6

CORRELATION OF BURST PRESSURE WITH PDA

The intent of the development of the burst correlation is to provide a tool for establishing a structural limit for circumferential cracks and for estimating the probability of burst for SG tubes with circumferential cracks. Two basic approaches may be considered to achieve these ends. The first approach treats the prediction of the burst pressure from a theoretical perspective using existing analytic, strength of materials techniques, e.g., postulate a geometry and perform a limit load type of analysis to predict a lower bound to the burst pressure. In the first case the only uncertainties to consider are those associated with the geometry of the degradation and with the variation of the material properties. This assumes that the theoretical model is validated by test data. If a limit analysis yields results significantly below the test data, the second approach would be expected to provide results more representative of the expected burst behavior of the tubes. The second approach is based on establishing an empirical correlation between the burst pressure and some geometry factor, i.e., the percent degraded area (PDA). If the second approach is used, the prediction of the burst pressure must also consider the uncertainties in the regression analysis or analyses and the regression assumptions must be verified. A schematic of the typical burst behavior of circumferentially cracked tubes which are laterally restrained by a tube support plate is illustrated on Figure 6-1. If there is no lateral restraint the burst pressures are significantly reduced.

If the burst pressure of laterally restrained SG tubes, e.g., by a tube support plate, is plotted against the PDA, three behavior patterns are evident. These are schematically illustrated on Figure 6-1. Up to about 25 to 35% degraded area (DA) the burst mode is characterized by an axial rupture of the tube. This is because the hoop stress is larger than the net section axial stress for throughwall cracks within this range of PDAs. Thus, less net area is required to resist the axial load due to the internal pressure. Beyond the axial rupture, up to about 75 to 80% DA, the burst resistance is governed by the bending strength of the degraded cross section of the tube if the degradation is mainly throughwall. Above a DA of about 80 to 85% the mode of failure is tensile, i.e., the burst resistance is governed by the axial strength of the remaining tube material area, regardless of the morphology of the flaw.

In the region from ~65 to ~85% degraded area, the dependence of the burst strength on the morphology of the flaw can be quite significant. For example, a bending failure mode would be expected for a single throughwall flaw, while a tensile mode would be

expected for a 360°, partial throughwall flaw. For a combination of both, the failure mode would be expected to be governed by the contribution of the material in the remaining ligament (outside of the throughwall flaw) to restricting the crack opening displacement at the elevation of the degradation. This is the transition area illustrated on Figure 6-1. The region of DAs in the vicinity of 80 to 85% is referred to as the *knee* of the burst resistance curve where the bending mode curve of Figure 6-1 intersects with the tensile overload curve.

Required margins of safety relative to tube rupture are delineated in RG 1.121 as a factor of three relative to the normal operating pressure differential and a factor of 1.43 relative to the postulated steam line break (SLB) pressure differential. The SLB pressure difference may be considered to be 2560 psid with an attendant critical pressure of 3657 psid. Values of three times the normal operating differential pressure may range from about 3750 to 4800 psi, depending on the plant. Since the normal operation critical pressures are greater than the SLB critical pressure, less degradation would be permitted. As it turns out, the critical region of the PDA for the normal operation required strength is near the *knee* of the burst resistance curve.

The development of a burst pressure correlation with the PDA started with a review and examination of the industry database on the subject and the identification of additional tests to be performed. The tests were conducted and the results examined, correlations with the PDA were developed and the results of the regression analyses were compared with the results obtained from the destructive testing of pulled tube sections and other laboratory specimen data.

6.1 Existing Industry Database

The purpose of this section is to provide a summary of existing data which was considered for inclusion in the EPRI circumferential cracking burst pressure database for nuclear plant steam generator (SG) tubes. Throughout this report, the word *flaw* is used to mean a crack or a narrow, say 6 to 10 mils, circumferential slit in a tube section that is pressurized to failure, e.g., circumferential cracking. This definition is independent of the means of effecting the flaw in the tube, e.g., the flaw may be a slit machined by an EDM process or a laser process, or an actual crack which has been chemically induced in a corrosive environment in a laboratory, model boiler, or steam generator (SG).

The purpose of compiling the database was to provide supporting data for efforts aimed at establishing guidelines for evaluating the structural integrity of SG tubes. For the data contained in this report, it is expected that the burst testing was performed in a manner similar, i.e., meeting the intent, or conforming to EPRI guidelines for leak and burst testing. The rationale for this is that, for the most part, the individuals responsible for the testing were also responsible for the development of the guidelines. The

database record is not all inclusive of every variable that could be varied during testing, thus, for future tests, some expansion of the database may be prudent if a particular variable is being investigated. For example, the EPRI guidelines specify a recommended pressurization rate. The database does not contain an entry for the pressurization rate, thus, if future tests are conducted to determine if some specific range of rates have an effect on the results, an additional column would be created to record the rate.

The earliest data reported in the surveyed database dates from 1981, although it is not considered to be currently useful because the testing was performed without the benefit of a lateral restraint of the tube. There was somewhat of a lull in the published data until the 1989 time frame, with much data reported between 1989, e.g., Reference 12, and 1991. A second lull occurred from 1992 through 1994, with additional data published in 1995 and 1996, e.g., Reference 10. It is beyond the scope of this report to discuss each of the salient references herein. For a variety of reasons, it is recommended later in this report that the historical data be relegated to a verification role relative to the data introduced in this report.

6.2 Additional Burst Tests

Based on the review of the existing database, a matrix of circumferential crack configurations was developed to be burst tested as part of the EPRI's program for circumferential cracking alternate repair criteria (ARC) development. The purpose of the test program was initially to obtain data, using the EPRI guidelines for burst testing of tubes with circumferential flaws, to supplement the existing database in areas where additional data was considered necessary. A committee of industry and vendor representatives was consulted in developing the test matrix.[1]

The purpose of the testing was not originally intended for the specific support of the development of a single analysis method for predicting the strength of tubes with circumferential indications or flaws. Methodologies based on theory already exist and generally predict quite similar burst pressure values for like morphologies in the range of degradation of most interest, i.e., when the percent degraded area (PDA) is greater than about 50%. For circumferential indications with less than or equal to a 50% degraded area (DA) the probability of a tube rupture is very small regardless of the morphology of the degradation. The intent of performing the tests was to obtain data to facilitate an understanding of the effect of morphology features such as deep penetration cracking (either uniform or outside of a main throughwall crack) on the burst strength, the effect of morphology on the transition from a bending dominated to a tensile dominated burst mode, and to develop data to support the development of

[1] The committee consisted of R. Keating (Westinghouse), P. Hernalsteen (Laborelec), J. Begley (Aptech), D. Ayres (ABB CE), R. Coe (FTI), and N. Cofie (SIA).

leak path analysis models which account for plastic deformation in the immediate vicinity of the flaw. In addition, the data were expected to support the statistical use of empirically developed relations for the burst pressure as a function of PDA. There were two anticipated uses for the burst database, to predict burst pressures based on the statistical variation of material properties about a structurally lower bound curve, and to predict burst pressures based on the statistical variation of the test burst pressures about an empirical fit of the data. It may be likely that information regarding both prediction methods will be needed to support the application of an ARC for circumferential cracks. One of the key outcomes here is that the data strongly support the use of empirical correlations. The development of ARC for circumferential degradation will likely be limited to beginning of cycle indications with PDAs less than to 50%, depending on the growth rate, to end of cycle indications with PDAs up to 80 to 90%. Thus, the range of interest for most of the testing is in the PDA range of about 60 to 90%.

In Section 7 of this report, analytic techniques for the prediction of leak rate from circumferential indications are developed. In order to complete this effort, predictions of total crack opening displacement (COD) and the crack tip opening displacement (CTOD) must be compared to empirical data. For this reason, some testing of throughwall slitted, full thickness ligament specimens with PDAs in the range of ~15 to 50% was desired.

It is noted that there can be a significant strengthening effect from axial ligaments between acoplanar multiple circumferential flaws. The effect may be governed by the ligament bending strength if the flaws overlap, by the shear strength if they project tip-to-tip, or by the tensile strength if they have significant circumferential separation. The empirical characterization of axial ligament strengthening is not part of this program, but a few tests to assess ligament strengthening were performed and are discussed later in this report section. It is clear from the data that consideration of a single throughwall flaw constitutes a lower bound for indications with less than ≈75% degraded area and a single partial throughwall by 360° constitutes a lower bound for indications with greater than 75% degraded area.

6.2.1 Test Program Objectives

Based on a review of the existing data and prediction formulae, the review committee agreed that the general aims of the test program should be to:

1. better define the *knee* region of the circumferential cracking burst curve by empirically evaluating the effect of deep wall penetration (expected to result in a lowering of the effective flow stress and a reduction in the critical CTOD),
2. determine the effect of a "tab", i.e., secondary, ligament within a large throughwall flaw, on the transition from bending to tensile failure in the region of the burst resistance curve just below the *knee*,

3. characterize the crack opening behavior as a function of pressure for some specific throughwall degradation lengths, and,
4. provide information contributing to the further understanding of the effect of test conditions, specifically different reinforcing foils, on the measured burst strength.

Using the test program aims as a guide, objectives were identified to provide direction on the specific configurations of the test specimens. These are summarized in Table 6-1, and a specific test configurations to address these objectives are given in Table 6-2. The first four objectives were mainly aimed at quantifying the effect of OD penetration of the ligament remaining outside of the throughwall portion of the flaw. This means verifying the tensile behavior of throughwall cracks with large crack angles, investigating the effect of *deeply* penetrating OD circumferential flaws, verifying the bending failure of throughwall flaws, and investigating the effect of OD penetration on bending failure. Figure 6-2 illustrates the cross section configuration for these specimens. At one extreme, the slit was entirely throughwall with the remaining ligament being full thickness, while at the other extreme there was no throughwall slit, the degradation being simulated entirely by a partial throughwall uniform depth slit.

Returning to Figure 6-1, the knee of the curve, corresponding to a throughwall length in the vicinity of 85% of the circumference of the tube, and the tensile behavior was not expected to be precisely as schematically illustrated. This is because the strength of the ligament outside of the throughwall region depends on the degradation depth. If no degradation is present, the net section stress at failure would be equal to the ultimate tensile stress of the material. When the depth of penetration is large, say 25% to 75%, the net section stress required to cause failure will be equal to the flow stress of the material. Finally, when the ligament degradation approaches throughwall, the failure stress is expected to be near the yield strength of the material. Thus, the effective flow stress is expected to vary from the ultimate tensile stress for minimum DA to the yield strength for maximum DA.

The fifth objective was to obtain COD and CTOD data as a function of differential pressure for a series of throughwall crack angles. The range of interest is illustrated on Figure 6-1. This information is needed to verify the analytical modeling of the plastic crack opening which is used to calculate the flow area of the leak from a throughwall flaw.

The sixth objective was aimed at better defining the effect of a small or "tab" ligament, within a large throughwall flaw, on the transition from bending to tensile failure in the vicinity of the *knee* region of the burst resistance curve. This is depicted as the shaded area on Figure 6-1. Figure 6-3 illustrates the remaining cross section area configuration for the specimens. The nondegraded area of the specimen is divided into two segments which are not equal in size. If all of the remaining area was concentrated in a single ligament, the rupture pressure would likely be dominated by the bending strength of the degraded cross section. The division of the remaining ligament into two sections,

a primary and a *tab* ligament as shown on Figure 6-3, should result in a burst pressure between that associated with bending and that associated with tensile overload, i.e., in the shaded are of Figure 6-1. Maximum strengthening should occur when the *tab offset* angle is zero degrees, diminishing only with tab length. No significant strengthening would be expected if the tab is nearly adjacent to the primary ligament, or if the tab is too narrow. Thus, the objectives of testing these configurations was to investigate the strengthening dependence on the size of the tab and how that dependence is affected by the magnitude of the tab offset. Because the center of the region of interest is in the total DA range of about 70 to 80%, the specimen configurations listed in Table 6-3 were selected for burst testing.

Finally, the seventh and eighth objectives were chosen to investigate the effect of different testing methods and to bolster the database of results for single throughwall flaws using the EPRI guidelines for burst testing of circumferential flaws. Of specific note is the comparison of results obtained from tests conducted using not lubricated 10 mil thick stainless steel foil with an ultimate tensile strength on the order of 1200 MPa (174 ksi) with those obtained using lubricated 6 mil thick brass foil with an ultimate strength on the order of 425 MPa (62 ksi). Four throughwall flaw sizes were selected for specific comparison. Four additional throughwall flaw sizes, large and not duplicating those already planned, were selected for throughwall flaw burst testing.

6.2.2 Test Conditions

The purpose of this section is to provide an overview of the test conditions, not the details of the test specification. All tests were conducted at room temperature using nominal 3/4" diameter by 0.043" thick mill annealed Alloy 600 SG tubing. The flaws were simulated by narrow EDM slits which had a width of ≈6 mils. The lower end of the tube was constrained by a clamp type tubesheet simulating collar, i.e., the tubes were not rolled into the collar, to prevent rotation within the collar. All of the specimens were also tested with lateral support provided by a 3/4" thick TSP simulant was located 37.75" above the top of the TS simulant. The diameter of the TSP hole was 0.784" ±0.003". A schematic of the test setup is illustrated on Figure 6-4.

For the COD and CTOD measurements, clip gages were used to measure the relative displacement of stand-off pieces which are glued to the tube, not to the collar. Measurements will be taken at the center of the silt, at one of the slit tips, and at the center of the remaining ligament. Displacement measurements were also recorded for the tab ligament specimens with the clip gages located at 120° intervals, with one of the gages centered with respect to the maximum slit.

The expected results in terms of the mode of failure are listed in Table 6-2 for the specimens fabricated with single throughwall slits and in Table 6-3 for the specimens aimed at investigating the effect of a *tab ligament*. The foil effect tests were performed to

confirm analytic results obtained by Paul Hernalsteen and presented to the EPRI ad hoc committee in February, 1996.

The testing program included obtaining the physical properties of the shim stocks used for the foil reinforcement of the throughwall cracks. The brass material was classified as half-hard, cold rolled CDA 260 alloy. The brass foil was tested in two thicknesses, 4 and 6 mils. The average yield strength from three tests was 39.6 ksi for the 4 mil foil and 32.2 ksi for the 6 mil foil. The respective ultimate tensile strengths were found to be 59.5 and 58.9 ksi. The stainless steel shim stock was full hard, cold rolled type 302. The average yield strength was measured to be 189.7 ksi and the average ultimate strength was found to be 202.5 ksi. Based on the stainless steel strength values it would be expected that the use of that foil could lead to strengthening of the specimen.

All of the test tubing was from heat NX9482 with an average outside diameter of 0.7513" and a thickness of 0.0428". The mechanical properties were found to be 54.9 ksi and 107.3 ksi for the yield and ultimate tensile strength respectively. The average value of the flow stress was 81.1 ksi.

6.2.3 Test Program Results

For single throughwall cracks with a PDA less than 15%, axial rupture occurs before circumferential rupture. For PDAs in the range of 15 to 80% the burst resistance is dominated by the bending load. Finally, for PDAs greater than 80% the burst pressure is governed by the tensile portion of the pressure load, i.e., the end cap load. The change from bending dominated to tensile dominated occurs at about 80% DA.
For 360° uniform depth cracks, the burst pressure is approximately governed by the net section stress, although there is evidence of some notch strengthening and ligament thickness effects on the flow stress.

For single throughwall cracks with a reduced ligament, for PDA > 65% the burst resistance is similar to uniform depth cracks. At PDA ~ 50% the burst resistance is about midway between the single throughwall and the 360° uniform. Bending leads to compression on some of the reduced ligament area, but it takes less CTOD to tear the ends.

For the double throughwall or tab ligament specimens, for 70% to 80% DA the burst behavior is similar to that for 360° uniform depth cracking. This indicates that the full CTOD is necessary to tear the material. Another observation from the testing was that the tab ligament always failed in tension, however, the main ligament may have failed in tension or in bending. If the main ligament failed in tension, it is likely that the main ligament and the tab failed simultaneously or near simultaneously since they would be subject to the same amount of strain as a function of time. If the main ligament failed in bending, it is implied but not required that the tab ligament failed first.

Throughwall Circumferential Crack Data

For the throughwall circumferential slit specimens, a variety of reinforcing foils was employed ranging from 4 and 6 mil brass to 10 mil stainless steel (SS) consisting of two layers of 5 mils each. All of the brass shims were lubricated before insertion into the tubes for testing (lubrication facilitates the insertion of the liner into the tube). Half of the tests with stainless steel were lubricated and half were not. The burst pressure of specimens with SS shims and without lubrication ranged from 4.4% for a PDA of 50% to 18.4% for a PDA of ≈80% greater than the corresponding burst pressure for non-lubricated specimens. The average increase in the burst pressure was 10% of that of the lubricated specimens. Moreover, an examination of the data indicated that the effect was approximately linear in the lubricated specimen burst pressure with a slope of about -4% per 1000 psi of burst pressure from a maximum of 118% for a lubricated specimen burst pressure of 5650 psi.

The effect of the difference in the thickness of the brass shims was essentially negligible. The average effect was to increase the burst pressure by 1.7% with a range from -2.6% to 6.6%. The effect of the non-lubricated stainless steel foil relative to the lubricated brass foils was to increase the burst pressure by an average factor of ≈26%, with a range from 20% for the large indications to 30% for the small indications. Finally, the average increase in burst pressure for lubricated SS foil relative to lubricated 6 mil brass foil was 12.6%, with a range of 1.8% for the 288° TW flaws to 20.6% for the 180° TW flaws. The conclusion from these comparisons is that the specimens tested with brass foils may be considered as one group for the analysis of the data, and that the specimens tested with SS foil should not be included in the correlation analyses.

6.2.4 EDM Simulation of Cracked Tubes

The circumferential cracking of the test specimens was simulated by machining narrow slits to the desired profile of the crack configuration to be tested. This is standard practice in the industry and has historically been demonstrated to be a valid approach. The narrow slits are machined using electrical discharge machining (EDM), although laser methods are also available, they tend to be significantly more expensive and have a longer lead time for fabrication. The slits tend to be on the order of 7 to 8 mils wide, not physically representative of a crack. However, because of the very ductile behavior of the nickel alloys used for SG tubes, extensive blunting of the crack tip occurs before the crack runs and failure occurs. If the crack is throughwall, blunting at the crack tips is on the order of the thickness of the tubes, e.g., about 40 to 45 mils. Thus, when the crack extends there is little influence of the initial radius of the crack tip. This has been confirmed by comparing the results of burst testing of axially fatigue cracked specimens versus EDM slit specimens.

A difference in the behavior of slit specimens relative to that of cracked specimens would be expected when the dimension of the ligament ahead of the tip of the crack is small. In essence, the material ahead of the crack tip must accommodate the strain necessary to achieve the crack opening displacement (COD) at the time of failure. If there is very little ligament left, the strain that can be accommodated is much less than the comparable strain if the ligament is large. It is not unreasonable to estimate the blunting that occurs for a partial depth indication as the remaining thickness fraction times the maximum value of 40 mils. For example, a 90% throughwall crack would be expected to blunt to about 4 mils before fracture occurred. For practical considerations, this may be accounted for by altering the magnitude of the flow stress used for burst prediction calculations base on theoretical considerations. One suggestion for such an adjustment is given in Reference 4.

6.2.5 Conclusions from the Results of the Test Program

The most significant conclusion from the test program results is that the prior domestic data should be omitted from the database used for developing correlations between the burst pressure and the size of the cracking. One of the reasons for this is that it is questionable as to whether or not a burst was achieved and a confident judgment is not possible because of the lack of load/displacement records. An examination of one of the Westinghouse specimens coupled with discussions with the testing engineer implies that a real burst of the tube was not achieved for most of those specimens. The second major conclusion is that the non-domestic data should be omitted from the database because of the variable uncertainty in adjusting the results to account for the use of 10 mil stainless steel foil. A single adjustment factor may be acceptable in estimating lower bound values but is not conducive to characterizing the variation of the data for correlation analyses. Also, a comparison of the paired data indicated that the effect of lubrication on the stainless steel foil results is a monotonically increasing function of the PDA or a decreasing function of the burst pressure. Thus, the SS foil data are considered to be useful for comparison to current results.

The final conclusion is that the results from the current test program should be segregated into two subsets and independent regression analyses should be performed using the data from the resulting subsets. A regression analysis of the bending mode data and a regression analysis of the tensile mode data should be performed, with the results from the other test specimens being examined relative the two bounding modes.

An alternative set of conclusions was provided via Reference 11. In summary, based on comparative analyses, it was concluded that only the strong foil results in reproducible results, i.e., tearing of the crack tips, from the burst testing and that the use of *weak* foil appears to require specific control of the lubricant and its application to make sure a true burst is achieved. In addition, the inability of some *weak* foil tests to achieve true burst for a PDA lower than 70% leads to concern with regard to prior test results, i.e., the data in these cases could be lower bound non-burst pressures. The limit model of

Reference 4 appears to be adequate [for lower bound analyses], but could be improved by modifying the flow stress for TW flaws in the bending mode (for a cracked ligament) and the tensile mode (for a full thickness ligament). It is noted that if actual burst is not achieved with a weak foil, the load displacement records can be used to determine if burst was imminent (these records were not available for the initial review of the results of the tests). Finally, the comparison of other test data obtained from both EDM slitted and corrosion cracked specimens with the regression results indicates that the data-derived relations are appropriate for predicting the burst pressure of corrosion cracked SG tubes.

6.3 Burst Pressure Correlation

A burst correlation for circumferential indications must, of necessity, be a composite of correlations for different crack configurations. The actual crack network may consist of:

1. Throughwall circumferential cracks, e.g., a single throughwall indication of some specific angular extent less than 360°, or multiple throughwall cracks separated by circumferential and/or axial ligaments, that could as a network extend 360° around the tube.

2. Partial throughwall cracks, e.g., a somewhat uniform crack that extends 360° around the tube at some average depth of penetration, or a group of partial throughwall cracks of varying depths around the tube.

3. A combination of throughwall and partial throughwall cracks that jointly extend up to 360° around the tube.

The burst correlation must be applied to as-measured RPC indications to assess tube integrity at the time of the inspection. In addition, the burst correlation must be applied to some projected end-of-cycle (EOC) crack morphology in order to assess the structural acceptability of indications detected at the beginning of the cycle. Hence, essentially all configurations must be considered. The use of the burst correlation will be to perform structural assessments based on the only available indication morphology information for an indication in a tube remaining in service being non-destructive examination data.

Because of the effect the complex geometries associated with circumferential cracks have on their structural performance relative to the performance of axial cracks, e.g., ODSCC at TSPs tends to be dominated by a pseudo-single largest crack, it is unrealistic to expect a correlation of bobbin or RPC voltage amplitude to burst pressure. This has been the industry experience. Hence, estimating the structural integrity of a circumferential indications relies on obtaining knowledge of the depth of the indication as a function of circumferential extent.

Given the cracked profile, the resistance of the indication to burst during normal and faulted operating conditions can be estimated. This however involves the use of

multiple analytical techniques, e.g., Paris instability per NUREG/CR-3464, to define regions of structural acceptability in depth/arc length space. The geometry of the tube support condition also contributes to the strength of circumferential cracks. For example, a tube with a large circumferential crack which is free to deform off-axis will have a significantly lower burst pressure than a similar tube which is restrained from lateral deflection. Thus, the lateral stiffness of the tube/support system, which is determined by its diameter, thickness, and length to the support structure, is a factor which must be considered in the analysis. Even so, the burst strength of a tube with circumferential cracking is not simply a function of the plastic instability strength of the remaining area. Thus, a tube with a 270° throughwall indication has less strength than a tube with a 360° indication which is 75% deep. This is because the neutral axis of the ligament area of the first example crack is not coincident with the axis of the tube, which is the loading axis for the crack. Hence bending loads are developed which affect the structural integrity for the throughwall configuration. If the remaining ligament is also partially cracked, the effect of the bending loads increases for larger crack angles.

Depending on the crack angle and morphology, the instability mode of failure may be governed by different predictive models. Moreover, ligaments between cracks may or may not be of sufficient size to contribute to the strength of the tube. Extension of the crack may be thought of as an inability of the material at the tip of the crack to accommodate the strain associated with the plastic opening of the crack tip. For single throughwall cracks, the tip of the crack becomes blunted on the order of the thickness of the tube before extension of the crack occurs. For partial depth cracks, the material in the radial direction cannot accommodate that level of deformation without tearing. For coplanar throughwall cracks separated by a ligament of tube material, the thickness of the ligament may or may not be sufficient to accommodate the plastic deformation at the tip of the cracks. Hence, the ligament may or may not contribute to the burst resistance of the crack network. An understanding of the potential ligament contribution to the strength of the tube is essential to predicting the limiting loads which the tube can sustain, as is an understanding of the contribution of radial ligaments for partial throughwall cracks.

Different approaches have been taken to justify the continued operation of plants where circumferential indications have been reported as being present in the SG tubes. These all share a common approach in that the strength of indications found during the current inspection, and judged to be bounding of the population of indications in the SGs, have been demonstrated to meet the requirements of RG 1.121 by testing of pulled tube specimens and/or in situ pressure testing. Thus, it is considered demonstrated that undetected indications at the beginning of the next operating cycle will not grow to any more significant extent than previously observed. Difficulties with this approach may arise when the next operating cycle is significantly longer than the previous cycle. In addition, the use of this approach requires the plugging of any tubes with detected circumferential indications.

Investigations of the strength of tubes with circumferential indications have been performed in specific circumstances to support the continued operation of specific plants. There has, however, been no unified approach which would be of benefit to the industry as a whole, and there has been no systematic attempt to estimate the strengthening effect of ligaments between the cracks. The intent of this effort was to provide that unified approach by documenting the various models employed and measuring their range of effectiveness relative to test specimens. Where multiple models were available for the same type of configuration, it was intended that a comparison be made and a *recommended* model selected. It was also intended to develop correlations based on dimensionless parameters (similar in concept to the EPRI axial throughwall crack burst correlation) that could be applied to different tube sizes. The burst capability for various crack angles and average crack depths was developed as a function of the percent degraded area.

It is to be noted that testing was performed in 1981 to determine the effect of offset TSP holes on the burst pressure of tubes with circumferential cracks at the top of the tubesheet. The results of these tests demonstrated that the offsets associated with the positioning of the TSP holes do not significantly affect the burst pressure. The worst case scenario would occur if the TSP hole is displaced in a direction through the centroid of the remaining ligament. However, TSP hole offsets are much less than the bending displacement that would occur if the plate was not present. Thus, the loads imposed by an initial deformation decrease (eventually to zero) as the tube deforms from the bending moment developed because the neutral axis of the remaining section does not intersect with the axis of the axial force imposed by the internal pressure.

Concerns could also be expressed relative to compressive loads being developed in *locked* tubes because of the average tube temperature increase, i.e., the throughwall temperature could become uniform at the primary temperature, that would be expected following a postulated steam line break (SLB) event. If the tube is in compression, then no tensile load is developed by the internal pressure. Thus, the only load acting to open the crack would be bending as a result of buckling of the tube. The axial position of the TSP would be governed by all of the locked tubes in the bundle, thus the compressive load in any single tube would be small relative to the total load on the plate. Since it would be extremely unlikely for a single tube to experience locking, the cracked tube cannot be compressed any more than it's neighbors. It is further noted that locking of the tubes would be expected at operating temperature. Hence, the change in the average temperature would only be on the order of 25°F. For a 36" long span, the axial compression assuming the TSP to be rigidly fixed would be on the order of 7 to 8 mils. The compressive load would then be on the order of 250 to 300 lbf. The amount of buckling deformation would be expected to be small relative to that needed to significantly open a circumferential crack in the tube.

To minimize the influence of scatter in the data (and for controlling the test specimens' configurations), the burst correlation was developed from EDM slitted specimen tests. To support further development of the correlation, twenty-three (23) burst test

configurations (with two replicates of each configuration) were tested. The final configurations were selected after a review of all the available data.

The final effort of the program was to correlate the predicted strength of circumferential indications based on the dimensions of the cracks with measured strengths from destructive examinations. Table 6-4 lists all of the test results from this program. The applicability of the correlations were assessed against burst data from other laboratory specimens which were made to simulate actual tube degradation measured on pulled tubes. Separate tables were also prepared to segregate the data as follows:

- Table 6-5 lists single throughwall slit specimen results extracted from the total database. This data was analyzed to calculate a regression line relating the burst pressure to the PDA for single, throughwall, circumferential slits of varying lengths. The regression analysis of these results essentially leads to a lower bound for the burst pressures up to about 75% DA because this is the weakest configuration for the geometry of the crack up to that depth.
- Table 6-6 lists the results from testing specimens with throughwall and/or reduced ligament slits. As expected, the specimens exhibited strengths greater than those of equivalent PDA throughwall slits and slightly less than equivalent PDA partial throughwall by 360° slits. There were not regression analyses performed using this data.
- Table 6-7 lists the results from the testing of the specimens with "tab" ligaments. These specimens tended to exhibit burst pressures equivalent to those from the 360° partial throughwall specimens, e.g., failure was by tensile overload, although some of the specimens did not exhibit tearing of the major ligament. No individual regression analyses were performed with this data, however, some of the data was included in the regression analyses to correlate burst pressure to PDA for tensile overload type failures.
- Table 6-8 lists the test results from the specimens which were considered for the correlation of the tensile or net section strength to the PDA. This includes large PDA data from single throughwall slits, data from double throughwall slits, and data from 360° partial throughwall slits. As discussed later, a reduced data set was selected for the regression analysis.

6.3.1 Analytical Models

Several analytical models have been employed to evaluate the structural integrity of tubes with circumferential cracks, e.g., References 1 through 3. In general, but not always, the integrity can be evaluated using tensile or bending limit load analysis considering the net area of the non-cracked material in the tube, i.e., one minus the fraction degraded area. Thus, as an initial observation, the strength of a tube should be approximately unaltered until the total area of the crack exceeds a value somewhat

lower than approximately one-half of the cross section area of the tube. This is simply based on the fact that the elastically calculated hoop stress is twice the axial stress, with the consideration that there is also a bending load. So, an axial rupture would be expected to occur prior to a circumferential rupture as long as somewhat more than one-half of the cross section is not cracked (the elastically calculated value neglecting bending, would be 1/2). The evaluations discussed are for: throughwall circumferential cracks, with unrestricted lateral motion, and with restricted lateral motion such as is provided by TSPs, partial throughwall cracks that extend less than and up to 360° around the tube, and throughwall plus partial throughwall cracks that jointly extend less than and up to 360° around the tube.

6.3.1.1 Limit Load Model

Hernalsteen, Reference 4, presented a general lower bound limit load model solution for a variety of idealized crack geometries ranging from uniform depth ID and OD cracks to throughwall cracks of limited circumferential extent. Specific accounting was made of the location of up to two lateral supports. A lower bound reference curve was recommended for general use, with techniques presented to adjust the results to account for plant specific geometries and material properties. A similar analysis for tubes without lateral support was recorded in Reference 14.

For uniform depth ID or OD cracks, the mode of rupture is by tensile overload of the remaining area and the burst pressure is approximately linear with the PDA. Hernalsteen refined the model to account for the effect of pressure on the flanks of the crack and the apparent change in the flow stress with ligament thickness.

$$P_n = \frac{t_l/t - \left(t_l/t - t_0/t\right)\alpha/\pi}{1 - t/R_m - \eta\left(2t/R_m\right)\alpha/\pi}, \qquad \text{(eq. 6-1)}$$

where t_l is the ligament thickness in the larger region of uniform depth of penetration extending over a circumferential length of 2α, t_0 is the ligament thickness in a local region, and η is a factor that accounts for the pressure acting on the flanks of the crack. For a uniform ID or OD crack, $\alpha = \pi$ or 0 and $t_l = t_0$, so Equation 6-1 becomes

$$P_n = \frac{t_l/t}{1 - \left(t/R_m\right)\left(1 + 2\eta\right)}, \qquad \text{(eq. 6-2)}$$

where η is then taken as -1 for a ID crack, indicating an unbalanced pressure load on the crack flanks, and zero for an OD crack. Making the appropriate substitutions, one obtains,

$$P_{n.ID} = P_{n.OD} \frac{R_m/t - 1}{R_m/t + 1} \qquad \text{(eq. 6-3)}$$

If necessary, this relation may be used to adjust allowable P_n values obtained from testing of OD indications to allowable values for ID indications. Most of the circumferential indications of interest are OD originated. For the SG tubes currently of interest, outside diameters range from 0.6875" to 0.875" with thickness values of 0.040" to 0.050", the ratio of Equation 6-2 may be taken as 0.774 with an error of no more than ±0.018.

In the limit of a throughwall crack, the load on the crack flanks could reduce the burst pressure by about 8%. The axial net section stress to cause failure of a tube with a uniform depth crack with the depth approaching zero is the ultimate tensile strength. At the other extreme, as the depth approaches 100%, the axial stress on the remaining ligament at the time of failure would be expected to be near the yield strength[2] simply because there would be no material in the ligament to accommodate plastic strain. Assuming a linear variation of the effective flow stress, σEF, with the thickness of the remaining ligament of material, t_l, the flow stress value to be used in Equation 6-11 (later in this section) would be given by,

$$\sigma_{EF} = \sigma_F \left(0.6 + 0.8 \frac{t_l}{t} \right) \qquad \text{(eq. 6-4)}$$

where the unadjusted flow stress is given as before (Reference 4). The constants in Equation 6-4 were developed based on the observation that the ratio of $\sigma Y/\sigma U$ for tubing fabricated by Westinghouse, Vallourec, and Sandvik is approximately constant at 0.43.

6.3.1.2 Plastic Zone Instability Model

Another possible failure mode to be considered is plastic bulging at the elevation of the crack. Burst pressures can be estimated by using a plastic zone instability (PZI) criterion, References 5, 6, 7, and 8, i.e., burst will occur when the plastic zone ahead of the crack is predicted to increase without bound. This analysis is intended to supplement the analysis of the previous section, not replace it. In other words, two separate failure modes are considered, the expected burst pressure corresponds to the mode with the lowest predicted burst pressure for the PDA of interest. A linear elastic

---

[2] Or more nearly 1.15% of the yield strength because thin ligaments will be in a state of plane strain, being restricted by the full thickness tube material adjacent to the crack.

fracture mechanics (LEFM) analysis of the crack leads to a solution for the plastic zone size ahead of the crack. For elastic-plastic material the crack length is replaced by an effective crack length which includes the plastic zone. For stable configurations, the effective crack length is adjusted iteratively until the plastic zone correction converges to a constant value. For an unstable configuration the iterative calculations will lead to a prediction of a massive plastic zone.

The LEFM stress intensity factor for a TW circumferential crack in a tube is (Reference 13),

$$K = \sigma\sqrt{\pi a}\left(0.9 + 0.25\frac{a}{\sqrt{R_m t}}\right), \qquad \text{(eq. 6-5)}$$

where a is the half-length of the crack, and σ is the applied far-field stress. The term in parenthesis is valid for normalized crack lengths, λ, in the range of 2 to 10, or larger, where,

$$\lambda = \frac{a}{\sqrt{R_m t}}. \qquad \text{(eq. 6-6)}$$

For a 7/8" diameter tube with a 0.050" thickness, Equation 6-5 is valid for total crack angles in the range of 40° to 200°. The plastic zone corrected crack length, i.e., effective crack length, a_e, is

$$a_e = a + \frac{K^2}{2\pi\sigma_f^2}. \qquad \text{(eq. 6-7)}$$

The effective crack length from equation 6-7 is then substituted into equation 5 to obtain a new estimate of K. This leads to a new estimate of a_e, et cetera. In practice, sufficient convergence to a solution for K is obtained with one iteration, i.e., one calculation of a_e. Substituting the internal pressure, p, and for the effective crack length leads to,

$$K = \frac{pR_i}{2t}\sqrt{\pi\left(a + \frac{K^2}{2\pi\sigma_f^2}\right)}\left[0.9 + 0.25\frac{\left(a + \frac{K^2}{2\pi\sigma_f^2}\right)}{\sqrt{R_m t}}\right]. \qquad \text{(eq. 6-8)}$$

The solution for the critical pressure is obtained by finding the value of K for which the derivative of p with respect to K is zero, or conversely the derivative of K with respect

to p is infinity, thus indicating that a_e is increasing without bound. Note, if λ is less than 1, a different expression from the one in square brackets is used.

6.3.1.3 Net Section Stress Model

If the degradation is somewhat uniform in depth and extends for 360° around the tube, the mode of failure will be a tensile separation in the axial direction. The same mode occurs for very long throughwall cracks. The remaining material fails by tensile overload without a significant contribution from the bending stresses. The burst pressure for this mode of failure is usually predicted using a net section stress approach. When the applied stress on the remaining section area of the material equals the failure stress, taken as the flow stress, the tube would be expected to separate.

By a straightforward force balance for an OD circumferential crack, the normalized burst pressure, P_n, is,

$$P_n = \frac{R_m}{t}\frac{t_{net}}{R_i}\left(1+\frac{1}{2}\frac{t_{net}}{R_i}\right), \qquad \text{(eq. 6-9)}$$

where t_{net} is the net remaining thickness of the tube, and R_m is taken for the non-degraded tube. If the circumferential crack is on the ID of the tube, the pressure load on the flanks of the crack must be considered. This results in a prediction of the normalized failure pressure as,

$$P_n = \frac{R_m}{2t}\left[\left(\frac{R_o}{R_o - t_{net}}\right)^2 - 1\right]. \qquad \text{(eq. 6-10)}$$

Note that by calculating the normalized burst pressure, the effect of changes in the flow stress and tube size are to be accounted for in the determination of the actual burst pressure.

The net section stress model does not replace either of the aforementioned models. Again, the estimated burst pressure would be that corresponding to the mode of failure with the lowest predicted burst pressure. From Figure 6-5, it is apparent that the lower bound burst pressure for circumferential indications in laterally supported tubes with PDAs above about 70 to 75% would be expected to be governed by the net section stress on the remaining ligament regardless of the way the degraded area is distributed around the tube circumference. For PDAs less than about 76%, some knowledge of the distribution of remaining area would be necessary to predict the mode of failure and the burst pressure. However, in this case one could use test data to establish two

empirical relationships, one corresponding to bending dominated failures and the other corresponding to tensile dominated failures.

6.3.1.4 Comparison of Analytical Models with Burst Data

A comparison of the lower bound theoretical models with the test data is provided on Figures 6-4 to 6-9. It is visibly evident that most of the burst pressures, and all of the data for PDAs $\geq$ 50%, significantly exceed the lower bound estimates. Based on this observation, it was judged appropriate to proceed with regression analyses of the data to develop predictive models for the burst pressure as a function of the PDA.

6.3.2 Burst Pressure Regression Analyses

The data obtained from the current program confirm that the limiting theoretical models of a 100% throughwall crack with a circumferential of less than 360° and a uniform partial throughwall crack with a circumferential extent of 360° bound the other cases. This was to be expected because in one limit assuming all of the degraded area to concentrated in one long circumferential crack represents the weakest configuration when the DA is less than about 80%. The data also indicate that the use of the limiting theoretical models introduces additional conservatism into the prediction of the burst pressure from the PDA. It is visibly apparent that the burst data are not distributed about the theoretical curves, thus the residuals from predictions would not be normally distributed about the theoretical curves.

Examination of the data of Figure 6-6 indicate that the burst behavior of the specimens could be described by fitting two regression lines, e.g., the first to the single throughwall data exhibiting a bending burst and the second to the 360° uniform depth, tab ligament and throughwall data exhibiting tensile failure of the remaining ligament.

6.3.2.1 Single Throughwall Crack Data Analysis

The single throughwall crack data is summarized in Table 6-5 and illustrated on Figure 6-7. The PDAs tested ranged from approximately 15 to 90%. The results from the tests were divided into two categories depending on whether the mode of failure appeared to be by bending or by tensile overload of the remaining area. The mode for each specimen is listed in Table 6-5. In order to fit a straight line in the region of interest, the Specimen 4A data were neglected. This would have the unnecessary effect of increasing the ordinate intercept and the slope of the curve.

The failures judged to be bending dominated tended to not tear before the foil and bladder lining. Thus, the burst pressures reported must be considered to be representative of lower bounds of the burst pressure corresponding to the measured PDAs. Each of the single throughwall test specimens was instrumented with three clip

gages to measure the deformation of the specimens during the pressurization to burst. The first gage was located at the center of the slit, the second at the center of the ligament, and the third at one tip of the slit. The pressure/time and pressure/displacement records for each specimen are contained in Appendix D of this report. Examination of the displacement records of specimens which did not tear gives insight as to whether or not burst was imminent. For example, if the record from clip gage #1 indicated that the rate of change of the pressure versus the displacement was approaching zero, it would be concluded that failure of the tube would have occurred at a pressure not significantly higher than that recorded. The behavior was verified by examining the record from clip gage #3 which recorded the crack tip opening displacement and clip gage #2 which measured the bending compression at the center of the ligament. Further confirmation was obtained by noting that the slope of the pressure/time history was constant until failure was achieved. This weakly implies that no significant extrusion of the foil/bladder occurred, thus indicating that a bending instability did occur.

For specimens designated as having failed in tension, it is apparent from the clip gage #2 displacement record that the ligament did experience some bending compression, but was in tension at the time the failure occurred. The record from specimen 2C (PDA of 90%) illustrates a minimum displacement of -6 mils[3] at a pressure of about 2000 psi followed by a displacement of 9 mils at a pressure of 3000 psi followed by failure of the specimen at a pressure of about 3100 psi. The displacement of clip gage #2 of Specimen 4I (PDA of 80% and burst pressure of ~5500 psi) is somewhat similar to those of the bending specimens, but total separation of the specimen occurred indicating a significant tensile mode contribution to the failure. These results are not inconsistent with the expected behavior transition from bending to tension in the degraded area range of ~75 to 80%, i.e., the results from the recent burst tests are in concert with the previously observed change in failure mode.

Two sets of data were considered for the regression analysis, those designated as bending failure, specimens 4B through 4G in Table 6-5, and the same data plus three data points designated as tensile failure, but consistent with the bending failure trend. The result from specimen 4A (PDA of 15% and burst pressure of 11500 psi) was omitted from consideration since it is out of the PDA range of structural interest. The first set of data, consisting of specimens 4B through 4G plus specimen 4F of Table 6-5 were selected for the analysis. Specimen 4F was designated a tensile failure, but had the same PDA and burst pressure as specimen 4G, which was designated to be a bending failure. Specimens 4I and 4J were considered for inclusion only because of their proximity to the data at 75% DA. Since tensile failures associated with a 80% DA would be expected

[3] The recorded displacement is greater than the deformation of the tube because the clip gages are mounted off the surface of the tube.

to exhibit close proximity to the bending failure data, it was decided that inclusion of that data was not justified. Regardless of which database was analyzed, the slope and intercept values were within 5% of each other. The results of the regression analysis are provided in Table 6-9.

It is apparent from the plot of the throughwall crack data that a linear regression equation relating the burst pressure to the PDA should be adequate. To verify this supposition the index of determination was calculated considering the pressure scale to be linear and logarithmic. The results were essentially identical, i.e., 97.5% and 97.3% respectively, hence, the use of a linear pressure scale is justified. It is noted that the logarithm scale is more attractive for making predictions because the distribution is skewed right and has a zero probability of occurrence of values of P_n less than or equal to zero. This simply means that the probability of burst during a SLB event would be calculated to be smaller using the logarithmic scale than the standard scale. To avoid the added complexity of dealing with a logarithm scale for the burst pressure, linear scale was selected for analysis.

The results of the regression analysis are provided in Table 6-9 and illustrated on Figure 6-10. A plot of the residual normalized burst pressures versus the predicted burst pressures is shown on Figure 6-11. The normal probability plot of the ordered residuals is shown on Figure 6-12. It is apparent from the plots that the predicted normalized burst pressures are not correlated to the residual normalized burst pressures and that the residuals appear to be normally distributed, see Reference 15. To quantify these observations, regressions of the ordinate values on the abscissa values for both sets of data were performed. The regression analysis of the predicted versus residual normalized burst pressure values resulted in an estimate of the slope of 0.0, i.e., flat line. The index of determination was calculated to be 0.0%, i.e., no correlation, and the p value for the slope parameter was found to be 100%. The intercept value was calculated to be 0.357 with a standard deviation of 0.014. In summary, the predicted values are indicated to be independent of the residuals.

The regression analysis of the expected normal deviates, per Reference 15, on the ordered residuals resulted in a predicted intercept of $\approx$0.0, a predicted slope

of 0.981, and an index of determination of 97.1%. In summary, the intercept and slope and index of determination are consistent with the assumption that the residuals are normally distributed.

In order to compare results for different tube sizes, the burst pressure is normalized by the mean radius, R_m, to thickness, t, ratio and the flow stress, σF, of the material. The normalized burst pressure, P_n, for axial cracking was defined as:

$$P_n = \frac{P_b R_m}{2 \sigma_F t}, \qquad \text{(eq. 6-11)}$$

where the flow stress, σF is usually defined as one half of the sum of the yield and ultimate tensile strength of the material. This definition is also suitable for circumferential cracks. Based on the test results, this is correlated to the PDA through a normalized crack length, λ. For axial cracks in tubes the crack length is normalized as,

$$\lambda = \frac{a}{\sqrt{R_m t}}, \qquad \text{(eq. 6-12)}$$

however, for circumferential cracks this relationship becomes,

$$\lambda = \theta \sqrt{R_m / t} = \rho 2\pi \sqrt{R_m / t}, \qquad \text{(eq. 6-13)}$$

where the equivalent throughwall angle θ is directly proportional to the PDA and ρ is the fractional degraded area. There is an inconsistency associated with the use of λ for circumferential cracks in that the limiting value of λ as $\rho \rightarrow 1$ is a function of the tube size. A consistent variable could be obtained by considering the ratio of λ to its maximum possible value, however, this ratio is linearly proportional to the PDA, hence, the appropriate choice for the independent variable is the PDA.

6.3.2.2 Uniform Depth Data Analysis

As with the throughwall analysis, multiple selections were considered for the uniform depth data analysis. The uniform depth specimens fail by tensile overload of the remaining section and a net section stress criterion may be developed. There were five (5) specimens in which the circumferential slit extended 360°. The actual PDAs for these specimens ranged from 69 to 79%. In addition, the double-slit specimens tended to fail in tension rather than in bending, although, for some specimens, for which the failure mechanism appeared to be bending, did not fully separate, i.e., the tab ligament broke and the sealing foil tore. The maximum pressure values for these specimens represents

a lower bound relative to burst, but, actual burst was not achieved. In addition, there were four specimens with single through wall slits that did separate to conclude the pressure test. Because of the thin section the limiting load is governed more by tension than by bending. Combining all of the above data resulted in a set consisting of the results of testing twenty-five specimens. All of the data are illustrated on Figures 6-10 and 6-13.

The single slit specimens would be expected to exhibit higher burst pressures than 360° uniform depth slit specimens for small remaining area. These specimens had remaining areas of 10 to 15%. For a 360° uniform slit specimen the remaining material ligament would be on the order of 4 to 6 mils deep. The remaining ligament of a uniform throughwall specimen would be on the order of 0.22 to 0.33" long with a width equal to the tube thickness. In essence, the second specimens would be able to absorb more plastic strain before separating and burst pressures would be expected to be higher. Based on this consideration it was decided that the single slit specimens would not be included in the database for the uniform thinning regression analysis.

Of the sixteen (16) double slit specimens that were tested with brass foil, five (5) failed in bending after the tab ligament tore. Since separation of the specimens did not occur, the results from these specimens were not included in the regression analysis. The final database consisted of five uniform depth and eleven double slit specimens.

It is apparent from an examination of the data, see Figure 6-13, that a simple linear first order regression would be expected to be sufficient. The trend of the data suggest that extrapolation to a PDA of 100 would be accompanied by a greater than zero burst pressure. In order to simplify the analysis the burst pressure was correlated to the percent remaining area. Since the regression must pass through zero for a remaining area of zero, it was considered appropriate to investigate whether or not weighted regression should be performed, i.e., by assuming the variance to be a linear function of the PRA. The weighted regression slope coefficient was essentially identical to the non-weighted slope value, hence, it was concluded that weighted regression was not necessary. The solution to the regression analysis was that the normalized burst pressure, P_n, may be predicted from the percent remaining area as,

$$P_n = 1.223\, A_R \,, \qquad \text{(eq. 6-14)}$$

where A_R is the percent remaining area. The standard error of the slope coefficient was calculated to be 0.0155 and the standard error of the residuals was found to be 0.0166. The regression line is illustrated on Figures 6-10 and 6-13. The 95% prediction bound illustrated on both figures was found as,

$$P_n = 1.223A_R - t_{(95,\upsilon)}s\sqrt{1+\frac{A_R^2}{\sum A_j^2}}\ , \qquad \text{(eq. 6-15)}$$

where t is the one-sided 95th percentile value of the t-distribution for ν degrees of freedom and s is the standard error of the residuals. Examination of the plot reveals that three of the five lower bound values from double slit specimens are at the 95% prediction bound. In addition, the four throughwall single slit results are at about the 95% upper bound.

Examination of the Residuals

Plot of the absolute residuals versus the predicted burst pressures is nondescript, Figure 6-14, indicating small to no dependence of the residuals on the predicted burst pressure. This observation was verified analytically by performing a regression analysis of the absolute residuals on the predicted burst pressures. The slope of the resulting regression line was near zero with an index of determination of about 15% and a slope p value of about 14%. This indicates no significant dependence of the variance of the residuals on the PRA, or PDA for that matter, supporting the performance of a non-weighted regression analysis. A normal probability plot of the ordered residuals indicates that a null hypothesis that the residuals are normally distributed about the prediction line would not be contradicted by the data. A graphical depiction of the results is provided on Figure 6-15. The regression of the normal distribution deviates on the observed standard deviates is parallel to the ideal relation line, a result of forcing the regression through the origin.

6.3.2.3 Concurrent Testing Program Data

To confirm the results of the regression analyses, data from a concurrent testing program of surrogate degradation profiles, i.e., to simulate degraded tubes, and from a previous surrogate tube simulation program were plotted with the current data and the regression lines, see Figure 6-16 (the R23C44 data were adjusted to reflect the fact that the slits were machined in a thinned section of the tubing). The regression results presented herein provide excellent predictions of the burst pressures of the surrogate specimens. For seventeen of the twenty test results the nominal regression curves provide a lower bound to the data.

6.3.2.4 Corrosion Degraded Tube Test Results

Further verification of the applicability of the regression curves was obtained by comparing the burst test results of thirty-nine (39) field and laboratory specimens with circumferential stress corrosion cracking. The data are plotted on Figure 6-17 relative to the two regression curves, corresponding to bending and tensile failure. Again, the

average regression predicted burst strengths constitute a lower bound to the actual test results, and not one falls below either of the regression curves. The burst pressure result for one other specimen, which is plotted for information on Figure 6-17 as a solid square, is below both of the regression curves, however, this specimen was severely damaged during the removal operation and thus exhibited a lower burst pressure than would have been achieved had the testing been performed in situ.

6.4 Probability of Burst

Since the errors of the regression were shown to follow a normal distribution, a deterministic estimate of the probability of burst of a single indication may be made using the Student's *t* distribution and the estimate of the variance of the product of the normalized burst pressure about the regression line and the material flow stress. This has been demonstrated to be a conservative practice in other applications because the burst pressure is essentially the product of the normalized burst pressure and the flow stress, i.e.

$$P_b = \frac{2\,t}{R_m} P_n S_f . \qquad \text{(eq. 6-16)}$$

The distribution of the product of the normalized burst and the flow stress is skewed right, hence the portion of the distribution in the lower tail is smaller than the portion of the distribution in the upper tail, whereas the Student's *t* distribution is symmetrical about the mean of the data. Thus, the following relationship is used to describe the distribution of the burst pressure about the regression curves,

$$P_b = t_{MinDoF}\left\{\left[a_0 + a_1\rho\right]\left(\frac{2t}{R_m}\right) S_f, s_b^2\right\} . \qquad \text{(eq. 6-17)}$$

Where s_b is the standard deviation of the product of the normalized burst pressure and the flow stress, adjusted for the ratio of the thickness to the mean radius of the tube. The use of the minimum DoF for determining the value of *t* adds margin to the calculation. The process for calculating the probability of burst for an indication is illustrated on Figure 6-18. In essence the distance from the regression line to the line representing the SLB differential pressure can be measured in terms of the number of standard deviations of the product distribution, *t*. The probability of burst is then estimated as the probability of obtaining the observed value of *t* at random. For these evaluations the distributions of the flow stress were obtained from the Westinghouse compendium of strength properties (available in the open literature), or from the specific room temperature properties listed for the tubes installed in the Arkansas Nuclear One SGs supplied by Combustion Engineering (CE). The same properties were assumed to apply

to 0.042" thick tubes in other CE supplied SGs. The adjustment for the decrease in strength with temperature was taken as that observed for tubes in *W* supplied SGs. The transition from bending to tensile dominated burst strength predictions occurs at a PDA of 75%. The probabilities of burst during a postulated SLB event range from $4 \cdot 10^{-7}$ to $3 \cdot 10^{-6}$ depending on the size of the tubing. The probability of burst as a function of the PDA for each of the tube sizes is shown on Figure 6-19. Note that all of the transitions from the bending dominated to the tensile dominated failure mode occur in the region of 72 to 75% DA regardless of the tube size. This is seen to be somewhat serendipitous since the standard error of the regression of the tensile failure data is about twice that of the bending data. Thus, it would be expected that the tensile failure line would dominate the probability of burst for at least some distance below the knee of the curve. However, the bending mode failure prediction line was obtained with about 60% of the number of data used for the tensile failure line, in effect making the product of the standard error and the *t* distribution deviate almost the same regardless of the failure mode. Although the probability of burst can also be estimated using the results of Monte Carlo simulations of the flow stress and normalized burst pressure distributions, such calculations were not considered to be necessary because of the low probability of burst values, e.g., on the order of 10^{-6} for PDAs as large as 75%, thus, the probability of one or more bursts occurring in a population of one-thousand tubes with PDAs on the order 75% is 10^{-3}.

Finally, a plot of the critical degraded area or percent degraded area as a function of the critical burst pressure is provided on Figure 6-20. Since the curves were developed from the lower 95% predictions using LTL material properties, the values presented represent structural limits in the sense of ODSCC ARC.

6.5 Conclusions

The evaluations performed of the existing data, the theoretical models and the additional test data indicate that the appropriate burst analysis method is to evaluate the circumferential crack area as a function of the tube circumference to establish the likely rupture mode, tensile versus bending, and to compare the result to the regression curves obtained from the analysis of the additional test data. It was also observed that the results of the regression analyses bounded the burst pressures for almost forty test results for tubes with corrosion induce degradation. Some specific conclusions from the overall are:

1. It is appropriate to remove the prior Westinghouse data from the analyses because it appears that burst was not achieved for almost all of the specimens and there are no load/displacement records available to determine if burst was imminent.

2. It is appropriate to remove the non-domestic data from the analyses because of variable uncertainty in adjusting the results to account for the use of 10 mil stainless

steel foil. A single adjustment factor may be sufficient for estimating lower bound values, but is not conducive to characterizing the variation of the data for the correlation analyses.

3. It is appropriate to segregate the results from the current test program and perform regression fits on the resulting subsets for bending failure and tensile failure modes, and then examine the results from the other tests relative to the two bounding modes.

Each of the above actions was completed for the analysis of the test data. The analysis of the data led to the following predictive conclusions:

1. Treating the PDA as that of a single TW crack provides a lower bound to the burst pressure, and mode, when correlated to the PDA. The test results demonstrated that the single TW crack and the uniform 360° crack constitute lower bounds relative to any other potential geometry of the circumferential cracks.

2. The presence of a *tab-like* ligament significantly increases the burst strength of the tube. For large PDA values, the presence of the tab-like ligament changes the mode of rupture from bending to tensile, and the burst pressures are similar to those for 360° uniform depth slits. For 70% to 80% DA the burst behavior is similar to that for 360° uniform depth cracking. Full CTOD is necessary to tear the material.

3. Single throughwall cracks — The burst resistance is dominated by the bending load for $15\% \leq PDA \leq 80\%$ and by the tensile portion of the load for $PDA > 80\%$. For $PDA < 15\%$ axial rupture occurs before circumferential rupture. For $PDA \geq 65\%$ the burst resistance is similar to uniform depth cracks. At $PDA \sim 50\%$ the burst resistance is about midway between the single throughwall and the 360° uniform.

4. Single throughwall with reduced ligament cracks — Bending leads to compression on some of the reduced ligament area, but it takes less CTOD to tear the ends.

5. 360° uniform depth cracks — Burst pressure is approximately governed by the net section stress. There may be some notch strengthening and ligament thickness effects on the flow stress.

6. The transition from bending dominated to tensile dominated failure occurs at about 75% DA. The probability of burst for degradation at this depth is on the order of 10^{-6}.

Moreover, the results from tests of surrogate specimens simulating observed field degradation were predicted well by the regression results, and the results from burst testing of almost forty corrosion cracked specimens were bounded by the regression predictions. It is also noted that the results from the test specimens tended to be

independent of shim thickness when brass was used and that while the use of 10 mil thick stainless steel elevates the burst pressure, it also appears to always result in tearing of the ends of the crack to terminate the test.

The main overall conclusion is that the two ideal models for evaluating the strength of the tubes, i.e., allocating the PDA to a 100% throughwall flaw or a uniform partial depth flaw over 360°, were confirmed to represent lower bounds for the burst pressure. Any flaw with a morphology at variance with these ideal representations has a greater burst strength than one conforming to the ideal representations. The strength of tubes with circumferential cracks can be predicted from the results of the regression analyses performed using the data from the throughwall and uniform depth specimens respectively.

6.6 References

1. EPRI NP-6301-D, "Ductile Fracture Handbook," Zahoor, A. (Novatech Corporation), Electric Power Research Institute, June, 1989 (Volume 1) to January, 1991 (Volume 3).

2. EPRI NP-5596, "Elastic-Plastic Fracture Analysis of Through-Wall and Surface Flaws in Cylinders," Kumar, V., and German, M. D. (General Electric Company), Electric Power Research Institute, January, 1988.

3. SRD-82-048, "Estimation Technique for the Prediction of Elastic-Plastic Fracture of Structural Components of Nuclear Systems, Contract RP1237-1, Combined Fifth and Sixth Semiannual Report, February 1, 1981 to January 31, 1982," Kumar, V., et al., General Electric Company (for the Electric Power Research Institute), March, 1982.

4. TR-95-030, Rev. 3, "Circumferential Cracks in Steam Generator Tubes: Structural Analysis Model and Integrated Burst Pressure Data Base," P. Hernalsteen, Tetra Engineering Group for the Electric Power Research Institute, October 11, 1996.

5. Vasquez, J. A., and Paris, P. C., "Plastic Zone Instability Phenomenon Leading to Crack Propagation," Proceedings of CSNI Specialists Meeting on Plastic Tearing Instability, St. Louis, MO, USNRC NUREG/CP-0010, pp. 601-631 (1979).

6. Vasquez, J. A., and Paris, P. C., "The Application of Plastic Zone Instability Criterion to Pressure Vessel Failure," Proceedings of CSNI Specialists Meeting on Plastic Tearing Instability, St. Louis, MO, USNRC NUREG/CP-0010, pp. 632-654 (1979).

7. Tada, H., Paris, P. C., and Loushin, L. L., *The Plastic Zone Instability Concept in Application to Analysis of Pressure Vessel Failure*, PVP-Vol. 336, American Society of Mechanical Engineers, New York, pp. 17-23 (1996).

8. NUREG/CR-3464, "The Application of Fracture Proof Design Methods Using Tearing Instability Theory to Nuclear Piping Postulating Circumferential Through Wall Cracks," U.S. Nuclear Regulatory Commission, September, 1983.

9. EPRI NP-6626-SD, "Belgian Approach to Steam Generator Tube Plugging for Primary Water Stress Corrosion Cracking," Electric Power Research Institute, March, 1990.

10. TR-96-016, Rev. 0, "Circumferential Flaws Burst Data - Evaluation of Foil Reinforcement Effects," P. Hernalsteen, Tetra Engineering Group for the Electric Power Research Institute, October 11, 1996.

11. "Circumferential Cracks in Steam Generator Tubes: Evaluation of the Results from the Westinghouse/EPRI Test Program," P. Hernalsteen (for Tractebel), November 15, 1996.

12. SG-89-12-004, "ASCO Unit 1 Tube Integrity Evaluation in Support of JCO," Begley, J., et al., Westinghouse Electric Corporation, December, 1989.

13. Tada, H. and Paris, P. C., *The Stress Analysis of Cracks Handbook, Second Edition,* Paris Productions Incorporated, St. Louis, 1985.

14. Cofie, N. G., and Froehlich, C. H., *Plastic Collapse of Pipes with Arbitrarily Shaped Circumferential Cracks*, PVP-Vol. 135, American Society of Mechanical Engineers, pp.39-46 (1988).

15. Draper, N. and Smith, H., *Applied Regression Analysis Second Edition*, Wiley, New York, 1981.

Table 6-1
SG Tube Circumferential Cracking Test Program Objectives

Objective	Discussion
1.	Verify the PDA range of tensile failure mode of throughwall flaws.
2.	Investigate the effect of uniform, i.e., 360°, OD penetration, especially *deep* penetration.
3.	Verify the PDA range of bending failure mode of throughwall flaws.
4.	Investigate the effect of OD ligament degradation (cracking) on the bending failure mode.
5.	Obtain COD data for verification of the leakage analysis model (the axial opening at the center and at the tip of the flaw is to be measured).
6.	Investigate the effect of a secondary (tab) ligament on the transition from bending to tensile failure mode for large throughwall flaws.
7.	Investigate the effect of different reinforcing foil material, thickness, and lubricity on the burst test results.
8.	Expand the database of throughwall indications tested in accord with the EPRI guidelines for circumferential crack testing.

Table 6-2
Identification of SG Tube Circumferential Cracking Burst Tests to be Performed

Percent Degraded Area	Throughwall Length (deg.)	Ligament Thickness (%)	Expected Failure Mode	Supported Test Objective	Number of Specimens
16.7%	60°	100	Axial/Bending	3, 5, 8	1
33.3%	120°	100	Bending	3, 5, 8	1
50.0%	180°	100	Bending	3, 5, 7[1], 8	4
60%	216°	100	Bending	3, 5, 7[1], 8	4
	120°	60	Bending	4	2
	72°	50	Bending	4,5	2
	0°	40	Tensile	2	2
65%	234°	100	Bending	8	2
70%	252°	100	Bending	3, 5, 7[1], 8	4
	144°	50	Bending	4,5	2
	90°	40	Bending	4	2
	0°	30	Tensile	2	2
75%	270°	100	Bending	8	2
80%	288°	100	Tensile ?	1, 5, 7[1], 8	4
	0°	20	Tensile	2	2
85%	306°	100	Tensile ?	8	2
90%	324°	100	Tensile	1, 5, 8	2
	0°	10	Tensile	2	2
			Total Number of Specimens		42

Note: 1. Two specimens are to be tested with lubricated 4/6 mil thick brass foil and two specimens are to be tested with non-lubricated 10 mil thick Type 302 SS foil with a minimum UTS of 185 ksi.

Table 6-3
PDAs Below the *Knee*[1] Circumferential Cracking Tests (Objectives 5 & 6)

Primary Ligament	Tab Ligament	Tab Offset	Expected Failure Mode	Number of Specimens
15% (54°)	5% (18°) (20% RA[2])	0	Tensile	2
		30	Tensile	2
		60	Tensile	2
20% (72°)	5% (18°) (25% RA)	0	Tensile	2
		30	Tensile	2
		60	Bending	2
	10% (36°) (30% RA)	0	Tensile	2
		45	Tensile	2
	Total Number of Specimens			16

Notes: 1. See Figure 6-1 for a schematic illustration of the *knee* of the burst curve.
2. Remaining area or one minus the total PDA.
3. Displacement measurements to be taken employing clip gages located at the center of the largest slit, and at ±120° to the first gage.

Table 6-4
New Circumferential Burst Test Results - All Data

		Specified (Measured)					Measured Dimensions			Specimen Info.			Test Results					
Test No.	Spec. No.	Main Ligament (*)	TW-1 Length (*)	Tab Ligament (*)	TW-2 Length (*)	Specified Main Lig. (% Wall)	TW-1 Width (inch)	TW-2 Width (inch)	Average Main Lig. (% Wall)	Tube OD (inch)	Tube ID (inch)	Shim(1) Code	Actual PDA	Burst Pres. (psig)	Normal Burst Pn	Time to Burst (sec)	Mode	Comments
42	3J	360°	0°			10%	0.006		21.3%	0.7515	0.6651	NBNS	78.7%	5.620	0.284	2.7	Tensile	Complete separation
35	3D	360°	0°			20%	0.005		29.3%	0.7516	0.6650	NBNS	70.7%	7.150	0.361	3.5	Local	0.10" circ breakthrough, minimal distortion.
36	3F	360°	0°			20%	0.005		30.2%	0.7514	0.6651	B	69.8%	6.990	0.354	3.4	Tensile	Complete separation
27	3B	360°	0°			30%	0.006		31.0%	0.7516	0.6650	NBNS	69.0%	7.060	0.356	3.5	Tensile	Complete separation
28	3C	360°	0°			30%	0.005		30.5%	0.7514	0.6651	NBNS	69.5%	7.210	0.365	3.6	Tensile	Complete separation
15	2K	360°	0°			40%	0.005		49.5%	0.7514	0.6648	NBNS	50.5%	10.490	0.529	5.8	Tensile	Complete separation
16	2L	360°	0°			40%	0.005		52.3%	0.7515	0.6650	NBNS	47.7%	10.820	0.546	6.0	Tensile	Complete separation
25	2O	269°	91°			40%	0.006		47.7%	0.7515	0.6651	6BL	64.4%	7.700	0.389	3.9	Tensile	Complete separation
26	3A	267°	93°			40%	0.006		45.4%	0.7515	0.6650	4BLNO	66.3%	7.450	0.376	3.8	Tensile	Complete separation
13	2G	288°	72°			50%	0.006		63.4%	0.7513	0.6647	6BL	49.3%	9.200	0.464	5.0	Tensile	Complete separation
14	2J	288°	72°			50%	0.007		59.7%	0.7515	0.6649	4BLNO	52.2%	8.880	0.448	4.8	Tensile	Complete separation
23	2M	214°	146°			50%	0.006		56.0%	0.7514	0.6651	6BL	66.7%	7.280	0.368	3.8	Tensile	Complete separation
24	2N	212°	148°			50%	0.006		51.0%	0.7516	0.6650	4BLNO	69.9%	6.780	0.342	3.3	Tensile	Complete separation
11	2D	243°	117°			60%	0.005		69.1%	0.7515	0.6649	6BL	53.4%	8.450	0.426	4.5	Tensile	Complete separation
12	2E	239°	121°			60%	0.006		67.6%	0.7514	0.6649	4BLNO	55.1%	8.230	0.415	4.4	Bending	0.20" circ tear each end, 0.12" width
1	4A	305°	55°			100%	0.006		100.0%	0.7514	0.6649	6BL	15.3%	11.500	0.580	6.8	Bending	No tear, 0.09" burst width (burst imminent)
2	4B	241°	119°			100%	0.005		100.0%	0.7513	0.6647	6BL	33.1%	9.180	0.463	4.9	Bending	No tear, 0.09" burst width (burst imminent)
3	1A	179°	181°			100%	0.005		100.0%	0.7515	0.6648	6BL	50.3%	7.880	0.397	4.1	Bending	Retest, no tear, 0.09" burst width (burst imminent)
4	1B	179°	181°			100%	0.005		100.0%	0.7516	0.6646	4BLNO	50.3%	7.650	0.384	4.1	Bending	No tear, 0.08" burst width (burst imminent)
7	1F	143°	217°			100%	0.005		100.0%	0.7514	0.6649	6BL	60.3%	7.190	0.363	3.8	Bending	No tear, 0.07" burst width (burst imminent)
8	1G	142°	218°			100%	0.005		100.0%	0.7515	0.6648	6BL	60.6%	7.060	0.355	3.6	Bending	No tear, 0.08" burst width (burst imminent)
17	4D	125°	235°			100%	0.005		100.0%	0.7514	0.6649	6BL	65.3%	6.840	0.345	3.6	Bending	No tear, 0.09" burst width (burst imminent)
18	4E	125°	235°			100%	0.005		100.0%	0.7514	0.6648	4BLNO	65.3%	6.800	0.343	3.6	Bending	No tear, 0.06" burst width (burst imminent)
19	1K	109°	251°			100%	0.005		100.0%	0.7514	0.6649	6BL	69.7%	6.750	0.341	3.6	Bending	Slight tear, 0.10" burst width (burst imminent)
20	1L	109°	251°			100%	0.005		100.0%	0.7516	0.6648	4BLNO	69.7%	6.330	0.318	3.1	Bending	Retest (not separated), torn (burst imminent)
29	4F	91°	269°			100%	0.005		100.0%	0.7513	0.6647	6BL	74.7%	6.060	0.305	3.1	Tensile	Complete separation
30	4G	91°	269°			100%	0.005		100.0%	0.7515	0.6650	4BLNO	74.7%	6.220	0.314	3.1	Bending	No tear, 0.07" burst width (burst imminent)
31	4I	73°	287°			100%	0.005		100.0%	0.7514	0.6648	6BL	79.7%	5.550	0.280	2.7	Tensile	Complete separation
32	4J	72°	288°			100%	0.005		100.0%	0.7514	0.6650	4BLNO	80.0%	5.460	0.276	2.8	Tensile	Complete separation
37	4N	55°	305°			100%	0.005		100.0%	0.7515	0.6650	6BL	84.7%	4.410	0.223	2.2	Tensile	Complete separation
38	4O	54°	306°			100%	0.005		100.0%	0.7514	0.6650	4BLNO	85.0%	4.440	0.224	2.2	Tensile	Complete separation

Table 6-4
New Circumferential Burst Test Results - All Data (continued)

		Specified (Measured)					Measured Dimensions			Specimen Info			Test Results					
Test No.	Spec. No.	Main Ligament (*)	TW-1 Length (*)	Tab Ligament (*)	TW-2 Length (*)	Specified Main Lig. (% Wall)	TW-1 Width (inch)	TW-2 Width (inch)	Average Main Lig. (% Wall)	Tube OD (inch)	Tube ID (inch)	Shim(1) Code	Actual PDA	Burst Pres. (psig)	Normal Burst Pn	Time to Burst (sec)	Mode	Comments
39	2B	35°	325°			100%	0.006		100.0%	0.7514	0.6646	6BL	90.3%	3.190	0.160	1.5	Tensile	Complete separation
40	2C	35°	325°			100%	0.005		100.0%	0.7514	0.6644	4BLNO	90.3%	3.090	0.155	1.4	Tensile	Complete separation
9	1I	145°	215°			100%	0.005		100.0%	0.7515	0.6649	10SL	59.7%	8.510	0.429	4.6	Tensile	Complete separation
10	1J	147°	213°			100%	0.005		100.0%	0.7515	0.6648	10SNO	59.2%	8.980	0.452	5.1	Tensile	Complete separation
5	1D	178°	182°			100%	0.005		100.0%	0.7516	0.6650	10SL	50.6%	9.500	0.479	5.2	Bending	0.10" circ tear each end + 0.5" axial 1 end, 0.17" wide
6	1E	180°	180°			100%	0.005		100.0%	0.7514	0.6650	10SNO	50.0%	9.810	0.496	4.8	Bending	No tear, 0.21" burst width (burst imminent)
21	1M	112°	248°			100%	0.005		100.0%	0.7515	0.6650	10SL	68.9%	7.410	0.374	4.0	Tensile	Complete separation
22	1N	112°	248°			100%	0.005		100.0%	0.7515	0.6649	10SNO	68.9%	8.110	0.409	4.2	Tensile	Complete separation
33	4K	73°	287°			100%	0.005		100.0%	0.7515	0.6649	10SL	79.7%	5.650	0.285	2.8	Tensile	Complete separation
34	4M	74°	286°			100%	0.005		100.0%	0.7514	0.6650	10SNO	79.4%	6.666	0.337	2.2	Tensile	Complete separation
49	5C	72°	135°	17°	136°	100%	0.007	0.007	100.0%	0.7512	0.6648	4BL	75.3%	5.640	0.285	2.7	Tensile	Complete separation
50	5D	71°	136°	17°	136°	100%	0.007	0.007	100.0%	0.7511	0.6650	6BL	75.6%	5.980	0.303	2.9	Bending	TW-1 opened 0.07", tab ligament separated
43	3K	60°	138°	21°	141°	100%	0.006	0.007	100.0%	0.7516	0.6650	6BL	77.5%	6.110	0.308	3.0	Tensile	Complete separation
44	3M	55°	143°	15°	147°	100%	0.007	0.009	100.0%	0.7514	0.6651	4BL	80.6%	4.790	0.242	2.4	Tensile	Complete separation
51	5E	73°	164°	17°	106°	100%	0.008	0.007	100.0%	0.7515	0.6648	4BL	75.0%	5.760	0.290	2.9	Tensile	Complete separation
52	5F	73°	164°	17°	106°	100%	0.006	0.006	100.0%	0.7513	0.6650	4BL	75.0%	5.460	0.276	2.6	Bending	TW-1 opened 0.08", tab ligament separated
45	3N	55°	173°	17°	115°	100%	0.006	0.006	100.0%	0.7519	0.6652	6BL	80.0%	5.200	0.262	2.4	Tensile	Complete separation
46	3E	54°	174°	17°	115°	100%	0.006	0.006	100.0%	0.7516	0.6650	4BL	80.3%	5.140	0.259	2.5	Tensile	Complete separation, 3E replaced 3O
53	5I	86°	172°	29°	73°	100%	0.006	0.006	100.0%	0.7514	0.6649	4BL	68.1%	7.120	0.359	3.6	Bending	TW-1 opened 0.10", tab ligament separated, arc error
54	5J	85°	171°	30°	74°	100%	0.006	0.006	100.0%	0.7515	0.6650	4BL	68.1%	7.060	0.356	3.6	Bending	TW-1 opened 0.10", tab ligament separated, arc error
47	5A	71°	187°	35°	67°	100%	0.006	0.006	100.0%	0.7512	0.6648	6BL	70.6%	7.280	0.368	3.6	Tensile	Complete separation, significant TW arc error.
48	5B	71°	187°	34°	68°	100%	0.006	0.006	100.0%	0.7516	0.6647	4BL	70.8%	7.210	0.362	3.6	Tensile	Complete separation, significant TW arc error.
55	5K	72°	126°	36°	126°	100%	0.007	0.008	100.0%	0.7517	0.6650	6BL	70.0%	7.500	0.378	3.8	Tensile	Complete separation
56	5L	75°	123°	38°	124°	100%	0.007	0.007	100.0%	0.7516	0.6648	4BL	68.6%	7.560	0.380	3.9	Tensile	Complete separation
57	5M	70°	173°	36°	81°	100%	0.008	0.006	100.0%	0.7516	0.6650	4BL	70.6%	7.070	0.356	3.5	Bending	No separation, TW-1 opened 0.06"
58	5N	74°	169°	37°	80°	100%	0.008	0.006	100.0%	0.7515	0.6650	4BL	69.2%	7.160	0.361	3.7	Tensile	Complete separation
AR1	1C	#N/A	#N/A	#N/A	#N/A	#N/A	#N/A	#N/A	100.0%	0.7515	0.6649	NBNS	0.0%	11.530	0.581	7.1	Axial	No EDM flaw. Burst opening = 1.40" L x 0.21" W
AR2	2F	#N/A	#N/A	#N/A	#N/A	#N/A	#N/A	#N/A	100.0%	0.7514	0.6648	NBNS	0.0%	11.560	0.583	7.1	Axial	No EDM flaw. Burst opening = 1.36" L x 0.22" W

Table 6-4
New Circumferential Burst Test Results - All Data (continued)

		Specified (Measured)					Measured Dimensions			Specimen Info			Test Results					
Test No.	Spec. No.	Main Ligament (*)	TW-1 Length (*)	Tab Ligament (*)	TW-2 Length (*)	Specified Main Lig. (% Wall)	TW-1 Width (inch)	TW-2 Width (inch)	Average Main Lig. (% Wall)	Tube OD (inch)	Tube ID (inch)	Shim(1) Code	Actual PDA	Burst Pres. (psig)	Normal Burst Pn	Time to Burst (sec)	Mode	Comments
AR3	3I	#N/A	#N/A	#N/A	#N/A	#N/A	#N/A	#N/A	100.0%	0.7515	0.6650	NBNS	0.0%	11.400	0.575	7.0	Axial	No EDM flaw. Burst opening = 1.38" L x 0.21" W
AR4	4L	#N/A	#N/A	#N/A	#N/A	#N/A	#N/A	#N/A	100.0%	0.7513	0.6651	NBNS	0.0%	11.440	0.579	7.1	Axial	No EDM flaw. Burst opening = 1.33" L x 0.21" W
AR5	5O	#N/A	#N/A	#N/A	#N/A	#N/A	#N/A	#N/A	100.0%	0.7514	0.6649	NBNS	0.0%	11.480	0.579	7.2	Axial	No EDM flaw. Burst opening = 1.40" L x 0.21" W
									Average	0.7515	0.6649							
									StDev	0.0001	0.0001							
											Note (1)	2BLNO:	2-mil brass, lubricated, no shim overlap					
												4BLNO:	4-mil brass, lubricated, no shim overlap					
												4BL:	4-mil brass, lubricated.					
												6BL:	6-mil brass, lubricated.					
												10S:	10-mil stainless steel, unlubricated (2 layers of 5-mil)					
												10SL:	10-mil stainless steel, lubricated (2 layers of 5-mil)					
												10SNO:	10-mil stainless steel, unlubricated (2 layers of 5-mil), no shim overlap					
												NBNS:	No bladder and no shim					
												B:	Bladder only					

Table 6-5
Single TW Slit Extracted Database Test Results

		Specified (Measured)					Measured Dimensions			Specimen Info.			Test Results					
Test No.	Spec. No.	Main Lig. (°)	TW-1 Length (°)	Tab Lig Length (°)	TW-2 Length (°)	Specified Main Lig. (% Wall)	TW-1 Width (inch)	TS-2 Width (inch)	Average Main Lig. (% Wall)	Tube OD (inch)	Tube ID (inch)	Shim Code	Actual PDA	Burst Pres. (psig)	Normal Burst Pn	Time to Burst (sec)	Mode	Comments
1	4A	305°	55°			100%	0.006		100%	0.7514	0.6649	6BL	15.3%	11.500	0.580	6.8	Bending	No tear, 0.09" burst width (burst imminent)
2	4B	241°	119°			100%	0.005		100%	0.7513	0.6647	6BL	33.1%	9.180	0.463	4.9	Bending	No tear, 0.09" burst width (burst imminent)
4	1B	179°	181°			100%	0.005		100%	0.7516	0.6646	4BLNO	50.3%	7.650	0.384	4.1	Bending	No tear, 0.08" burst width (burst imminent)
3	1A	179°	181°			100%	0.005		100%	0.7515	0.6648	6BL	50.3%	7.880	0.397	4.1	Bending	Retest, no tear, 0.09" burst width (burst imminent)
7	1F	143°	217°			100%	0.005		100%	0.7514	0.6649	6BL	60.3%	7.190	0.363	3.8	Bending	No tear, 0.07" burst width (burst imminent)
8	1G	142°	218°			100%	0.005		100%	0.7515	0.6648	6BL	60.6%	7.060	0.355	3.6	Bending	No tear, 0.08" burst width (burst imminent)
18	4E	125°	235°			100%	0.005		100%	0.7514	0.6648	4BLNO	65.3%	6.800	0.343	3.6	Bending	No tear, 0.06" burst width (burst imminent)
17	4D	125°	235°			100%	0.005		100%	0.7514	0.6649	6BL	65.3%	6.840	0.345	3.6	Bending	No tear, 0.09" burst width (burst imminent)
20	1L	109°	251°			100%	0.005		100%	0.7516	0.6648	4BLNO	69.7%	6.330	0.318	3.1	Bending	Retest (not separated), torn (burst imminent)
19	1K	109°	251°			100%	0.005		100%	0.7514	0.6649	6BL	69.7%	6.750	0.341	3.6	Bending	Slight tear, 0.10" burst width (burst imminent)
30	4G	91°	269°			100%	0.005		100%	0.7515	0.6650	4BLNO	74.7%	6.220	0.314	3.1	Bending	No tear, 0.07" burst width (burst imminent)
29	4F	91°	269°			100%	0.005		100%	0.7513	0.6647	6BL	74.7%	6.060	0.305	3.1	Tensile	Complete separation
31	4I	73°	287°			100%	0.005		100%	0.7514	0.6648	6BL	79.7%	5.550	0.280	2.7	Tensile	Complete separation
32	4J	72°	288°			100%	0.005		100%	0.7514	0.6650	4BLNO	80.0%	5.460	0.276	2.8	Tensile	Complete separation
37	4N	55°	305°			100%	0.005		100%	0.7515	0.6650	6BL	84.7%	4.410	0.223	2.2	Tensile	Complete separation
38	4O	54°	306°			100%	0.005		100%	0.7514	0.6650	4BLNO	85.0%	4.440	0.224	2.2	Tensile	Complete separation
40	2C	35°	325°			100%	0.005		100%	0.7514	0.6644	4BLNO	90.3%	3.090	0.155	1.4	Tensile	Complete separation
39	2B	35°	325°			100%	0.006		100%	0.7514	0.6646	6BL	90.3%	3.190	0.160	1.5	Tensile	Complete separation
9	1I	145°	215°			100%	0.005		100%	0.7515	0.6649	10SL	59.7%	8.510	0.429	4.6	Tensile	Complete separation
21	1M	112°	248°			100%	0.005		100%	0.7515	0.6650	10SL	68.9%	7.410	0.374	4.0	Tensile	Complete separation
33	4K	73°	287°			100%	0.005		100%	0.7515	0.6649	10SL	79.7%	5.650	0.285	2.8	Tensile	Complete separation
10	1J	147°	213°			100%	0.005		100%	0.7515	0.6648	10SNO	59.2%	8.980	0.452	5.1	Tensile	Complete separation
22	1N	112°	248°			100%	0.005		100%	0.7515	0.6649	10SNO	68.9%	8.110	0.409	4.2	Tensile	Complete separation
34	4M	74°	286°			100%	0.005		100%	0.7514	0.6650	10SNO	79.4%	6.666	0.337	2.2	Tensile	Complete separation
5	1D	178°	182°			100%	0.005		100%	0.7516	0.6650	10SL	50.6%	9.500	0.479	5.2	Bending	0.10" circ tear each end + 0.5" axial 1 end, 0.17" wide
6	1E	180°	180°			100%	0.005		100%	0.7514	0.6650	10SNO	50.0%	9.810	0.496	4.8	Bending	No tear, 0.21" burst width (burst imminent)

Table 6-6
Extracted Database Test Results

		Specified (Measured)					Measured Dimensions			Specimen Info.			Test Results					
Test No.	Spec. No.	Main Ligament (°)	TW-1 Length (°)	Tab Ligament (°)	TW-2 Length (°)	Specified Main Lig. (%Wall)	TW-1 Width (inch)	TW-2 Length (inch)	Average Main Lig. (% Wall)	Tube OD (inch)	Tube ID (inch)	Shim(1) Code	Actual PDA	Burst Pres. (psig)	Normal Burst Pn	Time to Burst (sec)	Mode	Comments
36	3F	360°	0°			20%	0.005		30.2%	0.7514	0.6651	B	69.8%	6.990	0.354	3.4	Tensile	Complete separation
42	3J	360°	0°			10%	0.006		21.3%	0.7515	0.6651	NBNS	78.7%	5.620	0.284	2.7	Tensile	Complete separation
35	3D	360°	0°			20%	0.005		29.3%	0.7516	0.6650	NBNS	70.7%	7.150	0.361	3.5	Local	0.10" circ breakthrough, minimal distortion.
27	3B	360°	0°			30%	0.006		31.0%	0.7516	0.6650	NBNS	69.0%	7.060	0.356	3.5	Tensile	Complete separation
28	3C	360°	0°			30%	0.005		30.5%	0.7514	0.6651	NBNS	69.5%	7.210	0.365	3.6	Tensile	Complete separation
15	2K	360°	0°			40%	0.005		49.5%	0.7514	0.6648	NBNS	50.5%	10.490	0.529	5.8	Tensile	Complete separation
16	2L	360°	0°			40%	0.005		52.3%	0.7515	0.6650	NBNS	47.7%	10.820	0.546	6.0	Tensile	Complete separation
26	3A	267°	93°			40%	0.006		45.4%	0.7515	0.6650	4BLNO	66.3%	7.450	0.376	3.8	Tensile	Complete separation
14	2J	288°	72°			50%	0.007		59.7%	0.7515	0.6649	4BLNO	52.2%	8.880	0.448	4.8	Tensile	Complete separation
24	2N	212°	148°			50%	0.006		51.0%	0.7516	0.6650	4BLNO	69.9%	6.780	0.342	3.3	Tensile	Complete separation
12	2E	239°	121°			60%	0.006		67.6%	0.7514	0.6649	4BLNO	55.1%	8.230	0.415	4.4	Bending	0.20" circ tear each end, 0.12" width
25	2O	269°	91°			40%	0.006		47.7%	0.7515	0.6651	6BL	64.4%	7.700	0.389	3.9	Tensile	Complete separation
13	2G	288°	72°			50%	0.006		63.4%	0.7513	0.6647	6BL	49.3%	9.200	0.464	5.0	Tensile	Complete separation
23	2M	214°	146°			50%	0.006		56.0%	0.7514	0.6651	6BL	66.7%	7.280	0.368	3.8	Tensile	Complete separation
11	2D	243°	117°			60%	0.005		69.1%	0.7515	0.6649	6BL	53.4%	8.450	0.426	4.5	Tensile	Complete separation

Table 6-7
Extracted Database Test Results - Tab Ligament Data

		Specified (Measured)					Measured Dimensions			Specimen Info.			Test Results					
Test No.	Spec. No.	Main Ligament (°)	TW-1 Length (°)	Tab Ligament (°)	TW-2 Length (°)	Specified Main Lig. (% Wall)	TW-1 Width (inch)	TW-2 Width (inch)	Average Main Lig. (% Wall)	Tube OD (inch)	Tube ID (inch)	Shim(1) Code	Actual PDA	Burst Pres (psig)	Normal Burst Pn	Time to Burst (sec)	Mode	Comments
49	5C	72°	135°	17°	136°	100%	0.007	0.007	100.0%	0.7512	0.6648	4BL	75.3%	5.640	0.285	2.7	Tensile	Complete separation
50	5D	71°	136°	17°	136°	100%	0.007	0.007	100.0%	0.7511	0.6650	6BL	75.6%	5.980	0.303	2.9	Bending	TW-1 opened 0.07", tab ligament separated
51	5E	73°	164°	17°	106°	100%	0.008	0.007	100.0%	0.7515	0.6648	4BL	75.0%	5.760	0.290	2.9	Tensile	Complete separation
52	5F	73°	164°	17°	106°	100%	0.006	0.006	100.0%	0.7513	0.6650	4BL	75.0%	5.460	0.276	2.6	Bending	TW-1 opened 0.08", tab ligament separated
53	5I	86°	172°	29°	73°	100%	0.006	0.006	100.0%	0.7514	0.6649	4BL	68.1%	7.120	0.359	3.6	Bending	TW-1 opened 0.10", tab ligament separated, arc error
54	5J	85°	171°	30°	74°	100%	0.006	0.006	100.0%	0.7515	0.6650	4BL	68.1%	7.060	0.356	3.6	Bending	TW-1 opened 0.10", tab ligament separated, arc error
44	3M	55°	143°	15°	147°	100%	0.007	0.009	100.0%	0.7514	0.6651	4BL	80.6%	4.790	0.242	2.4	Tensile	Complete separation
43	3K	60°	138°	21°	141°	100%	0.006	0.007	100.0%	0.7516	0.6650	6BL	77.5%	6.110	0.308	3.0	Tensile	Complete separation
46	3E	54°	174°	17°	115°	100%	0.006	0.006	100.0%	0.7516	0.6650	4BL	80.3%	5.140	0.259	2.5	Tensile	Complete separation, 3E replaced 3O
45	3N	55°	173°	17°	115°	100%	0.006	0.006	100.0%	0.7519	0.6652	6BL	80.0%	5.200	0.262	2.4	Tensile	Complete separation
48	5B	71°	187°	34°	68°	100%	0.006	0.006	100.0%	0.7516	0.6647	4BL	70.8%	7.210	0.362	3.6	Tensile	Complete separation, significant TW arc error.
47	5A	71°	187°	35°	67°	100%	0.006	0.006	100.0%	0.7512	0.6648	6BL	70.6%	7.280	0.368	3.6	Tensile	Complete separation, significant TW arc error.
55	5K	72°	126°	36°	126°	100%	0.007	0.008	100.0%	0.7517	0.6650	6BL	70.0%	7.500	0.378	3.8	Tensile	Complete separation
56	5L	75°	123°	38°	124°	100%	0.007	0.007	100.0%	0.7516	0.6648	4BL	68.6%	7.560	0.380	3.9	Tensile	Complete separation
57	5M	70°	173°	36°	81°	100%	0.008	0.006	100.0%	0.7516	0.6650	4BL	70.6%	7.070	0.356	3.5	Bending	No separation, TW-1 opened 0.06"
58	5N	74°	169°	37°	80°	100%	0.008	0.006	100.0%	0.7515	0.6650	4BL	69.2%	7.160	0.361	3.7	Tensile	Complete separation

Table 6-8
Extracted Database for Tensile Failure Curve Analysis

		Specified (Measured)					Measured Dimensions			Specimen Info.			Test Results					
Test No.	Spec. No.	Main Ligament (°)	TW-1 Length (°)	Tab Ligament (°)	TW-2 Length (°)	Specified Main Lig. (% Wall)	TW-1 Width (inch)	TW-2 Width (inch)	Average Main Lig. (% Wall)	Tube OD (inch)	Tube ID (inch)	Shim(1) Code	Actual PDA	Burst Pres. (psig.)	Normal Burst Pn	Time to Burst (sec)	Mode	Comments
36	3F	360°	0°			20%	0.005		30.2%	0.7514	0.6651	B	69.8%	6.990	0.354	3.4	Tensile	Complete separation
42	3J	360°	0°			10%	0.006		21.3%	0.7515	0.6651	NBNS	78.7%	5.620	0.284	2.7	Tensile	Complete separation
35	3D	360°	0°			20%	0.005		29.3%	0.7516	0.6650	NBNS	70.7%	7.150	0.361	3.5	Local	0.10" circ breakthrough, minimal distortion.
27	3B	360°	0°			30%	0.006		31.0%	0.7516	0.6650	NBNS	69.0%	7.060	0.356	3.5	Tensile	Complete separation
28	3C	360°	0°			30%	0.005		30.5%	0.7514	0.6651	NBNS	69.5%	7.210	0.365	3.6	Tensile	Complete separation
49	5C	72°	135°	17°	136°	100%	0.007	0.007	100.0%	0.7512	0.6648	4BL	75.3%	5.640	0.285	2.7	Tensile	Complete separation
51	5E	73°	164°	17°	106°	100%	0.008	0.007	100.0%	0.7515	0.6648	4BL	75.0%	5.760	0.290	2.9	Tensile	Complete separation
44	3M	55°	143°	15°	147°	100%	0.007	0.009	100.0%	0.7514	0.6651	4BL	80.6%	4.790	0.242	2.4	Tensile	Complete separation
43	3K	60°	138°	21°	141°	100%	0.006	0.007	100.0%	0.7516	0.6650	6BL	77.5%	6.110	0.308	3.0	Tensile	Complete separation
46	3E	54°	174°	17°	115°	100%	0.006	0.006	100.0%	0.7516	0.6650	4BL	80.3%	5.140	0.259	2.5	Tensile	Complete separation, 3E replaced 3O
45	3N	55°	173°	17°	115°	100%	0.006	0.006	100.0%	0.7519	0.6652	6BL	80.0%	5.200	0.262	2.4	Tensile	Complete separation
48	5B	71°	187°	34°	68°	100%	0.006	0.006	100.0%	0.7516	0.6647	4BL	70.8%	7.210	0.362	3.6	Tensile	Complete separation, significant TW arc error.
47	5A	71°	187°	35°	67°	100%	0.006	0.006	100.0%	0.7512	0.6648	6BL	70.6%	7.280	0.368	3.6	Tensile	Complete separation, significant TW arc error.
55	5K	72°	126°	36°	126°	100%	0.007	0.008	100.0%	0.7517	0.6650	6BL	70.0%	7.500	0.378	3.8	Tensile	Complete separation
56	5L	75°	123°	38°	124°	100%	0.007	0.007	100.0%	0.7516	0.6648	4BL	68.6%	7.560	0.380	3.9	Tensile	Complete separation
58	5N	74°	169°	37°	80°	100%	0.008	0.006	100.0%	0.7515	0.6650	4BL	69.2%	7.160	0.361	3.7	Tensile	Complete separation
50	5D	71°	136°	17°	136°	100%	0.007	0.007	100.0%	0.7511	0.6650	6BL	75.6%	5.980	0.303	2.9	Bending?	TW-1 opened 0.07", tab ligament separated
52	5F	73°	164°	17°	106°	100%	0.006	0.006	100.0%	0.7513	0.6650	4BL	75.0%	5.460	0.276	2.6	Bending?	TW-1 opened 0.08", tab ligament separated
53	5I	86°	172°	29°	73°	100%	0.006	0.006	100.0%	0.7514	0.6649	4BL	68.1%	7.120	0.359	3.6	Bending?	TW-1 opened 0.10", tab ligament separated, arc error
54	5J	85°	171°	30°	74°	100%	0.006	0.006	100.0%	0.7515	0.6650	4BL	68.1%	7.060	0.356	3.6	Bending?	TW-1 opened 0.10", tab ligament separated, arc error
57	5M	70°	173°	36°	81°	100%	0.008	0.006	100.0%	0.7516	0.6650	4BL	70.6%	7.070	0.356	3.5	Bending	No separation, TW-1 opened 0.06"
37	4N	55°	305°			100%	0.005		100%	0.7515	0.6650	6BL	84.7%	4.410	0.223	2.2	Tensile	Complete separation. Single TW slit.
38	4O	54°	306°			100%	0.005		100%	0.7514	0.6650	4BLNO	85.0%	4.440	0.224	2.2	Tensile	Complete separation. Single TW slit.
40	2C	35°	325°			100%	0.005		100%	0.7514	0.6644	4BLNO	90.3%	3.090	0.155	1.4	Tensile	Complete separation. Single TW slit.
39	2B	35°	325°			100%	0.006		100%	0.7514	0.6646	6BL	90.3%	3.190	0.160	1.5	Tensile	Complete separation. Single TW slit.

Table 6-9
Regression Parameters for the Correlation of P_n to PDA for the Bending Failure Mode

Parameter	Value
Intercept, $b0$	0.57326
Slope, b_1	-0.35281
Standard Error of P_n	0.007503
Number of Data, N	11
Index of Determination, R^2	97.5%
p Value for the Slope	$1.7 \cdot 10^{-8}$

Table 6-10
Regression Parameters for the Correlation of P_n to PDA for the Tensile Failure Mode

Parameter	Value
Intercept, $b0$	0.0000(1)
Slope, b_1	1.2227
Standard Error of P_n	0.016631
Number of Data, N	16
Index of Determination(1), R^2	88.1%
p Value for the Slope	$2.5 \cdot 10^{-8}$

(1) By definition for regression through the origin.
(2) The index of determination for regression through the origin is shown for information only.

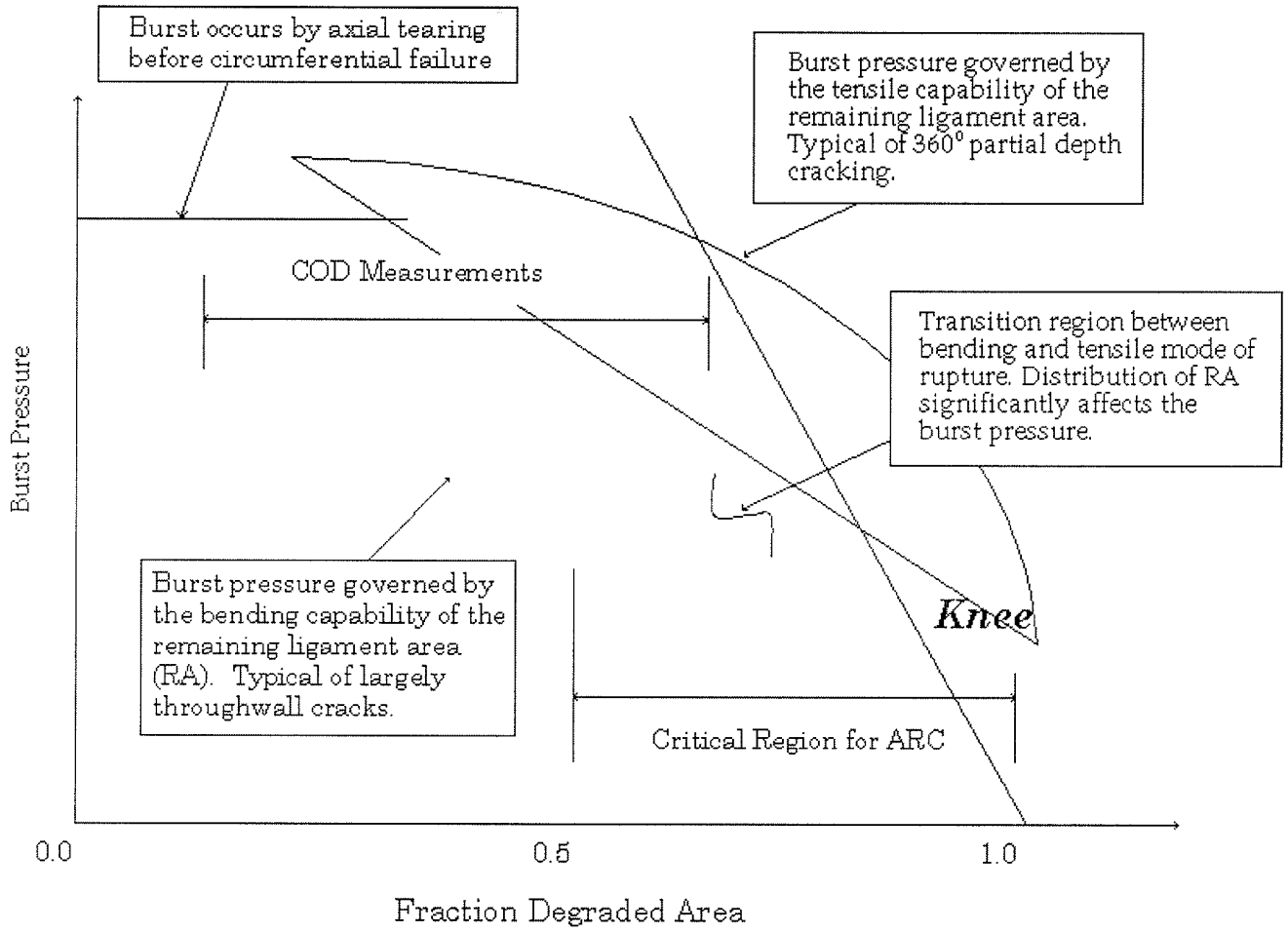

Figure 6-1
Burst Curve Schematic

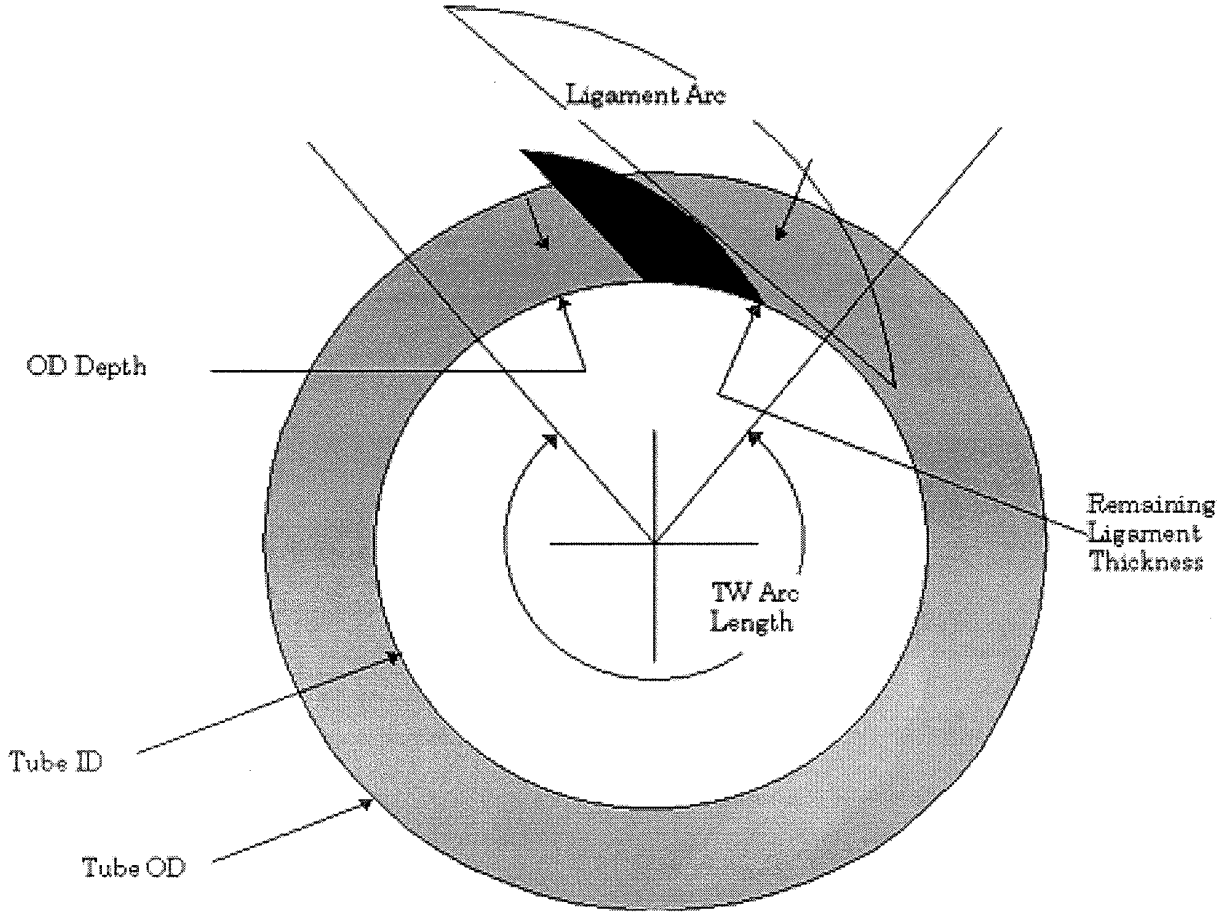

Figure 6-2
Section Geometry, Objectives 1-5

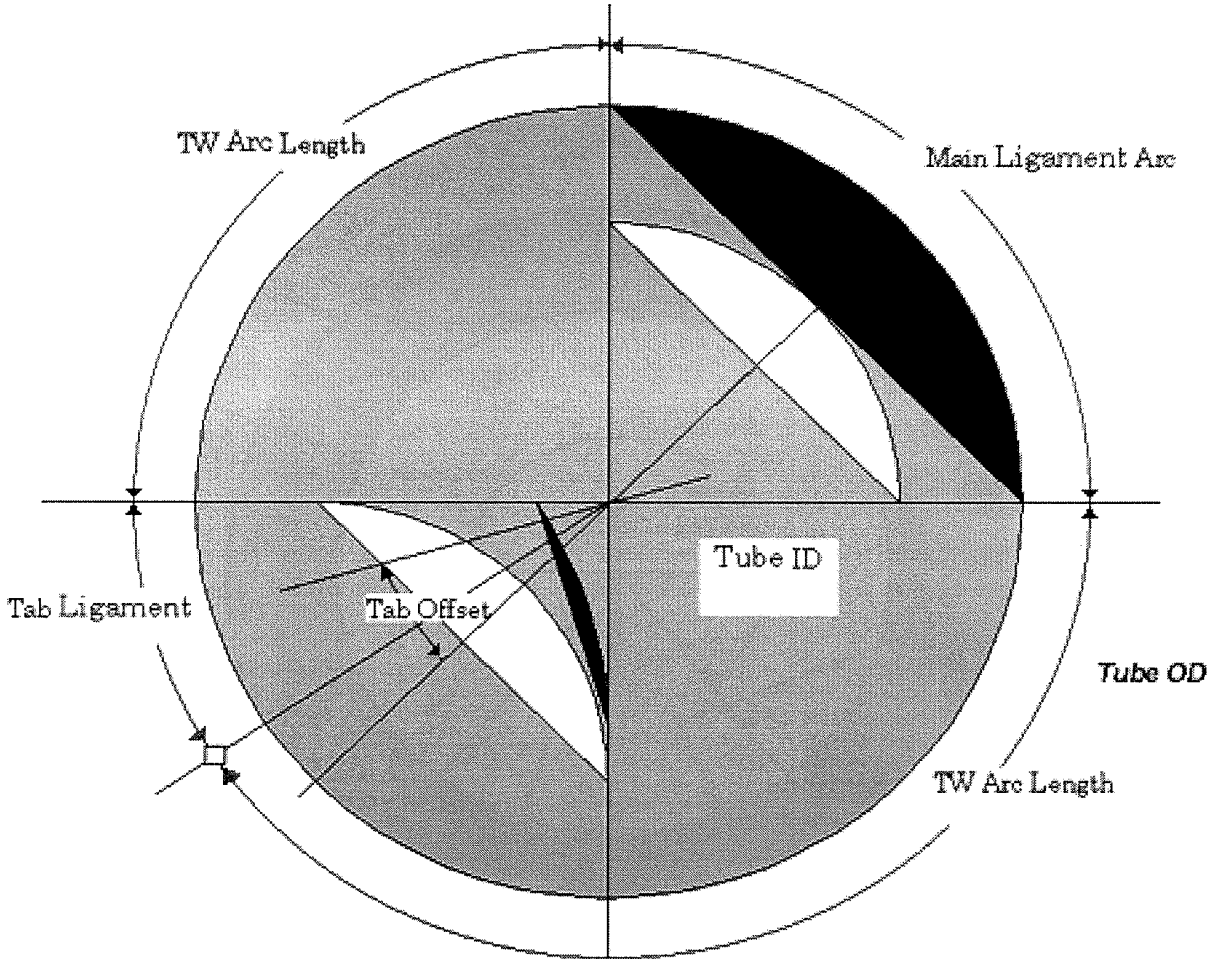

Figure 6-3
Section Geometry for Objective 6 Tests

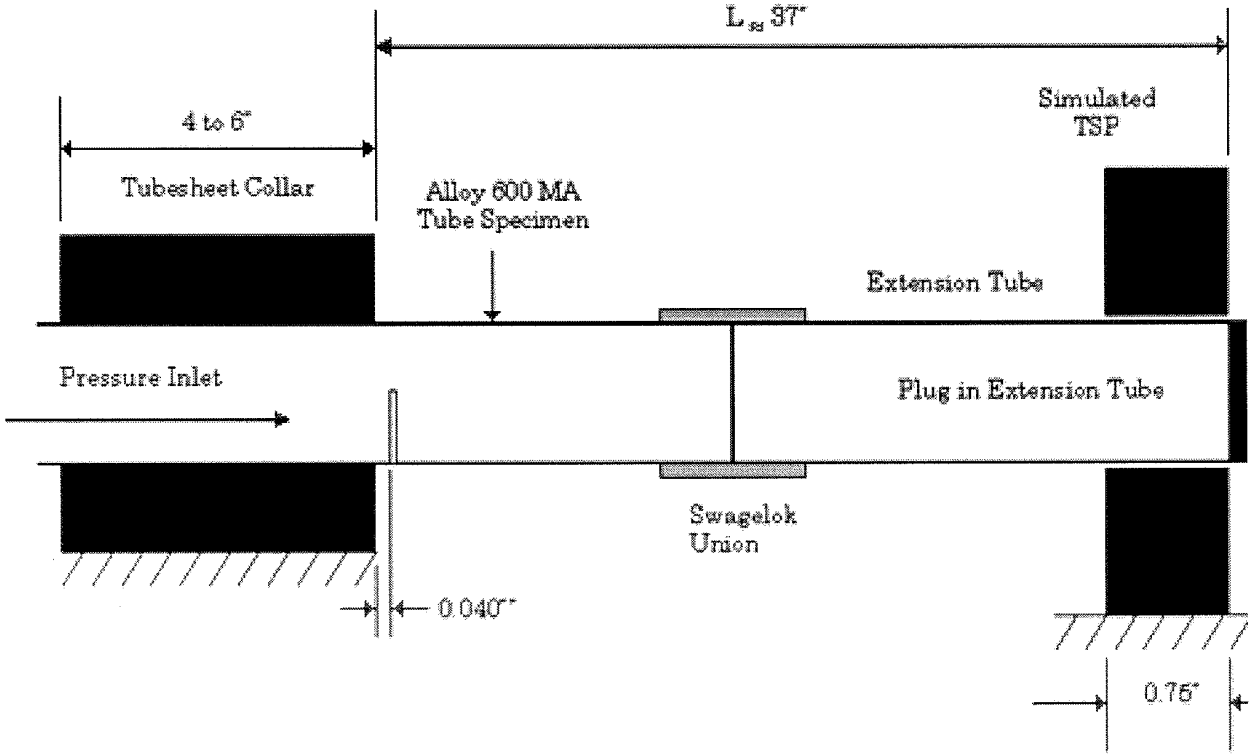

Figure 6-4
Test Setup

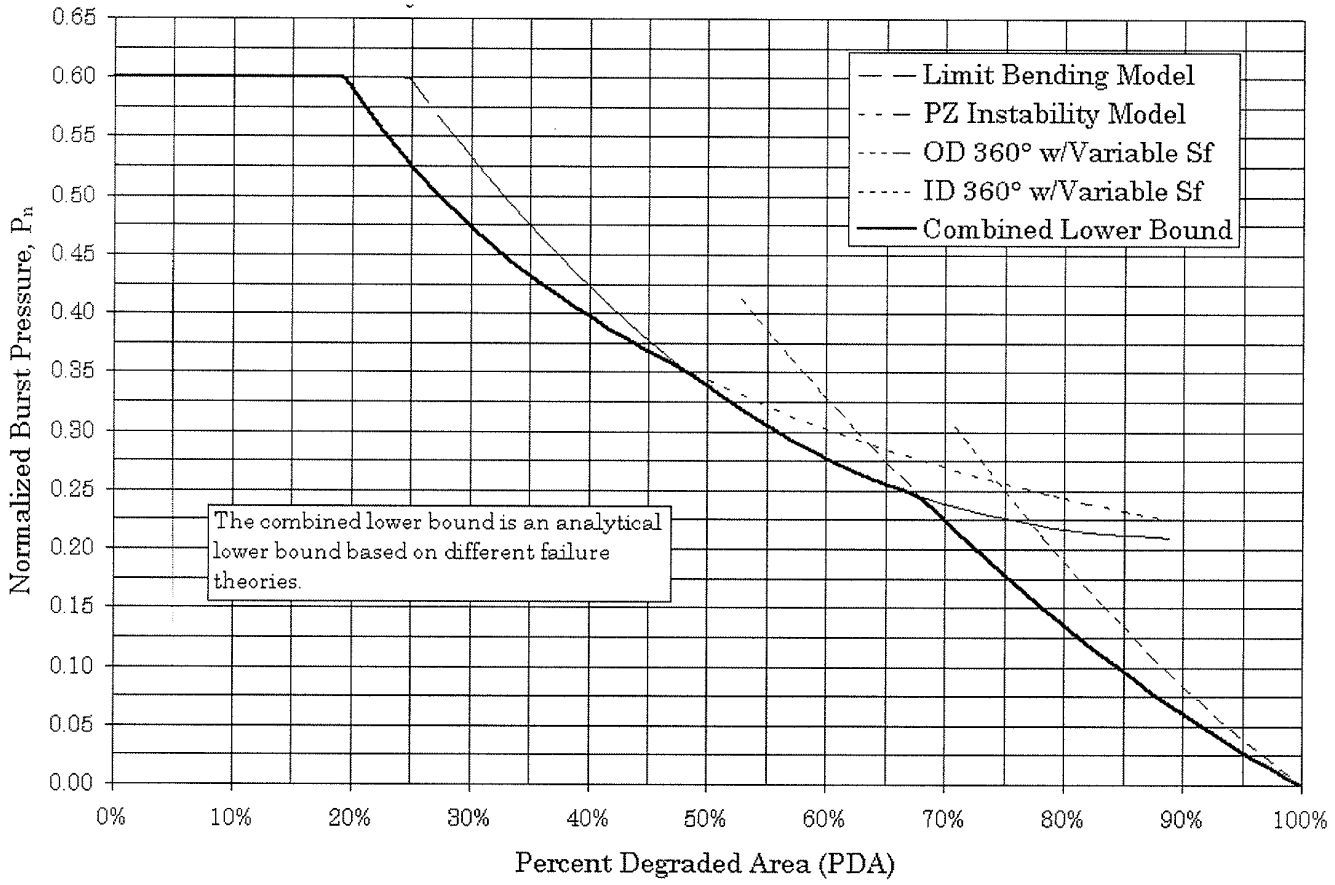

Figure 6-5
Normalized Burst Pressure vs. PDA Models for Alloy 600 SG Tubes with Circumferential Cracks

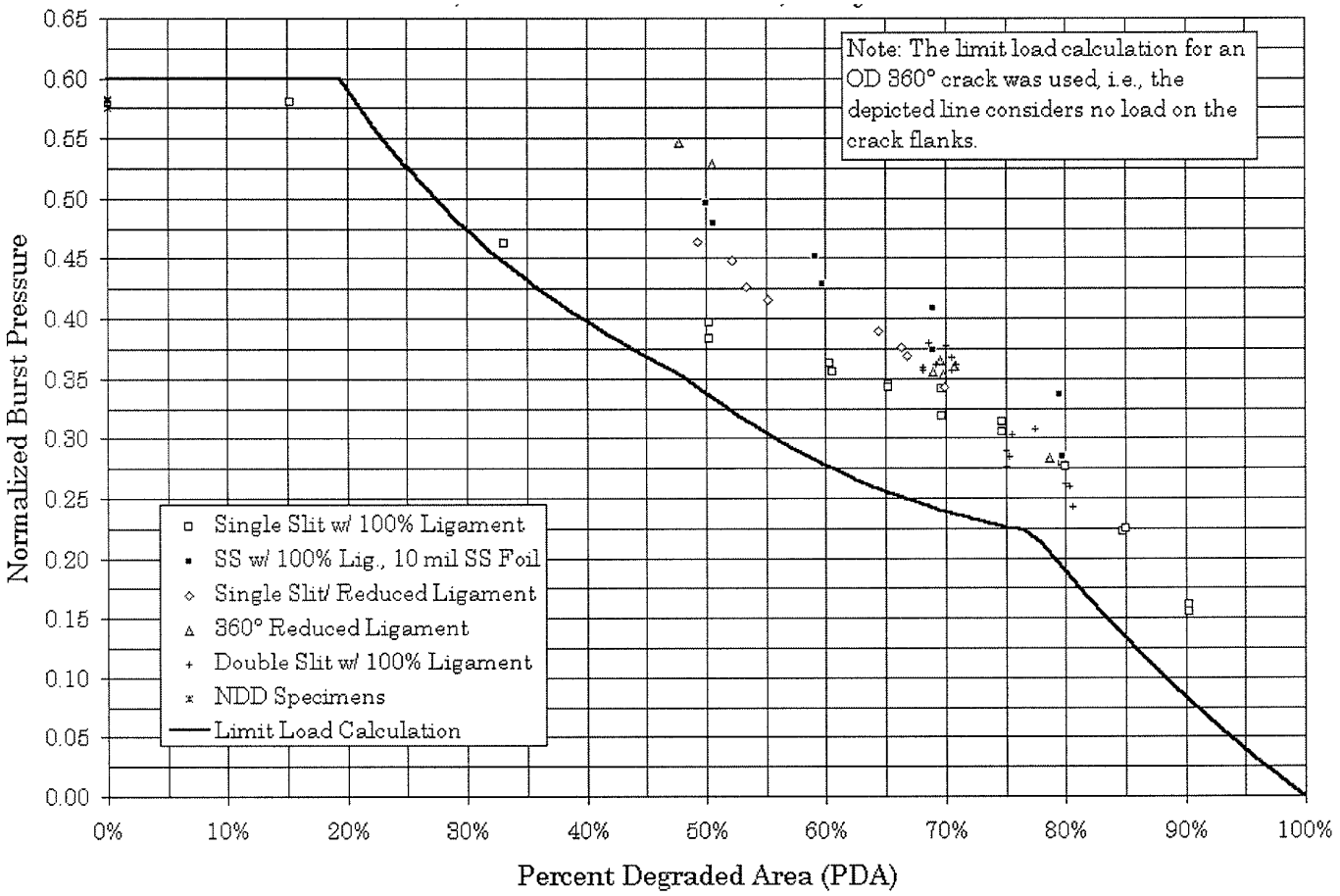

Figure 6-6
Normalized Burst Pressure vs. Percent Degraded Area All New Data, ¾" x 0.043" Nominal, Alloy 600 SG Tubes

Correlation of Burst Pressure with PDA

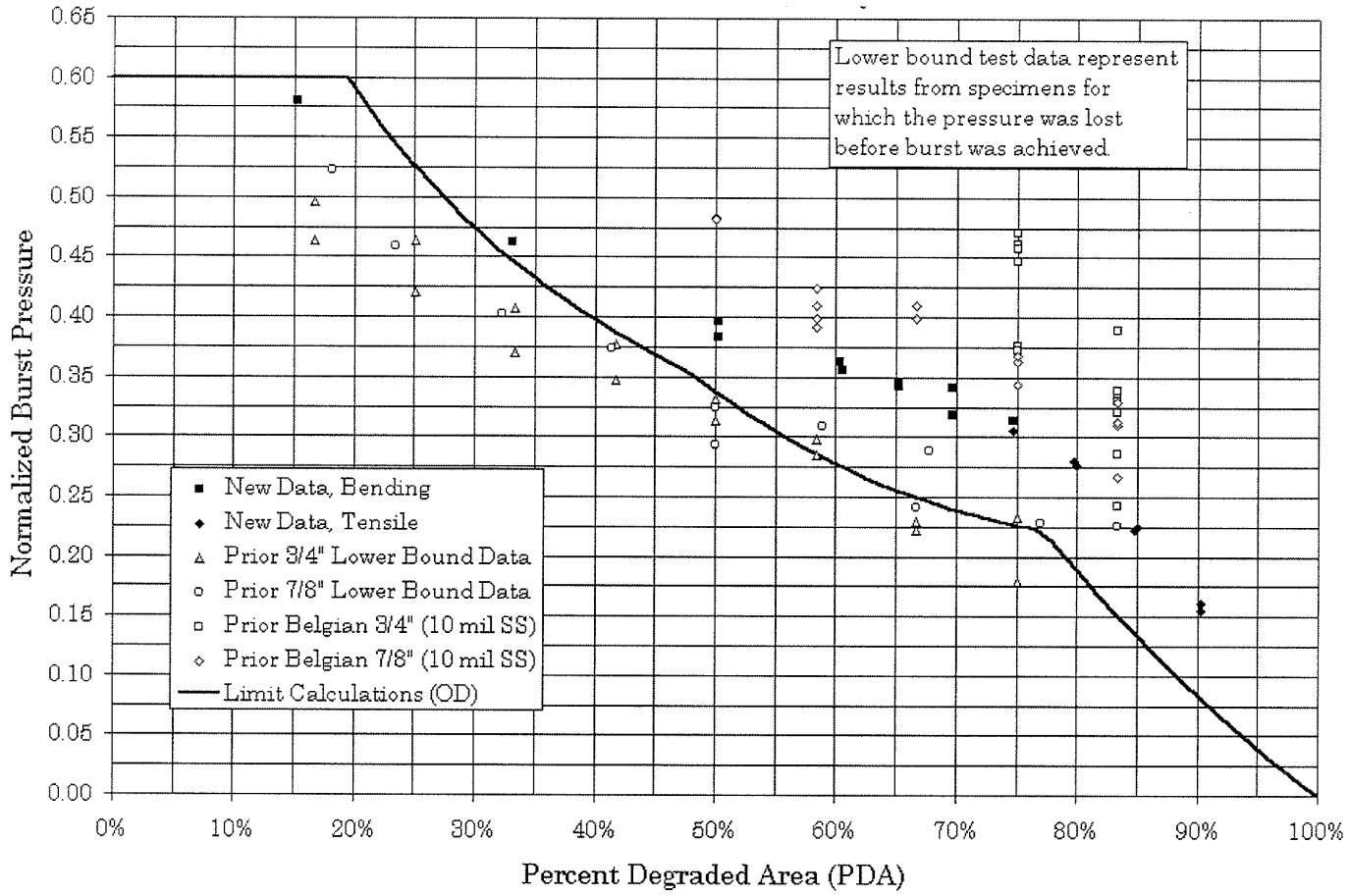

Figure 6-7
TW, Single Slit Circumferential Burst vs. PDA New Data for ¾" x 0.043" Nominal, Alloy 600 SG Tubes

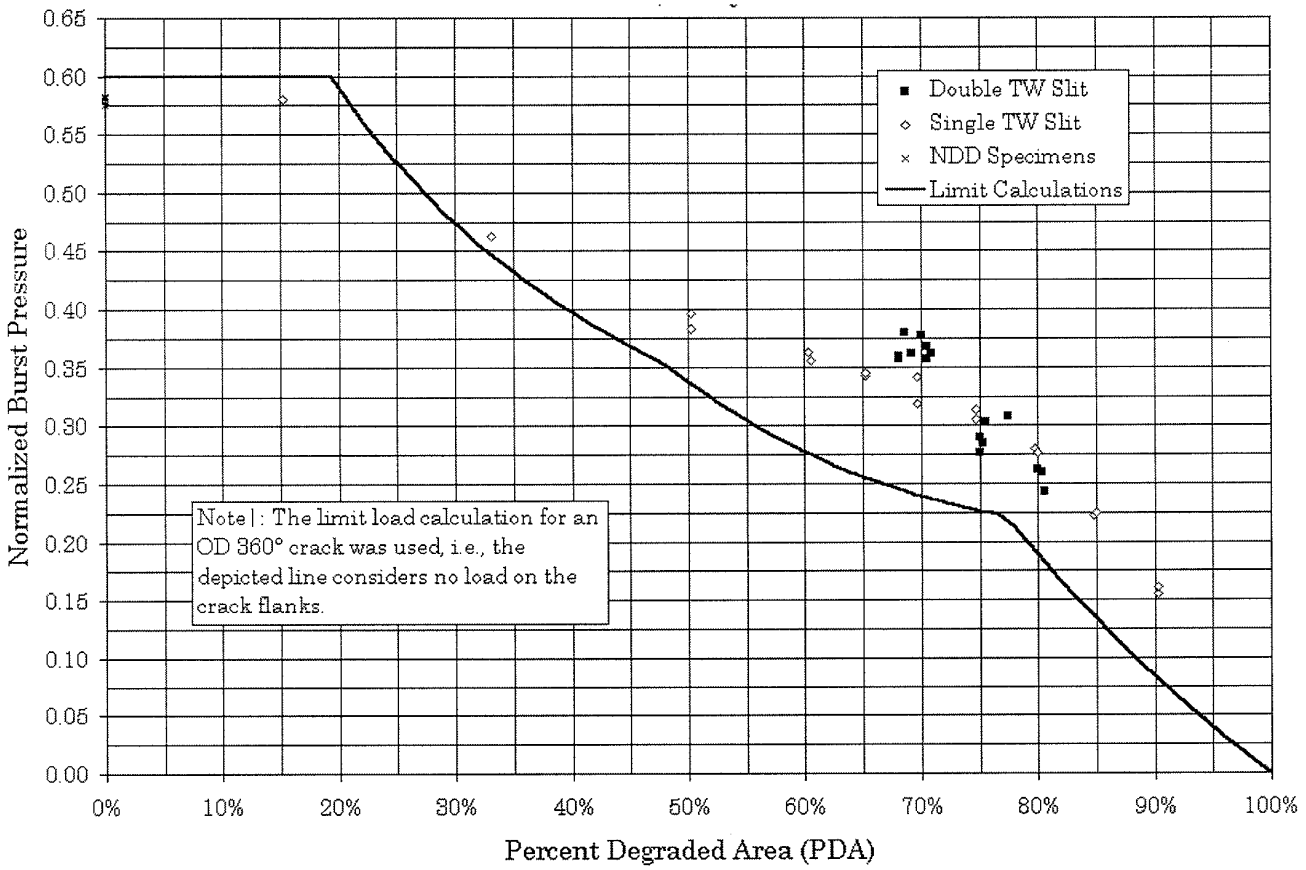

Figure 6-8
Double Slit Burst Pressure vs. Percent Degraded Area ¾" x 0.043" Nominal, Alloy 600 SG Tubes

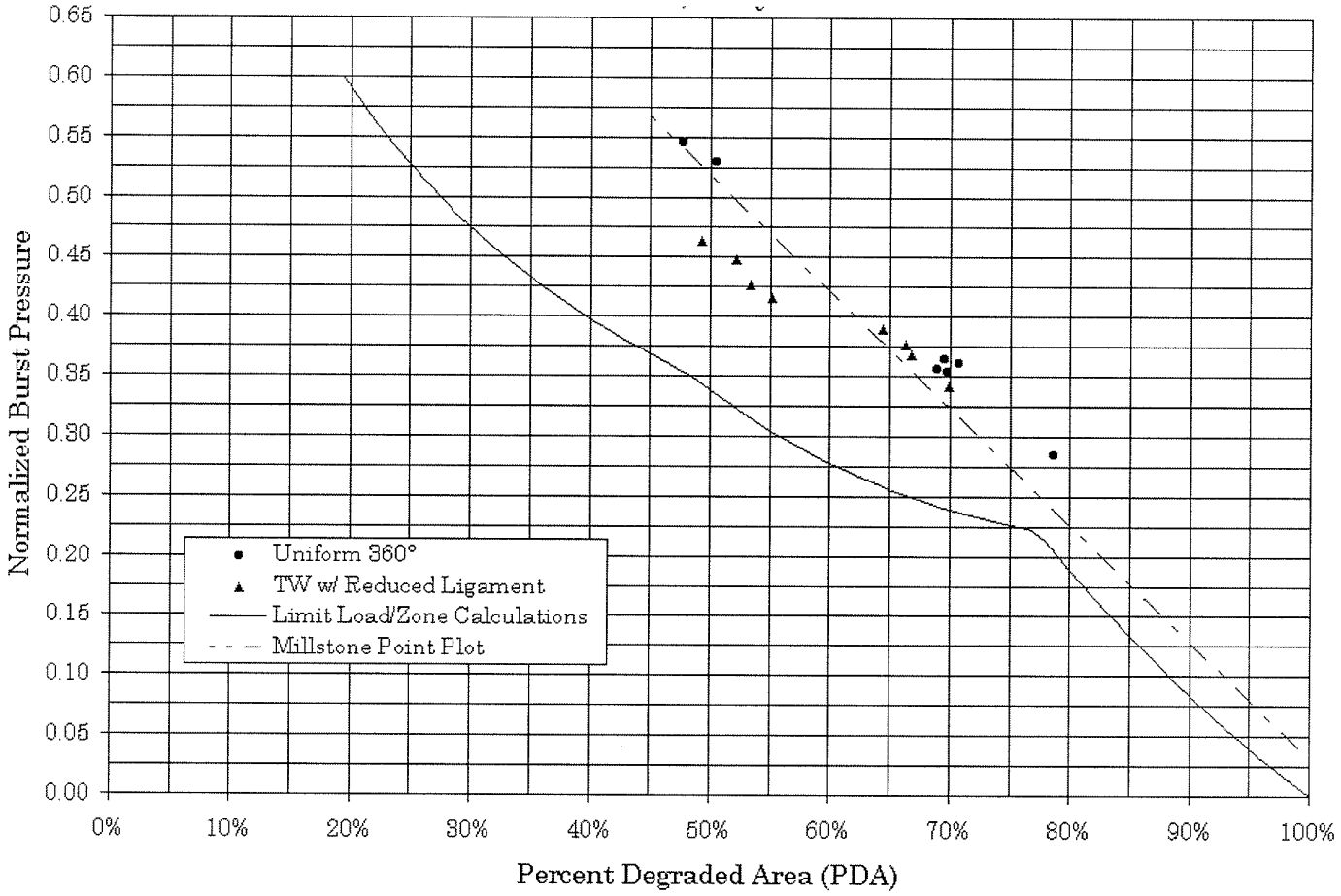

Figure 6-9
Uniform Depth Circumferential Burst vs. PDA ¾" x 0.043" Nominal, Alloy 600 SG Tubes

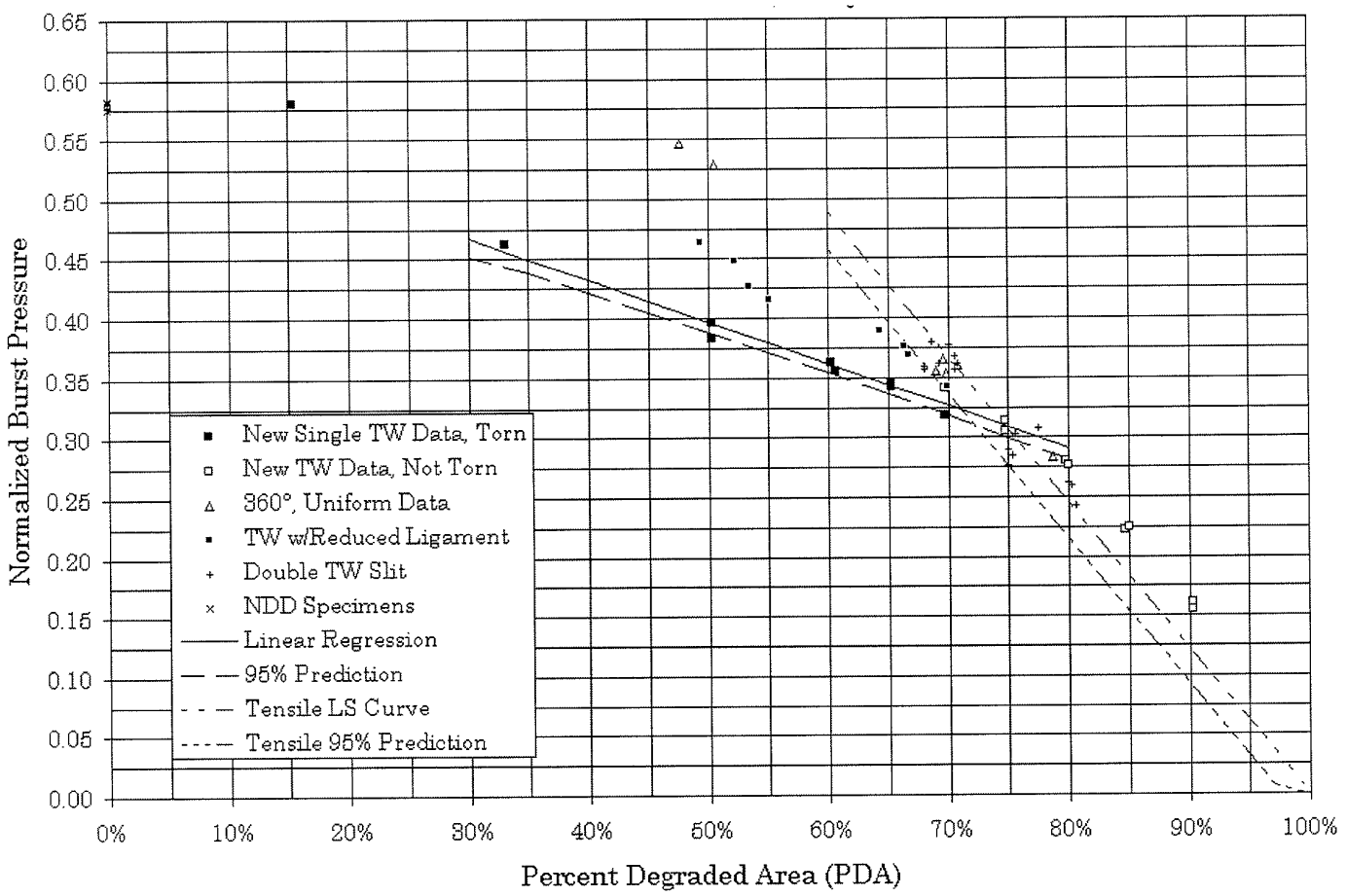

Figure 6-10
TW, Single Slit Circumferential Burst vs. PDA New Data for ¾" x 0.043" Nominal, Alloy 600 SG Tubes

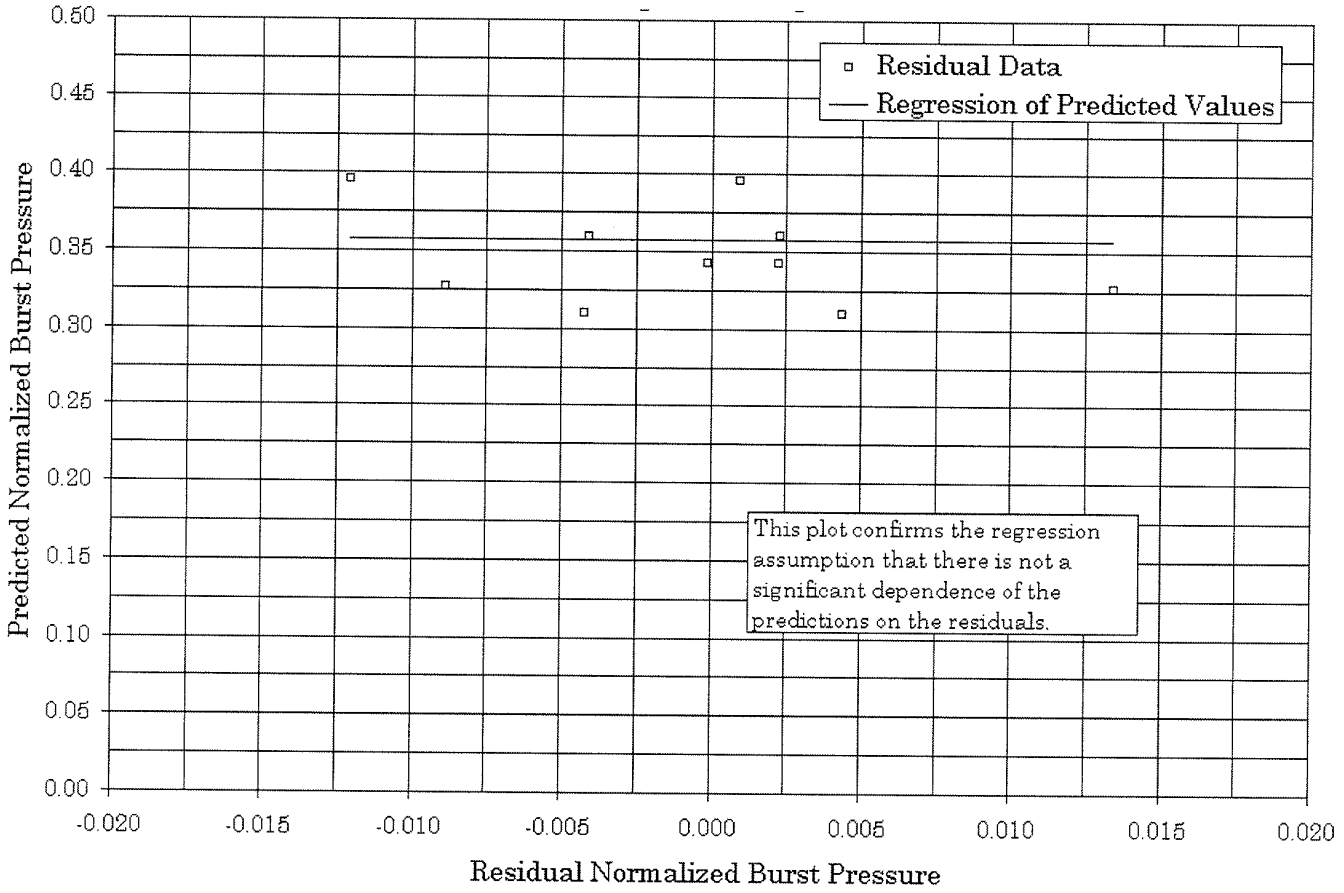

Figure 6-11
Scatter Plot of the Residuals of the TW Regression Equation

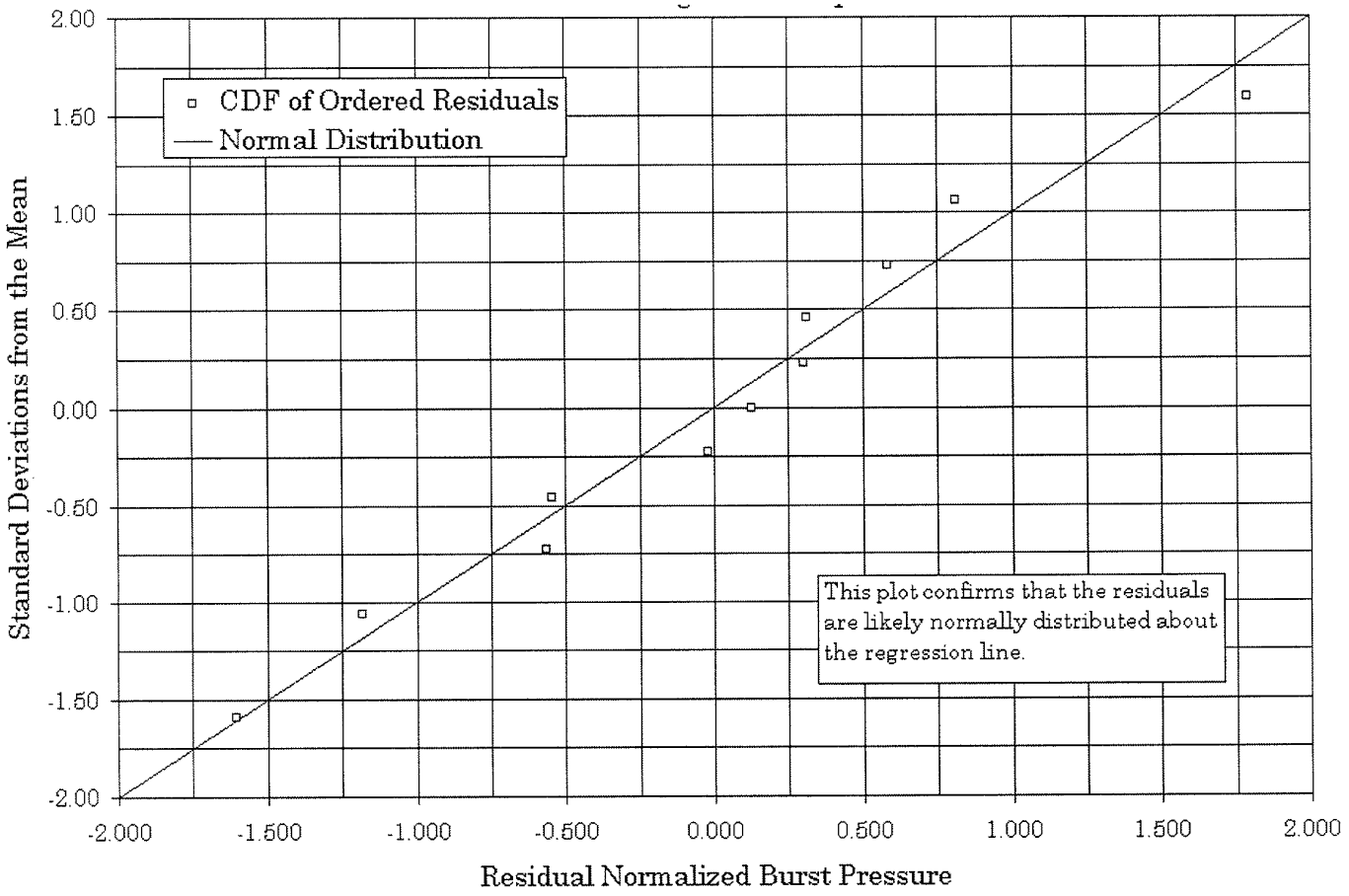

Figure 6-12
Normal Probability Plot of the Residuals of the TW Burst Regression Equation

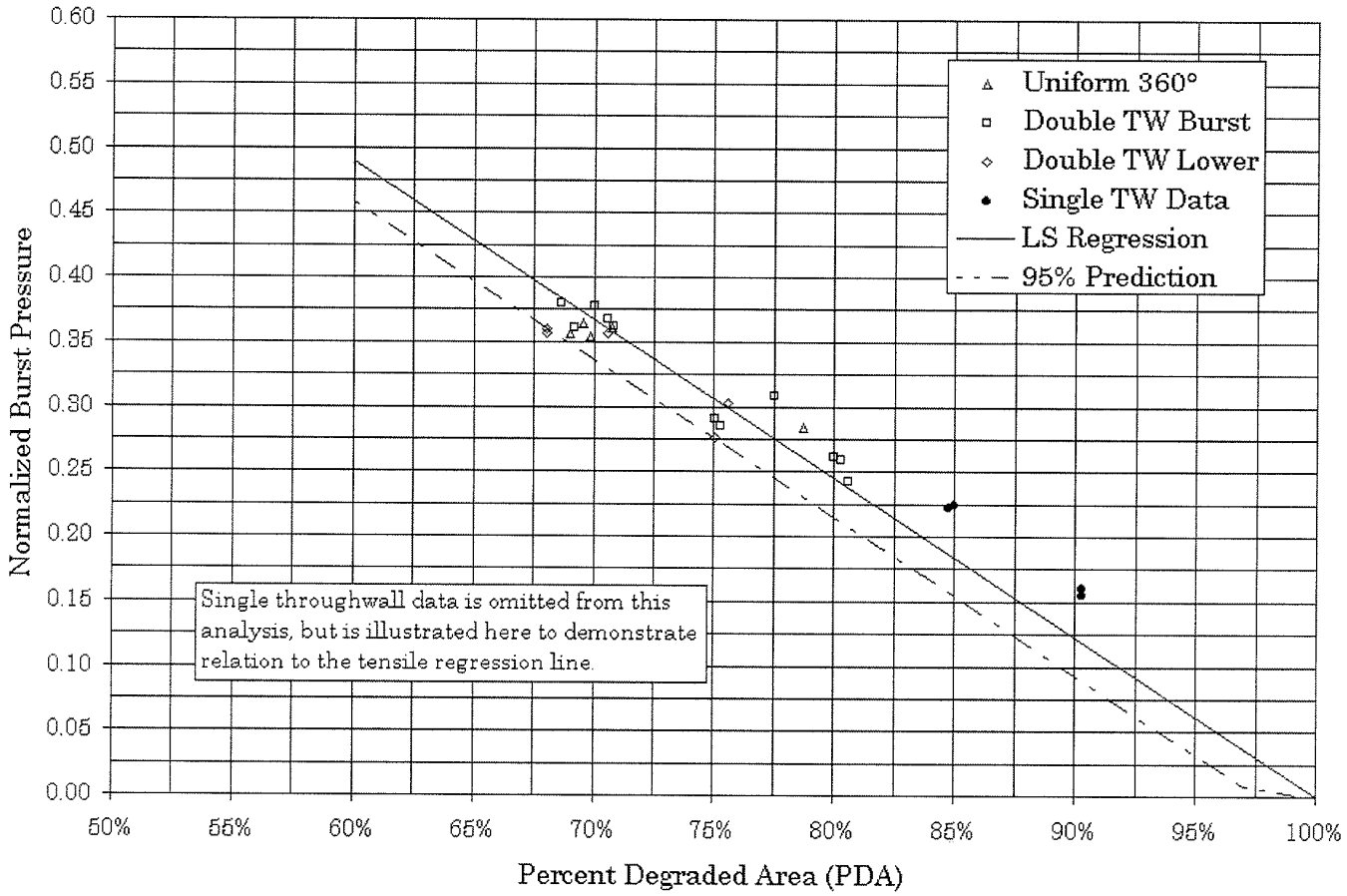

Figure 6-13
Normalized Burst Pressure versus PDA Tensile Failure Mode Data

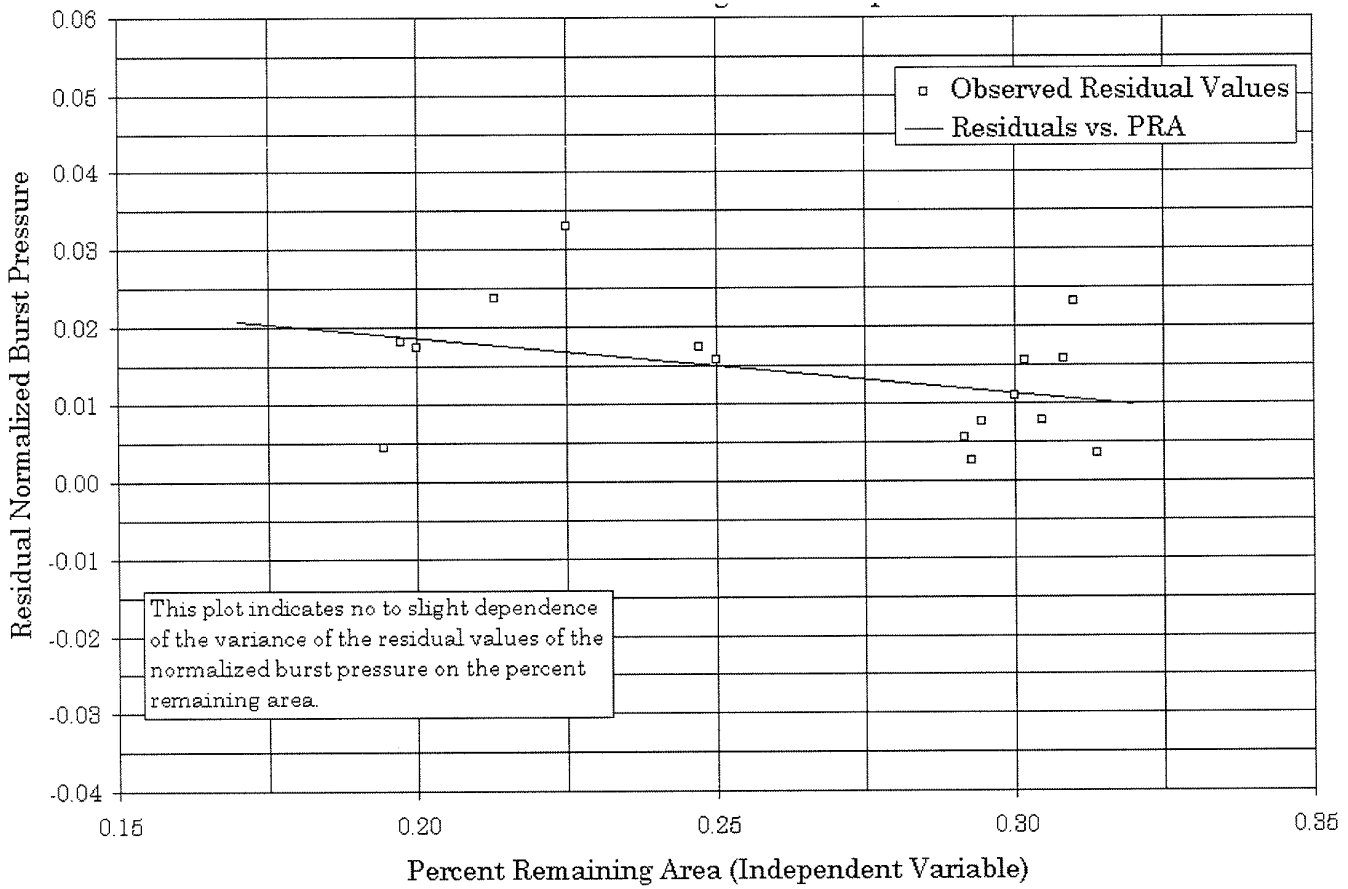

Figure 6-14
Scatter Plot of the Absolute Residuals of the Tensile Failure Regression Equation

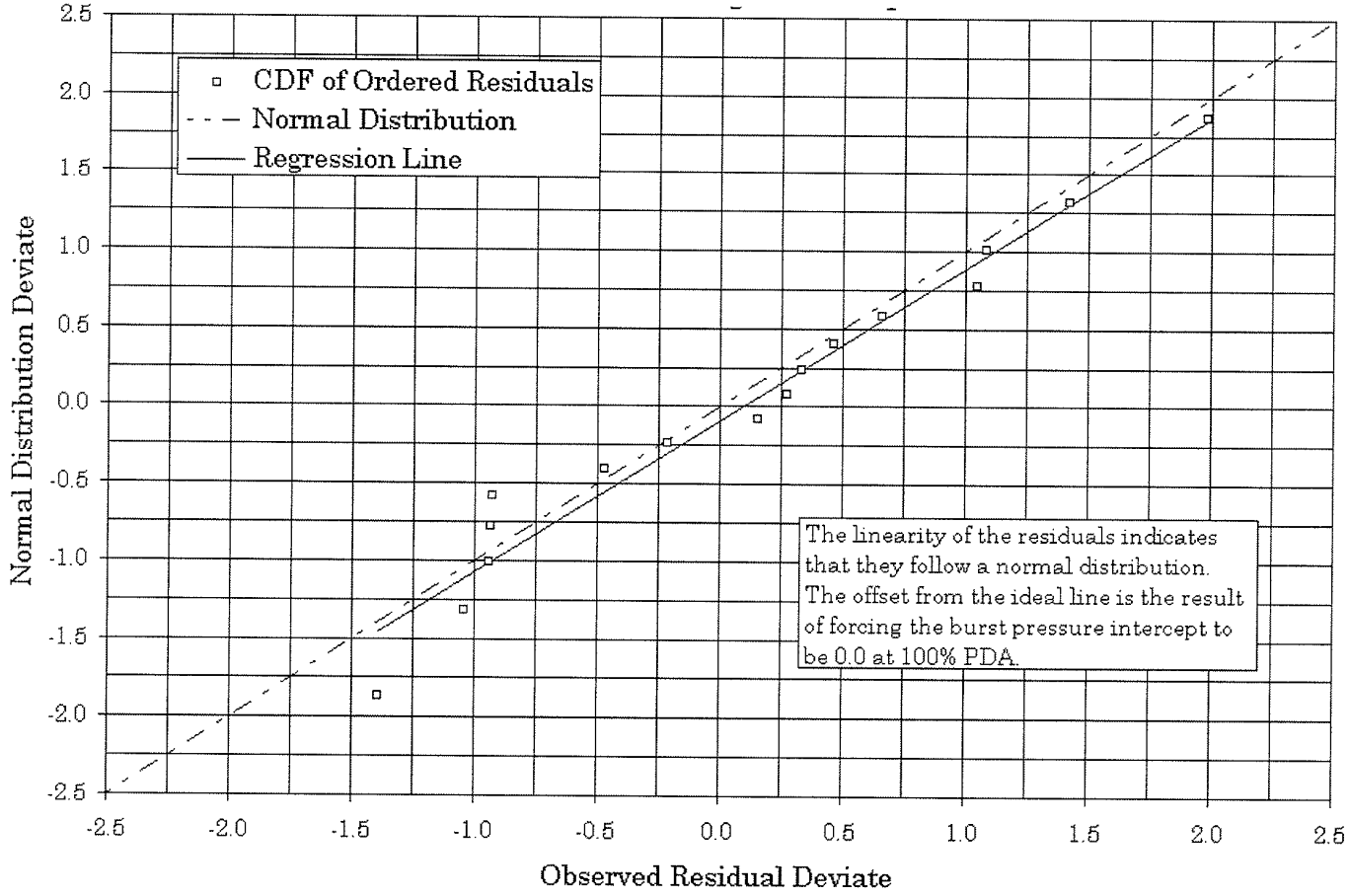

Figure 6-15
Normal Probability Plot of the Residuals of the Tensile Regression Equation

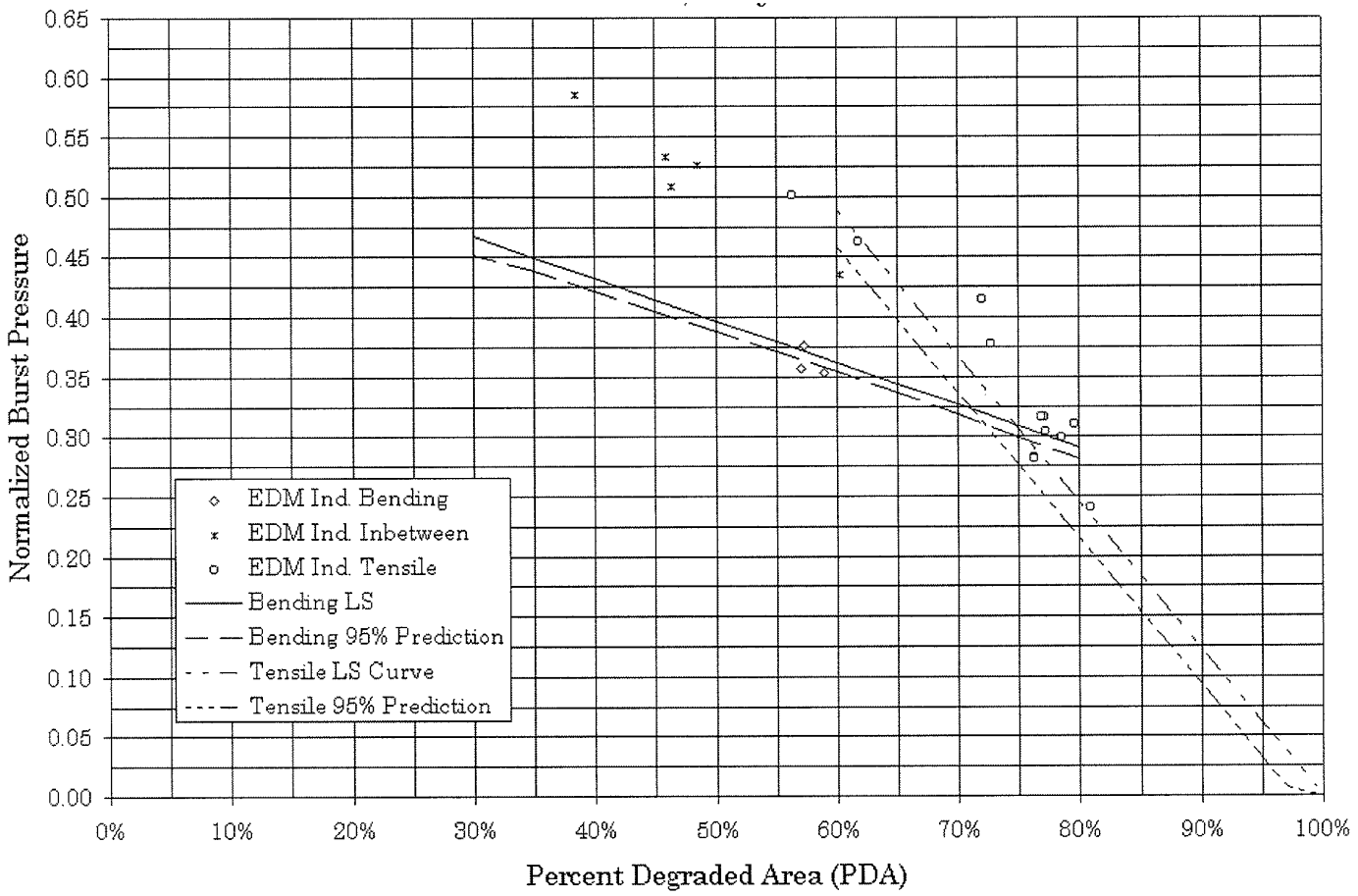

Figure 6-16
TW, Single Slit Circumferential Burst vs. PDA EDM Simulations of ¾" x 0.043", Alloy 600 Tube Indications

Correlation of Burst Pressure with PDA

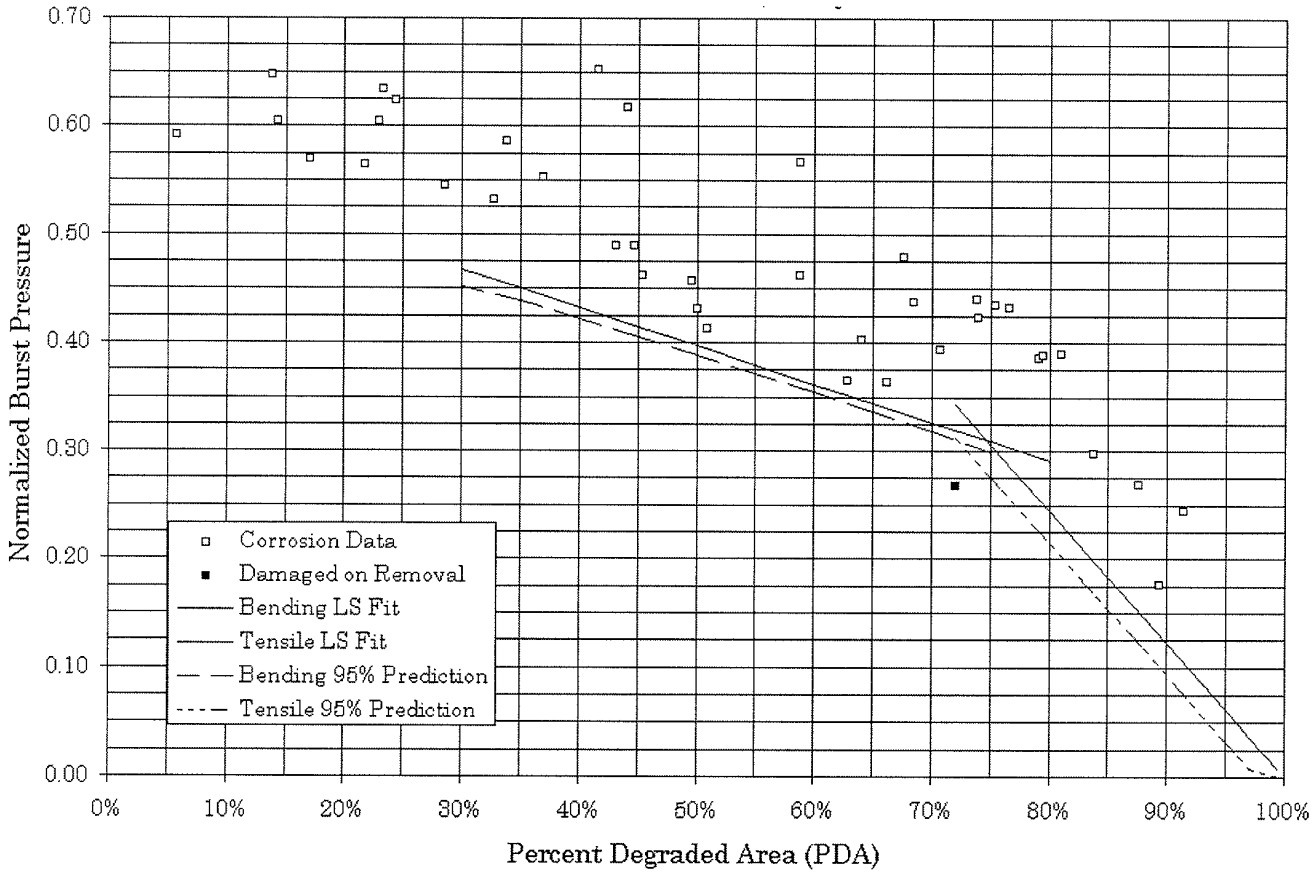

Figure 6-17
TW, Single Slit Circumferential Burst vs. PDA New Data for ¾" x 0.043" Nominal, Alloy 600 SG Tubes

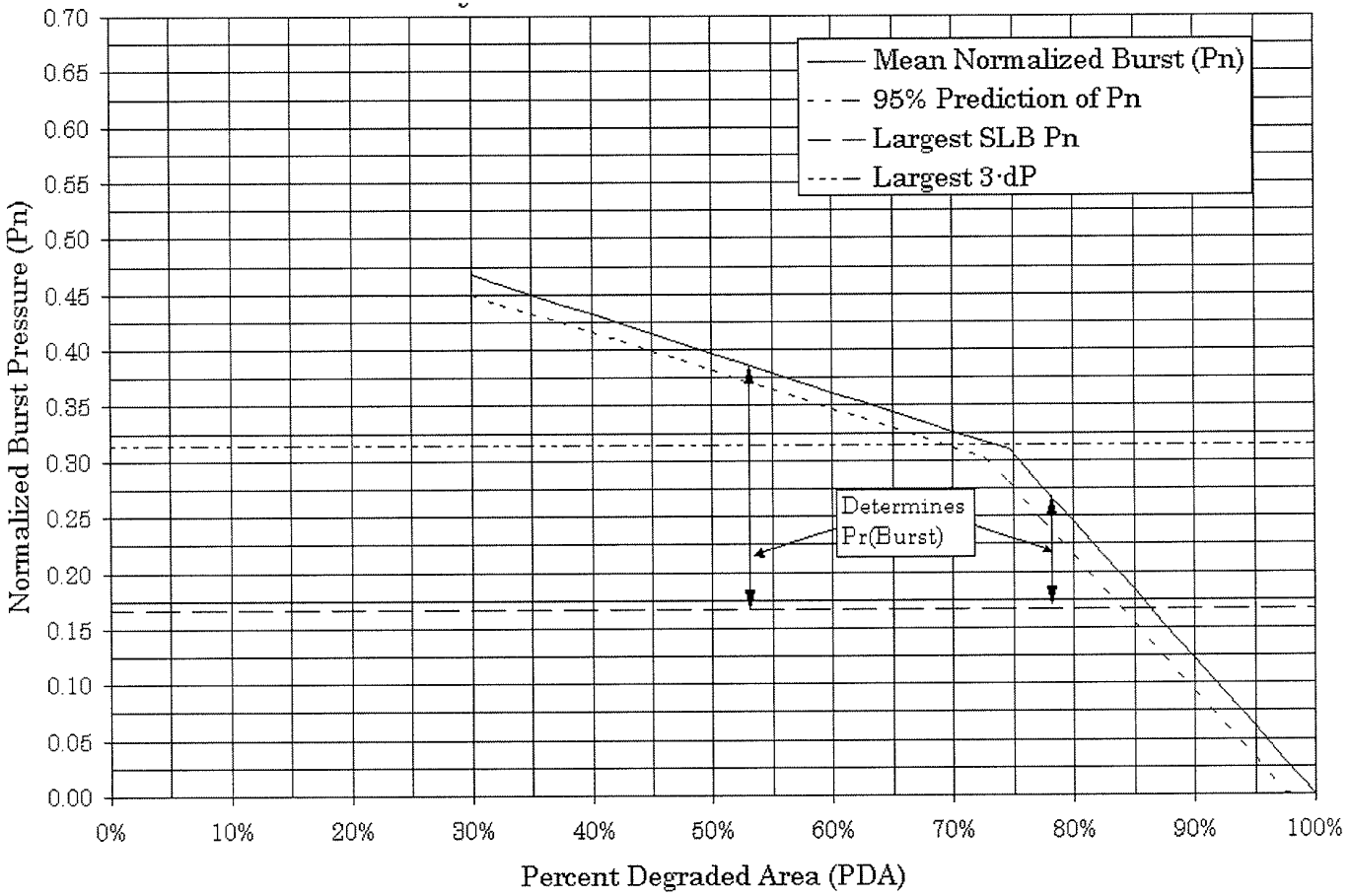

Figure 6-18
Development of Structural Limit Alloy 600MA Steam Generator Tubes

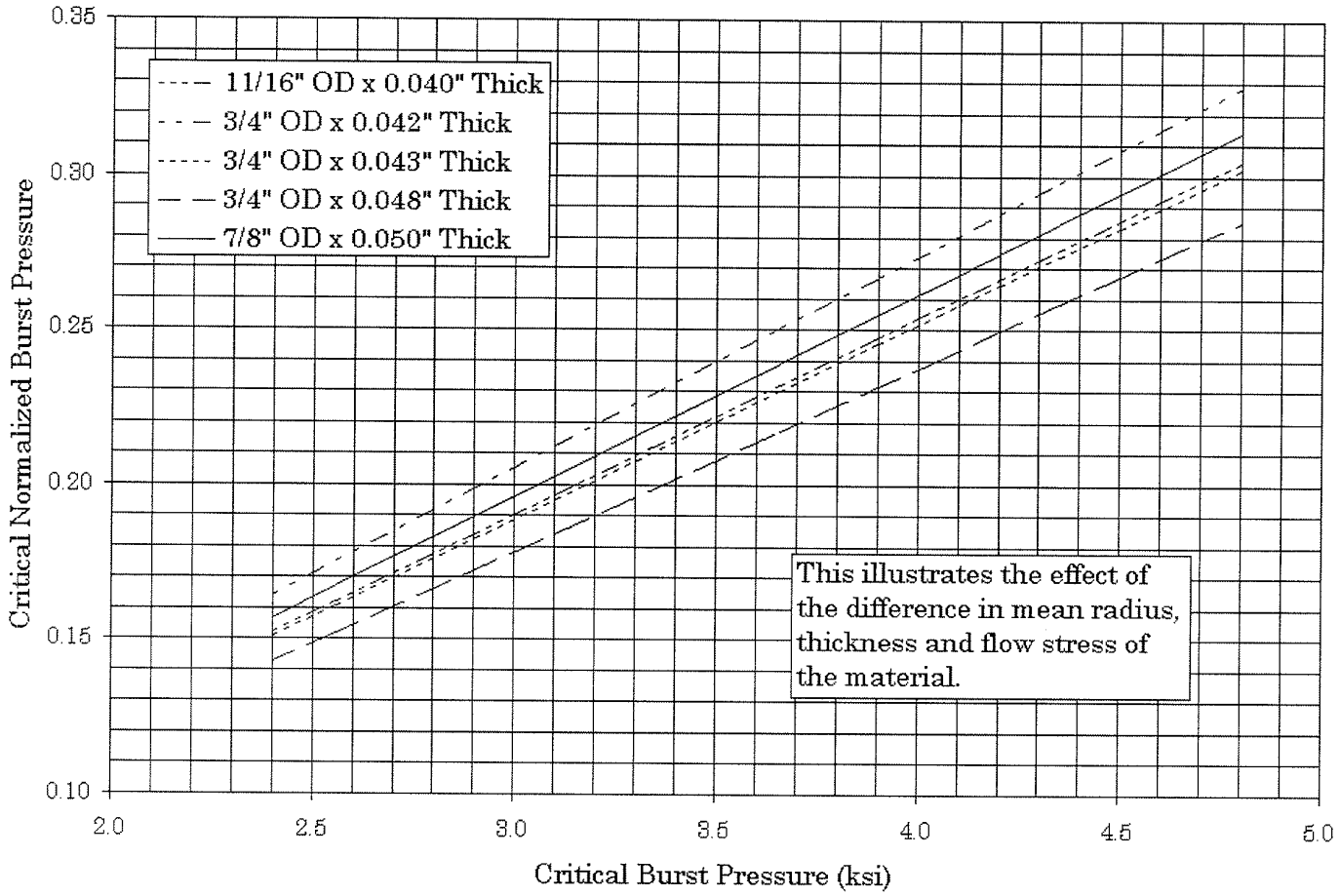

Figure 6-19
Comparison of Critical Values of P_n to P_B Alloy 600 MA Steam Generator Tubes w/LTL Flow Strength

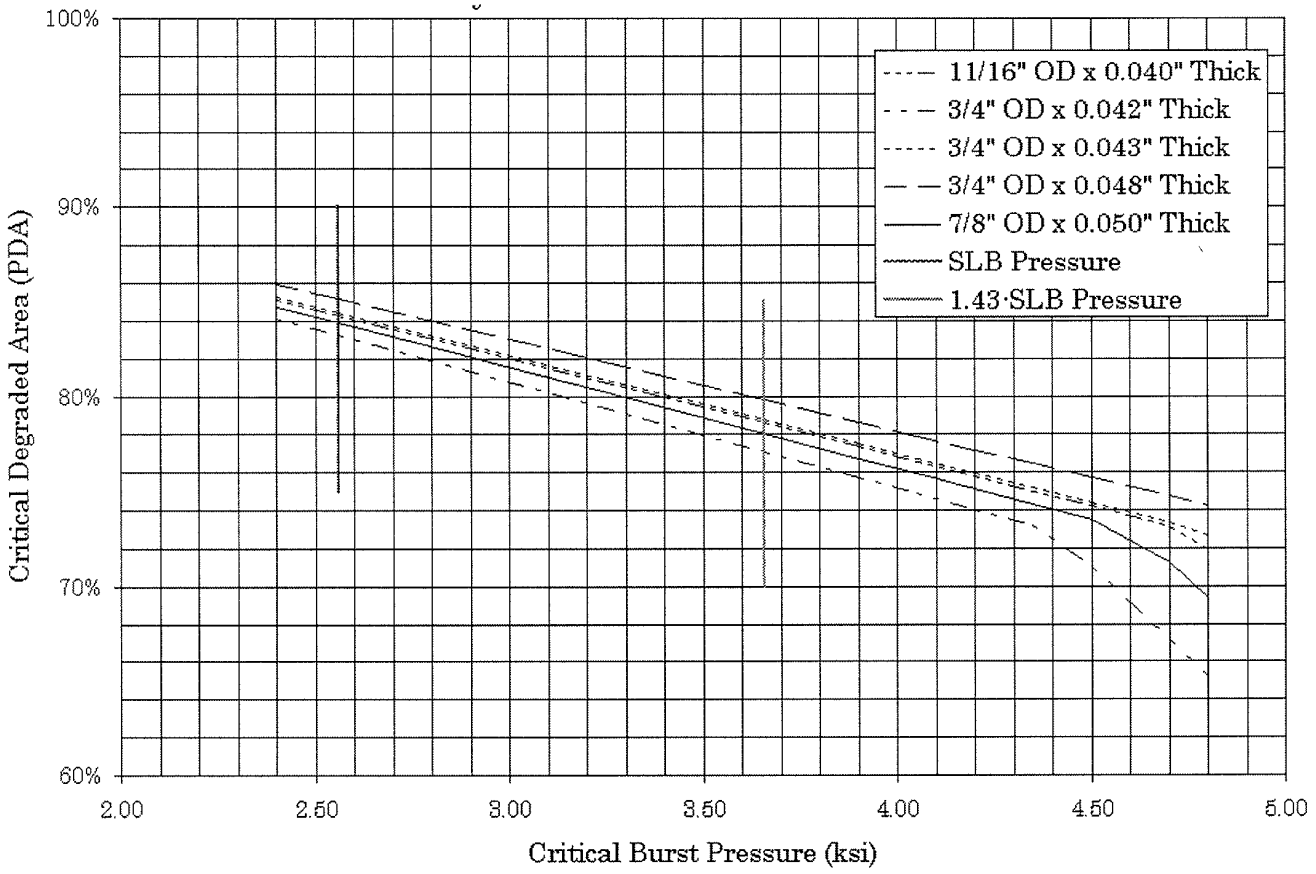

Figure 6-20
Critical PDA vs. Critical Burst Pressure for Alloy 600MA Steam Generator Tubes

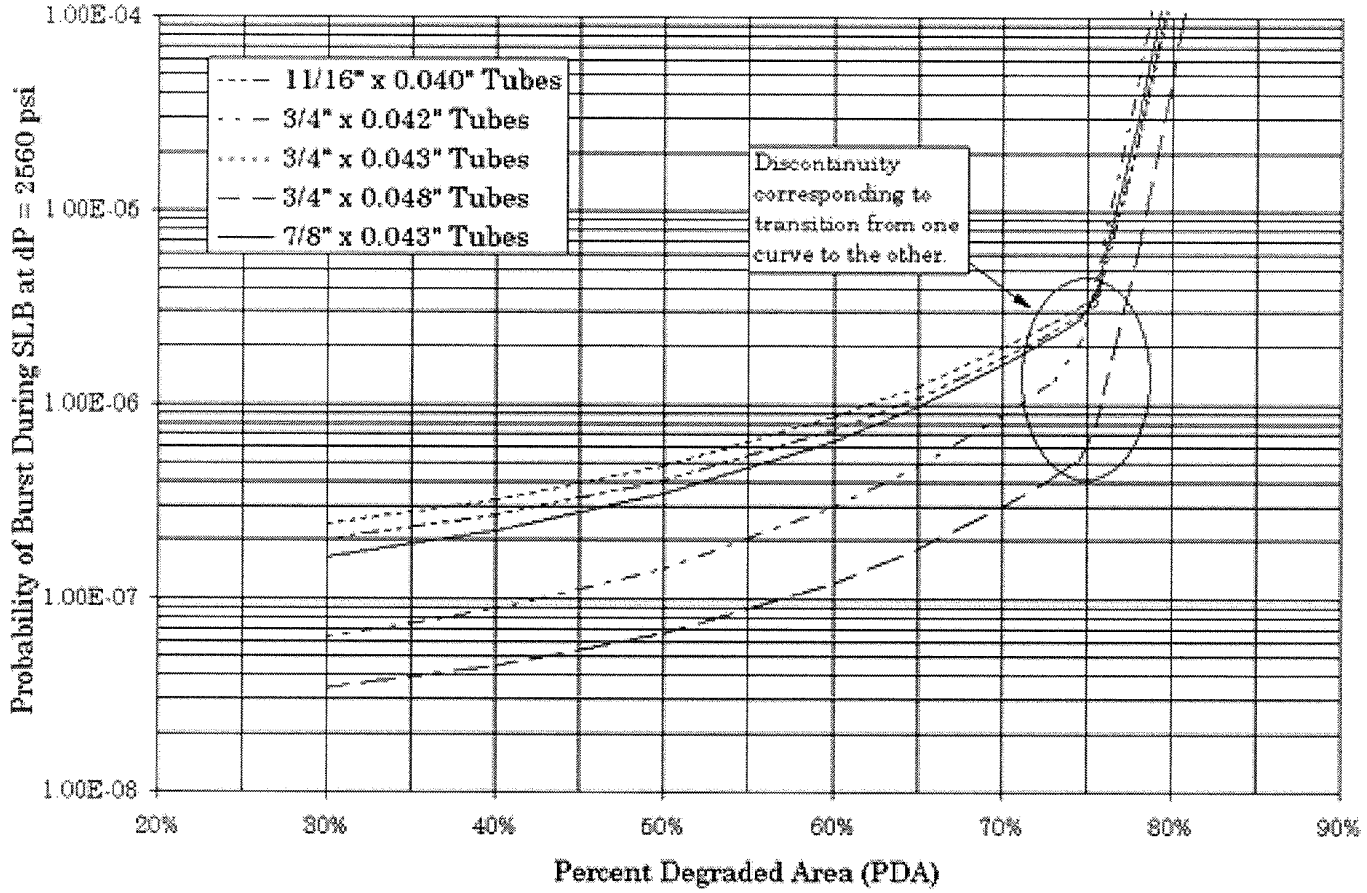

Figure 6-21
Probability of Burst During SLB vs. PDA Circ. Indications in various Sizes of Alloy 600MA SG Tubes

7

ANALYTIC MODELLING FOR LEAK RATES

There are four principal elements in the modeling of leak rates for steam generator tubing exhibiting circumferential corrosion degradation. These elements are;

- Development of relationships for leak rates as a function of temperature, pressure, crack length and crack opening area
- Calculation of crack opening area as a function of temperature, pressure, crack length and tubing dimensions
- Benchmarking of leak rate calculations
- Projection of end of cycle degradation severity.

The above topics are discussed in the following portions of this section. Leak rate equations are presented relating leak rates to temperature, pressure, crack length and crack opening area. Equations for calculating crack opening areas are then discussed. Benchmarking of leak rate calculations is described in detail with consideration of uncertainties. The treatment of projected end of cycle degradation severity covers only one aspect of the problem. A technique is presented to obtain the distribution of through wall leaking crack lengths for a given value of percent degraded area, PDA. The methodology for projecting end of cycle PDA values is covered in Section 9.

7.1 Leak Rate Regression Equations

Version 3.0 of the PICEP two phase flow algorithm was used to compute flow rates through cracks in steam generator tubing as a function of pressure (p), temperature (T), crack opening area (A), and total through wall crack length (L). This code was developed by EPRI and models the physical processes of two phase flow through a long narrow crack. For illustration purposes see Figure 7-1. Leak rate calculations are based upon Henry's homogeneous non-equilibrium critical flow model with several modifications to account for friction, crack turns and fluid conditions.

The flow conditions considered were:

- single phase flow at room temperature
- steam line break accident conditions
- normal operating conditions

These conditions cover in situ testing for condition monitoring purposes, leak before break and technical specification considerations at normal operating conditions and information required for dose assessments, that is, projected leakage at postulated steam line break conditions. Room temperature is considered to be 70°F. The temperature range at accident and normal operating conditions is taken as 565°F to 620°F. As noted above, friction effects and crack surface roughness were included in the model. The PICEP input parameters were:

- surface roughness, EK = 0.0002
- exit/inlet area ratio, AR = 1
- crack path tortuosity, $N_{90} = 0$, $N_{45} = 1.2$
- entrance loss coefficient, CD = 0.61
- friction factor, FFRED = 0

Given these input parameters and appropriate pressures, crack lengths and crack opening areas were systematically varied and leak rates were calculated. These calculations are appropriate for 0.875, 0.750 and 0.625 inch diameter steam generator tubing with wall thickness ranging from 0.034 to 0.050 inches.

Leak rates calculated by PICEP for the variety of the above conditions were fitted to regression equations. The primary side pressure is termed, $p_{prim,}$ and the secondary side pressure is termed p_{sec}. The PICEP based leak rate regression equations are given as:

- Single-phase flow for room temperature water:

$$Q = a\,\{1\text{-}exp\,[b\,(A/L)^{0.5} + c\,(A/L)\,]\}\,A\,p^{0.5}$$

where: $p = (p_{prim} - p_{sec})$, $a = 16.92894$, $b = -24.72647$, and $c = -202.3061$.

- Accident conditions (two-phase flow):

$$Q = \{a + b\,exp\,[c\,(A/L)^{0.451} + d\,(A/L)\,]\}\,A\,p^{1.333}$$

where: $p = (p_{prim} - p_{sec})$, $a = 0.0137492$, $b = -0.01382257$, $c = -18.076667$, and $d = -395.8772$.

- Normal operating conditions (two-phase including choked flow):

$$Q = \{a + b \exp [c (A/L)^{0.564}] A p^N$$

$$N = \{1 - d \exp [e A^{4.259}] \}$$

where: $p = (p_{prim} - p_{sec})$, $a = 24.02751$, $b = -23.90614$, $c = -57.78132$, $d = 0.602285$, and $e = 0.981541$.

The leak rate Q is expressed in terms of gallons per minute at room temperature (70°F). To convert to gallons per minute at any other temperature, multiply the calculated Q by the ratio of the specific volume of water at temperature (T) to the specific volume of water at 70°F. The pressure, p, is in units of psi, A is in inches^2 and L is in inches. Given these equations, leak rates can be calculated for the conditions of interest in tube integrity evaluations if crack opening areas are specified. Calculation of crack opening areas is discussed below. Note that the expression of leak rates as volume per unit time at room temperature effectively removes any explicit temperature terms from the leak rate regression equations. Note too that the regression equations do not depend on the crack orientation. The regression equations can be used for axial as well as circumferential cracking if the appropriate crack opening areas are calculated.

7.2 Calculation of Crack Opening Areas

The opening area of circumferential throughwall crack in a steam generator tube can be calculated from standard solutions in the EPRI Ductile Fracture Handbook. In the typical case where lateral displacement is restricted by tube support structures, the applicable solution is that of an internally pressurized thin walled cylinder with a throughwall circumferential crack. This solution neglects bending effects and thus is consistent with restricted lateral displacement. A single Irwin type plastic zone correction to the crack length is all that is required to account for plasticity effects in the range of crack lengths and loading conditions that are of practical interest for leak rate calculations.

Crack opening area calculations are straightforward. The parameters required are tube wall thickness, t, mean tube radius, Rm, total crack length, L, elastic modulus, E, differential pressure, p, axial pressure stress, σ, and yield strength, σ_{yp}. The stress intensity factor, K, is first calculated to permit a plastic zone adjustment to the crack length.

$$K = \frac{pR_m}{2t}\frac{\sqrt{\Pi L}}{\sqrt{2}}\left(0.8875 + \frac{0.2625L}{2\sqrt{R_m t}}\right)$$

The effective crack length is then taken as,

$$L_{effective} = L_f = L + \frac{1}{\Pi}\left(\frac{K}{\sigma_{yp}}\right)^2$$

The normalized crack length is defined as,

$$\lambda_f = \frac{1}{2}L_f / \sqrt{R_m t}$$

The crack opening area is then given by,

$$A = 2\Pi R_m t\frac{\sigma}{E}\left(0.02 + 0.81\lambda_f^2 + 0.3\lambda_f^3 + 0.03\lambda_f^4\right)$$

Displacement measurements versus internal pressure were conducted as part of this program's burst test studies. These measurements were obtained at three different circumferential locations on the crack plane. Crack opening as a function of position was calculated from these displacement measurements and thus crack opening areas were obtained. Figure 7-2 shows excellent agreement between calculated and measured crack opening areas. Total crack lengths ranged from 60° to 180° and maximum test pressures were just over 5000 psi. Figure 7-3 illustrates the vastly over-conservative result that is produced if the restriction of lateral displacement is ignored. Figure 7-3 clearly demonstrates that the appropriate crack opening area solution has been selected. Crack opening area calculations are well benchmarked and can be used with very high confidence.

7.3 Benchmarking of Leak Rate Calculations

Since crack opening area calculations are well benchmarked, the adequacy of the leak rate regression equations can be evaluated. Two avenues are open. One is a comparison with previous leak rate calculations and the other is the comparison of measured and calculated leak rates. Previous published calculations for leak rates through cracks in steam generator tubing are based on a semi-empirical orifice type approach. Crack opening area calculations are very similar between the current approach and the semi-empirical orifice approach. A range of leak conditions and formulations were

compared. Figure 7-4 illustrates the general result. The PICEP based regression equations predict leak rates in general agreement with previous calculations. Leak rates at lower crack lengths tend to be somewhat higher than previous calculations. This is to be expected since the semi-empirical approach reflects the experimental fact that some throughwall cracks do not leak. The conclusion of the comparison with previous calculations is that the current approach is similar but somewhat more conservative for the crack lengths of practical interest.

The comparison of measured and calculated leak rates began with the leak test results generated on this program (see Section 4). Figure 7-5 shows the circumferential crack profile of a specimen cracked in the laboratory. The through wall crack length is approximately 200° and this assumes that a 40° sector with a depth of 5% of the wall thickness will fracture during leak rate testing. Room temperature leak rate tests were conducted prior to testing at elevated temperatures. Figure 7-6 shows that the current leak rate calculation methodology agrees well with measured cold test data. Best agreement is obtained for a crack length of 202°. Leak test results at elevated temperatures and pressures for the same specimen are shown in Figure 7-7. The predicted leak rates again agree well with measurements. However, best agreement is obtained with a throughwall leaking crack length of 209° not 202° as for the lower pressure room temperature tests. Crack tearing during pressurization is the fundamental problem in comparing measured and calculated leak rates of tubes with stress corrosion cracks. Figure 7-8 illustrates the right side of the crack profile of Figure 7-5 but drawn to scale this time. The tapered, very shallow ligament must tear to some extent during pressurization for leak rate testing. A tear of only 7° can have a significant impact on the leak rate. Hence, with stress corrosion samples, the comparison of measured and calculated leak rates is complicated by geometry changes during testing.

Samples with fatigue cracks instead of stress corrosion cracks tend to exhibit relatively uniform crack fronts through the wall thickness especially for axial cracking. Hence geometry (length) changes during pressurization for leak testing are minimized. The definitive comparison of the leak rate regression equations with measured leak rate data is considered to be that of Figure 7-9. Measured leak rates under normal operating conditions are plotted versus axial crack length for fatigue crack samples and a selection of stress corrosion cracked samples. Crack opening area calculations for axial cracks are benchmarked versus experimental data eliminating this factor of uncertainty. Prediction of leak rates under normal operating conditions is a greater challenge than steam line break conditions. The calculated leak rates are just below the measured data for fatigue cracked samples but bound the data for stress corrosion samples.

Figure 7-9 demonstrates that the current leak rate equations provide an excellent bounding result. The much smoother fatigue crack samples are expected to bound the data for stress corrosion samples, perhaps by a substantial margin. A good yet realistic bound for stress corrosion cracks is a calculated result just below the data for the fatigue

cracked samples but at the upper bound for stress corrosion samples. Calculated leak rates can be regarded as a good bounding result. Consideration of uncertainty would lead to lower leak rates as crack morphology and roughness effects become dominant. The controlling uncertainty in leak rate calculations is not any uncertainty regarding the bounding leak rate regression equations but the uncertainty of projected end of cycle leaking crack lengths.

7.4 Projection of Leaking Crack Lengths

Section 9 provides a description of methodology to project EOC degradation severity. For burst calculations it is practical to consider the worst case crack morphology for a given value of percent degraded area, PDA. A single through wall is the worst case geometry but in burst calculations the penalty of assuming this bounding morphology is not totally unreasonable. This is not the case with leak rate calculations. If the absolute worst case morphology is assumed, then cracks which do not change the burst pressure from its undegraded value would be assumed to leak at more than 0.5 gpm. Clearly a more practical approach to the conservative estimation of leaking crack lengths is needed.

The description of crack morphology in Section 3.2 provides a picture of deep crack segments against a shallower background of corrosion degradation. Leakage will develop as these deep crack segments penetrate the wall thickness.

The question of which, if any, deep crack segments penetrate the wall depends on both the PDA value and the apportionment of PDA between the shallow crack background and the deep crack segments. As presented below, measured crack profiles of pulled tubes are used to determine what fraction of PDA is available to drive deep crack segments throughwall and what fraction resides in background cracking. Note that the fraction of deep crack PDA is defined as that fraction of the total PDA which is above background in the deep crack segments.

Even if crack profiles are known with virtual certainty from destructive examination, the question of effective leaking crack lengths is not trivial. As discussed in an earlier section, cracking tearing as the test pressure is increased to levels appropriate for postulated steam line break events can significantly increase the leaking crack length compared to measured 100% throughwall crack lengths based on fractographic appearance. Conversely, crack path tortuosity, surface roughness, ligaments and other impediments to flow can lead to much reduced leak rates compared to expectations from fractographic observations.

Figure 7-10 shows a plot of measured leak rates at SLB pressure differentials from circumferentially cracked tubes versus leak rates predicted from post test fractographic measurements of 100% throughwall crack lengths. The bounding nature of the PICEP

based leak rate equations has been established. The scatter in Figure 7-10 is due to the uncertainty is estimating the effective leaking crack lengths. As expected, scatter above and below the mean curve is evident. If the effective leaking crack length is equated with the crack length at a fractographically established crack depth of 80% throughwall, an upper bound leak rate is obtained. This is illustrated in Figure 7-11. Hence, if a circumferential crack profile is determined from destructive examination, an upper bound leak rate for that particular tube can be determined easily. Note that this upper bound leak rate effectively accounts for crack coalescence, since separate cracks on the basis of 100% fractographic depth may sometimes form one single large crack at the 80% depth level. Similarly the phenomena of "popin", or mechanical tearing throughwall without a full tube burst is included.

The pulled tube crack profiles presented in Section 3 were analyzed to determine the fraction of PDA associated with the background and deep crack segments as a function of PDA level. The deep crack segment fraction of PDA versus PDA level is plotted in Figure 7-12 based on the conservative, bounding assumption that a depth of 80% throughwall represents a leaking crack. Note that certain crack profiles have a zero deep crack fraction of PDA, that is, the upper bound leak rate is zero for some PDA levels. Figure 7-13 shows a plot of leaking (1) and non-leaking (0) cracked tubes versus PDA level. This figure is simply a transformation of Figure 7-12 where any tube with a non-zero deep crack PDA fraction is assigned a probability of leaking of 1. Figure 7-13 includes two additional pulled tube indications that had very large PDAs (above 90%) with deep crack PDA fractions approaching unity. If there are no deep crack segments greater than 80% throughwall, the deep crack PDA fraction is zero and the probability of leaking is 0. A log logistic fit to the binary data of Figure 7-13 results in a probability of leakage curve (POL) versus PDA, as shown in the figure. The equation for this curve is;

$$POL = 1/\left(1+\exp\left(12.320 - 7.969\log 10(PDA)\right)\right)$$

When projected end of cycle PDA values are obtained, the POL curve is applied first to determine when leak rates are to be computed. Given that a leak rate computation is warranted for some selected PDA value, the number of deep crack segments is selected according to the frequency of occurrence table in Section 3. The lengths of deep crack segments are selected from the Weibull length distribution of Section 3. The remaining question is the selection of the fraction of PDA which is applied to deep crack segments to drive them throughwall. Figure 7-12 provides one basis to determine the deep crack PDA fraction. At first glance, a Monte Carlo approach with a random deep crack PDA fraction between 0 and 0.7 seems a likely choice. However this figure is based on the bounding assumption that the leaking crack length is equal to the length at a depth of 80% throughwall. Figure 7-14 shows a plot of deep crack fraction versus PDA where the leaking crack length is based on 100% wall penetration. In this case, the deep crack PDA fraction is closer to a random number between 0 and 0.1.

The preferred conservative approach to estimating leaking crack lengths, once a deep crack PDA fraction has been selected, is to assign this fraction to the deep crack segments in a manner that produces the largest leak rate. That is, the deep crack PDA fraction is not equally apportioned to all deep crack segments in a tube. In order to maximize the leak rate, all of the deep crack PDA fraction may be assigned to a single deep crack segment in order to create a leaking crack.

At this point we have an upper bound leak rate equation, a deep crack PDA fraction based on the bounding assumption that an 80% deep crack is a leaking crack and a scheme to assign the deep crack portion of PDA to maximize the resulting leak rate. Hence the possibility of calculating substantially overconservative leak rates for steam generators with circumferential corrosion degradation at expansion transitions must be evaluated.

Operating experience at normal conditions and in situ testing data relative to accident conditions provide a means to benchmark leak rate calculations. Early benchmarking evaluations with even more conservative leak rate methodologies considered instances of relatively few degraded tubes without obvious difficulty. However, when the full range of circumferential degradation observed in service was considered, the compounding effects of several upper bound assumptions led to calculated total steam generator leak rates much in excess of field experience. Even lower 5th percentile leak rates at normal operating conditions would routinely indicate forced outages and BOC leak rates at normal operating conditions (after plug on detection and return to power) which exceed administrative limits and in some cases technical specification limits. Consequently, one bounding assumption was relaxed to a degree.

The deep crack PDA fraction is sampled as a random number between 0 and 0.3. This is, in effect, a compromise between the data of Figure 7-14 where leaking crack lengths are based upon 100% throughwall fractographic observations and Figure 7-12, where leaking crack lengths are based upon 80% throughwall fractographic observations. A deep crack PDA fraction sampled between 0 and 0.3 leads to a conservative calculation of leaking crack lengths, approximately midway between essentially a best fit estimate and an upper bound estimate. An upper bound leak rate equation coupled a with final deep crack PDA apportionment scheme to maximize the leak rate on a per tube basis argues for the overall conservatism of the approach. When considering a total steam generator leak rate, a further element of conservatism is added; a 95/95 leak rate is calculated using rank order statistics.

The leak rate methodology can be summarized a follows. In a given Monte Carlo simulation trial of a steam generator, a list of EOC PDA values is generated. Both detected and undetected populations of PDA values are to be considered. For each PDA trial value (PDA_{sample});

1. Use the POL curve to determine if a leak rate is to be calculated for PDA_{sample}, otherwise assign a zero leak rate

2. If a leak rate is to be calculated, select the number of deep crack segments according to the frequency of occurrence table in Section 3

3. For each deep crack segment obtain a deep crack segment length from the Weibull distribution presented in Section 3

4. Pick a random number between 0 and 0.3. This is the fraction of the total PDA value (PDA_{sample}) that resides in the total deep crack segment length (sum over all deep crack segment lengths)

5. Compute the background degradation depth for the PDA not in the deep crack segments as $(1\text{-}PDA_{deep\ crack\ fraction})PDA_{sample}$

6. Compute the total deep crack area above background as $(PDA_{deep\ crack\ fraction})PDA_{sample}$

7. Consider each deep crack segment to determine if the total deep crack area is sufficient to drive the segment throughwall (100% depth is assumed to be throughwall)

8. Assign the total deep crack segment area to drive the largest crack throughwall (100% depth) and maximize the calculated leak rate

9. Store the leak rate value.

After steps 1 through 9 are completed for each EOC PDA value, the sum of these leak rates is the total steam generator leak rate for the given simulation. After many simulations are performed, the different total leak rates are sorted from low to high. Using rank order statistics, the 95/95 total leak rate is calculated. For example, in an ordered list of 1000 leak rates, the 961st largest leak rate is the distribution free 95% confidence estimate of the 95 percentile leak rate.

7.5 Adjustments of In Situ Measured Leak Rates to Operating Conditions

In situ leak rate measurements are commonly made at room temperature and at pressure differentials that may differ from the desired reference conditions such as a SLB pressure differential of 2560 psi. In some cases, it may be desirable to adjust an operating plant leak rate to another pressure differential. The leak rate equations of Section 7.1 with the crack opening areas of Section 7.2 should be used for the adjustment of circumferential crack in situ measurements to the desired conditions.

The adjustment of a room temperature, in situ measurement to a SLB leak rate at operating conditions is obtained by multiplying the measured leak rate by the calculated ratio of the accident condition (two-phase flow) leak rate to the single-phase flow for room temperature water using the Section 7.1 equations. Adjustments relative to normal operating conditions would use the corresponding normal operating condition equation of Section 7.1. It is preferable that the room temperature in situ measurement used for the adjustment be made at a pressure differential higher (about 10% higher) than the reference value in order to account for potential ligament tearing at operating temperatures as discussed in the in situ guidelines given in Appendix F. The calculated adjustment ratio then corrects the in situ measurement for operating temperature and for the over-pressure test condition. The crack opening equations of Section 7.2 require the crack length and material yield strength as input. For consistency in the adjustment practice, it is recommended that the crack length be selected such that the calculated leak rate at the measurement condition (temperature, pressure) is about a factor of 1.5 to 2 higher than the measured value. If the tube specific yield strength is known, it should be used in the analysis. If not known, it is recommended that nominal material properties be used. Similarly, nominal tube dimensions should be used in the analysis.

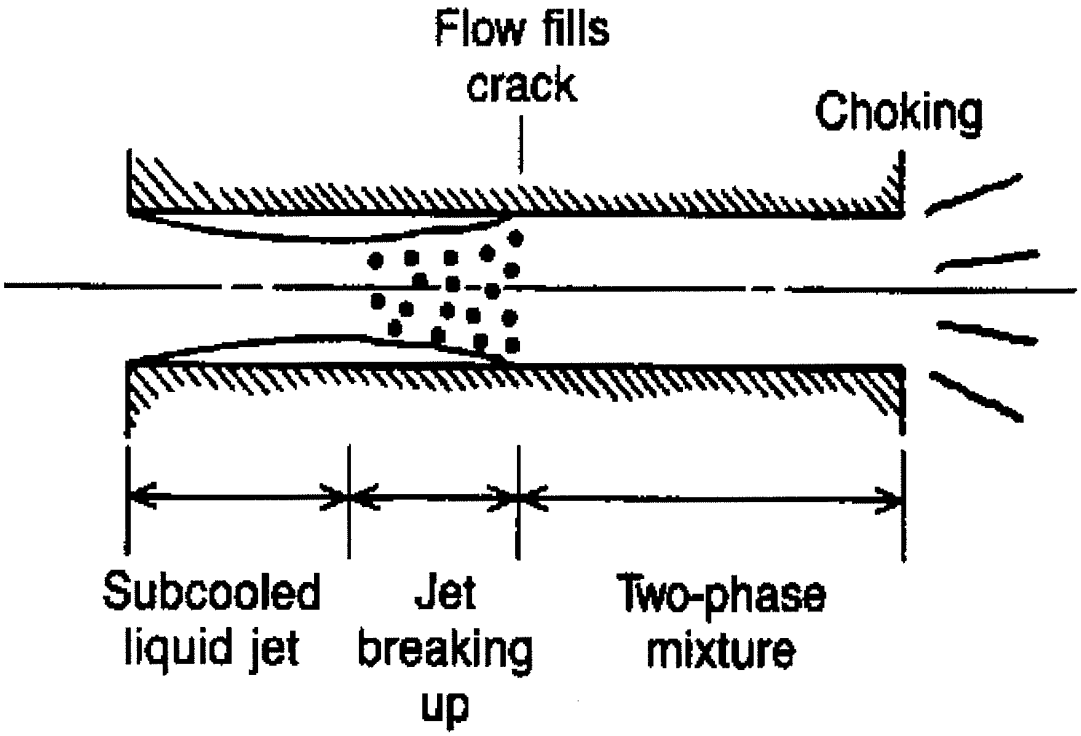

Figure 7-1
Physical Processes Occurring During Flow Through a Long, Narrow Crack

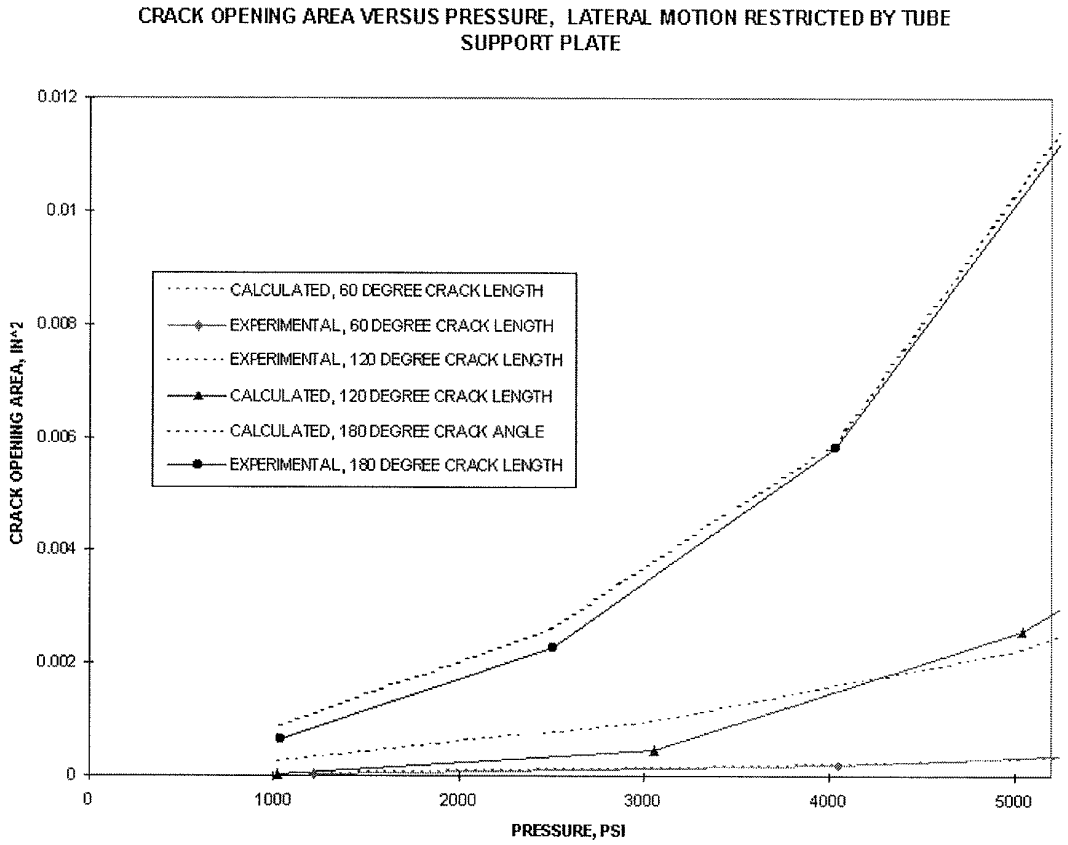

Figure 7-2
Circumferential Crack Opening Area Versus Pressure; Comparison of Measured and Calculated Values, Lateral Motion Restricted

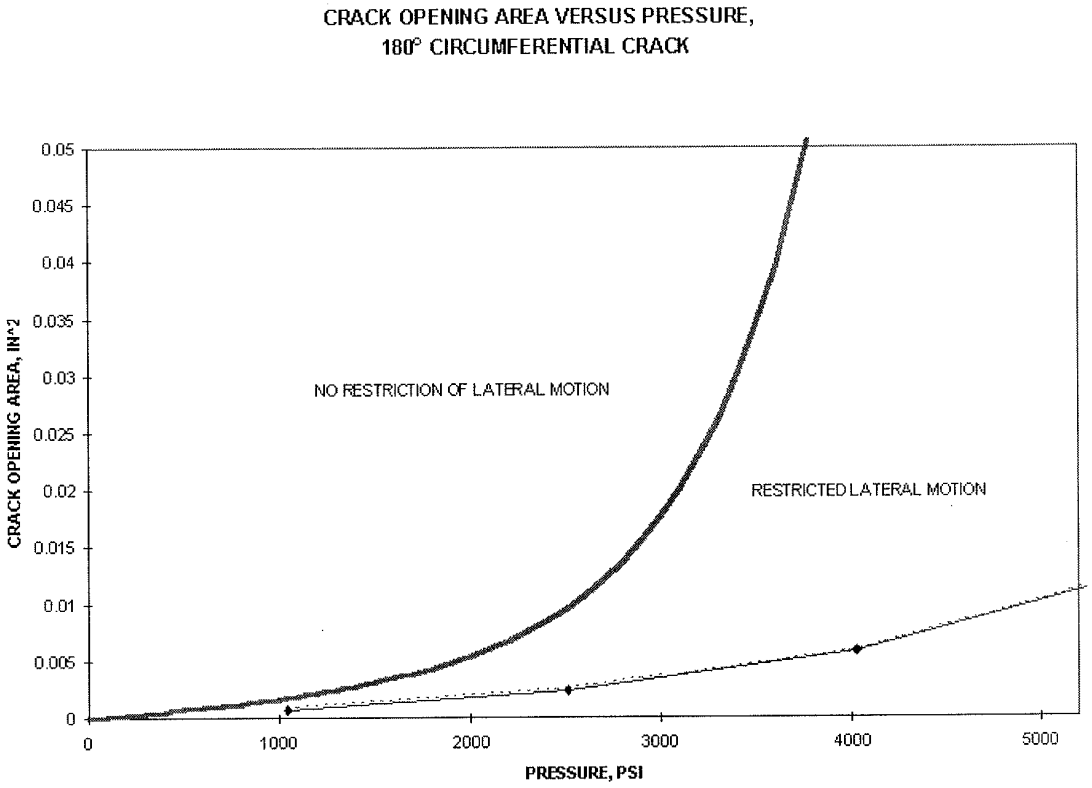

Figure 7-3
Circumferential Crack Opening Area Versus Pressure; Effect of Restriction of Lateral Motion

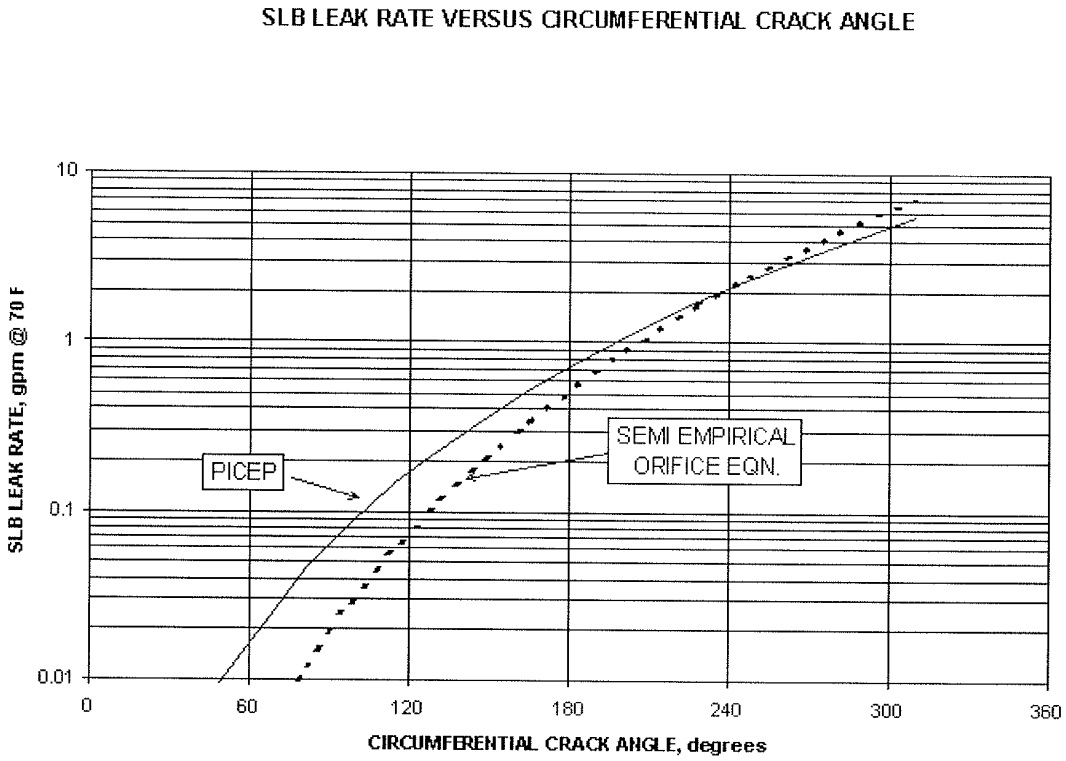

Figure 7-4
Comparison of SLB Leak Rates Calculated by PICEP Based Regression Equations and a Semi-Empirical Orifice Type Approach

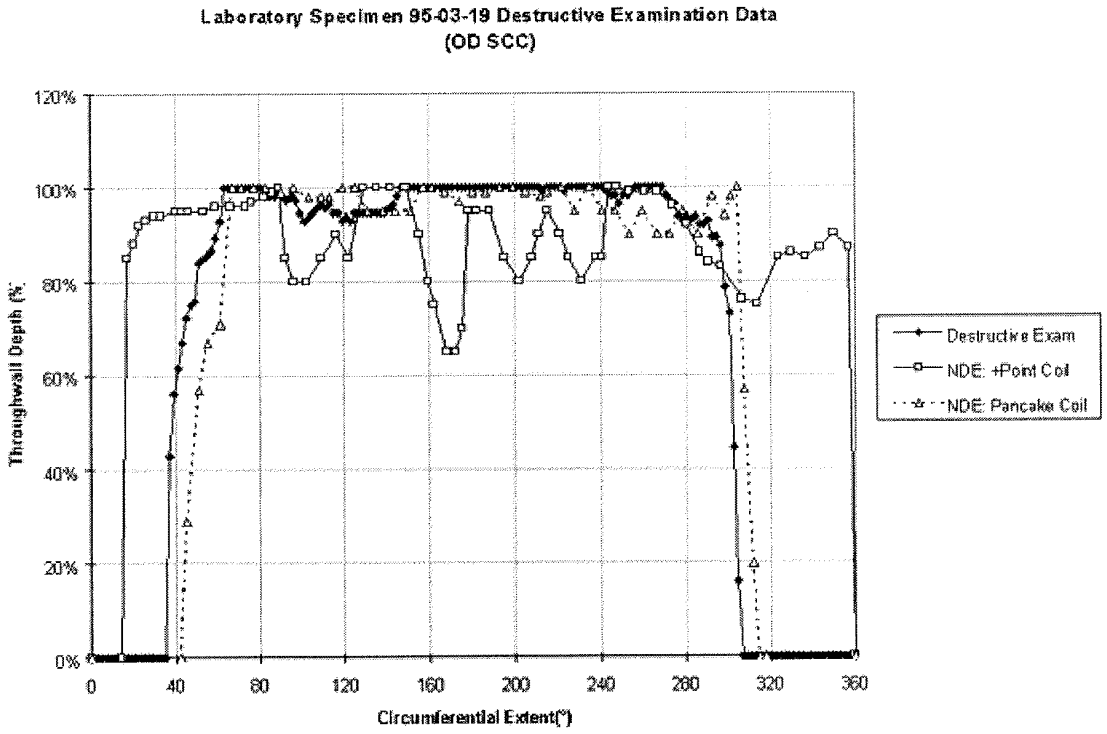

Figure 7-5
Circumferential Crack Profile of ODSCC Laboratory Cracked Specimen (95-03-19)

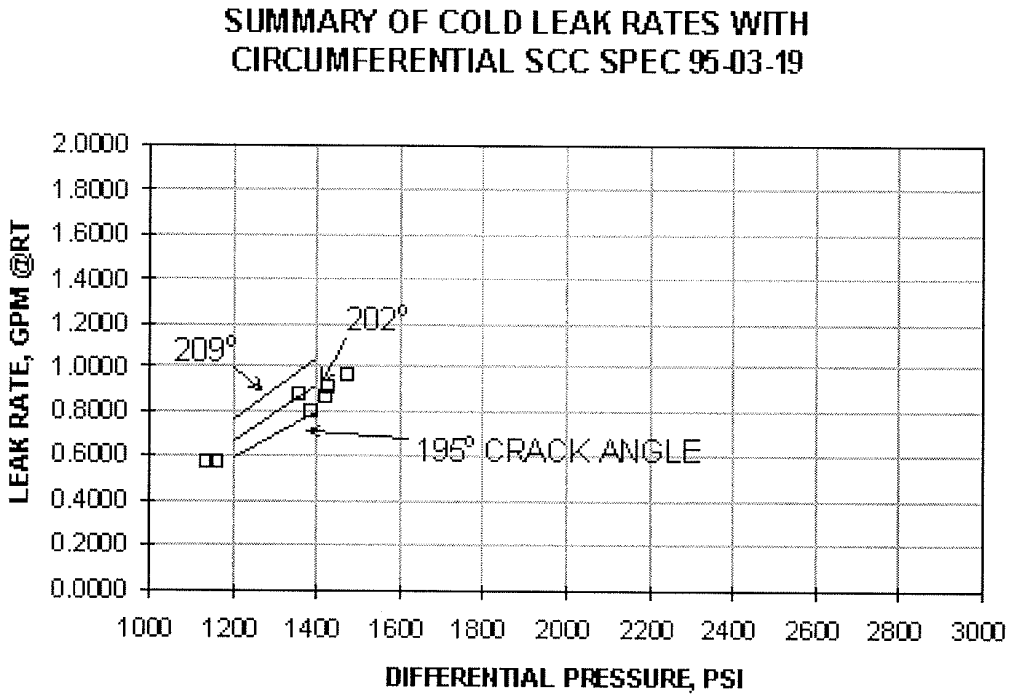

Figure 7-6
Room Temperature Leak Rate Versus Differential Pressure for Specimen 95-03-19

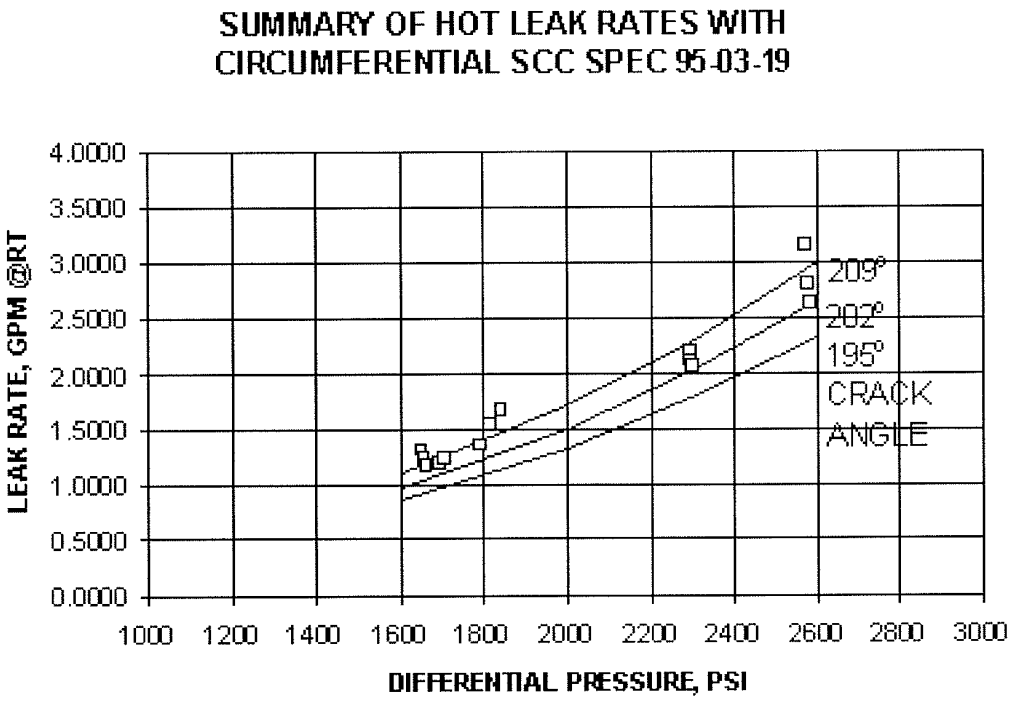

Figure 7-7
Elevated Temperature Leak Rate Versus Differential Pressure for Specimen 95-03-19

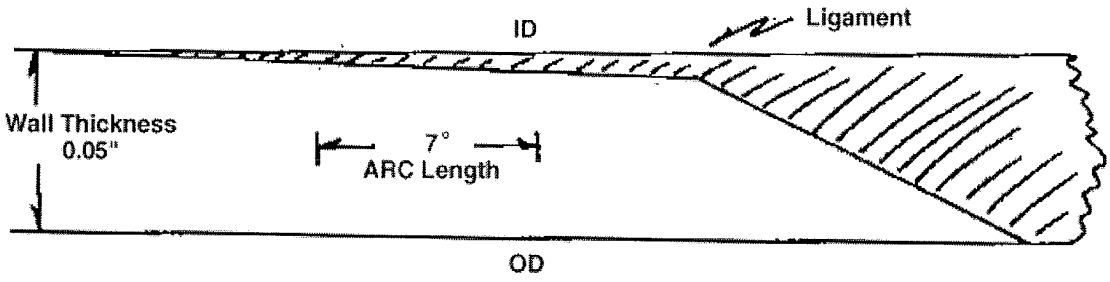

RIGHT SIDE CRACK TIP OF SPECIMEN 95-03-19
APPROXIMATELY DRAWN TO SCALE

Figure 7-8
Expanded Local View of Circumferential Crack Profile of Specimen 95-03-19, Drawn on Scale

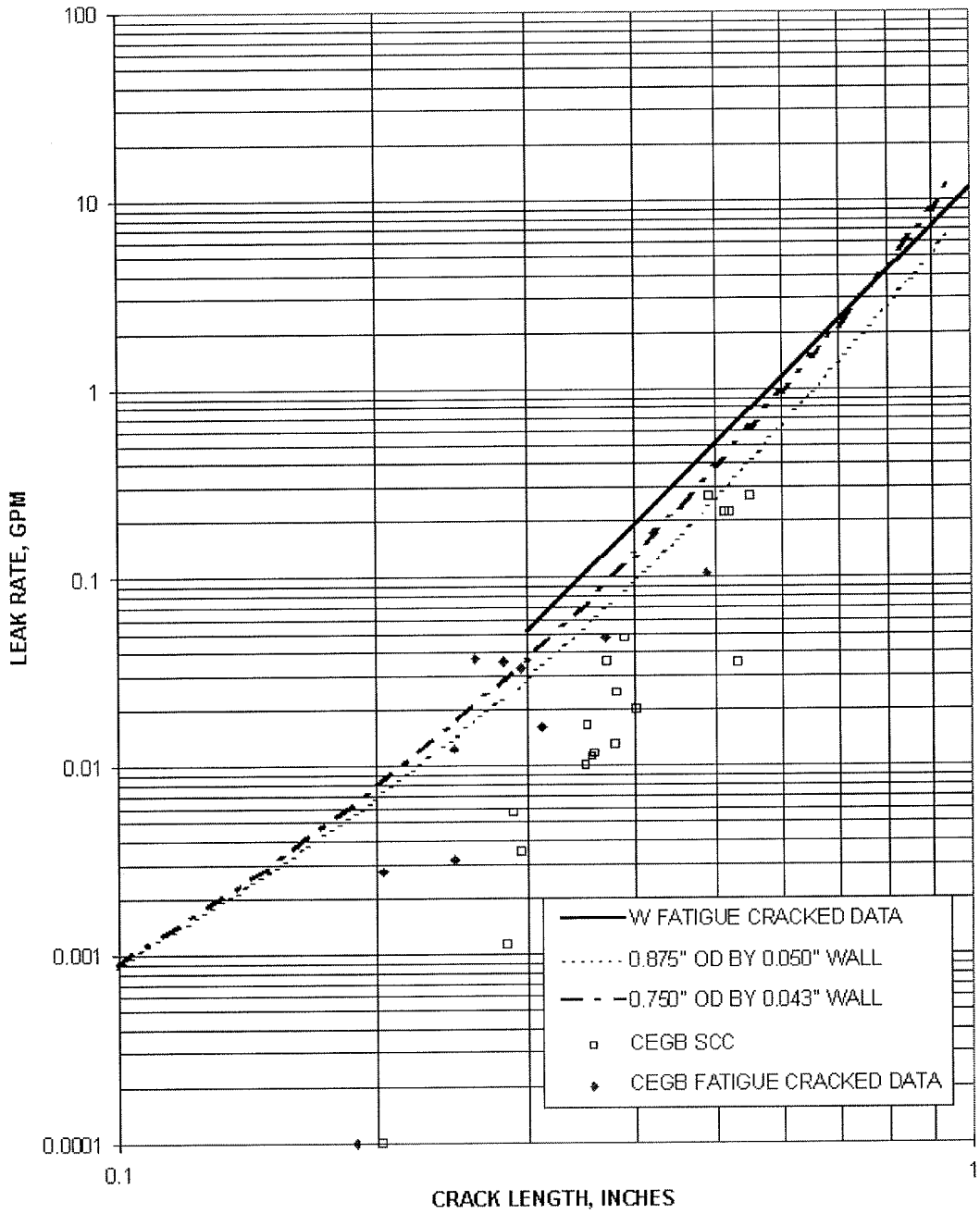

Figure 7-9
Comparison of Measured and Calculated Leak Rates Through Axial Cracks in Steam Generator Tubing at Normal Operating Conditions

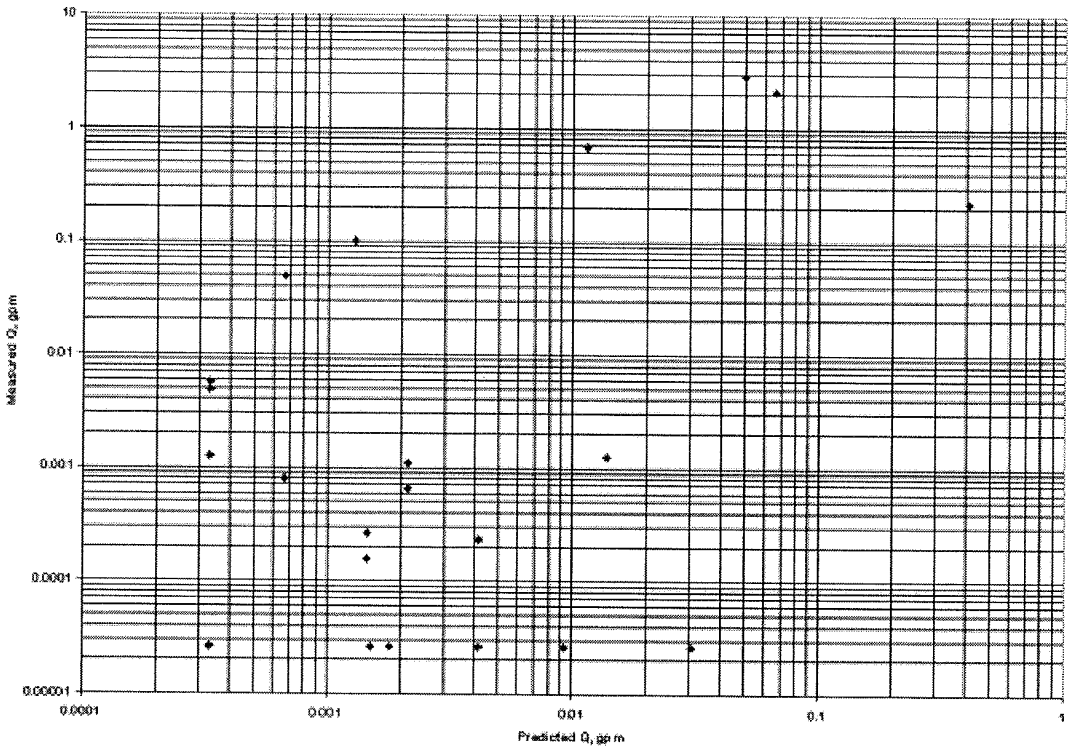

Figure 7-10
Measured vs. Predicted SLB Leak Rates in Circumferentially Cracked Specimens; Leaking Crack Lengths Based on 100% Throughwall Cracking Per Fractographic Observations

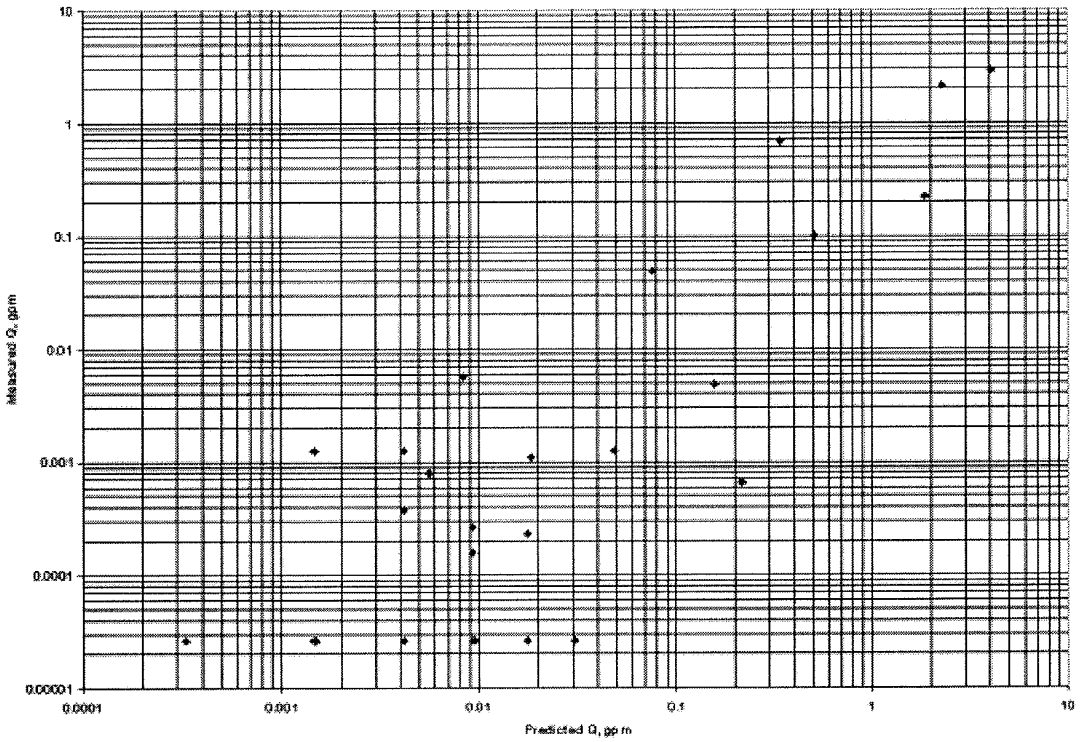

Figure 7-11
Measured vs. Predicted SLB Leak Rate in Circumferentially Cracked Specimens; Leaking Crack Lengths Based on 80% Throughwall Cracking Per Fractographic Observations

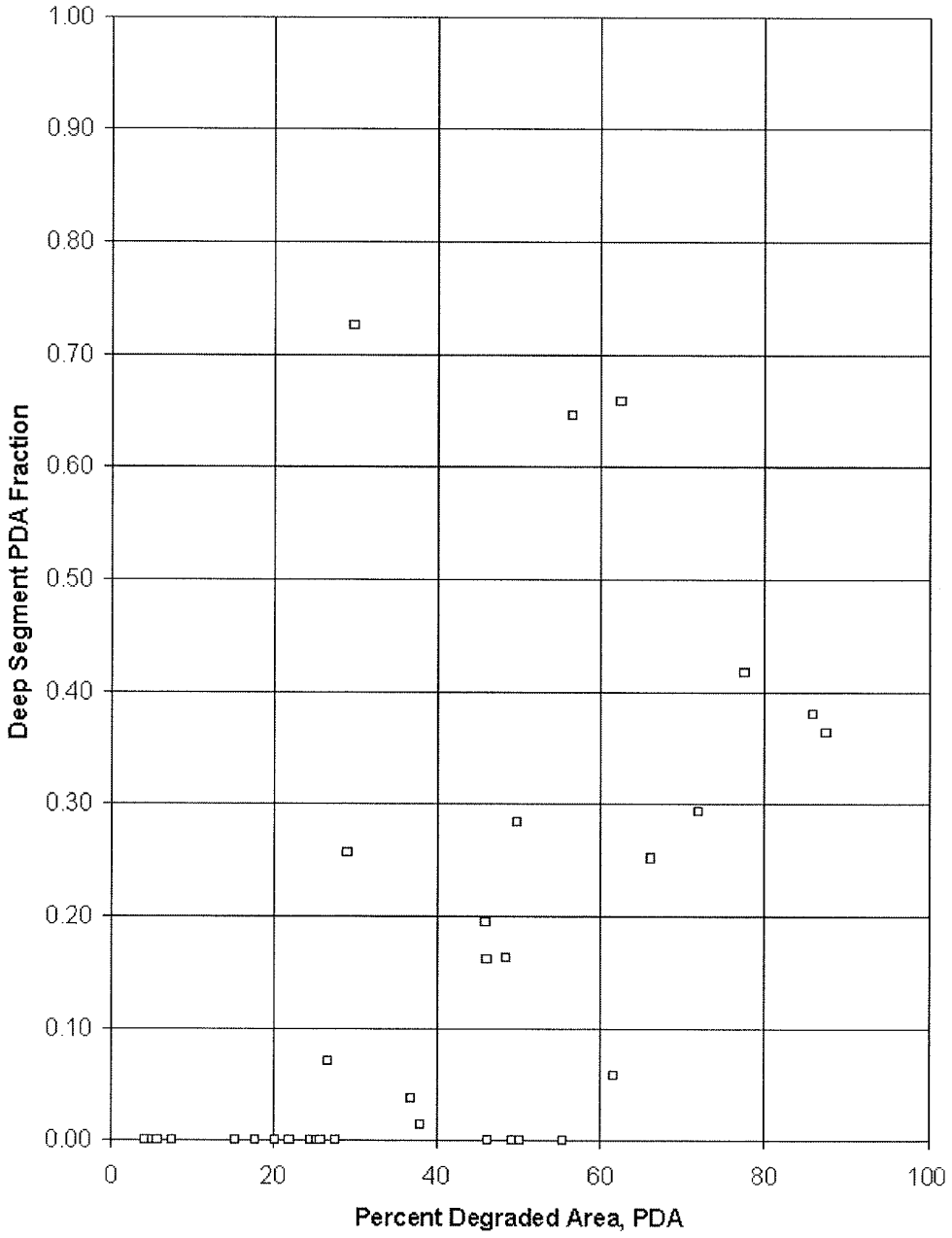

Figure 7-12
Deep Crack Segment PDA Fraction Versus PDA; 80% Throughwall Assumed as a Leaking Deep Crack Segment

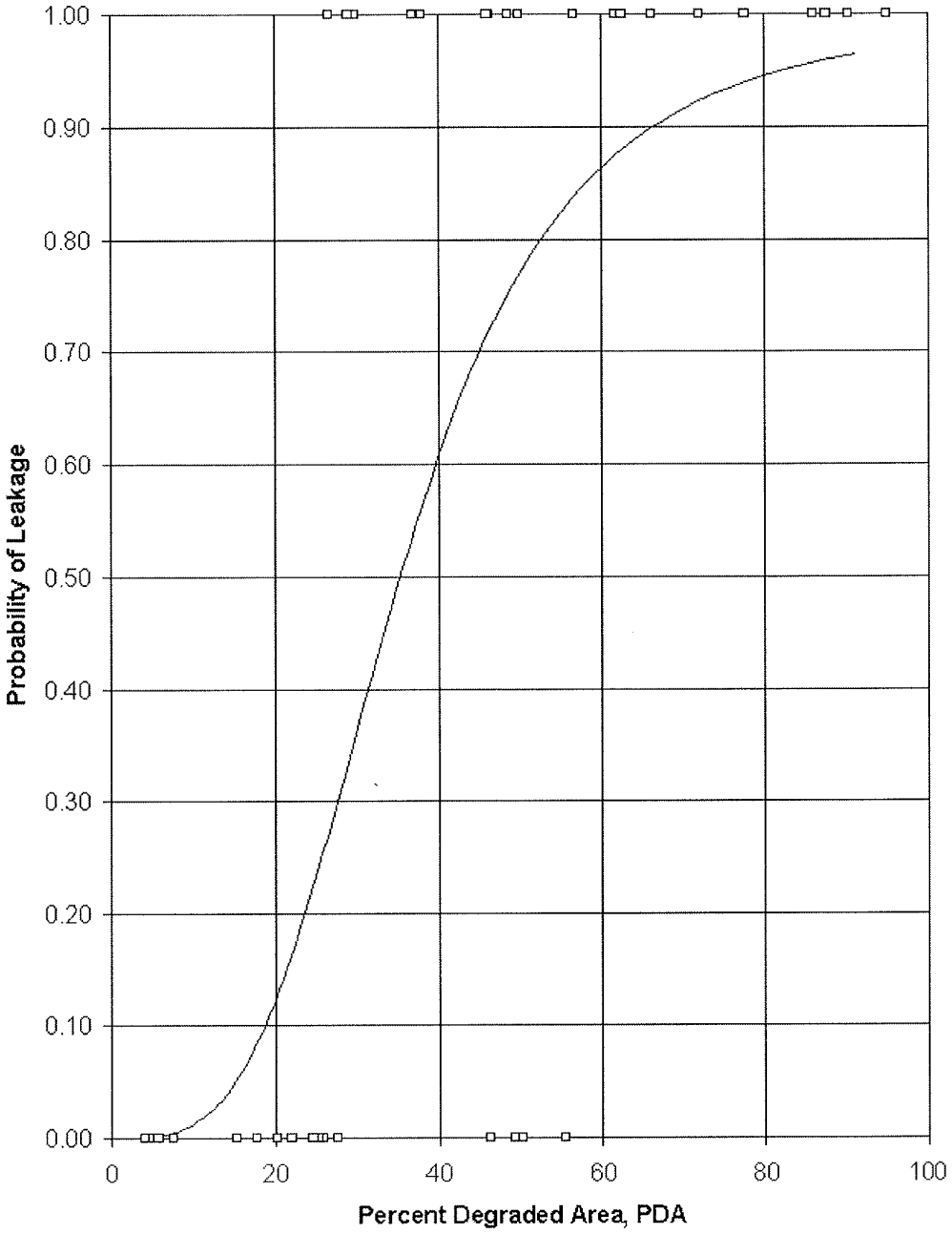

Figure 7-13
Probability of Leakage Versus PDA; 80% Throughwall Assumed to Characterize a Leaking Crack Segment

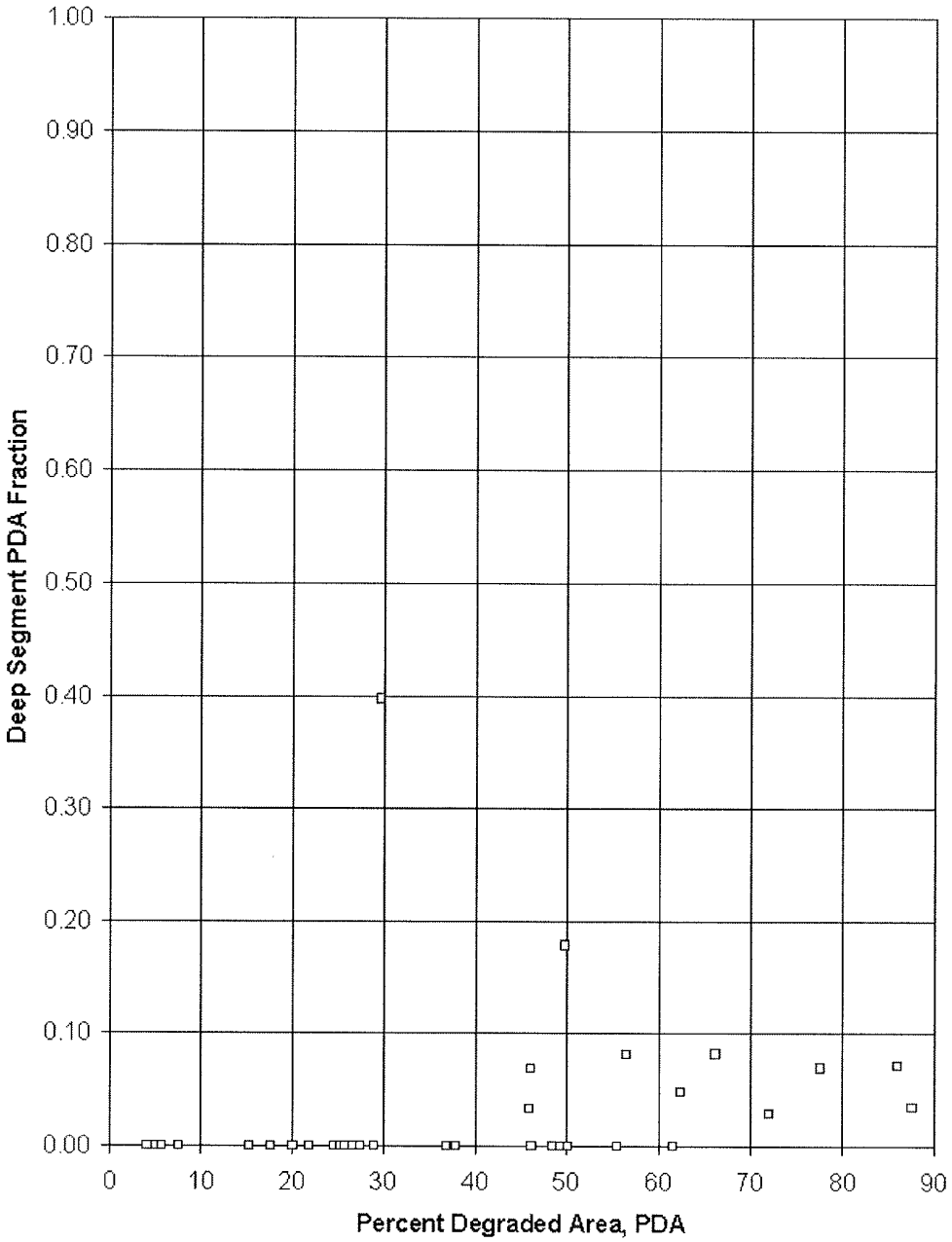

Figure 7-14
Deep Crack Segment PDA Fraction Versus PDA; 100% Throughwall Assumed to Characterize a Leaking Crack Segment

8

LEAK AND BURST ASSESSMENT METHODS FOR MEASURED INDICATIONS

This section describes the elements of the process for evaluation of the as-found condition of tubing for a steam generator affected by circumferential cracking. This process corresponds to that of the condition monitoring assessment described in Reference 1. In addition, the specific role of in-situ pressure testing as an important supplement to NDE/analytical based evaluation, is discussed.

With a deterministic structural performance criteria, the worst case degraded tube should meet a minimum burst pressure of 3ΔP (or 1.4 SLB whichever is greater). This can be accomplished by analysis or by testing. With an analysis approach, the worst case, as measured, degraded tube should meet the 3ΔP burst criterion with a probability of 0.95 at 50% confidence (Reference 1) when NDE sizing errors, tensile strength variations and burst relationship uncertainties are properly considered. Given the data in this report, calculation of an acceptable maximum measured PDA value for a deterministic structural performance criterion is straightforward. With a probabilistic structural performance criterion, condition monitoring assessments are somewhat more involved.

For a probabilistic structural performance criterion, the basic condition monitoring question is, "Given a set of EOC measured PDA values and perhaps in situ testing burst and leak data, is the as found conditional probability of tube burst at projected SLB conditions less than 0.01?". If an in situ testing approach is followed and it can be established that the lowest burst strength has been found and measured, the conditional probability of tube burst for the as found condition of the steam generator will then be determined as either 0 or 1. This does beg the question as to whether or not the probabilistic technology used to project the condition of the steam generator is reasonably correct or conservative versus unconservative to the point of unacceptability. In general, this question, along with determining whether or not the measured EOC PDA values imply an acceptable conditional probability of burst, can only be treated by recourse to some relatively sophisticated calculations. The following subsections discuss such calculations in essentially increasing order of complexity. The simplest approaches have the disadvantage of over conservatism.

The condition monitoring process deals explicitly with the set of observed defects. These are defects which have been detected and measured. In the case of circumferential cracking, the measurements which characterize the defect are in terms of percent degraded area (PDA). As discussed in Section 5, the uncertainty in this measurement is significant even for the less adverse case of explosive expansion. This measurement uncertainty is additive and on the order of 13% in terms of standard deviation. The PDA measurement uncertainty dominates other components of uncertainty in the condition monitoring process, particularly with regard to structural integrity which is determined principally by the extreme value of PDA for the observed defects.

Two methods have been investigated for dealing with PDA uncertainties in terms of the condition monitoring process. The first involves a direct approach and is appropriate for moderate cases in which the largest measured defect does not appear to challenge structural limits. The second method uses an indirect probabilistic approach and may be useful when the largest observed defects are closer in value to structurally limiting PDA values.

8.1 Burst Analyses

The information available for the evaluation in structural integrity consists of N measured PDA values [DM1, DM2, ... DMN]. Corresponding to this measured array will be a set of N "true" PDA values [D1, D2, ..., Dj, ... DN]

Where:

$$DM_j = D_j + E \qquad \text{(eq. 8-1)}$$

E = measurement error

The process of measurement described in equation 8-1 results in a measured distribution with higher variation than the underlying true distribution. This is shown in Figure 8-1 for a 13% additive measurement uncertainty. This behavior and its consequences regarding the overall conservative nature of the measured distribution is discussed in detail in Section 9.1.1. It can be concluded that the measured distribution is, in general, a conservative representation of the true PDA distribution and that the effect of large measurement uncertainty is to shift moderate PDA values into the upper tail of the observed (measured) distribution. This behavior is justification for using the measured PDA values without adjustment for computations sensitive to general distributional properties of PDA. In the case of burst under accident conditions, which depends on the extreme of the PDA distribution, a more definitive treatment of measurement uncertainty is required.

For modest PDAs, the structural limits from the Section 6 burst pressure correlation and the associated burst probability analyses permit application of deterministic analyses. The structural limits can be reduced by NDE uncertainty to obtain an acceptable PDA. The burst probability per indication for PDAs < 75% are < $4x10^{-6}$ but increase sharply for PDAs > 75%. If all measured PDAs adjusted for NDE uncertainty are < 75%, the burst probabilities would be negligible. The confidence level applied to the NDE uncertainties is a function of the number of indications near the acceptable PDA level. For example, the NDE uncertainty at 99% confidence (2.32 sigma) can be added to the measured value for comparison with the 75% PDA value. With the explosive expansion NDE uncertainty (1.3% mean, 13.4% standard deviation) from Section 5 at 99% confidence is 32.5%. Thus, measured PDAs less than about 43% readily satisfy burst criteria. For a small number of indications in this range, the acceptable PDA can be moderately increased using the burst probabilities of Section 6.4. For a very large number of indications, it may be necessary to increase the confidence level applied to the NDE uncertainties to conservatively bound the burst probability at < 10^{-2}. When NDE uncertainties are large, such as found for circumferential indications in hardroll expansions, this approach is generally too conservative and increased emphasis on in situ testing may be necessary.

8.1.1 Direct Addition of Measurement Uncertainties

The most straightforward treatment of NDE measurement uncertainties is to apply Equation 8-1 in inverse form:

$$DSYN_j = DM_j - E \qquad \text{(eq. 8-1A)}$$

$DSYN_j$ = synthesized "true" PDA of j^{th} indication

This will result in a true PDA distribution with a higher variance than the measured distribution, but avoids the computational difficulties associated with a true probabilistic inverse. The process of evaluating the condition of the tubes is by repeated application of Equation 8-1A in conjunction with sampling of material flow stress and computation of burst pressure as shown in Figure 8-2. This process is essentially the same as applied in the ARC for ODSCC at TSP intersections as given in NRC Generic Letter 95-05. NDE uncertainty, burst pressure and leakage are a function of PDA rather than voltage for GL 95-05.

The sequence for one Monte-Carlo trial includes:

- Computation of true defect sizes [DSYN] for all N observed defects
- Sampling of flow stress [FS] for all N defects
- Computation of burst pressures (see Section 6) for all N defects [PB]
- Ordering of burst pressure array [PB], determination of minimum value
- Testing minimum burst pressure against performance criterion

The process is repeated until an acceptable confidence level estimate of burst frequency for the specified performance criterion is obtained. In the case of steam-line-break an acceptable condition monitoring outcome is a frequency of burst less than 10^{-2}.

It should be noted that an acceptable outcome for this approach, in terms of meeting the acceptance criterion, may require a 3-sigma margin between the largest observed PDA and a PDA challenging the burst pressure requirement. The sigma referred to is one standard deviation in the sizing error statistic. This, of course, is for larger defect population sizes and depends also on the precise nature of the upper part of the order statistic of observed PDA values. The condition monitoring probability of burst obtained by adding measurement error to the observed EOC PDA values typically over estimates the true probability of burst by an order of magnitude or more. Hence, more sophisticated analyses are required for condition monitoring when the true conditional probability of burst approaches the limit of 0.01.

8.1.2 Discriminant Analysis Approach

The direct method described in the previous section requires a significant PDA margin between the largest observed value and the "limiting" PDA value which is approximately 82%-90% (dependent upon tube size) for circumferential cracks under steam-line-break conditions. In the presence of large measurement uncertainty, there is a distinct possibility that large measured PDA values are the result of measurement uncertainty applied to a relatively innocuous true distribution. The discriminant analysis method developed in this section provides a process by which the properties of the measured distribution order statistics are used to evaluate the relative probability of the data belonging to an underlying population for which the probability of burst under steam-line-break conditions is unacceptable.

This indirect process was developed using training sets for which the underlying probability of burst was known. The training sets were samples taken from three gamma functions, each representing a "true" underlying population.

Three basic gamma sampling distributions were chosen for training set development. Each gamma distribution had a shape parameter of 3 and a scale parameter adjusted to give a specific probability of having a maximum true PDA value exceeding 90% for a sample of 1000 defects.

The training set development process for a given gamma distribution consists of steps:

- A sample of size 1000 is drawn from the distribution
- The sample is processed through a probability of detection function (POD: see Figure 9-3) to obtain a detected subset
- A measurement uncertainty is applied to obtain the as-measured PDA set
- The measured subset order statistics are developed (these include PDA_{MAX} and other properties of the distribution tail

This process is repeated 1000 times for each basic sampling distribution.

Three basic sampling distributions were selected. Distribution 1 represents an underlying situation with a burst probability significantly less than 10^{-2}. The scale parameter of Distribution 1 was 4.5. Distribution 2 represents the marginal case in which the probability of burst is approximately 10^{-2}. The scale parameter for this case is 5.0. Distribution 3 represents the clearly unacceptable underlying tube condition for which the probability of burst is greater than 10^{-1}. In this case the scale parameter was 6.0. In each of these cases observed PDA value in excess of 90% are *expected.* The training sets, therefore, test the ability of the method to differentiate between situations in which the maximum observed PDA values may be identical while the underlying burst probabilities vary by order of magnitude.

Figure 8-3 shows the three training sets each as a two-dimensional cluster. Each point in the cluster is defined by two order statistics from one sample of which 1000 are taken for each underlying distribution. The first order statistic plotted is the maximum observed value from the sample. The second order statistic is the average of the 50 largest observed PDA values in the sample. A third order statistic (not shown), is the standard deviation of the set of 50 largest PDA values from the sample. The training sets shown in Figure 8-3 were all developed using a 13% additive measurement uncertainty. As can be seen from the figure, there is very limited separation between the three clusters.

The training sets were subjected to a formal discriminant function analysis (Reference 8-2). This analysis is classically used to determine which variables discriminate between two or more defined groups. In this case properties of the order statistic are examined to determine the set which best discriminates between groups of differing burst probability.

The most important output from the discriminant factor analysis is the identification of the most important factors. In the case of the present training set, the average of the largest 50 data points is the most important discriminating variable. Discriminant analysis has the capability of providing classification functions. Application of the classification functions to the training sets results in the classification results shown in Table 8-1. The diagonal elements in the matrix given in Table 8-1 represent the correct classification count by group (distribution). The off-diagonal elements are essentially misclassifications. In the case of group 2 (distribution 2), the process would have classified samples from this marginal case as clearly good in 147/1000 cases and clearly bad in 10/1000 cases. It should be noted that this classification matrix represents a process capability. Actual performance would probably be somewhat lower. It can also be seen from the table that in *no case* was a sample taken from the clearly bad distribution, classified as clearly good.

The process of logistic regression was utilized to develop a decision function for the training set, specifically for the discrimination between the acceptable and marginal cases (distributions 1 and 2). The logistic regression approach has a distinct advantage in that the classification function provides an explicit probability estimate which in its more familiar NDE form is probability of detection. In this study the dependent variable is the probability of belonging to the more adverse group.

Figure 8-4 shows two traces of the two-dimensional classification function for the distribution 1 and 2 training sets. The independent variables are the maximum observed PDA value and the average of largest 50. The value of the average of the largest 50 sample observations, which minimizes the probability of belonging to the more adverse group, is a function of the largest observation. For an observed maximum PDA value of 95%, the average of the largest 50 observations should be less than 58%. For observed maximum of 70%, the average should be less than 55% to minimize the probability of the sample having originated from the more adverse set. For intermediate values of observed maxima the relationship is approximately linear. This can actually be seen more clearly in the central graph in Figure 8-3.

This indirect process will require training set development for alternative sample sizes. The present training sets were developed for a situation in which the observed number of indications would exceed 500. Custom training sets would be required with plant-specific attributes such as POD functions and sizing uncertainties appropriate for the specific inspection process.

The indirect process does appear to have significant promise in terms of distinguishing between acceptable and unacceptable conditions in the presence of high levels of measurement uncertainty and maximum observed PDA values near structural limits.

8.2 Leak Rate Assessments

Leak rate assessments for condition monitoring by analysis are a direct application of the leak rate methodology presented in Section 7. The as measured PDA values of the steam generator at end of cycle are the input data. Repeated leak rate calculations for the total steam generator leak rate are performed and the 95th percentile leak rate is identified. This serves as a 50% confidence estimate of the upper 95% leak rate. It is argued that the measured PDA values provide a good to conservative estimate of the true severity of degradation. The leak rate calculation methodology for a given PDA value is conservative. The end result is a conservative SLB leak rate calculation. As discussed later, in situ testing should routinely lead to lower total SLB leak rates and this is an attractive alternative approach.

8.3 Utilization Of In Situ Test Results

Selection of tubes for in situ testing is discussed in detail in Appendix E. Appendix F describes guidelines for the performance of in situ pressurization tests. The interpretation of in situ testing data depends on whether a deterministic or probabilistic approach to tube integrity is under consideration. As noted in the beginning of this section, interpretation of in situ test data relative to deterministic structural performance criteria is relatively straightforward. Condition monitoring relative to probabilistic performance criteria adds a degree of complexity.

If in situ testing is carried to the point where the lowest burst pressure has been identified, then the as found conditional probability of tube burst at postulated SLB conditions can be established as essentially 0 or 1. An answer of 0 in one particular instance does not say that degradation management practices or the computations of a projected EOC degradation state are appropriate. This one particular answer could be generated either through good fortune or good technology. Deciding between good technology or good fortune is possible by using the methodology of Section 9 to predict the probability of encountering the lowest observed burst pressure. If there is less than a 0.1 projected chance of encountering the lowest observed EOC in situ burst pressure, then the adequacy of the prediction methodology and input data such as growth rates and POD curve must be reviewed. Revision of growth rate data and POD curves to match in situ test burst data allows recalculation of the EOC probability of burst. This recalculated value then provides a reasonable condition monitoring check of the conditional probability of burst and the adequacy of degradation management practices.

With regard to total steam generator leak rates, in situ testing can provide a direct measure providing all degraded tubes with a reasonable chance of leaking are tested. The guidelines of Appendix E provide good selection criteria. Leak rate calculations based on measured PDA values are conservative. In situ testing provides a means to demonstrate actual leakage integrity at postulated SLB conditions.

8.4 References:

1. Draft Regulatory Guide DG-1074, Steam Generator Tube Integrity [Draft], USNRC, September 1996.

2. STATISTICA Release 5, StatSoft, Inc., Tulsa, OK, 1995.

Table 8-1
Classification Matrix Statistical Discriminate Analysis

Group	Percent Correct	G1	G2	G3
G1	86.30	863	137	0
G2	83.70	147	837	16
G3	97.80	0	22	978
Total	89.27	1010	996	994

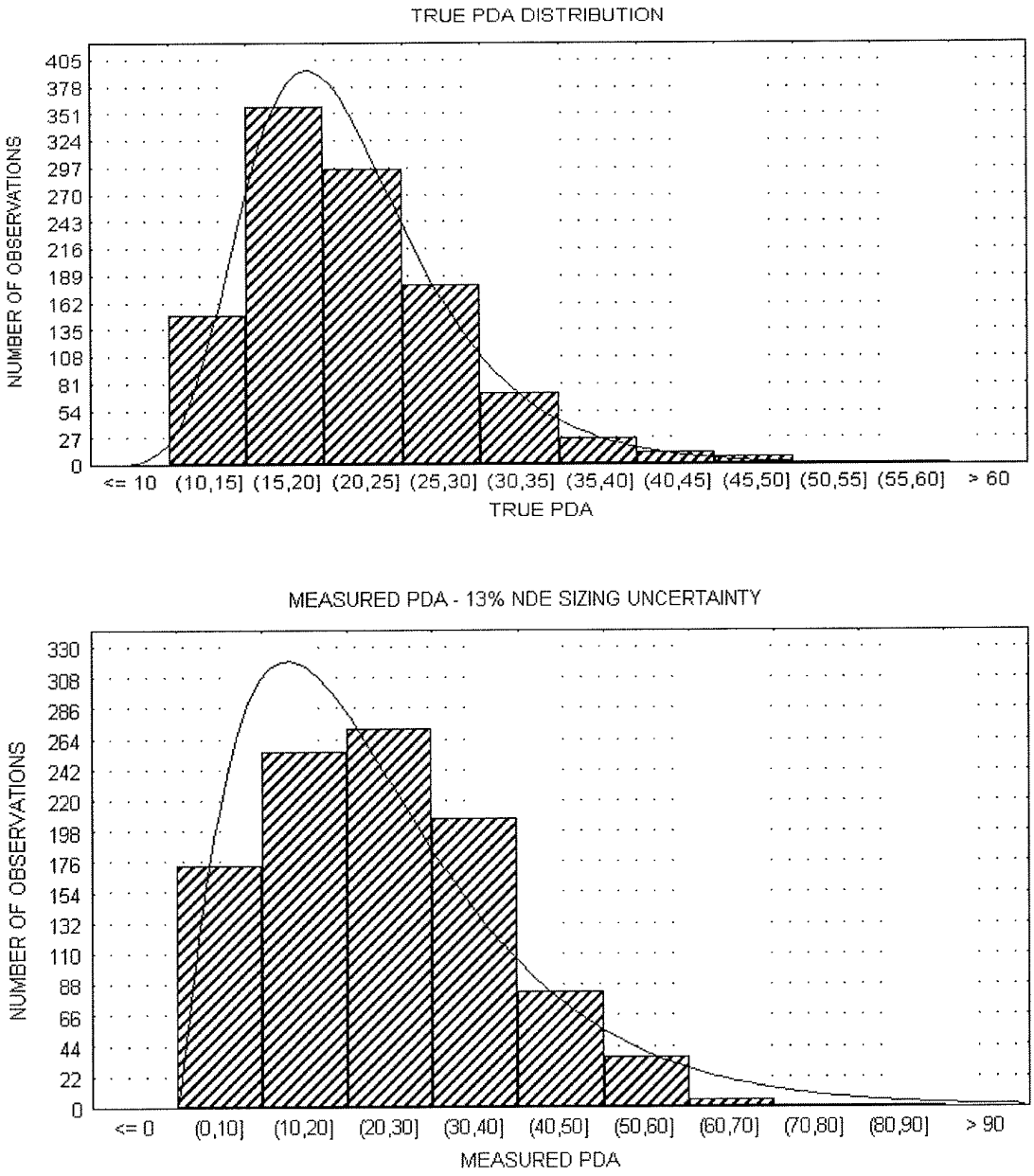

Figure 8-1
Comparison of True and Measured PDA Distributions

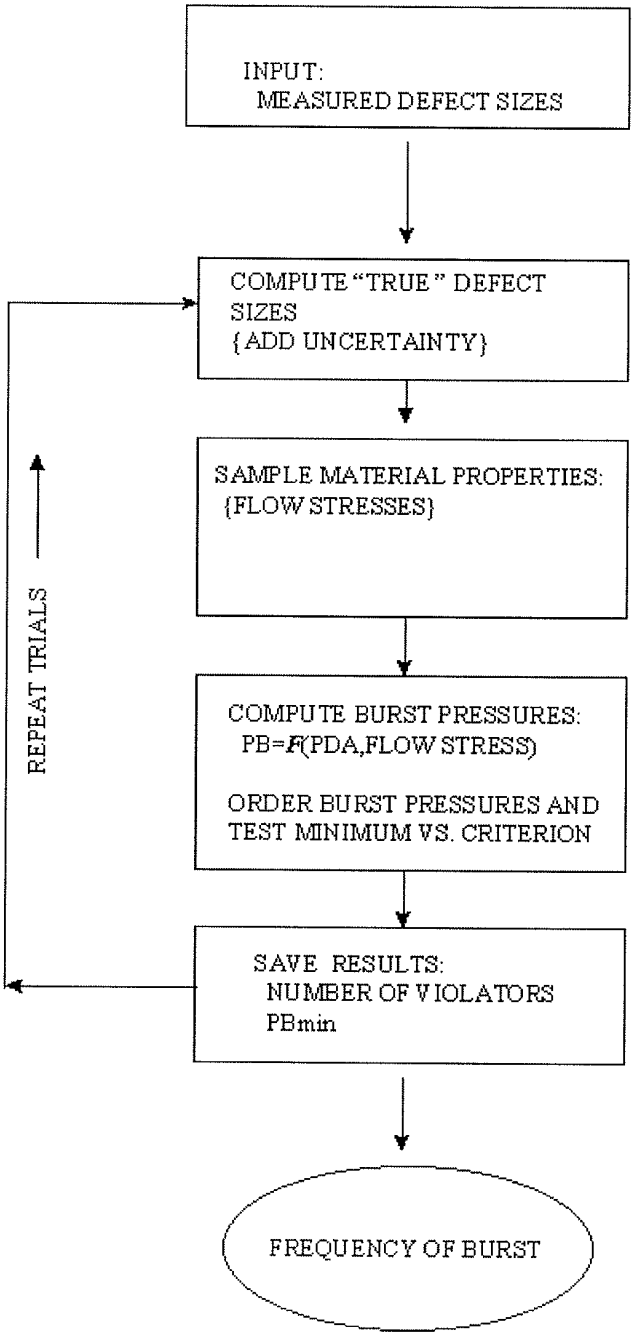

Figure 8-2
Flow Chart for Direct Method Condition Monitoring

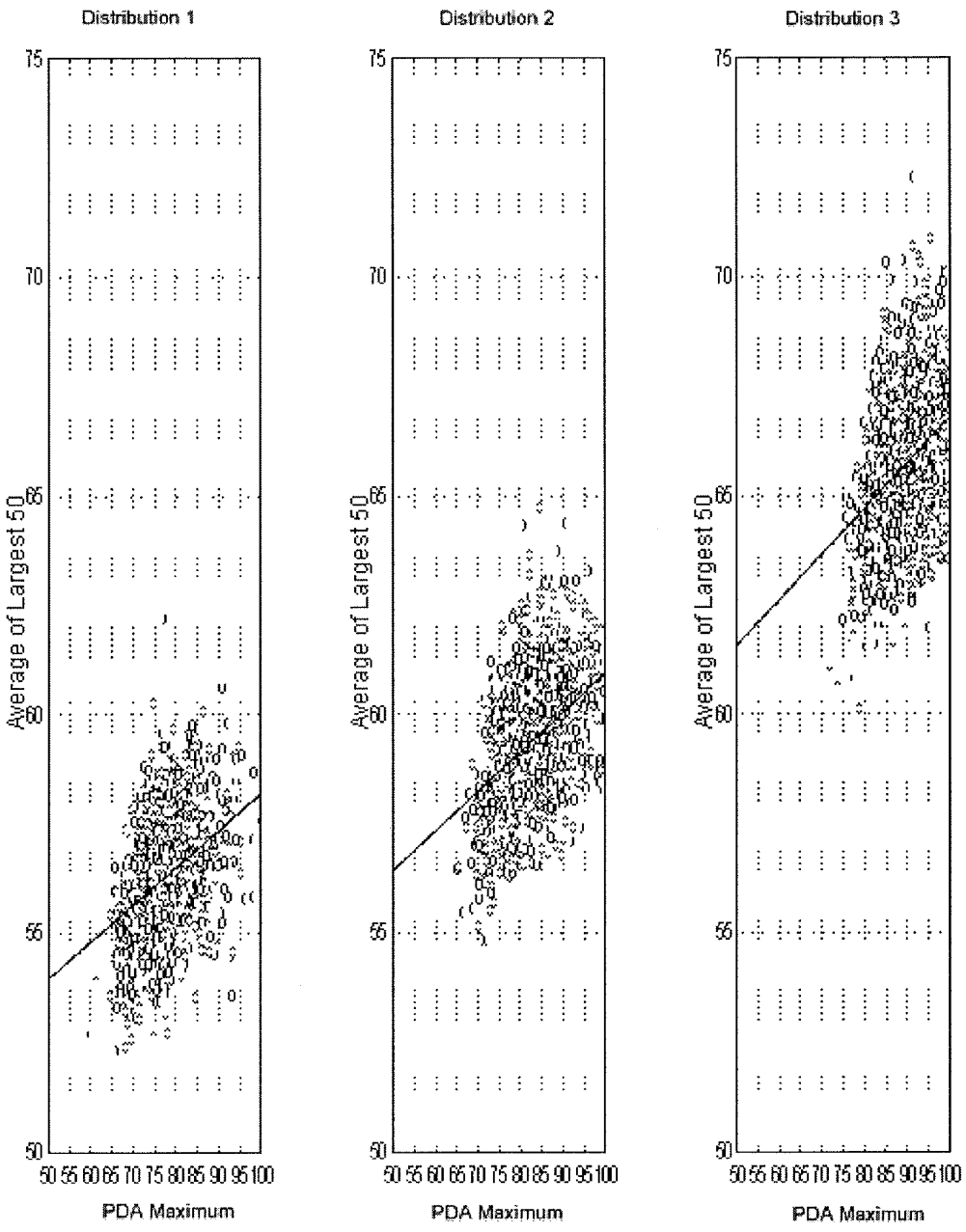

Figure 8-3
Training Sets For Discriminant Analysis

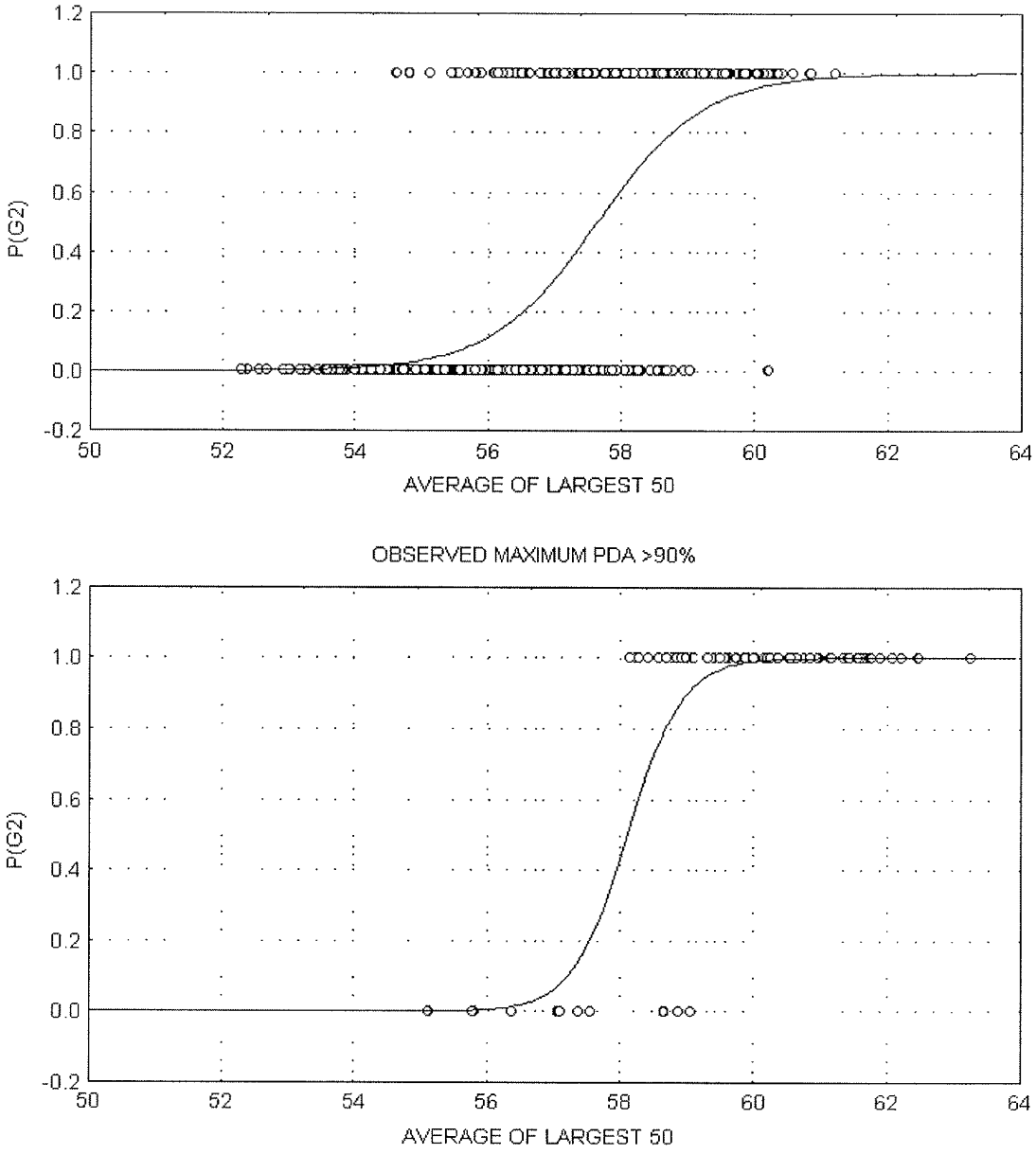

Figure 8-4
Probability of data belonging to Adverse Population as function of upper order Statistic Observed largest PDA <75%

9

LEAK AND BURST ASSESSMENT METHODS FOR PROJECTED EOC CONDITIONS

This section describes the elements of a single-cycle process for the evaluation of burst and leak rate probabilities for a steam generator affected by circumferential cracking. In addition, examples are provided illustrating the application of the process to the evaluation of burst probability and leak rates for a relatively severe situation in which several hundreds of defects are present.

The basic single-cycle process has been extensively used for the evaluation of ODSCC at TSP intersections (Reference 9-1). The methodology developed in this document for circumferential cracks differs from that in Reference 9-1 in two principal ways. The first is the ability to model the undetected portion of the defect population using a size dependent probability of detection (POD). The increased complexity of this approach is warranted based on the work described in Section 5.8 of this report. A significant gain in available margin for defect growth is achieved with the incorporation of this feature which provides a more realistic assessment of the BOC defect state in the generator.

A second major difference between the circumferential cracking methodology and that in Reference 9-1 is in the treatment of NDE sizing uncertainty. This contrast reflects fundamental differences in the basic predictive approaches for the two situations. In the case of ODSCC at TSP intersections, the burst probability is obtained using a correlation relating burst pressure to NDE voltage. The component of variance which dominates this computation is related to the correlation uncertainties. The uncertainties associated directly with the NDE voltage measurement are small compared to depth sizing and the specifics of their treatment has less impact on the probabilistic assessments which are dominated by the correlation uncertainties.

The current models describing burst and leakage for circumferential cracks (see Sections 6 and 7) are physically based and have relatively small components of variance associated with modeling or correlation uncertainties. The impact of NDE measurement uncertainties, specifically regarding defect sizing, dominate the probabilistic computations. The treatment of this component of uncertainty is very critical in the probabilistic computations for circumferential cracks. Consequently, significant attention has been given to the way in which this component of uncertainty has been embedded in the circumferential cracking evaluation process.

The basic elements in the evaluation process for circumferential cracking include:

- Modeling of the BOC defect population
- Projection of the defects to EOC conditions
- Evaluation of burst probability under SLB conditions
- Evaluation of leak rate probability under SLB conditions

9.1 Development of BOC Distributions

The first step in a single-cycle evaluation process is the development of the BOC (beginning-of-cycle) defect distribution. This distribution characterizes the initial condition for the steam generator in terms of defect population. The complete set of defects in the BOC population consists of two subpopulations as shown in Figure 9-1. The first of these is made up of unrepaired defects which have been left in service (arc only). These are a subset of the measured defect population from the previous operating cycle. The size of this subpopulation is known as is the measured PDA value associated with each defect.

The second subpopulation consists of defects which were undetected at the end of the previous operating cycle. None of the attributes of this subpopulation can be directly measured. As shown in Figure 9-1, the subpopulation size and distributional character must be inferred from information regarding the observed (detected and measured) population and in POD function.

The process of determining the size and distribution of this subpopulation of "hidden" defects is the core process in the probabilistic evaluation model. The characterization of the BOC hidden population is one of a class of inverse probabilistic problems for which indirect solutions are required. The problem is best understood in terms of an idealized process involving a conceptual population of true defect depths as shown in Figure 9-2. This allows a straightforward examination of the processes involved using direct simulation methods.

9.1.1 Inspection and Measurement Effects

Figure 9-2 illustrates qualitatively the effects of detection and measurement on an idealized defect population. In essence, the observed defect population is the result of a sorting and distortion process on a larger true/total defect population.

The first operation on the true distribution of defect depths is a probabilistic sorting process resulting from a depth dependent POD function (Figure 9-3). This operation

splits the true/total population into true/detected and true/hidden subpopulations. In the case of a constant POD, the two subpopulations are identically distributed with relative numbers of defects determined by the POD value which is typically on the order of 60%. In the case of a depth dependent POD, the two subpopulations are no longer identically distributed. The increased POD at higher defect depths results in a shift of the detected subpopulation to the right and the undetected subpopulation to the left. This can be seen in Figure 9-2. In this sense it can be seen that a monotonically increasing POD as a function of depth results in a detected subpopulation more adverse in the distributional sense than the hidden subpopulation.

The true/detected subpopulation is subjected to an additional process, that of depth measurement. In the case of circumferential cracking, the depth sizing error is substantial (>13% PDA). The effect of the error addition part of the process is to broaden the distribution of the true/detected subpopulation into the measured/detected subpopulation as shown in Figure 9-2. This is typical of a process where a random measurement error component is present.

The broadening effect of measurement on a distribution can be illustrated using a component of variance argument. In the absence of systematic bias, the principal effect of measurement on a distributional quantity is to add a component of variance to that quantity. Figure 9-4 illustrates this for a simple case in which the true distribution and measurement error are both normally distributed. In this situation the measured distribution can be constructed by direct simulation:

$$Xm_i = Xt_i + N_i\sigma_m \qquad \text{(eq. 9-1)}$$

where: Xm_i = ith measured value

Xt_i = ith true value

N_i = ith normal standard deviate

σ_m = measurement error.

Alternatively, the measured distribution can be obtained parametrically by adding a component of variance to the true distribution.

$$\overline{Xm} = \overline{Xt}$$

$$\sigma_m = \sqrt{\sigma_t^2 - \sigma_c^2}$$

where:

$\overline{X}m$ = *mean of measured distribution*

$\overline{X}t$ = *mean of true distribution*

σm = *standard deviation of measured distribution*

σt = *standard deviation of true distribution*

σe = *measurement error*

As seen in Figure 9-4, both the direct simulation (eq. 9-1) and parametric estimation process produce the same measured distribution. For this simple example, the parametric process can be applied to the inverse problem where the measured values are known and the true distribution, without measurement error, is desired.

In this case:

$$\overline{X}t = \overline{X}m$$

$$\sigma t = \sqrt{\sigma m^2 - \sigma e^2}$$

It is important to note that the direct simulation of eq. 9-1 *cannot* be used to obtain the true distribution. The result of the direct simulation process is always to increase the variance of the dependent variable no matter how the equation is recast. The obviously incorrect result of this application is a process by which the measurement error results in an apparent reduction of uncertainty in the measured distribution by comparison with the true distribution.

Unfortunately, the parametric process for establishing the true distribution in the presence of a known measurement error is not generally appropriate for non-normal distributions such as those typical of observed depths for circumferential cracks. For this application indirect methods are required.

As shown in Figure 9-2, the measured defect depth distribution can be obtained for any true distribution if the POD, and measurement uncertainties are known. In developing a procedure for the establishment of a BOC depth population, a process qualification approach has been taken in which the direct simulation approach is used to validate the BOC population characterization process. In essence, the procedure in Figure 9-2 is augmented by a simulation of the BOC population characterization process. Since the character of the true hidden population is known in the simulation, a direct comparison can be made between the true and inferred BOC populations for any situation of interest. The process is shown conceptually in Figure 9-5.

9.1.2 Procedure for BOC PDA Distribution

Of the four distribution functions discussed in Section 9.1.1, only the detected/measured distribution of PDA values is available to the analyst. This data in conjunction with knowledge of the uncertainty in the measurement process and the nature of the POD function must provide the basis for inferring the "hidden" BOC PDA distribution. Conceptually, this process involves two inverse operations on the measured/detected data. The first is a removal of the measurement uncertainty from the data, the second operation is the inverse version of the detection process in which the undetected defects corresponding to each detected defect are characterized.

The inverse POD process is straightforward. Consider a set of N measured PDA values [DM_1, DM_2 ... DM_i, ... DM_N] representing the inspection results. There will be a set of "true" PDA values corresponding to the detected set given by:

[D1, D2, ... Di, ... DN]

where: DMi =Di + E

E = Measurement Error

Corresponding to each true PDA value (Di), there exists a probability of detection value (PODi). This implies that for each defect detected and measured, there exists JI hidden defects where:

$$Ji = 1/PODi - 1$$

$$[0, 1, 2, 3 \ldots] \qquad \text{(eq. 9-2)}$$

For a set of detected PDA values, Ji can be evaluated using a series of binomial trials as shown in Figure 9-6. This permits construction of a hidden population consisting of N groups each having identical within-group PDA values. The total number of groups corresponds to the number of defects detected. It should be noted that a group can have a zero membership which is usually the case for higher POD situations.

The process has been tested by simulation using the logic of Figure 9-5 for the case of zero measurement uncertainty. The true undetected population [UD1, UD2 ... UDM] is compared with that obtained using the above process [UDS1, UDS2 ... UDSMS].

Three figures of merit are used in the comparison. The first is the ratio of the predicted undetected population size (MS) to that of the true size (M). The second figure of merit is the ratio of the largest PDA value in the synthesized population to that of the largest in the true undetected population. The third figure of merit is the ratio of the Nth

largest PDA values for the synthesized and true populations where the Nth largest value is the 95th percentile of the true distribution order statistic. Table 9-1 shows the comparison of true and synthesized undetected populations for a simulation of 1000 trials. The values shown in the table are means and standard deviations of the specific figure of merit. A value greater than 1.0 indicates that on average the inverse process produces a sample with a more adverse characteristic. As can be seen, the process provides best estimates of the characteristics of the undetected population.

The case of a non-zero NDE measurement uncertainty produces a measured/detected population that differs from the true detected population. The addition of variance as part of the measurement process results in a broadened distribution. This measured distribution (DM) can be used as a surrogate for the true distribution in conjunction with the inverse POD process to infer the hidden population. As would be expected, the distortion caused by measurement error results in biased estimates of the characteristics of the undetected population. A comparison of the true and synthesized undetected populations is shown in Table 9-2 for 5%, 13%, and 20% additive NDE measurement uncertainties. Each of these cases consisted of 1000 trials. The true/total distribution for each case was a Gamma with a shape parameter of 3 and a scale parameter of 5. The sampling distribution is shown in cumulative form in Figure 9-6. As can be seen from Table 9-2, the procedure of using the measured/detected PDA population to infer the characteristics of the hidden population provides a generally conservative estimate for the upper tail of hidden population. The degree of conservatism in terms of the 95th percentile and the extreme value increases with the magnitude of the uncertainty as shown in Figure 9-7.

9.1.3 Process Qualification for BOC PDA Distribution

The process for inferring the undetected BOC population has been shown to be conservatively biased by the presence of measurement uncertainty for a reasonable choice of underlying PDA distribution. A more extensive process qualification using a wide range of Gamma distributions and population sizes was undertaken. The range of parameters used in the study is given in Table 9-3. Cases were run parametrically in uncertainty level and consisted of 10,000 trials each. The domain of the underlying PDA distributions is shown in Figure 9-8 in CDF form.

The results of the process qualification are consistent with the more limited study performed in the previous section. The agreement between the distributional parameters (maximum PDA and 95% PDA) for the synthesized and true undetected populations, is insensitive to the underlying distribution. This can be seen in Figures 9-9 and 9-10 which show the parameters as functions of the median of the underlying PDA distribution. The same is not true, however, for the prediction of undetected population size. Figure 9-11 shows a distinct systematic behavior with the median of the underlying PDA distribution. It should be noted that this trend

disappears as the additive NDE uncertainty goes to zero. It should also be noted that the process *over predicts* the size of the undetected population, as the underlying PDA distribution becomes more adverse.

The cumulative distribution function (CDF) of the ratio of synthesized maximum PDA to true maximum PDA is shown in Figure 9-12 for the 13% NDE uncertainty case. In only 20% of the cases is the extreme PDA generated from the detected/measured population less than the true maximum undetected PDA.

The CDF of a similar ratio involving the 95th percentile order statistic is shown in Figure 9-13. A similar level of conservatism is present regarding the proportion of synthesized samples with less adverse tails beyond the 95th percentile.

The process qualification study leads to the following conclusions:

- The measured PDA distribution [DM] can be used to synthesize a surrogate [UDS] for the undetected population [UD]. (See Figures 9-5, 9-6.)
- The presence of an additive/size-independent NDE measurement uncertainty will result in [UDS] probabilistically more adverse than [UD].
- The relative conservatism of the synthesized undetected PDA distribution increases with the level of NDE uncertainty.

9.1.4 Including Defects Left in Service

The hidden population [UDS] can be augmented by a subset of the measured/detected population [DM] to form the total BOC population of defects. Presumably, the subset to be left in service will be chosen by PDA value. The presence of NDE uncertainty requires adjustment of the subset of the measured/detected population chosen to be left in service. The simplest procedure in this situation is to add the NDE uncertainty to the measured values [DM]. This is, of course, double accounting, but should have little impact for reasonable repair thresholds. The total BOC PDA distribution is simply the total membership of the two arrays.

9.2 Development of EOC Distribution for PDA

The end-of-cycle (EOC) distribution of PDA is inferred from the BOC PDA distribution as developed in the previous discussion, in conjunction with a random sample of defect growth rates developed from evaluation of plant data:

$$PDA_{eoc,i} = PDA_{boc,i} + G_i \Delta T \qquad \text{(eq. 9-3)}$$

where: $PDA_{eoc,i}$ = EOC PDA for i^{th} defect

$PDA_{boc,i}$ = BOC PDA for ith defect

G_i = random growth rate for ith defect

ΔT = cycle length

The process of evaluation of the EOC PDA distribution is assumed to utilize direct Monte-Carlo simulation of eq. 9-3. The EOC distribution for a given trial will be equal in size to the BOC population (undetected + unrepaired).

The growth rates are treated probabilistically in the EOC simulation. For each defect, a random value of growth rate is obtained from a growth rate sampling distribution without regard to the BOC PDA value for that defect. The selection of growth rates can be accomplished in at least two ways:

- Sampling with replacement from a set of growth rate values
- Sampling from a piecewise continuous or analytical CDF.

It should be noted that data obtained from field NDA examinations often has a significant percentage of apparently negative growth rates. In such a situation the negative values should be treated in the simulation as zero growth. Figure 9-14 shows a typical CDF for PDA growth rate in plants with explosive expansion transitions.

At this point in the simulation, the basic physical characterization of the circumferential defects is complete in terms of having the information necessary to predict structural and leakage integrity for a given period of operation. The EOC PDA value for a given defect is the basic characterization factor for both burst and leakage.

9.3 Structural Integrity Projections

The burst pressure for a circumferential crack has been shown to be bounded by a relatively simple function of PDA, material flow stress, and tube geometry (Reference 9-2). For a given defect:

$$PB_i = F\left(PDA_{eoc,i}, S_i\right) \qquad \text{(eq. 9-4)}$$

Where: Pb_i = burst pressure of i^{th} defect

F = functional form of burst equation (Section 6)

$PDA_{eoc,I}$ = PDA of i^{th} defect at EOC

S_i = randomized sum of yield and ultimate strength at temperature of interest

At this point in the simulation, burst pressures are computed for each of the defects originally present at BOC. This allows a direct assessment of the number of defects with burst pressures less than some chosen criteria.

Figure 9-15 shows a conceptual flow chart of the simulation process for structural integrity projections. The entire process is repeated 10,000 times to assess the probability of tube burst. Equation 5-32 of Reference 9-1 can be used to obtain high confidence estimates of burst probability.

It should be noted that the example methodology used a lower limit burst equation and accounted for the uncertainty in the material strength. Hence, there are no modeling or correlation uncertainties present. The large uncertainties in the example are due solely to the uncertainties associated with the PDA. In actual practice, the burst pressure versus PDA correlations would also be simulated, and as demonstrated in Section 6, the probabilities of burst would be expected to be very small.

9.3.1 Example SLB Burst Probability Analysis

The process described in Figure 9-15 was used in the analysis of a representative test case for a plant with active circumferential cracking. The previous cycle EOC PDA measurements used in the analysis are shown in Figure 9-16 in histogram form. The growth rates, POD function, and material properties used in the analysis are shown in Figures 9-14, 9-3, and 9-17 respectively.

The typical EOC PDA distribution for this case is shown for a 1.5 EFPY operating period in Figure 9-18. The minimum burst pressure distribution for 10,000 trials is shown in Figure 9-19 for the 1.5 EFPY operating period.

The most important result which is the probability of burst as a function of operating time is shown in Figure 9-20. Figure 9-20 also shows the effect of ARC level on probability of burst. As can be seen from the figure, the 13% NDE uncertainty results in a dominance of the unrepaired subpopulation as a risk contributor. For this example, a 20% PDA repair limit would permit a 1.25 EFPY operating cycle and satisfy a 10^{-2} burst probability.

9.4 Leakage Integrity Evaluation

The final element in the circumferential cracking simulation is the evaluation of leakage from the defect population. A detailed description of the leakage model for an individual defect is given in Section 7.

Unlike the computation of burst pressure, the leakage computation for circumferential cracks is functionally complex. The EOC PDA distribution does, however, remain the basic defining quantity. For each EOC PDA value in a given Monte-Carlo trial a basic probability of leakage can be computed. On the basis of a single binomial trial for each defect, potential leakers are identified for further analysis. Virtually any size crack can, in fact, leak (see Figure 7-14).

The group of defects in a given trial determined to be leakers are processed per Section 7 to determine the individual and cumulative leak rates under SLB conditions. The cumulative leak rate for each Monte-Carlo trial is saved to construct the distribution function for total leak rate under SLB conditions.

9.4.1 Example SLB Leakage Evaluation

The example case described in Section 9.3.1 was extended to the evaluation of leakage under SLB conditions. The distributions of total leak rate as predicted by the Monte Carlo leak rate simulation, are shown in Figure 9-21 for three operating periods. A leak rate of 4.5 gpm at 95% cumulative probability is obtained for operating cycles up to 1.5 EFPY.

9.5 References

9-1 Keating, R. F., "SLB Leak Rate and Tube Burst Probability Analysis Methods for ODSCC at TSP Intersections," Westinghouse Electric Corporation, Report WCAP-14277, December, 1996.

9-2 Begley, C.J., Woodman, B.W., Begley, J.A., "A Probabilistic Operational Assessment of Steam Generator Tube Degradation at SONGS Unit 2 for Cycle 9," Aptech Engineering Services, Inc., report AES 97043057-1-1, September, 1997.

Table 9-1
BOC PDA Inference Process
(Zero NDE Uncertainty)

	Mean	Std. Deviation
N_{SYN}/N_{TRUE}	1.0007	.1084
$PDA_{95/SYN}/PDA_{95/TRUE}$	.9999	0529
$PDA_{MAX/SYN}/PDA_{MAX/TRUE}$	1.0117	.1648

Table 9-2
BOC PDA Inference Process: Effect of Uncertainty

NDE Error - %PDA

	5	13	20
N_{SYN}/N_{TRUE}	1.25	1.36	1.22
$PDA_{95/SYN}/PDA_{95/TRUE}$	1.014	1.056	1.076
$PDA_{MAX/SYN}/PDA_{MAX/TRUE}$	1.034	1.164	1.304

Typical True PDA Distribution

Table 9-3
Process Qualification Study Input

	MIN	MAX
Gamma-Shape	1.5	6.5
Gamma-Scale	3	6
Population Size	300	1500
NDE Uncertainty	0	20 % PDA

Table 9-4
Process Qualification Results

NDE Error - % PDA

	0	5	13	20
N_{SYN}/N_{TRUE}	1.005	1.23	1.56	1.54
$PDA_{95/SYN}/PDA_{95/TRUE}$	1.0014	1.017	1.06	1.08
$PDA_{MAX/SYN}/PDA_{MAX/TRUE}$	1.012	1.035	1.169	1.30

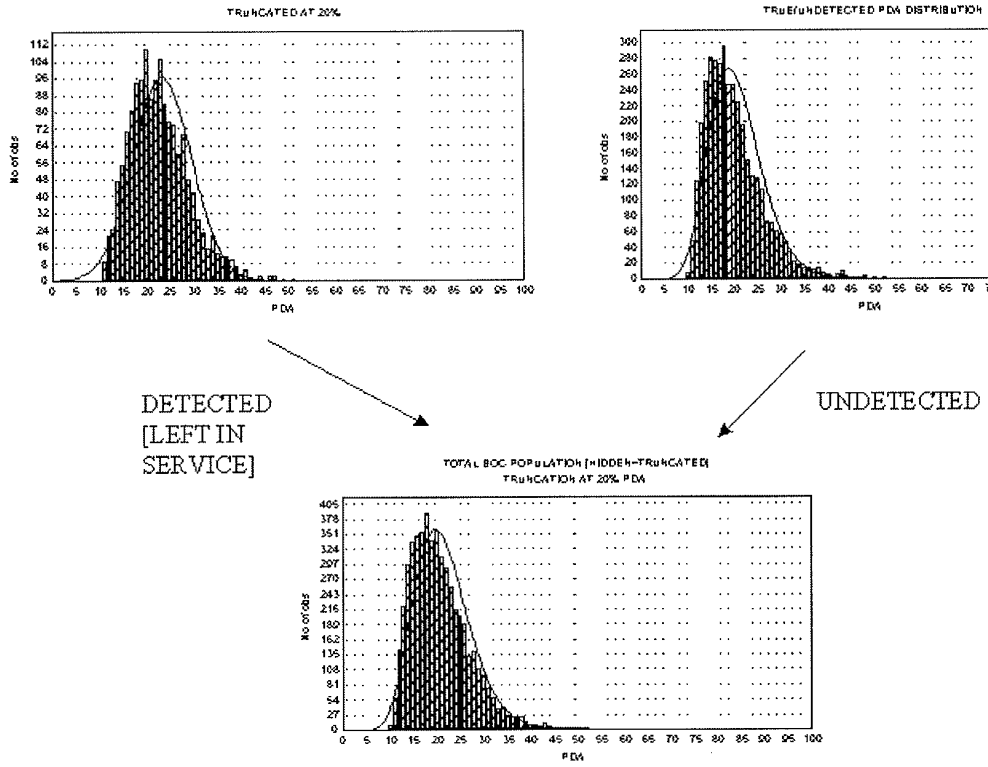

Figure 9-1
Components of BOC PDA Distribution

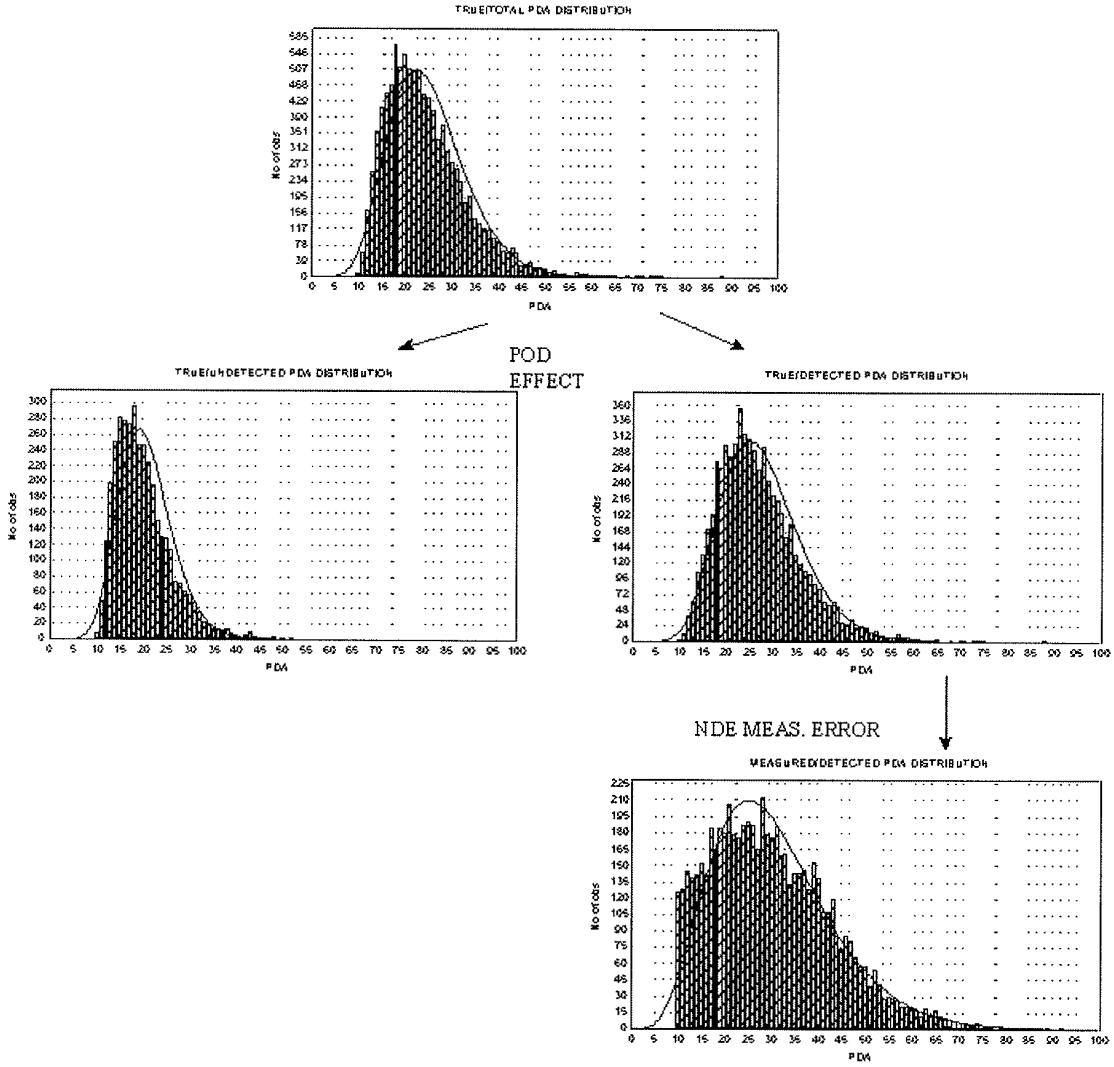

Figure 9-2
Detection and Measurement Effects

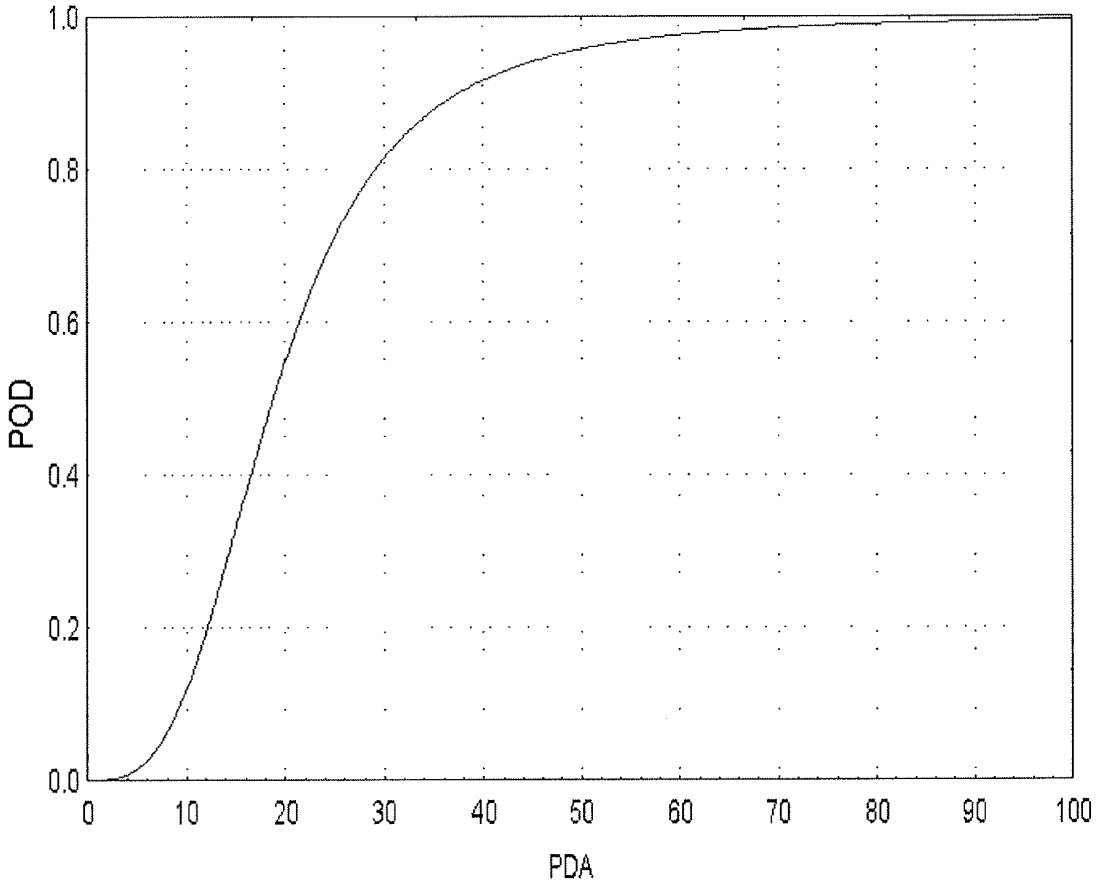

Figure 9-3
POD Function for Circumferential Cracks

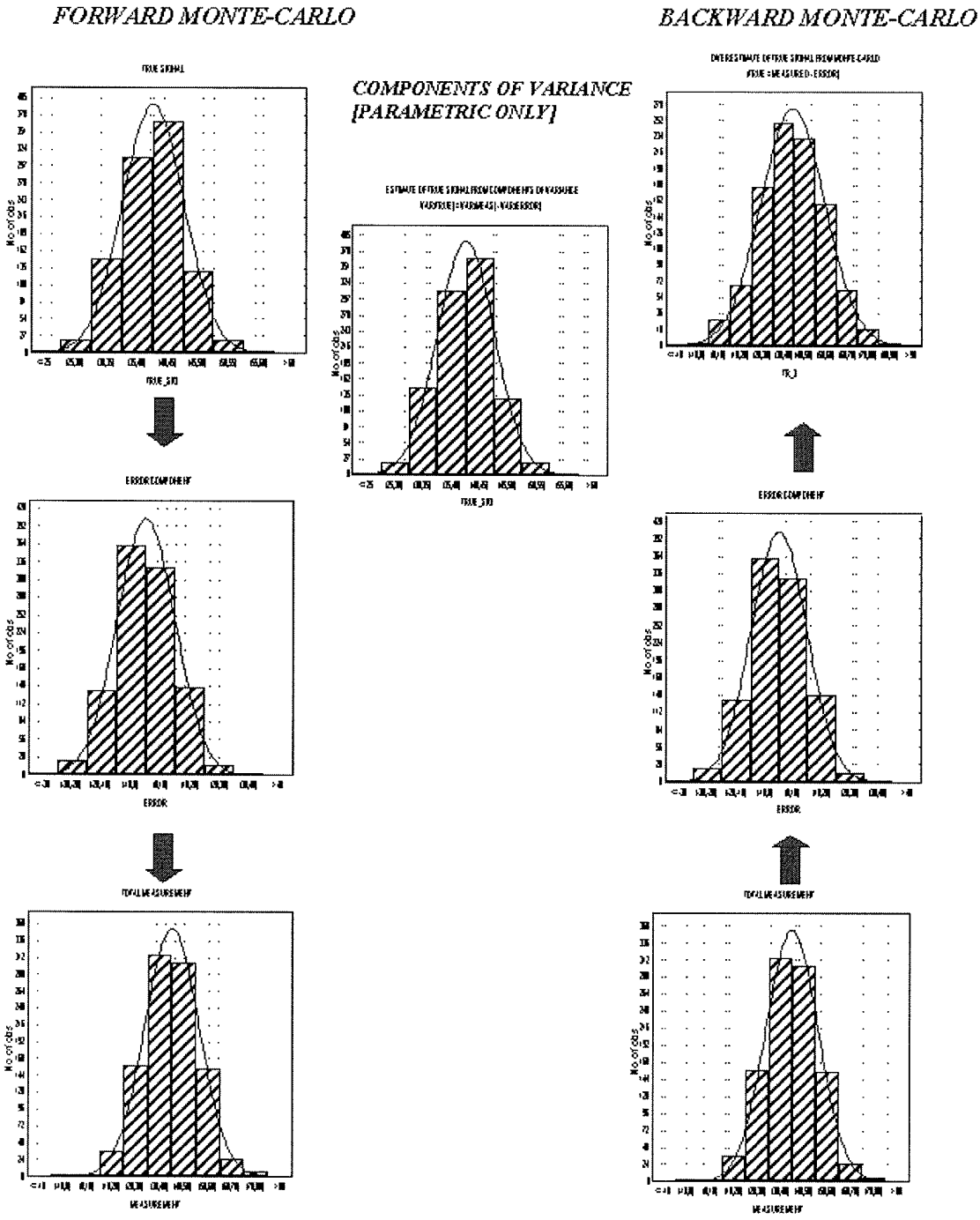

Figure 9-4
Components of Variance [Parametric Only]

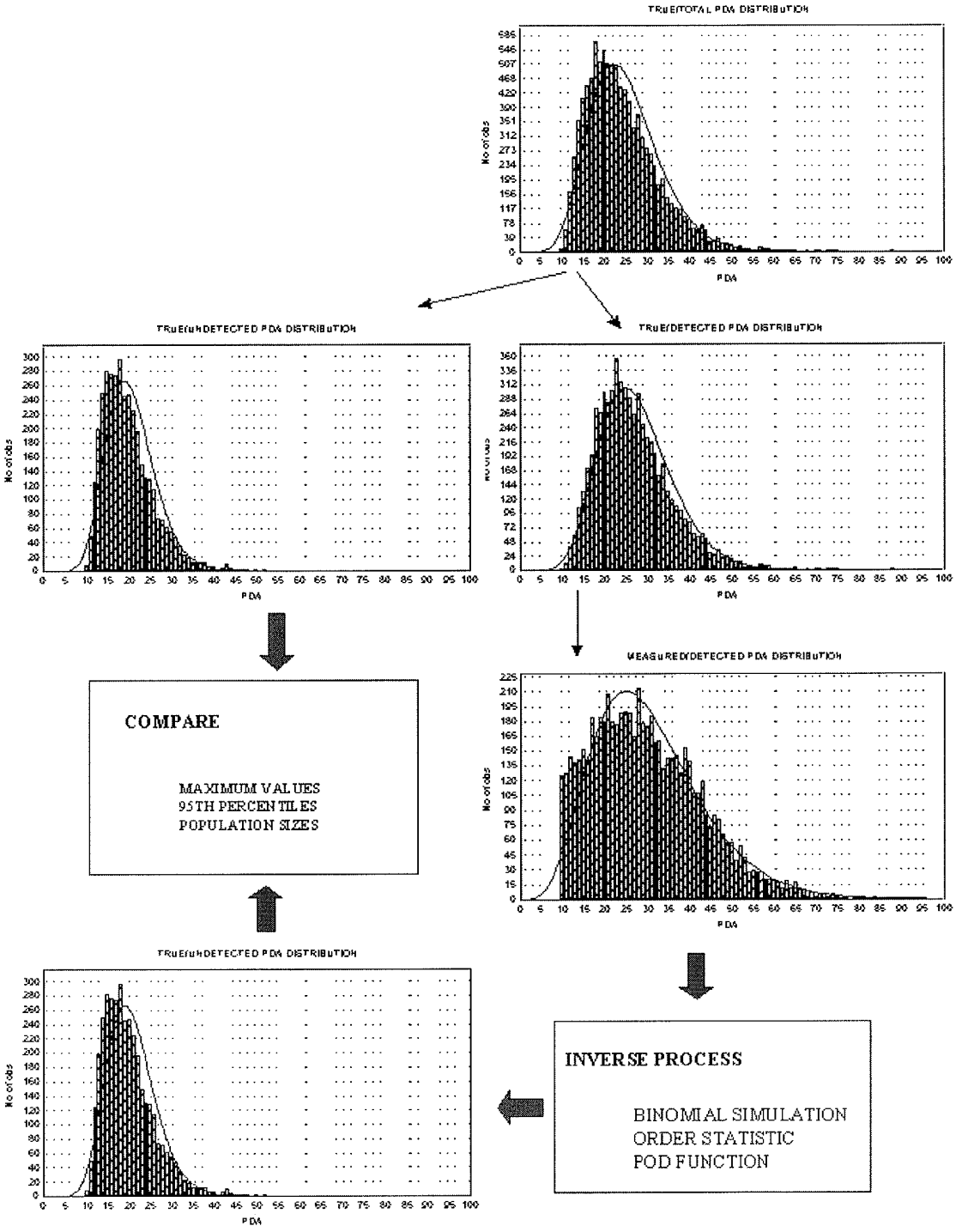

Figure 9-5
Logic for BOC Synthesis

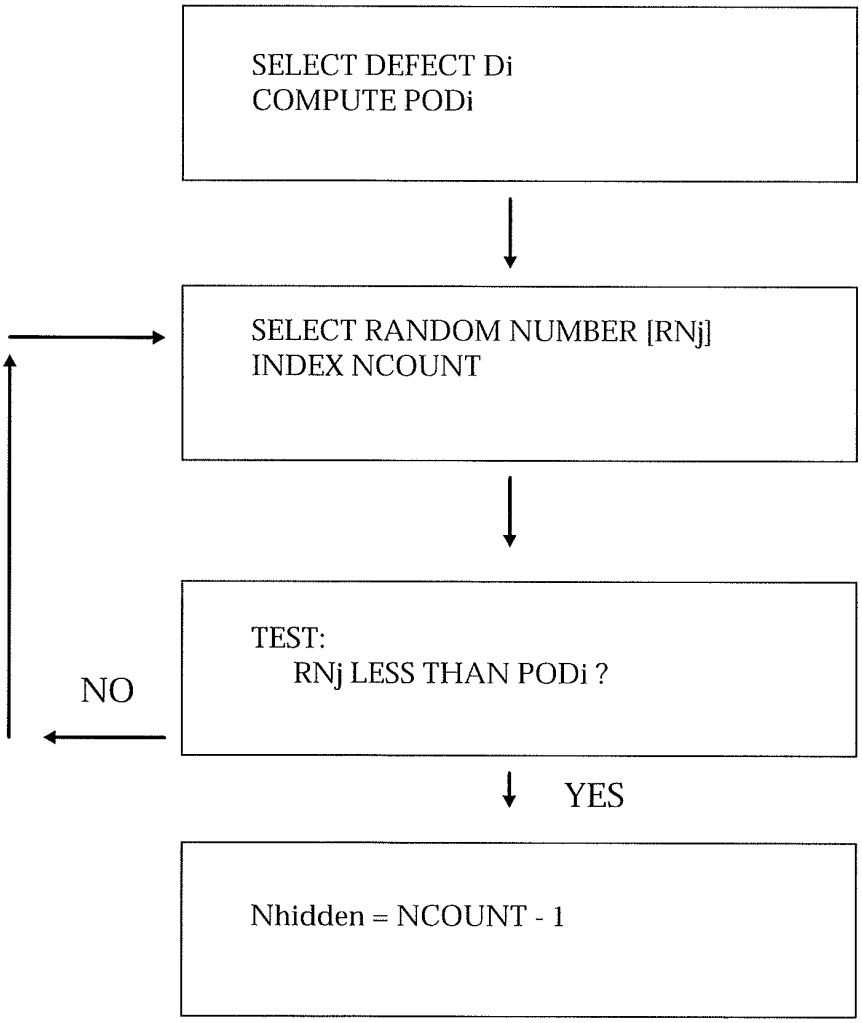

Figure 9-6
Logic Chart for Inverse Detection

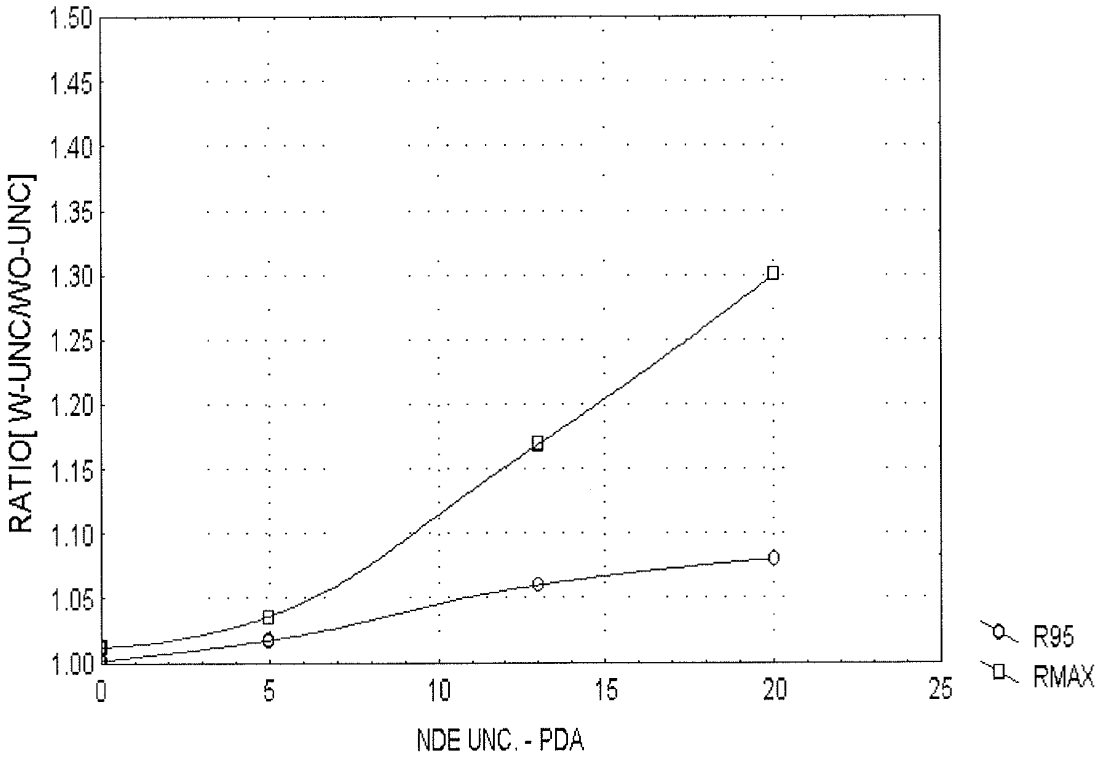

Figure 9-7
Effect of NDE Uncertainty on Prediction of Hidden Population Attributes

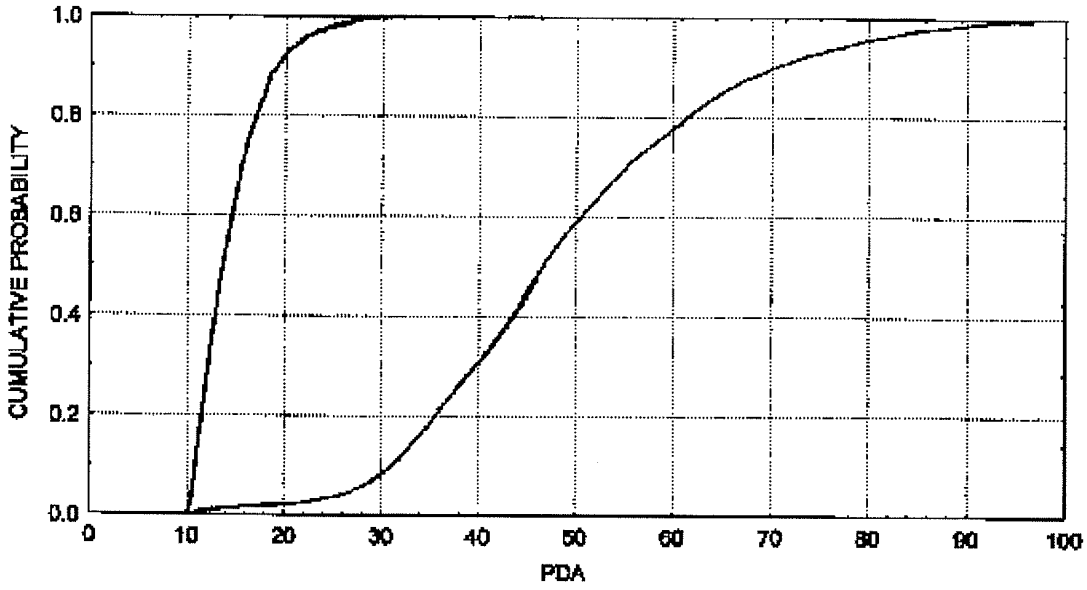

Figure 9-8
Domain of CDF's for Process Qualification

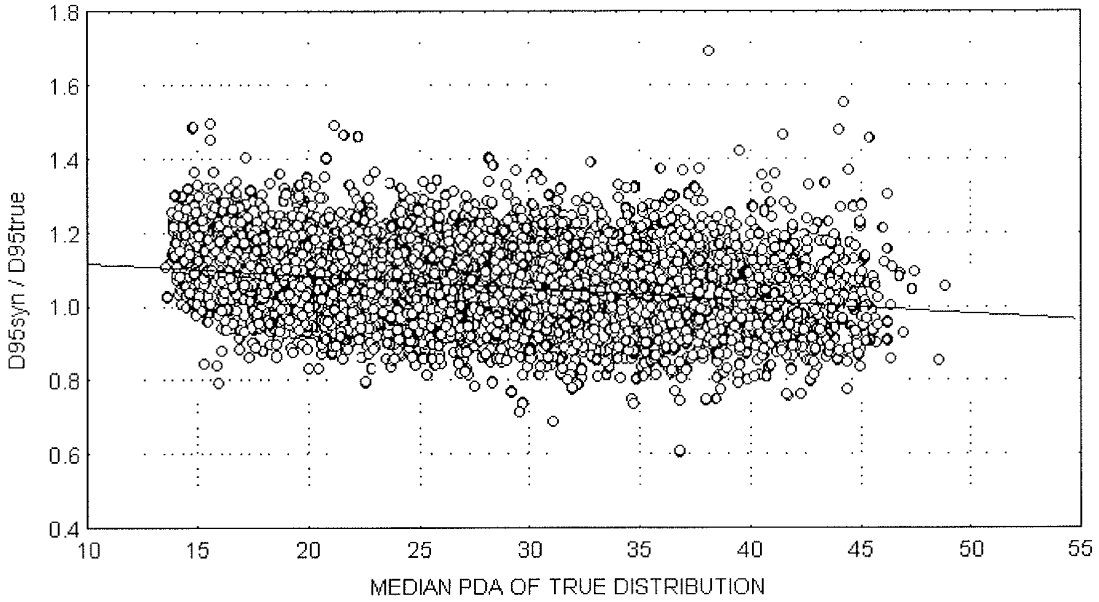

Figure 9-9
Ratio of 95th Percentiles VS Median of True Distribution

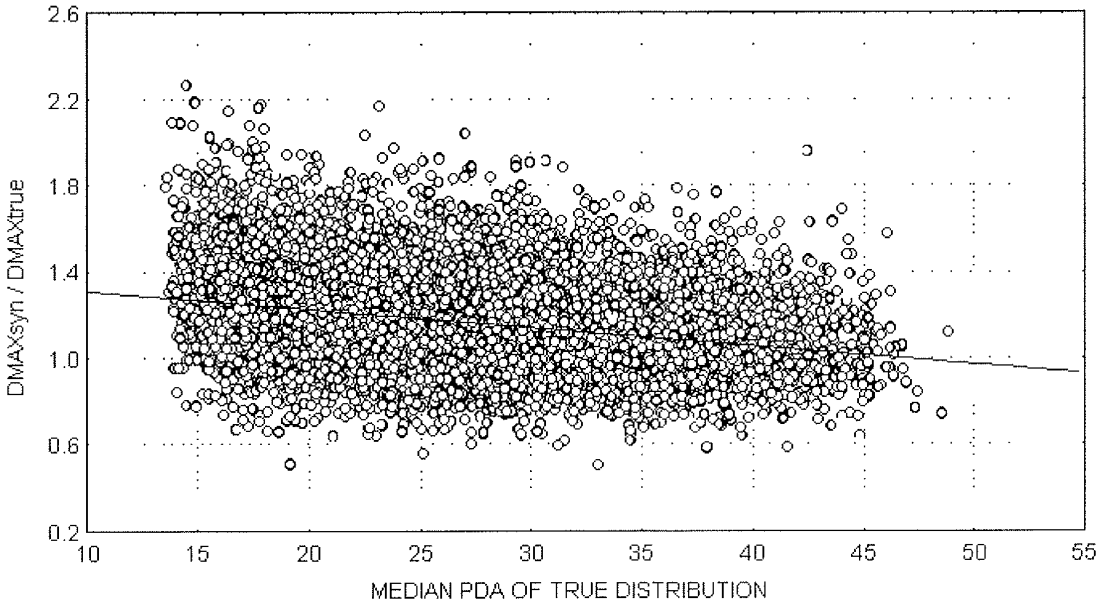

Figure 9-10
Ratio of Maximum Values VS Median of True Distribution

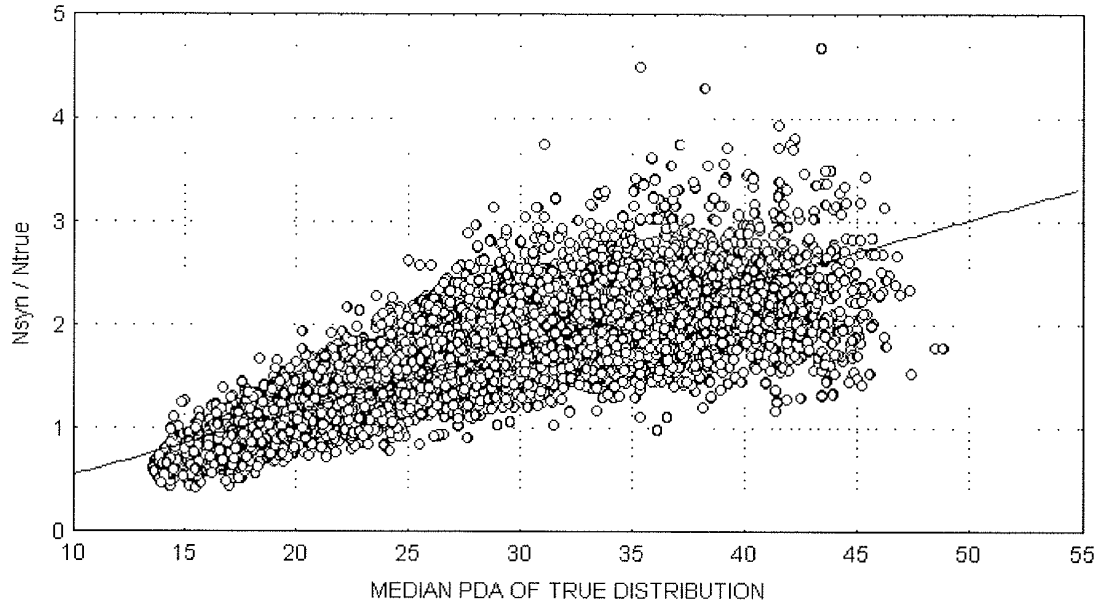

Figure 9-11
Population Size Ratio VS Median of True Distribution

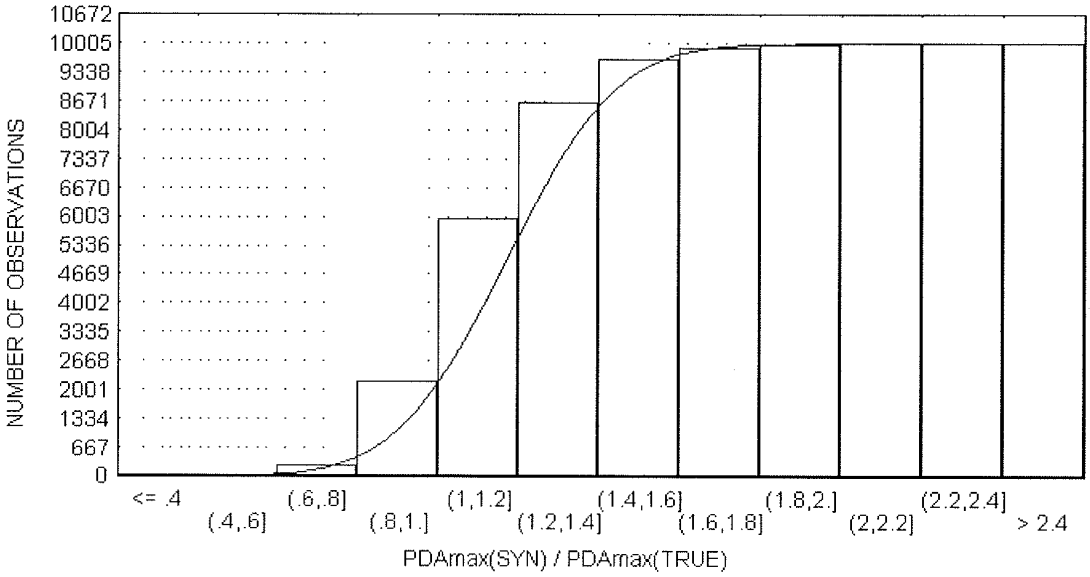

Figure 9-12
CDF of PDA Maxima Ratio
13% NDE Uncertainty

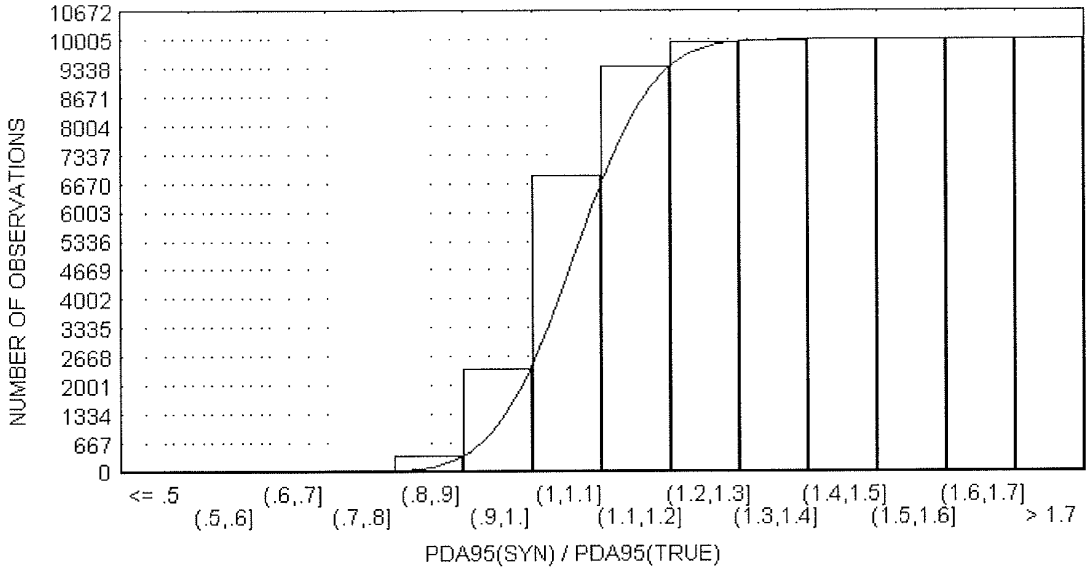

Figure 9-13
CDF of PDA 95% Ratio
13% NDE Uncertainty

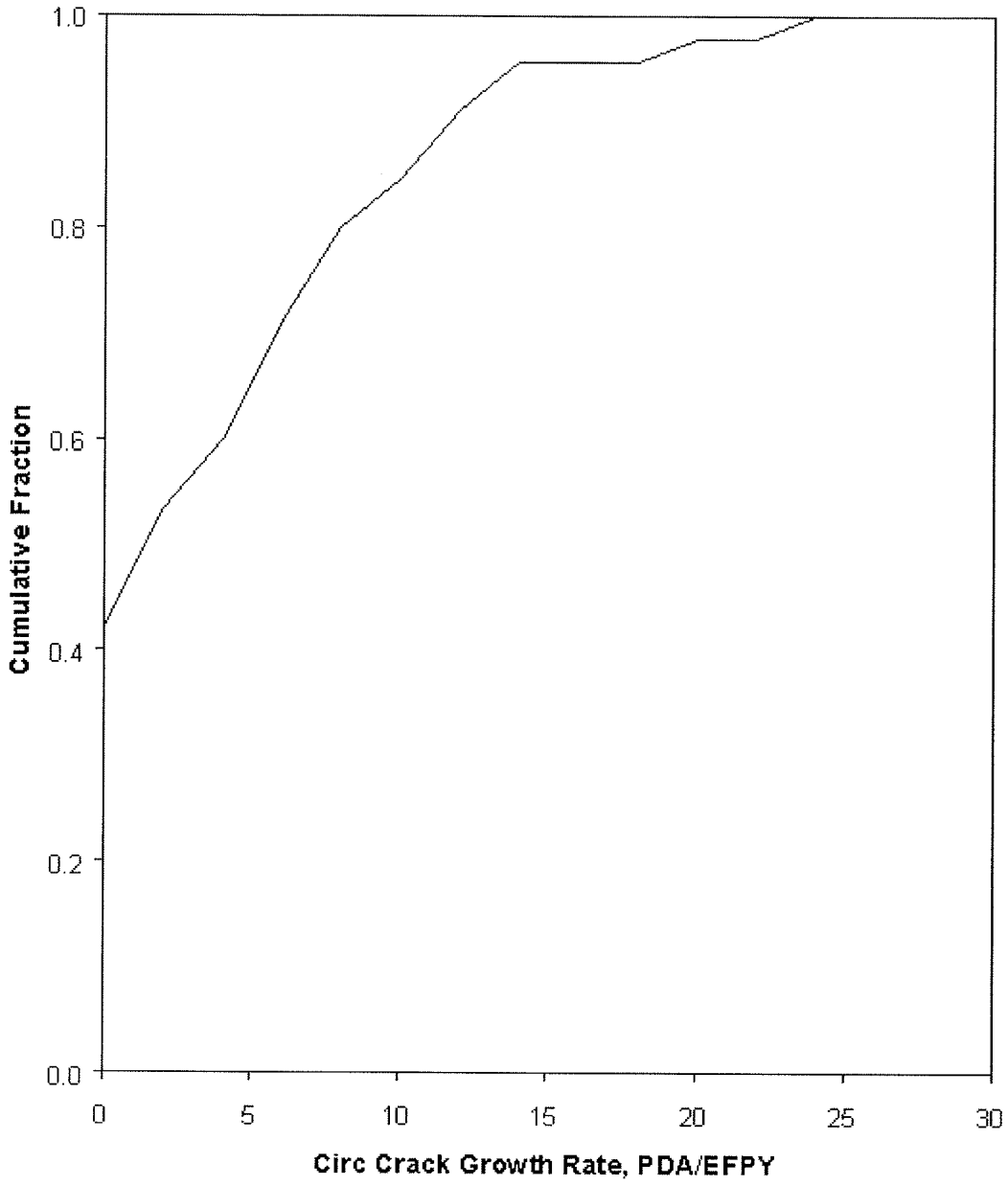

Figure 9-14
PDA Growth Rates for Explosive Expansions

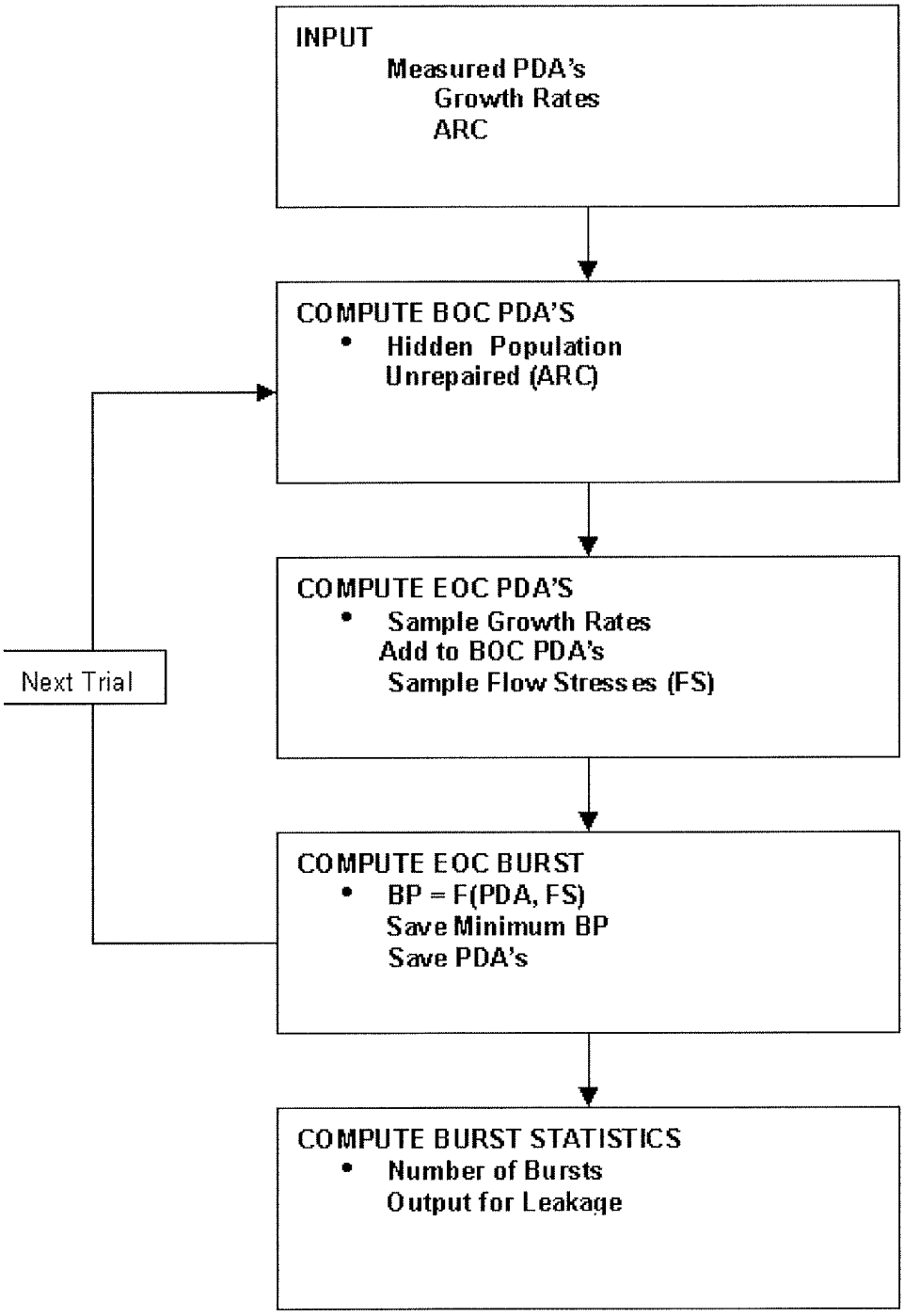

Figure 9-15
Flow Diagram for Burst Simulation Process

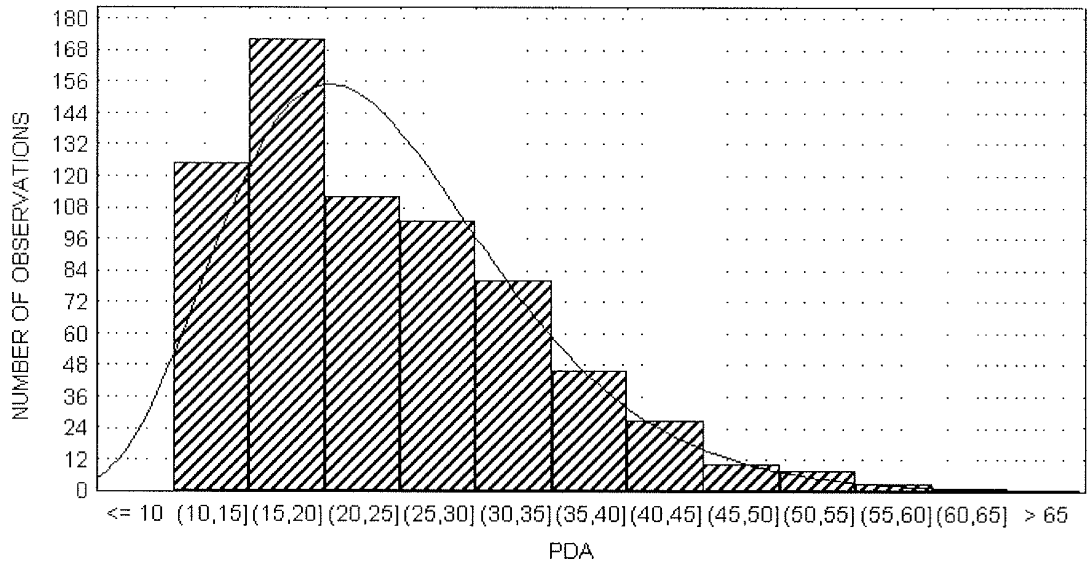

Figure 9-16
PDA Distribution at Previous EOC Conditions
13% NDE Error

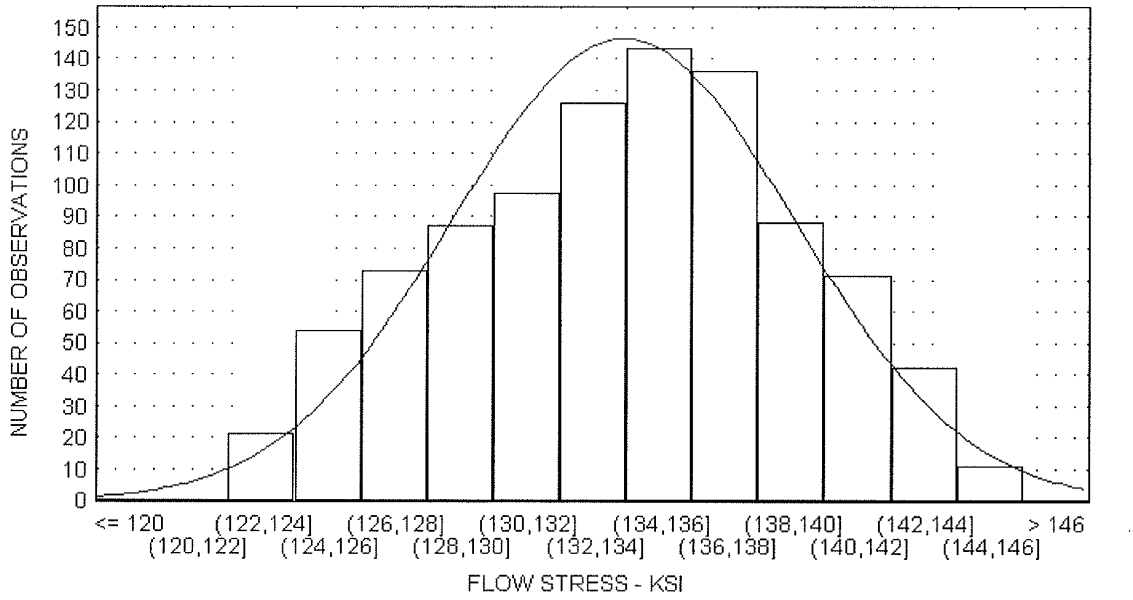

Figure 9-17
Flow Stress Distribution for Sample Cases

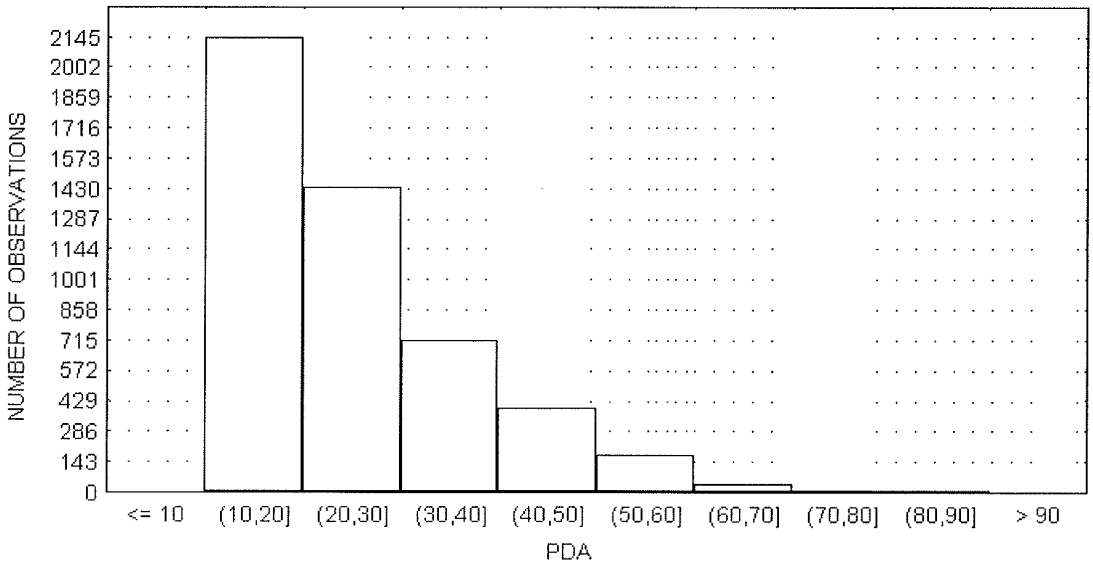

Figure 9-18
EOC PDA Distribution
1.5 EFPY Run Time : Zero Arc

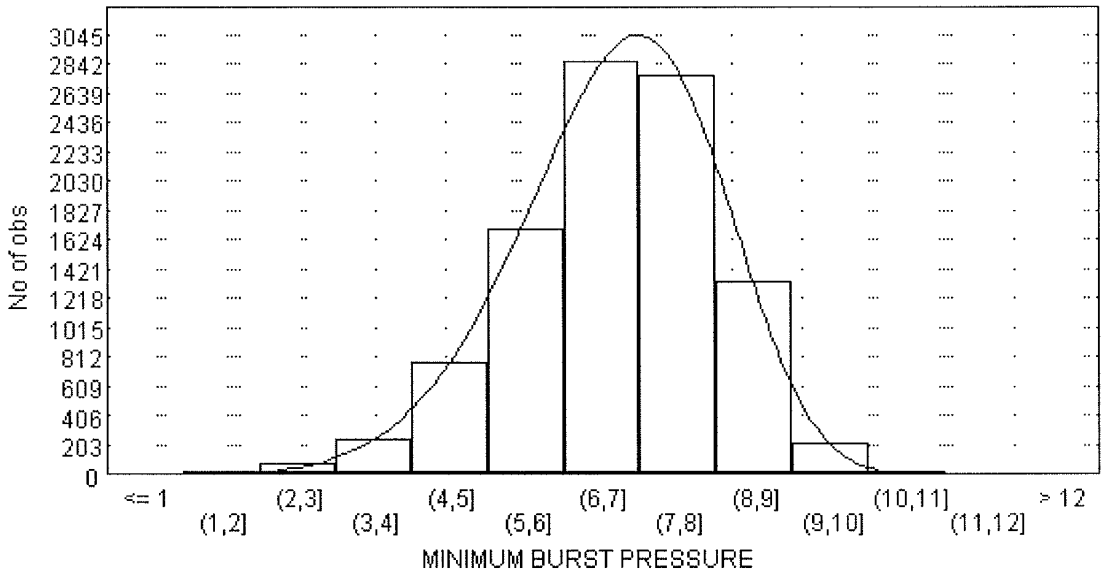

Figure 9-19
Distribution of Minimum Burst Pressures
13% NDE Uncertainty : 1.5 EFPY Run Time

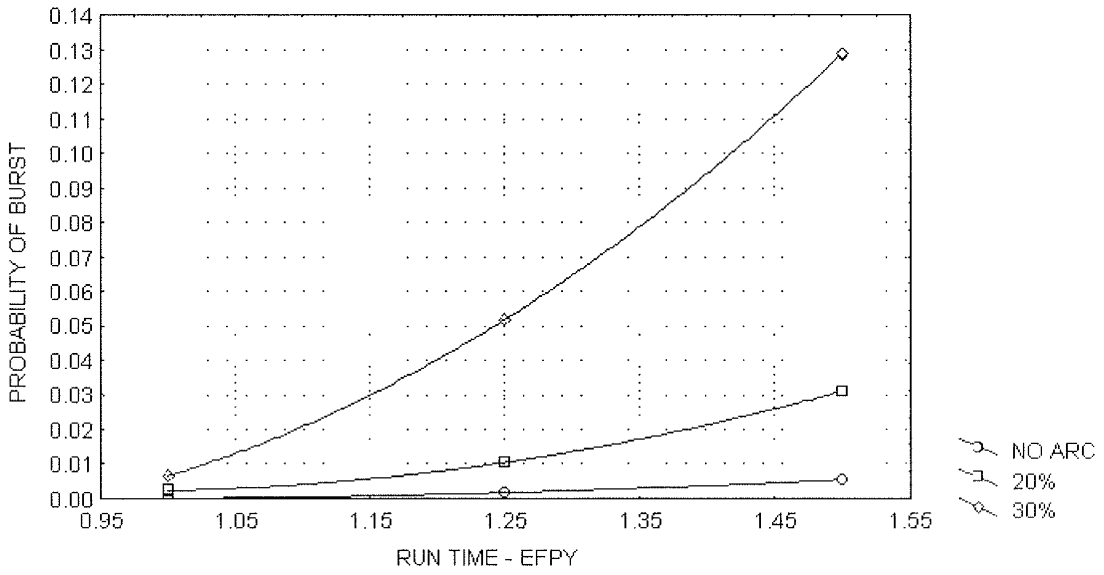

Figure 9-20
Probability of Burst Under SLB Loading for Various Arc Levels

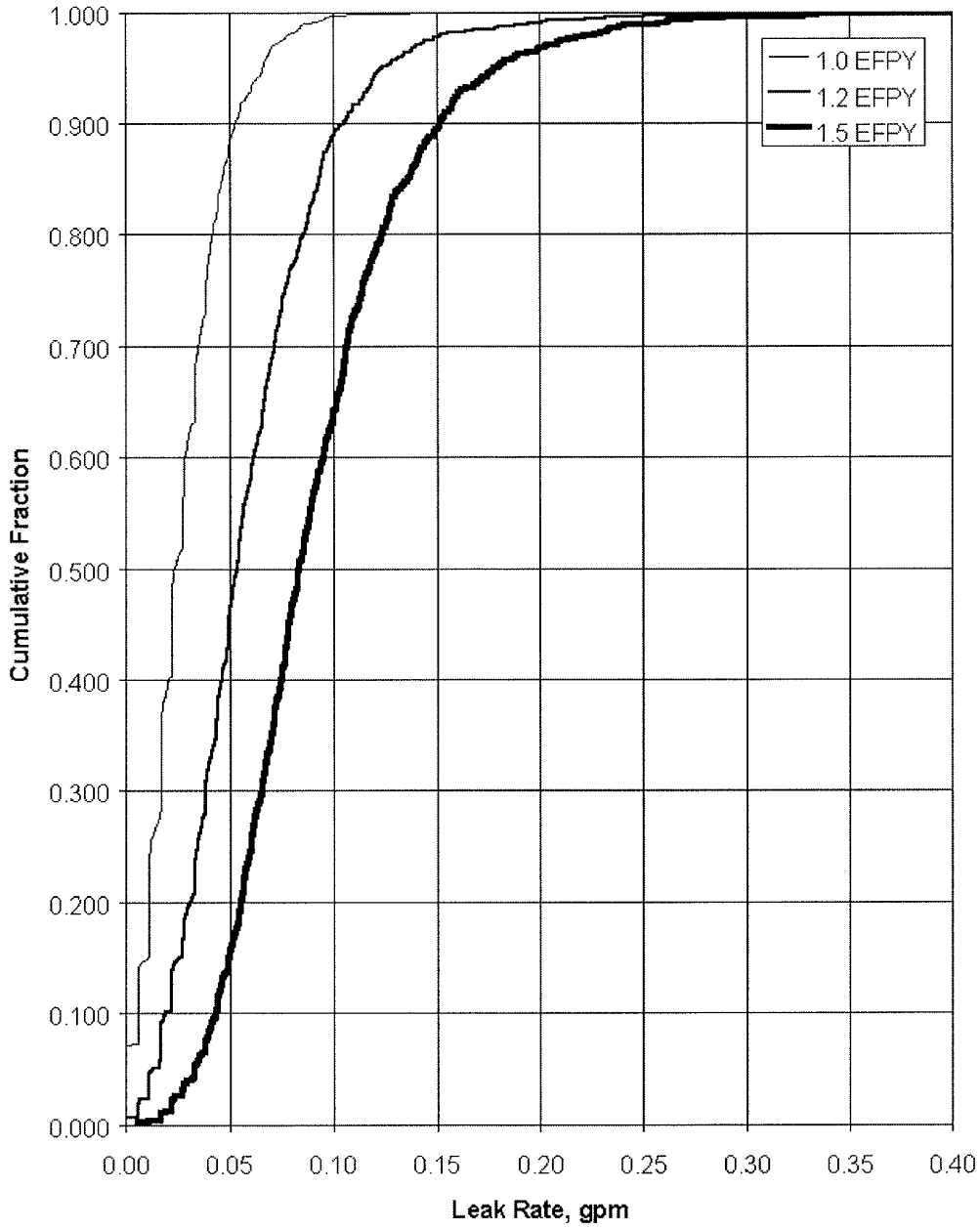

Figure 9-21
Simulated Leak Rate Distributions

A

NDE GUIDELINES FOR DEPTH ANALYSES

Alternate Repair Limit for
Circumferential Cracking at Expansion Transitions

Eddy Current Testing, Data Analysis and Engineering
Data Requirements

Arkansas Nuclear One Unit #2

November, 1996

CONTENTS

1.0 Introduction

This document provides the basis for eddy current (EC) inspection and analysis guidelines to be applied in conjunction with the implementation of Alternate Repair Criteria (ARC) for circumferential outside diameter stress corrosion cracking (ODSCC) in the explosive transitions at the top of the tubesheet (TTS) in the steam generators (Sgs) in the Arkansas Nuclear One Unit #2 (ANO) nuclear plant. An expansion transition zone is created in a tube during steam generator manufacturing by elimination of the tube to -tubesheet crevice. Enlargement of the nominal tube diameter within the tubesheet was accomplished by ABB-CE (ASEA Brown Boveri-Combustion Engineering) using explosive manufacturing techniques. The expansion transition zone is defined as the length of tube encompassing the change in tube diameter from the nominal to maximum diameter.

The purpose of this document is to provide background material for steam generator engineering personnel, eddy current data analysts, and regulators. Eddy current rotating probe data acquisition and analysis guidelines for the detection and characterization of circumferential cracks will be provided as a separate document, consistent with the bases established herein. Crack characterization is achieved using a profiling technique in which the data matrices are scanned in a direction perpendicular to the crack major axis and by amplitude measurements derived from the c-scan presentation of the circumferential indications. Rigorous reporting requirements are imposed in order to satisfy engineering analysis data requirements. All tubes which exhibit circumferential cracking requiring repair should be given due consideration for structural integrity and the need for stabilization.

Section 2 describes engineering data requirements necessary to characterize the state of the tube for determining structural integrity. Section 3 addresses eddy current data acquisition requirements for instrumentation, probes, coil test frequencies, cabling, and calibration standards. The overall eddy current data analysis activity is accomplished in two stages; 1) data screening and 2) crack characterization. Data screening is addressed in Section 4 with specific requirements established for analyst training and performance demonstration, data quality monitoring, and reporting. Section 5 describes additional data analyst training requirements, and data analysis requirements for the characterization of indications reported during data screening using profiling analysis and amplitude measurement methods. Separate data analyst training and performance demonstration requirements are imposed on analysts for data screening and characterization.

The requirements specified herein are to be incorporated into the plant steam generator inspection program for ANO. Steam generator engineering personnel have the responsibility to ensure that 1) eddy current data acquisition and analysis guidelines are appropriately modified and followed, 2) site-specific data analyst training and performance demonstration programs are implemented and 3) crack profile analysis and amplitude measurement results are monitored for compliance with engineering data requirements.

2.0 Engineering Data Requirements

Expansion zone alternate repair criteria impose special engineering data requirements on eddy current data analyses in order to ascertain the structural condition of the tube. These requirements include the measurement of crack and ligament lengths as well as the depth profiles for the cracks; the measurement of indication voltage behavior will also be correlated to the structural performance criteria, such as burst strength and leakage. This section defines and describes the engineering data requirements for detailed circumferential crack characterization; the requirements for characterization of axial cracks is also provided to cover situations in which mixed mode degradation must be evaluated.

2.1 Length measurements

2.1.1 Crack Length Determination

Circumferential crack length is defined as the arc length between crack endpoints and is reported in degrees. Crack endpoints are defined as the angular position of the first and last indications associated with a crack. The endpoints of the crack may be initially determined using the slope-intercept method in which the indication leading and trailing edges are used to define the crack endpoints. The slope-intercept method extrapolates the slope of the edges to the baseline where the sample point intersection values are determined. The difference in sample point values corresponds to the crack length.

The slope-intercept technique utilizes the total vertical channel data profile of the crack to predict the actual crack length. This technique yields measurements which are less affected by the shape of the crack than does the amplitude threshold technique. In the event that signal to noise ratios near the ends of the indication do not permit use of the slope-intercept approach, identification of the departure from null points for the indication response may be used as indication endpoints.

Identification of the slope-intercepts or points of departure from null should be done at high screen amplification factors (low numerical span settings). Since the deepest portion of the crack may produce large amplitudes which require low gain to permit viewing of the indication without saturation, high gain display permits a realistic estimate of the potential continuous crack length more consistent with metallurgical confirmation of pulled tubes.

No correction should be applied for coil field spread, as this may vary with length and crack depth. Appropriate adjustment will be made in the structural evaluation of the flaws for NDE uncertainty.

Measurements are made within individual scan lines; usually only the scan line with the longest arc length is used, but for distributed cracking (i.e., multiple cracks over portions of the circumference) which has a finite axial extent, it is appropriate to report the overlapped extent from consecutive scan lines to derive a true estimate of the total arc length.

A finite number of consecutive scan lines may exhibit flaw behavior for a circumferential crack. It is important to estimate the total length as the combination of offset arc lengths when consecutive scan lines present offset flaw segments as shown in Figure A-1. In this case the indication arc length should be reported as approximately 75°, representing the combination of the maximum single scan line plus the adjacent scan line offset. This may be accomplished by "stacking" the affected scan lines, as described in Section 5.

Figure A-1
Schematic Drawing Showing Total Arc Length Concept for Offset Scan Lines.

2.1.2 Ligament Estimation, Angular Spacing

The arc length between multiple circumferential indications, or between axial and circumferential indications in mixed mode cracking, is critical to structural evaluation of degraded tubes. It is important to establish the fact of separation as well the angular extent of separation.

When more than one indication is observed in an expansion transition isometric, sufficient information must be developed to define both angular and axial relationships among the flaw segments. The axial positions and the axial crack lengths provide dimensional information which is combined with circumferential crack lengths and their angular positions for evaluation of the structural capability of a tube with mixed mode degradation. The angular arc lengths of the circumferential flaws observed plus the ligaments separating them must total 360 degrees when they are in the same plane.

To classify as a ligament by rotating probe inspection, the amplitude should return to the null point for background response. Ligament length is estimated in degrees arc length in the same fashion as circumferential flaw arc lengths are determined. The positions of the endpoint of flaw #1 and the beginning of flaw #2 on the scan line

are subtracted to obtain the ligament arc length. The difference between 360 degrees and the sum of the arc lengths of Flaw #1, Flaw #2, and the measured ligament represents the "back ligament"; at minimum the shortest of the ligaments present should be reported. See Figure A-2.

Figure A-2
Schematic Showing Ligament Concept.

2.2 Profiling Requirements

2.2.1 Depth Profiles

Software improvements have facilitated the estimation of flaw depth for both circumferential and axial cracks. Rotating probe computer analysis software assembles the data from successive scans into a matrix which stores the data from each line in the rows of the array. The helical translation is typically displayed on a per revolution basis, so that the plotting of successive revolutions or scans representing the 360° of the tube ID produces the familiar pseudo-isometric or C-scan display; the data from each scan line is individually analyzed. Analysis of successive lines produces an axial profile of the tube condition.

Eddy current data analyzed parallel to the crack major axis have yielded inadequate information about the depth profile *along* the length of the crack. Addressing the data array in a column-wise fashion instead of the usual row-wise approach permits the generation of axial Lissajous figures. The resulting orthogonal intersect of the data stream with the plane of the circumferential cracks permits phase angle measurement and depth sizing in a manner analogous to what is done for axial cracks.

The axial Lissajous patterns created by angular indexing through the data array can be used to generate depth estimates at each angular position; the result is a circumferential depth profile which can be compared to destructive examination results. Detection sensitivities can be derived from the multiple data points in the destructive depth vs axial Lissajous phase angle-based depth comparison, and the identification of potential ligaments can supplement the tube integrity evaluation. It will be required for structural analysis of circumferential cracks to produce depth estimates using the axial Lissajous phase angles at intervals sufficient to characterize depth variations (typically about 5 degrees) over the observed length of the crack.

2.2.3 Maximum Depth Locations

The region of maximum depth in the crack should be characterized versus length in sufficient detail to define the profile of the maximum depth region. Closely spaced analyses (e.g., at 5 intervals) should be performed to characterize the portion of the length of the crack that is the maximum depth region.

A fixed sampling rate for profiling, such as every n-degrees, is not recommended, since details of the crack profile may be lost in the interval between points analyzed. All sample points should be used to provide reliable information for crack profiling.

2.2.4 Profiling of Closely Spaced Parallel Circumferential Cracks

Closely spaced multiple indications separated axially should be profiled individually with the start and finish angles reported for each crack.

2.3 Application of Crack Profiles for Average Depth Calculation

2.3.1 Crack length averaged depth

Calculations for crack length average depth are based on the area under the depth/angular position curve as defined above, divided by the total angle of the crack between the leading and trailing endpoints.

It is possible to have multiple cracks in the same plane. Depths reported as <XX% will be applied as XX% in the analysis. If NQS (non-quantifiable signals) points are reported, the average should be developed in a conservative manner to obtain a bounding average depth. For example, NQS = average of adjacent depth calls.

2.3.2 360 degree averaging

Calculations for tube section 360° average depth are based on the cumulative area under the depth/angle curve as defined above for all of the cracks in a plane, divided by 360.

2.3.3 Calculation of Average Crack Depth

From the axial profile measurements along the circumferential crack length, perform a weighted average calculation using segments no greater than 10°. In regions where rapid changes in depth and amplitude are apparent, it may be appropriate to use 5° segments to capture the profile detail in the average depth calculation.

$$\text{Average depth} = \sum_{i=1}^{n} (\%\ \text{Depth}_i \times \text{arclength}_i) \ / \ \text{Total Arclength}^{*} \qquad \text{(degrees)}$$

for each of n segments

where i = index identifying successive segments of the profile and

arclength = circumferential length (degrees) of n-th segment

* For average over crack length, use measured total Arclength; for average affected cross section, use 360°.

The arclength of the i-th segment for use in average crack depth determination is obtained by subtracting the i-th position (degrees) from the (i+1)th position; for this purpose the 1st and last positions are the NDD positions at each end of the indication being analyzed.

For structural integrity considerations, use is made of the Percent Degraded Area (PDA); this value differs slightly from the average depth calculation described above in that account is taken of the ID/OD origin of the cracking. The degraded area of a toroidal sector in the form

$A_1 = \theta/2 * (\%\ \text{depth} * R_{MI})^2$, (θ in radians is the angular width of the sector)

is calculated for each depth measurement. In each sector the mean radius R_{ml} is identified as the average of two adjacent depth estimates.

2.4 Amplitude Measurements

The same c-scan profiles which are analyzed for flaw depth along the length of the indication will be addressed with "voltage integral" software; this permits determination of the maximum voltage along the c-scan lines and provides an average voltage over the length of the indication, or 360° if preferred.

2.4.1 Maximum Voltage

Individual c-scan lines which comprise a circumferential indication will be assessed to find the point along the composite of flaw responses which exhibits the maximum amplitude. Application of specialized analysis software, e.g., "voltage integral" software incorporated in EDDYNET 95, provides a convenient and reliable tool for determination of voltage levels along chosen scan lines. The site specific guidelines should detail the specific steps required to assure proper identification of the voltage value corresponding to the point of maximum amplitude. Correlation of this value with structural parameters provides a part of the rationale for the subject circumferential repair criteria.

2.4.2 Average Voltage

Using "voltage integral" tools applied to the rotating probe c-scan lines, it is possible to synthesize a representation of the maximum amplitude portions of consecutive scan lines such that the average area under the curve, i.e., the synthesized scan line, is a conservative representation of the degradation response. This average voltage then is an alternative parameter against which the structural parameters which provide the basis for the repair criteria can be correlated.

2.5 Reporting Requirements

For each expansion transition indication the following information should be recorded:

Tube Identification.....Steam Generator, Row, Column

Type of Indication.....3 Letter Code

SCI for Single circumferential Indication

MCI for Multiple

Maximum Signal Amplitude.....Volts

Average Voltage.....Volts

Phase Angle (at Max. Voltage)...Degrees

Degradation Length.....Tip to Tip Length of Indication

(degrees)

Ligaments.....Separations between ends of adjacent indications, circumferential and axial (degrees)

This information documents the indications on which circumferential depth profiling may be performed. For each segment (arc length) for which flaw depth information is obtained, it is necessary to report the following standard information :

1. Degrees arc position relative to a fixed reference point
2. Phase angle (degrees) at the point of maximum depth for the signal evaluated and its corresponding amplitude (volts)
3. Maximum amplitude (volts) of the signal as determined with "voltage integral" software and the phase angle at that point.

3.0 Eddy Current Data Acquisition Requirements

3.1 Scope

This section defines data acquisition requirements for expansion transition examination using multiple-frequency eddy current instrumentation in conjunction with rotating probes.

3.2 Instrumentation

Multiple-frequency eddy current instrumentation capable of generating four frequencies as a minimum with digitized outputs is required.

Eddy current instrumentation shall be qualified for detection and sizing in accordance with Appendix H to EPRI document NP-6201 Rev. 4. The Appendix H *Acquisition Techniques Sheets* (*ACTS*) shall specify essential test variables including coils, cabling, test frequencies, drive voltages, receiver gains, etc.

3.2.1 Digitizing Rate

A minimum digitizing rate of 30 samples per inch of helical travel for both axial and circumferential extents should be used. Combinations of probe speed and instrumentation sample rates are chosen such that:

$$\frac{\text{Sample Rate (Samples/Second)}}{\text{Rotating Probe Speed (Inches/Second)}} \geq 30 \text{ (samples/inch)}$$

where Rotating Probe Speed is translated into rotations per minute as a function of the tube dimensions using the following equation:

$$\text{Rotating probe speed (in/sec)} = \text{Rotation rate (rpm)} * \ * t_m / 60$$

where t_m tube mid-wall diameter (in)

Probe rotation rate should be established to assure data quality. It may be necessary to reduce rotation rates to decrease or eliminate excessive noise caused by higher probe rotation rates.

3.3 Probes

Industry data available from pulled tubes has established that significant cracks are not satisfactorily detected with bobbin coils at expansion transitions. Therefore coils which reduce the effect of the expansion transition are commonly used to inspect expansion transitions.

3.3.1 Recommended Coils

For detection and sizing of circumferential cracks, whether initiated from the ID or the OD, *coils* recommended for expansion transition examination should be qualified in accordance with Appendix H. Such other or new techniques as may satisfy the Appendix H criteria may also be employed. The measurement techniques in this document apply to rotating probe characterization, and more specifically to +Point coils. This emphasis on +Point analysis reflects the interim recommendation issued by EPRI [1] (11/20/95) that circumferential crack measurement data be collected uniformly to the extent possible; for the Spring 1996 outage season it was recommended that all measurements be made with +Point coils.

For irregularly formed expansions, large liftoff signals may occur with standard rotating probe designs. Special probe designs incorporating a gimbaled shoe with a single +Point ™ may yield data with improved signal to noise. In addition, the use of magnetically biased coils may be necessary to provide improved data quality in the presence of permeability variations.

3.3.2 Data Acquisition

Rotating probe data acquisition for expansion transitions shall occur during probe insertion (on the "push"). To ensure that crack length measurement uncertainty meets the requirements for the alternate repair limits, positive position control such as might be assured with probe tensioning devices or position encoders integrated into the probe delivery system is recommended.

3.4 Test Frequencies

The frequencies at which the applied technique was qualified should be specified for the field application. As an example, recommended individual coil test frequencies for a 3-coil probe head are listed in Table A-1. For Alloy 600 tubing, the frequencies include a 600 kHz high frequency for detection of ID initiated cracks, a mid-range frequency 300 kHz for detection of OD initiated cracking, a supplemental low range frequency (100 kHz to 150 kHz) for mixing purposes and a structure sensitive frequency in the range of 10 - 30 kHz for location. Additional frequencies may be used in conjunction with those recommended above, as special interest requires.

---

[1] "ECT Data Collection for the Application of Crack Sizing Techniques", Letter from EPRI Steam Generator Management Project to Distribution, dated November 20, 1995.

Table A-1
Recommended Test Frequencies

Coil	Primary	Aux 1	Aux 2	Locator
+Point	300 kHz	Optional	100-150 kHz	NA
0.115" Pancake Coil [1]	300 kHz	Optional	100-150 kHz	10-30 kHz
0.080" Pancake Coil [2]	600 kHz	Optional	100-150 kHz	NA

Notes:
[1] Unshielded
[2] Shielded

Frequencies and/or coils other than those specified in Table A-1 may be used for detection and sizing provided these alternative methods are *demonstrated* to give results comparable to or better than those obtained with the recommended coils and frequencies.

3.5 Cabling

The impact of system cabling including probe shaft assembly length, pusher-puller slip rings, and sacrificial extension cables on data quality should carefully be assessed. System cabling configurations which provide best data quality in the context of signal amplitude or signal-to-noise ratio are preferred.

The length of the shaft assembly supplied with rotating probe motor units is typically 50 feet. If additional length shafts are used, caution should be exercised when higher test frequencies, >300kHz, are used to ensure the signal amplitudes are not significantly diminished. Probe extension lengths should also be minimized and should be manufactured with high performance low-loss cable.

3.6 Calibration Standard

3.6.1 Standard Configuration

Table A-2 provides a listing of required discontinuities for both 3/4-inch and 7/8-inch OD tubing. Hole diameters and tolerances for flat-bottom holes (FBH) are as specified by current plant ASME Code requirements. All freespan EDM notches should be at least 0.25" long to counter the influence of edge effects; those located in the expansion transition shall be 0.25" long. Notch widths shall be no greater than 0.006". The tolerance for widths and depths of the notches shall be 0.001". The tolerance for the slot lengths shall be 0.010".

In addition to the tube wall discontinuities listed in Table A-2, a simulated tube sheet segment 270 degrees in circumferential extent, at least 0.75" thick, fabricated from SA-285 Grade C carbon steel or equivalent, may be incorporated into the calibration standard for process channel suppression. The edge to edge distance between the support plate and the nearest slot shall be at least 0.5.

Other reference signal sources e.g., copper, ferrite, etc., may be incorporated into the calibration standard at the discretion of the user.

Table A-2
Calibration Standard
Reference Discontinuity Configuration

Orientation	Surface	Location	Depth, %				Comments
			20	40	60	100	
Circ	ID	Freespan	x		x	x	ID/OD Same notch
Circ	OD	Freespan	x	x	x	x	"
Axial	ID	Freespan	x		x	x	"
Axial	OD	Freespan	x			x	"
FBH	OD	Freespan	x		x	x	ASME
Circ	ID	Exp		x			
Circ	OD	Exp		x			
Axial	ID	Exp		x			
Axial	OD	Exp		x			

4.0 Eddy Current Analysis - Data Screening Requirements

4.1 Scope

This section defines data analysis requirements for data screening in which tubes with potential indications at or near the expansion transition are reported. Once identified, data from these tubes are examined in further detail in accordance with Section 5 for more detailed characterization of the reported indications.

4.2 Personnel Qualifications

4.2.1 Analyst Training

Data analysts shall be given specific training in 1) industry experience with expansion zone cracking and 2) current industry analysis practices for crack detection and characterization.

Training data sets shall be prepared for analyst familiarization. These data sets shall include examples of expansion zone indications reflecting a diversity of test conditions including but not limited to; 1) large and small amplitude indications, 2) indications in the presence of extraneous test variables. e.g., secondary-side deposits, permeability, excessive expansion zone geometry changes, etc., and 3) indications which illustrate the engineering data requirements listed in Section 2.

4.2.2 Analyst Performance Demonstration

All data analysts shall successfully pass a site-specific practical examination. The examination should consist of data sets that demonstrate depth profiling skills using appropriate analysis software. Analysts may qualify separately for detection and depth profiling.

4.3 Analysis Setup

The setup instructions provided in this section apply to a rotating probe incorporating a +Point coil. Consistent setup information should be provided as required by the qualification parameters for other techniques.

4.3.1 Channel Assignments

In addition to the normal assignment of channels for the individual frequencies from rotating coil probes, separate +Point analysis channels should be set up for axial and circumferential cracks in which flaw signals are directed upwards. This analysis aid allows the analyst to evaluate the data in a manner consistent with industry practice for pancake coils.

4.3.2 Spans

Initial span settings should be set in accordance with applicable procedures or at the discretion of the user if not so specified. However, at a minimum, expansion transitions should be viewed at a span setting that permits viewing of the calibration standard 40% OD EDM notch located in the expansion transition at no less that 1/2 full screen height.

4.3.3 Rotations

Rotations can be set in accordance with applicable procedures or at the discretion of the user if not so specified. It is recommended that the phase angle be rotated to the highest possible angle allowed to identify small amplitude ID indications while still maintaining a minimal signal to noise ratio.

4.3.4 Voltage Normalization

Primary analysis channel voltages for the three coils listed in Table A-1 should be individually set to 1 volt using the calibration standard 40% OD axial EDM notch.

While the voltage associated with a crack indication is not regarded as a reliable indicator of depth, standard flaw voltage profiles can be used for comparison with structural performance parameters, e.g., burst strength, leakage, if a normalized voltage calibration is provided. Adoption of an common voltage calibration technique will facilitate the industry-wide comparison of indications.

4.3.5 Calibration Curves

No phase angle-depth calibration curves are required for the initial data screening process. For depth analysis of the maximum voltage point for circumferential indications, it will be necessary to establish a phase angle vs depth curve in the Axial Liz window.

4.4 Data Evaluation

4.4.1 Data Quality

Calibration Verification - The four EDM notches located within the expansion zone transition of the calibration standard shall be visible.

Probe Noise - Degradation channel data with electrical noise in excess of an established limit will be rejected and the tube reexamined.

Tube Noise - The acceptance of data from tubes with excessive noise due to extraneous test variables such as probe motion, permeability, and tube deposits shall be carefully assessed. Where possible, consideration shall be given to using other NDE methods or techniques to ensure that potential crack indications are not being masked.

4.4.2 General Analysis Requirements

The potential for PWSCC is well documented for roll expansions, including both axial and circumferential orientations. The presence of ODSCC in both orientations at or near the expansion transition has precedents in numerous plants. Recent experience in

hydraulic expansion transitions as well as broader industry experience in both mechanical roll and explosive expansion units has raised industry awareness of the need for careful analysis of data from all types of transitions.

With liftoff or probe motion set on the horizontal, the presence of signal trajectories in the upper impedance plane shall be regarded as reflecting possible degradation. While calibration standard signals exhibit predictable phase angle rotation with changing frequency, this behavior should not be relied upon for in-plant conditions. For example, clockwise vs counter-clockwise, ID to OD, or OD to ID shifts with frequency are within the range of expected patterns of behavior for flaw signals. Detection of flaw behavior in a degradation analysis channel should cause the signal to be evaluated as an indication of degradation, notwithstanding conflict with other channels or with other coils, unless the signal in the context of its occurrence is more reasonably explained as arising from extraneous factors. Care should be exercised to avoid nullifying a flaw signal call on the basis that a data channel more susceptible to interference does not present clear flaw behavior.

Filters and/or line "nulling" techniques are often used as an analysis aid to remove geometric or high frequency noise. However, the lack of filtered data channel confirmation of a potential indication observed on a raw or unfiltered data channel should not be the basis for non-reporting.

Expansions transitions which are not symmetric and smoothly varying, may cause liftoff signals to follow a trajectory in the upper impedance plane. In these cases, a coordinated review of the C-scan and Lissajous behavior may resolve the signal as representing liftoff.

Similarly interference's arising from the presence of metallic copper deposits or magnetite which may be detectable in the upper impedance plane should be screened carefully to avoid mis-identification of flaws as extraneous variables.

4.4.3 Data Screening

Data acquisition test extent during expansion transition zone examination typically consists of 2 inches above the top of the tubesheet to 3 inches below the top of the tubesheet. For mis-placed transitions the test extent should be adjusted to assure an adequate examination of a tube length centered on the bottom of the expansion. All data acquired from this region shall be screened using *both* impedance plane and terrain plot analysis techniques.

Strip Chart Analysis -Strip chart evaluation techniques for data screening are prohibited!

Impedance Plane Analysis - Primary, secondary, and process degradation channels, if used, shall be scrolled for potential indications. The use of multiple-channel analysis software display features is encouraged to accomplish this requirement in an efficient manner.

Conservative analysis criteria shall be used for screening purposes. No voltage threshold shall be used. In addition, requirements for phase angle correlation between degradation analysis channels, and/or confirmation between different coils is not required for reporting an indication. Potential indications observed in any of the degradation analysis channels shall provide a basis for reporting.

Terrain Plot Analysis - Terrain plots shall be generated and reviewed for all primary, secondary, and process degradation analysis channels. Signal features observed on terrain plots shall be reviewed in the impedance plane for evidence of degradation.

Voltage Integral Analysis - Single and/or multiscan graphics documenting the maximum and average voltages shall be generated for each circumferential indication from the primary degradation analysis channel. The depth corresponding to the point of maximum amplitude on the scan line shall be determined and reported.

4.5 Reporting Requirements

4.5.1 Recording of Results

Analysis Codes - Appropriate three-letter analysis codes that reflect indication orientation and frequency of occurrence shall be adopted. Typical industry codes for indications attributable to cracking include SAI and MAI for single and multiple axial indications, SCI and MCI for single and multiple circumferential indications, and MMI for mixed mode indications in which both orientations are present.

Final Report Entry - The record of each tube analyzed shall include the Tube ID, the VOLTS, DEG, analysis code, CH#, axial location and test extent for each detected flaw.

Attachment A

Measurement of Circumferential Cracks

1. Scope

1.1 The purpose of this section is to provide a step-by-step guideline to promote consistent measurement of length and/or depth of crack-like indications in non-ferromagnetic tubing. In accordance with the November 1995 letter from EPRI, the following guideline applies to data collected using Zetec, Inc. +Point rotating probes, and analyzed using Eddynet 95 software. The qualification of other coils, software, and analysis techniques should be accompanied by a similar guideline. Length and/or depth measurements of these indications should be performed with caution and consistency.

2. Training

2.1 Analyst Training

Analyst training shall meet the requirements specified in Section 4.2.1.

2.2 Analyst Performance Demonstration

Performance Demonstrations shall meet the requirements specified in Section 4.2.2.

3. Reporting Requirements

3.1 Indication Length

a) Identify all indication endpoints (start and finish) with 0% depth notation.

b) Include defect-free lengths that may lie within the overall indication length.

c) The 0% depth points should be as close as possible to the indication endpoints used to define the length.

3.2 Labels

In the COMMENT field for the depth profile data point being reported, apply labels to indication data points indicating the following, if appropriate:

CP Points at which the indication changes from ID to OD, or OD to ID. The reference phase angle is the angle associated with the 100% through-wall EDM notch.

MD Minimum depth estimate (data not obtainable from lissajous)

FP Indication present but depth cannot be assigned.

These labels are used to facilitate engineering evaluation of the reported depth profile information; decisions related to the treatment of crack segments for which ambiguous or marginal data is provided are aided by using the analyst's judgment concerning the severity of the indications evaluated.

4. Analysis Setup

NOTE: These setup parameters are provided as an example only, with regard to a multi-coil rotating probe containing .115 pancake / +Point / 0.080 pancake coils. Any +Point rotating probe and/or configuration can be substituted. A specific analysis technique sheet must be completed to show actual set-up parameters for the applicable probe type & configuration.

4.1 Channel Assignments

Establish recommended or required Process channels for the appropriate +Point channels.

4.1.2 Identify channels in the System Info Screen as appropriate:

Coil #1= .115 Pan

Coil #5= PlusCirc

Coil #7= .080 Pan

Coil #4= Trigger

Process channels = PlusAx (as appropriate)

Low frequency channel(s) = Locator

4.1.3 Set the following parameters in the MRPC window:

a) Set RSLEW to ON.

b) Set the X and Y scales to 2.0/2.0.

c) Set the X rotation to 60 and the Y rotation to 35, or as desired for optimum viewing.

Using the User Selectable option functions, set the following parameters:

a) Set TUBING DIAMETER as applicable. (Note: when measuring ID indications it is recommended that the ID diameter is used and when measuring OD flaws it is recommended that the mid wall diameter be used.)

b) Set TRIGGER channel to the appropriate channel number.

c) Activate LISSAJOUS.

d) Activate CIRC LINE FILTER and AXIAL LINE FILTER.

e) Set Report Angle as ACTUAL DEGREE.

f) Set Report % as ARC/LEN.

g) Turn Arrow on.

4.1.4 Set the following parameters in the main Lissajous window:

a) For left strip chart, select the vertical component of the primary frequency +Point channel.

b) For right strip chart, select the vertical component of the primary frequency pancake coil channel.

c) For main Lissajous, select the primary frequency +Point channel.

d) From the Tools menu, Data Slewing:
Slew the data channels as follows:

Coil #5 (PlusCirc) = 120 Degrees
Coil #7 (.080Pan) = 240 Degrees

4.1.5 Set the axial scale between corresponding features on two known artifacts on the calibration standard (refer to the drawing for the as-built dimension)

4.1.6 Set channel rotation as follows:

Raw data analysis channels (0.115 Pancake, +Point Circ, 0.080 Pancake):

a) Set rotation such that the phase of the 40% ID circumferential EDM notch is at 15 Degrees (Peak to Peak).

Process channels (PlusAx):

a) Set rotation such that the phase of the 40% ID axial EDM notch is at 15 Degrees (Peak to Peak).

Locator channel(s):

a) Set rotation such that the phase response of the TSP or the TTS is in the downward direction.

Trigger channel:

a) Set rotation such that the minor pulses are horizontal and the major pulse is upward.

4.1.7 Select the primary frequency +Point channel, and locate the response of the 40% OD axial EDM notch. Set voltage on this signal to 1.00 volt (Peak to Peak), and normalize to all channels.

4.1.8 Establish phase vs. depth curves as described, using ACTUAL percentage values from the appropriate standard drawing for the calibration standard described in Section 2.4

a) Select the primary frequency +Point channel (PlusCirc) in the main Lissajous window. Under "System" select "Create Cal Curve". Within the "Cal Curve" window select "Type"; then select "ANGLE". Establish a 3-point OD curve using the response from the 100%, 60%, and 40% nominal OD circumferential EDM notches. Establish a 4-point ID curve using the 100%, 40%, and 20% nominal ID circumferential EDM notches (ID point 4 is 0 degrees=0%).

b) Select the primary frequency +Point process channel (PlusAx) in the main Lissajous window. Under "System" select "Create cal Curves". Within the "Cal Curves" window select "Type"; then select "ANGLE" curve. Establish a 3-point OD curve using the response from the 100%, 60%, & 40% nominal OD axial EDM notches. Establish a 4-point ID curve using the 100%, 40%, & 20% nominal ID axial EDM notches (ID point 4 is 0 degrees=0%).

4.1.9 Adjust span such that the Lissajous response of the 40% OD axial EDM notch is 1/2 of full screen (main Lissajous window) height for all applicable analysis channels.

4.1.10 Store setup.

5. Data Evaluation

5.1 TTS Circumferential Arc Length Measurement

The start and end of an indication should be entered as 0% outboard from the endpoint indications.

5.1.1 Load the tube to be measured, and label the TTS by monitoring the locator channel.

5.1.2 Plot the primary frequency +Point channel (PlusCirc).

5.1.3 Locate an area of the plot that does NOT exhibit the presence of a circumferential indication (this is an area that exhibits ONLY roll transition geometry response); see Figure A-3.

> *Caution: There may not be a defect-free portion of the scan. Conservative analysis should be practiced, and the application of filters should only be done when there is an apparent return-to-null in the scan.*

5.1.4 Scroll the Axial Line Filter cursor to the defect free portion of the scan; see Figure A-4. Apply the axial line filter to the data; see Figure A-5.

5.1.5 While scrolling the circumferential scan line, monitor the axial Lissajous window for initial flaw response. Note the circumferential position of the arrow at that point (this is the start of the indication); see Figure A-6.

(Figure A-7 shows the peak amplitude of the circumferential crack indication.)

Continue scrolling the circumferential scan line and monitor the axial Lissajous window for the end of flaw response. Note the position of the arrow at that point (this is the apparent end of the indication); see Figure A-8.

5.1.6 Scroll the axial scan line to "stack" the circumferential lines; see Figure A-9.

5.1.7 Place the FROM / TO range markers at the outer-most edges of the stacked circumferential scan lines (the first & last points where the data departs from null). Care should be taken to ensure that the area discussed in Section 5.1.5 is encompassed within the FROM / TO area, as shown in Figure A-9.

Caution should be exercised if a balance condition is not obtained; in such a case, the complete arc length should be reported as one indication.

5.1.8 Enter the indication length (ARC=/DEG=) to the final report.

5.1.9 Repeat steps 5.5.1.4 through 5.5.1.8 if multiple TTS circumferential indications exist in the tube.

5.1.10 Graphics are required for all reported indications; see Figure A-9.

5.2 TTS Axial Length Measurement

5.2.1 Load the tube to be measured and label the TTS by monitoring the locator channel.

5.2.2 Plot the primary frequency +Point process channel (PlusAx).

5.2.3 Locate an area of the plot that does NOT exhibit the presence of an axial indication (this is an area that exhibits ONLY roll transition geometry response); see Figure A-10.

Caution: Conservative analysis should be practiced, and the application of filters should be done with discretion.

5.2.4 Scroll the Axial Line Filter cursor to the defect free portion of the scan. Apply the axial line filter to the data; see Figure A-11.

5.2.5 While scrolling the axial scan line, monitor the circumferential Lissajous window for initial flaw response. Note the axial position of the arrow at that point (this is the apparent start of the indication); see Figure A-12. (Figure A-13 shows the peak amplitude of the axial crack indication).

Scroll the axial scan line and monitor the circumferential Lissajous window for the end of flaw response. Note the position of the arrow at that point (this is the apparent end of the indication); see Figure A-14.

5.2.6 Scroll the circumferential scan line to "stack" the axial lines; see Figure A-15.

5.2.7 Place the FROM / TO range markers at the 0% points adjacent to the outer-most edges of the stacked axial scan lines (the first & last instance where the data departs from null). Care should be taken to insure that the area discussed in section 4.4.5 is encompassed within the FROM / TO area; see Figure A-16.

5.2.8 Enter the indication length (AX LEN=) to the final report.

5.2.9 Repeat steps 5.2.4 through 5.2.8 if multiple TTS axial indications exist in the tube.

5.2.10 Graphics are required for all reported indications; see Figure A-16.

5.3 Depth Measurement of Axial Indications

5.3.1 Follow steps in the LENGTH MEASUREMENT section (5.2) to identify & measure the length of the axial indication.

5.3.2 Return to the main Lissajous window, and display the primary frequency +Point process channel (PLUSAX). Locate the first scan which is part of the subject axial indication.

5.3.3 Isolate the signal within the window, and perform VOLTS_P/P on the positive leg of the signal. (If the phase angle is not best measured from the positive leg, measure the value from the negative leg or exit transition and enter a comment so indicating). Enter the percentage value to the final report, along with the phase angle, percent depth, and the analysis code as appropriate.

5.3.4 Locate the next successive scan line of the subject indication.
Repeat step 5.3.3.

5.3.5 Repeat step 5.3.4 until all scans have been entered to the report.

5.3.6 Repeat steps 5.3.1 through 5.3.5 until all subject axial indications in the tube have been entered to the report.

5.4 Circumferential Indication Depth Measurement

5.4.1 After loading the calibration standard, establish a phase vs. depth curve in the AXIAL LIZ window as described, using ACTUAL percentage values from the appropriate calibration standard drawing;

a. In the MRPC window, select the primary frequency +Point channel, and plot the calibration standard.

b. Scroll the cursor to locate the largest amplitude scan of the 100% circumferential EDM notch (or other appropriate signal), and re-plot the display.

c. In the AXIAL LIZ window, normalize voltage to the main Lissajous display using "Set Circ & Axial to Main Eddy".

d. In the AXIAL LIZ window, select ANGLE VS. DEPTH curve.

e. Use the FROM -TO range markers to isolate the upward excursion portion of the signal within the AXIAL LIZ window, then perform VOLTS_P/P. Use that measurement to establish the appropriate point(s) on the ANGLE VS. DEPTH curve.

f. Repeat steps described 4.1.8 to establish a 3-point OD curve using the 100%, 60%, and 40% nominal OD Circumferential EDM notches.

g. Repeat steps described in 4.1.8 to establish a 4-point ID curve using the100%, 60%, and 20% nominal ID Circumferential EDM notches (ID point 4 is 0 degrees = 0%).

5.4.2 Follow steps in the appropriate LENGTH MEASUREMENT section to measure the arc length of the circumferential indication.

5.4.3 Plot the primary frequency +Point channel (PlusCirc). Locate the largest amplitude scan of the subject circumferential indication, then scroll the circ cursor to identify the initial departure from null of the circumferential indication within the AXIAL LIZ window.

5.4.4 Use the FROM/TO range markers to isolate the signal within the AXIAL LIZ window, and perform VOLTS_P/P on the positive leg of the signal. Enter the percentage value to the final report.

5.4.5 Step the circ cursor to the next successive angular position of the subject indication. Repeat step 5.4.4.

5.4.6 Repeat step 5.4.5 until the depth values for all angular positions of the indication(s) have been entered into the report.

5.5 Voltage Integral Evaluation of Circumferential Cracks

Evaluation of circumferential indications using the "Voltage Integral" software begins with C-scan data collected using a rotating coil probe, in this case a +Point configuration. After a circumferential indication has been identified, using signal interpretation guidelines based on an Appendix H qualified procedure using EDDYNET95 analysis software, the "Voltage Integral" software will be used to identify the maximum vertical amplitude component from the c-scan data and to obtain an

average amplitude estimate based on the area under the c-scan curve. These parameters will be correlated with pertinent tube integrity parameters to develop criteria which might be components of alternate repair criteria for circumferential cracks.

This work will be performed using the 300 kHz data from the +Point PlusCirc channel.

5.5.1 Access the MRPC window, choose "User Selectables", and "Activate Liz".

5.5.2 Using the Circ Liz window, set up the phase calibration and voltage scale as follows:

a. Set the phase for the largest signal for the 100% deep circumferential EDM slot from the calibration standard data at 30°.

b. Set the peak to peak voltage for this signal at 20 volts.

c. Set the phase angle vs depth curve in the Axial Liz window.

d. Store the setup using the "File" option of the EDDYNET95 window.

5.5.3 From the MRPC window, under "User Selectable Options", set the following parameters:

a. Arrow "on"

b. Cross-hatch "off"

c. Axial and circumferential line filters "on"

d. Set other options as needed

5.5.4 Perform crack sizing using the voltage integral software.

a. Identify the scan line giving the largest amplitude signal in the MRPC window.

b. Choose "User Selectables" and toggle "Voltage Integral" to ON.

c. Click on "Plot Cursor Scan" in the Voltage Integral window.

d. Click on "Set to zero".

e. Click on "3/4 Plot".

(It may be necessary to use "Scale/2", "Scale 2", or "3/4 Plot" option to bring the voltage within the boundaries of the degree plot available in this window.)

f. Move the vertical line in the Voltage Integral plot to the circumferential location of the maximum voltage (Figure A-17).

g. Click on "RPT Entry" to store this data.

5.5.5 Using the Axial Liz window, measure the phase angle and corresponding depth associated with the maximum voltage position; enter this data in the report.

5.5.6 Return to the RPC scan window; use the "Axial from" and "Axial to" options to cover all scan lines which exhibit any segment of the circumferential flaw. (Figure A-18)

(Covering a few extra scan lines is recommended unless they may contain large contributions from tubesheet deposits or the tubesheet transition signal.)

5.5.7 Go to the "Voltage Integral" window:

a. Click on "Plot Multiscan Peaks".

b. Move the vertical line to the new peak it presents.

c. Click on "RPT entry" to store this data.

This step produces a result with approximately the same maximum amplitude, but an increase in average voltage should be expected.

(In the event the data contains Mixed Mode cracking, use the "Voltage Threshold" arrows to move the "zero voltage" line so that negative signals from axial cracks are eliminated from the estimate.)

5.5.8 Repeat steps 5.5.4 to 5.5.7 for other circumferential indications separated from the initial indication by returns to null (ligaments of sound tubing) if it is desired to assess each of multiple circumferential indications individually.

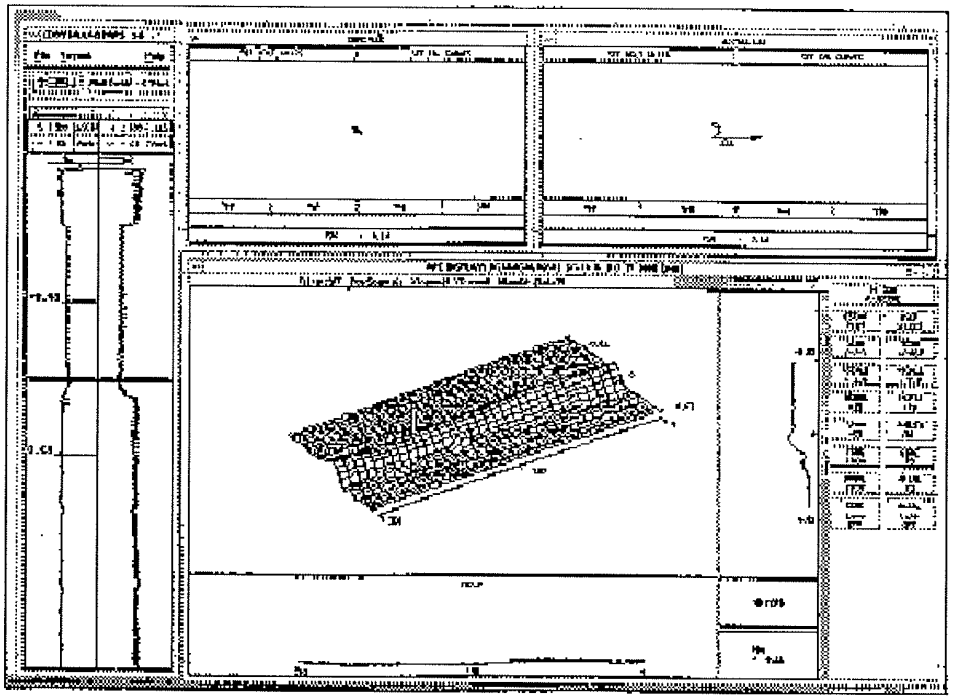

Figure A-3
Indication-free scan line in the roll transition geometry response.

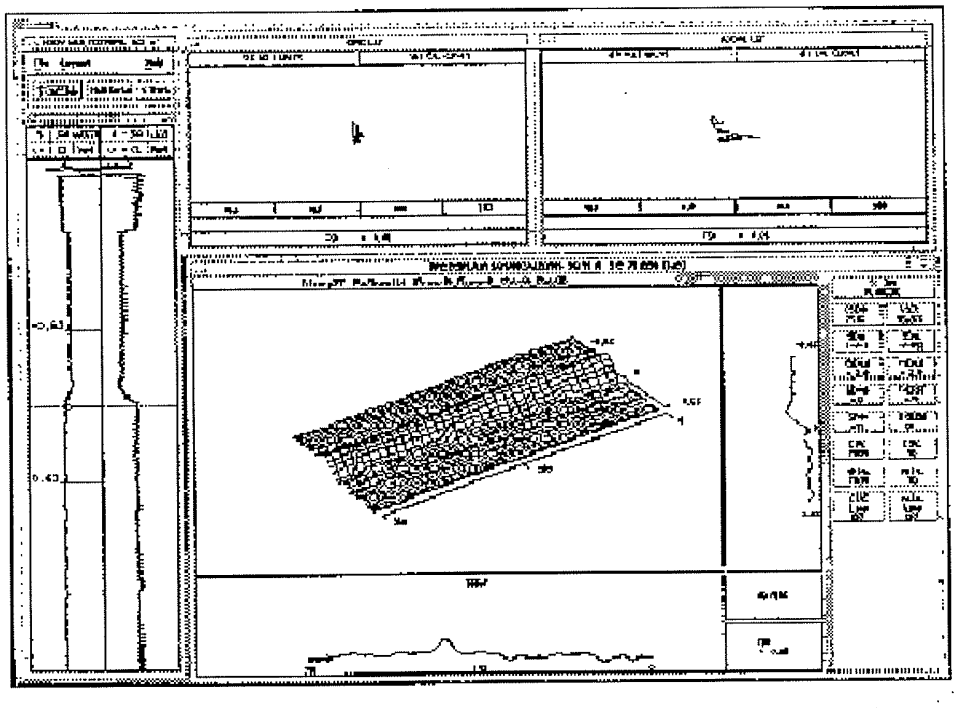

Figure A-4
Defect-free position on scan line which exhibits circumferential indication

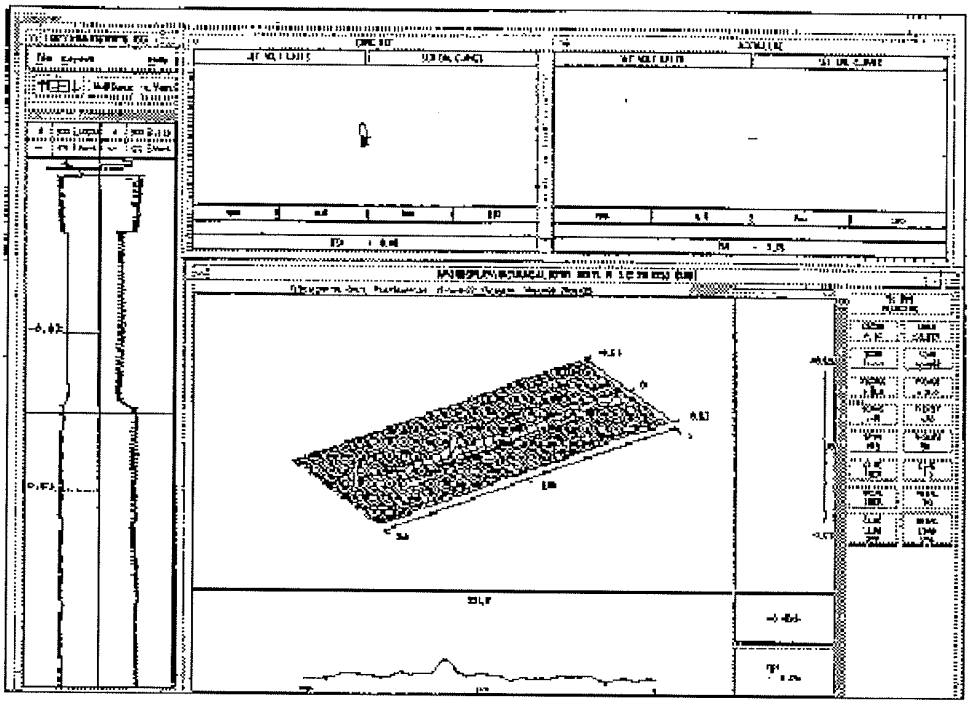

Figure A-5
C-scan after application of axial line filter

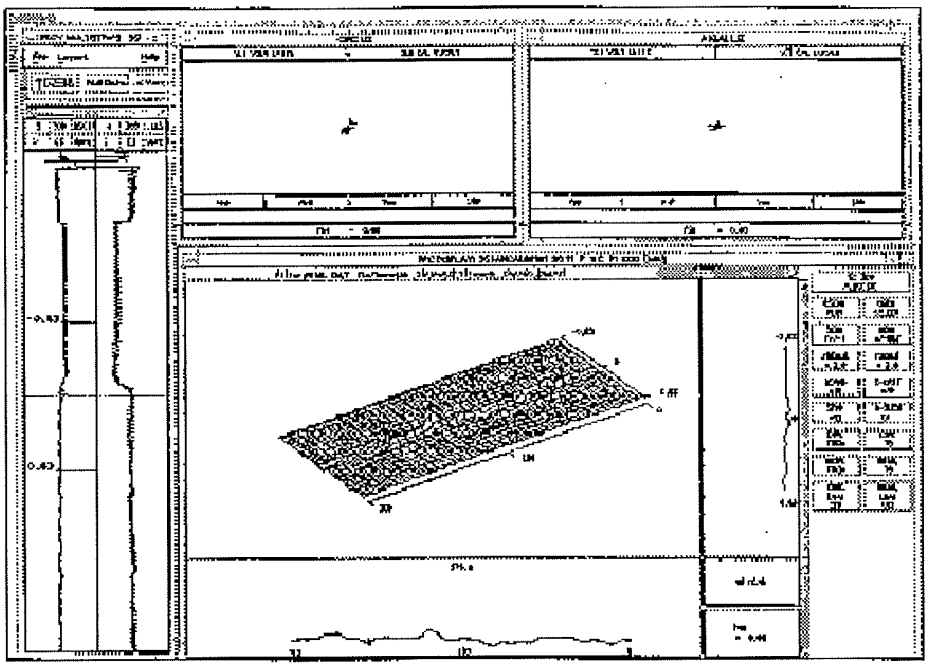

Figure A-6
Cursor at start of circumferential indication in axial lissajous window

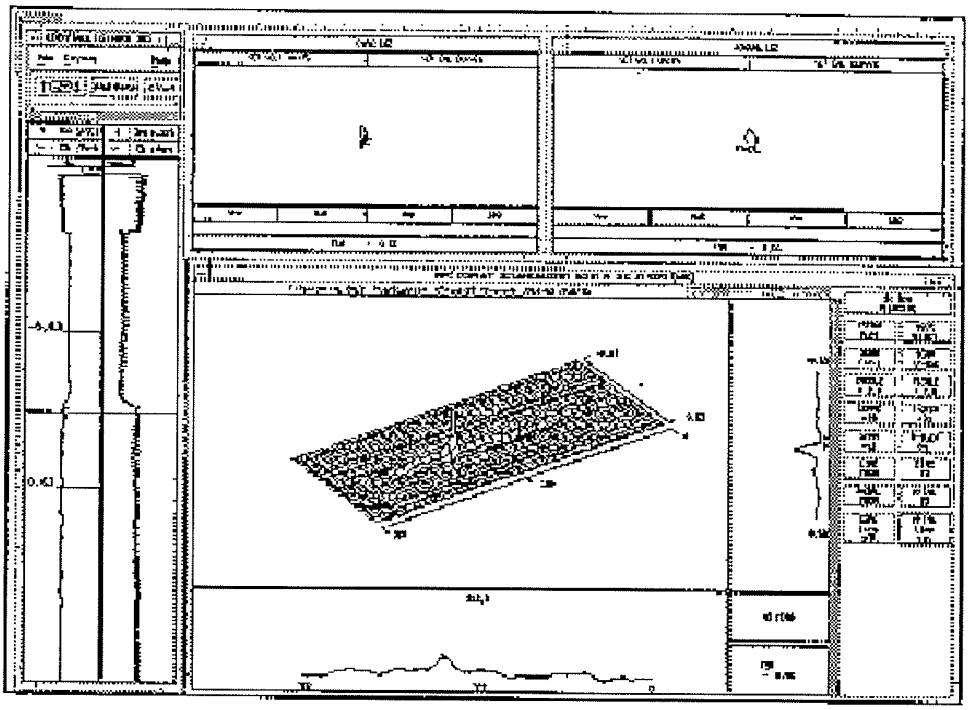

Figure A-7
Cursor at position of peak amplitude of the circumferential indication

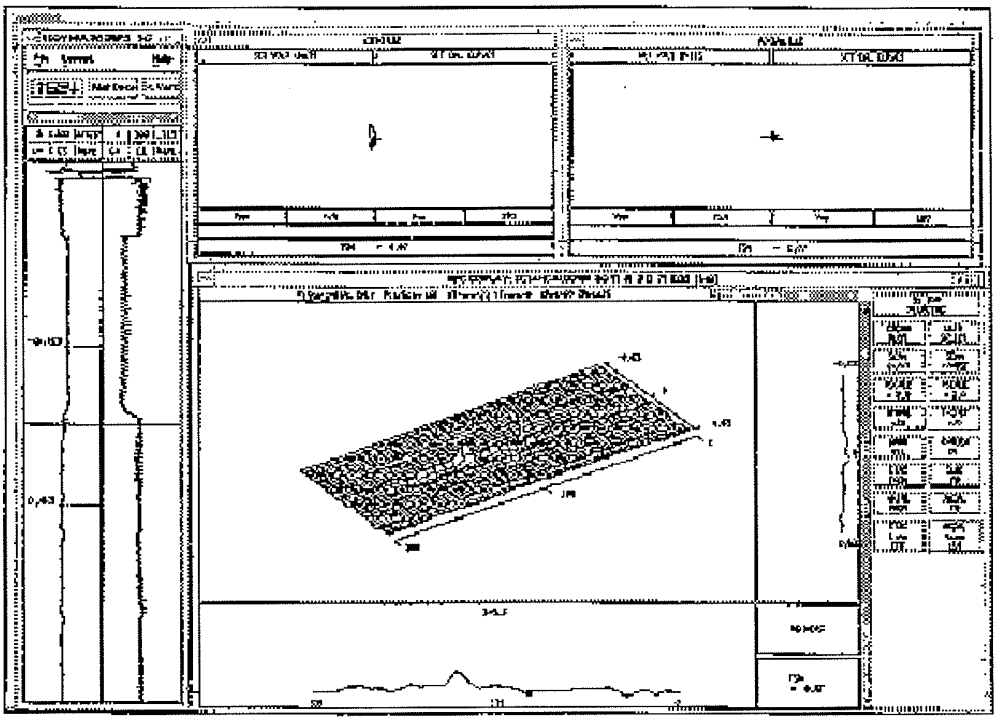

Figure A-8
Cursor at the end of the circumferential indication in the axial lissajous window

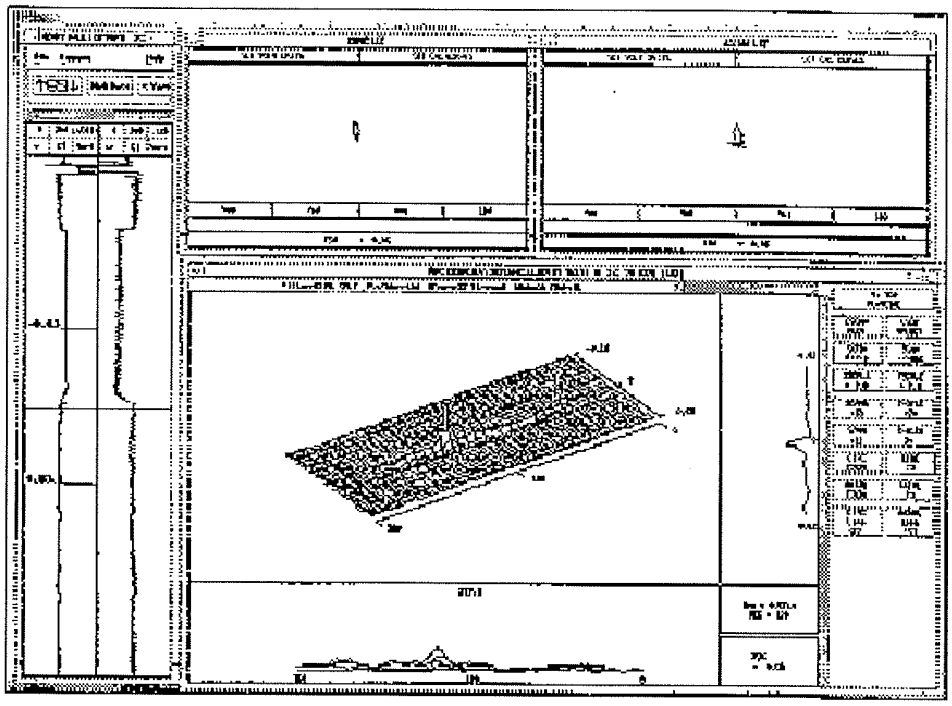

Figure A-9
"Stacked" scan lines affected by the circumferential indication

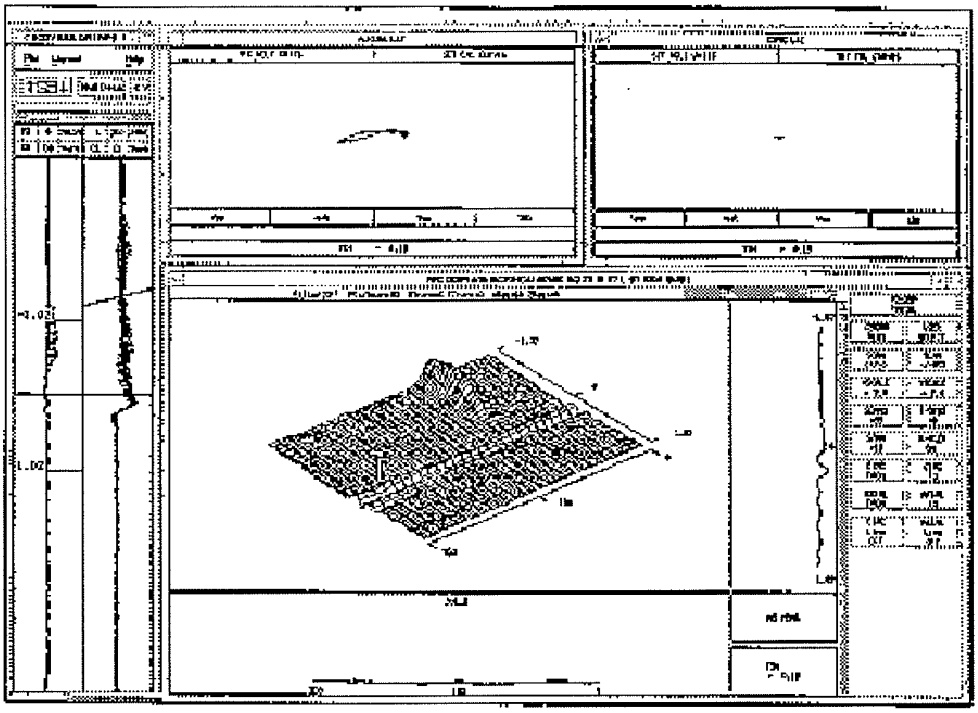

Figure A-10
Cursor at position on roll transition geometry response free from axial indications

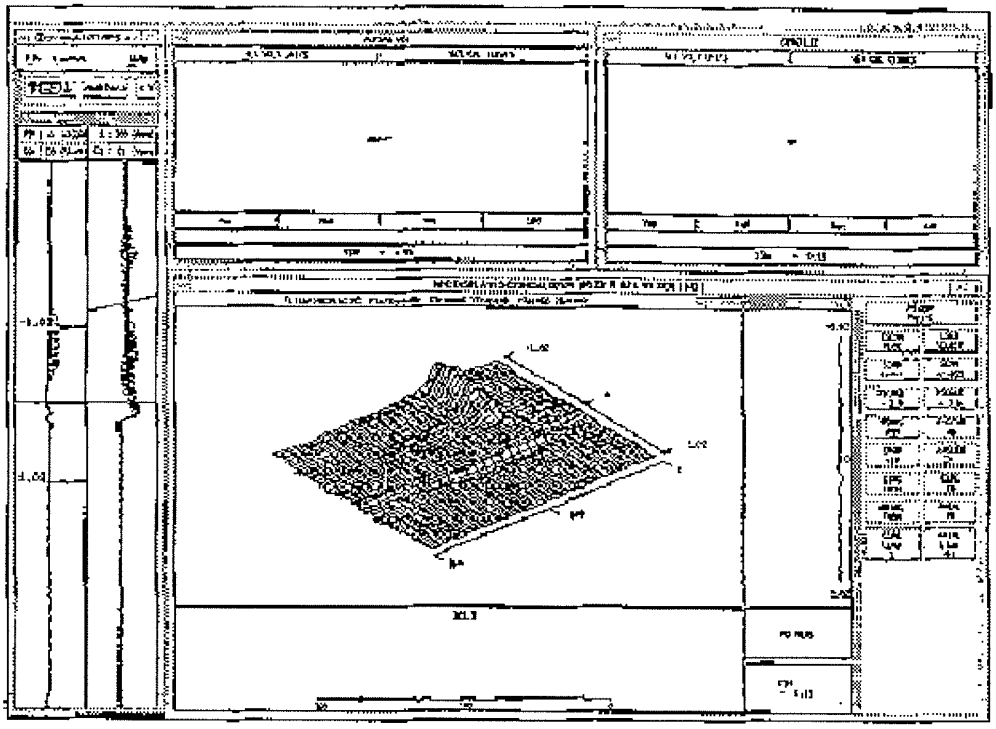

Figure A-11
Cursor at position of roll transition geometry response after axial line filter application

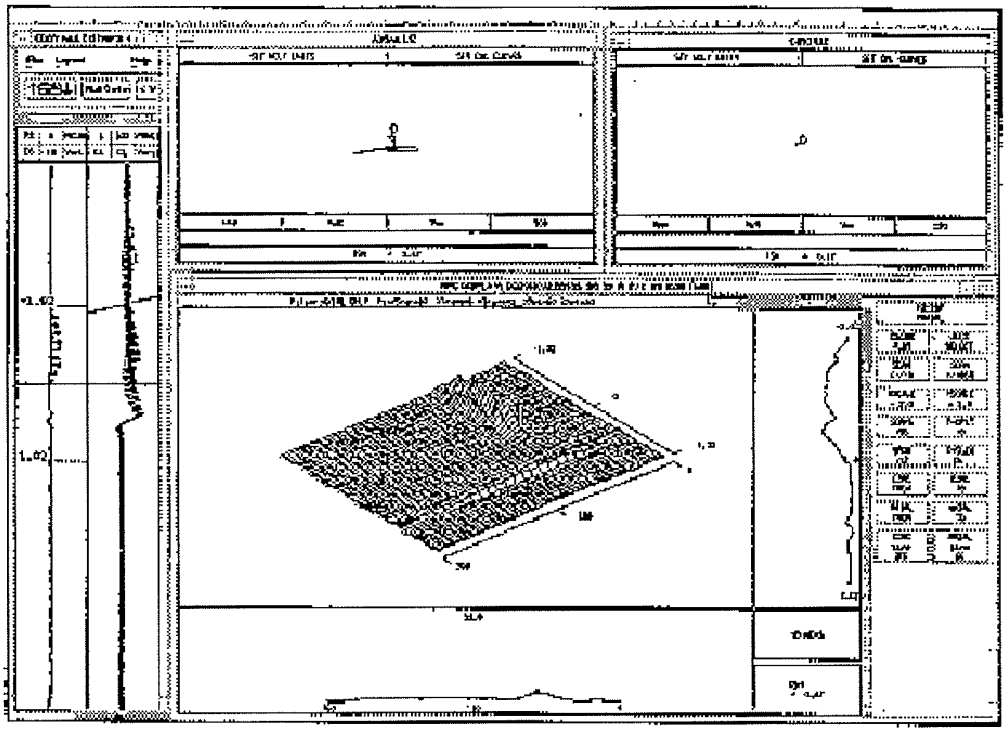

Figure A-12
Cursor at the start of an axial indication in the circumferential lissajous window

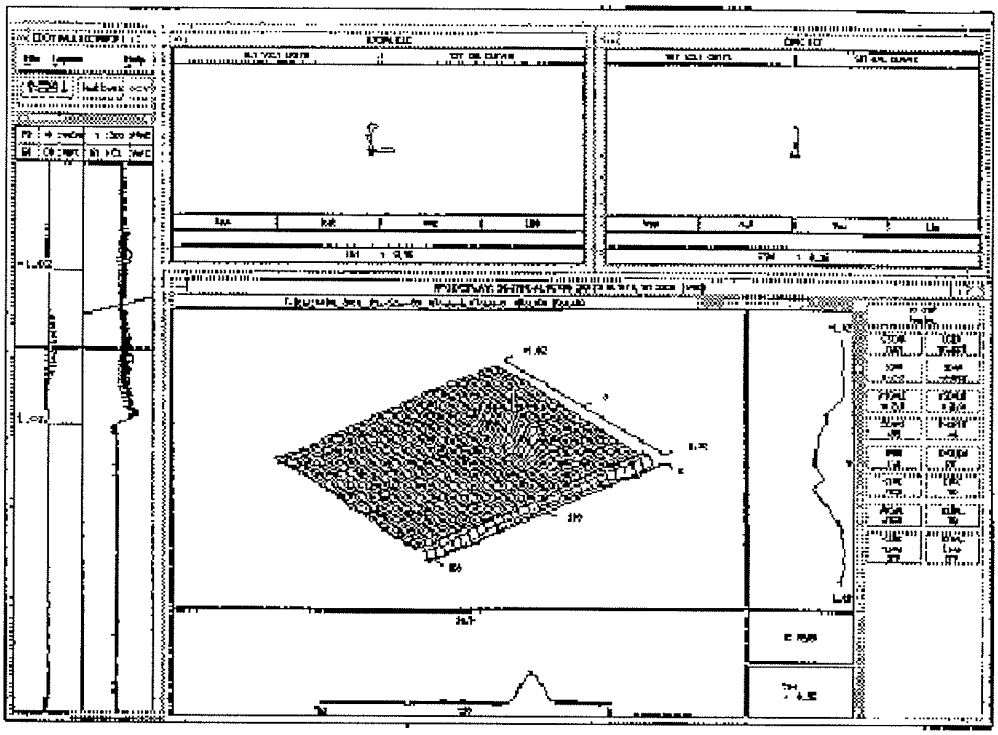

Figure A-13
Location of peak amplitude of the axial indication in the circumferential lissajous window

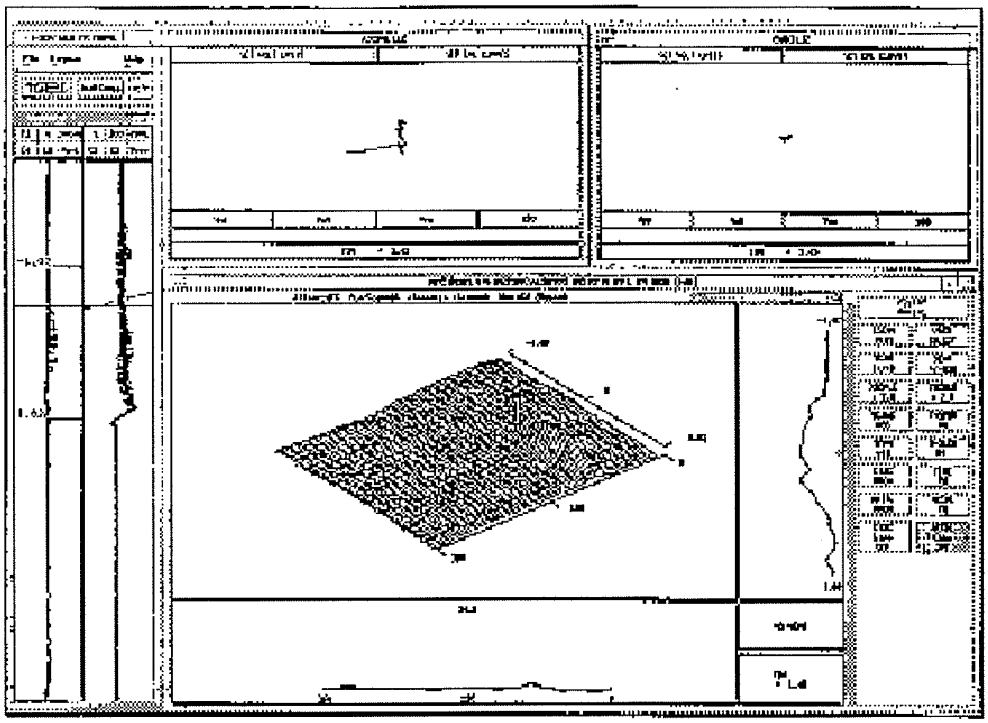

Figure A-14
Cursor at the end of the axial indication in the circumferential lissajous window

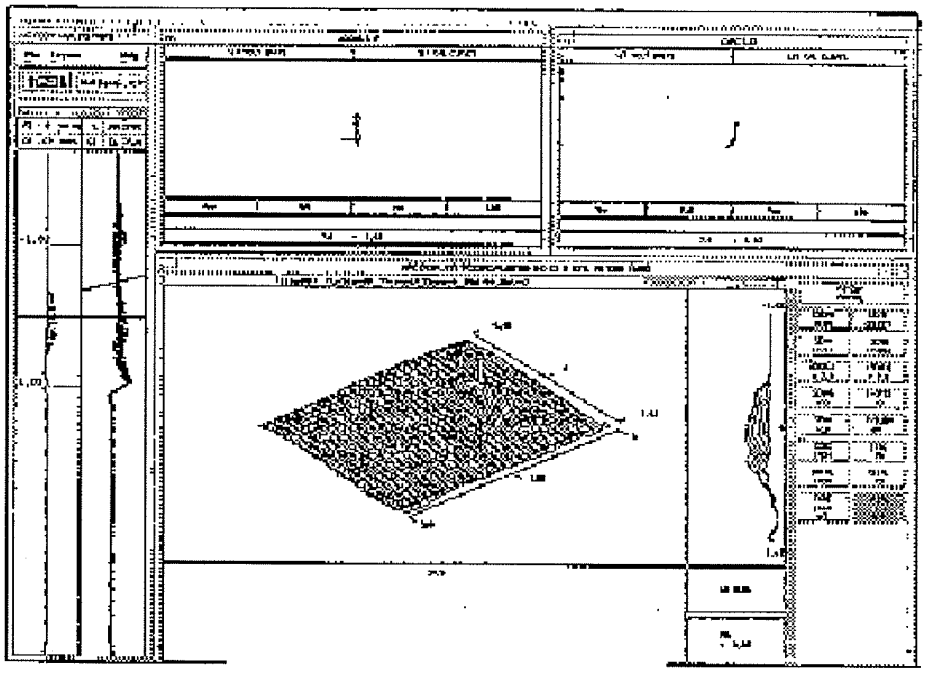

Figure A-15
"Stacked" axial lines affected by the axial indication

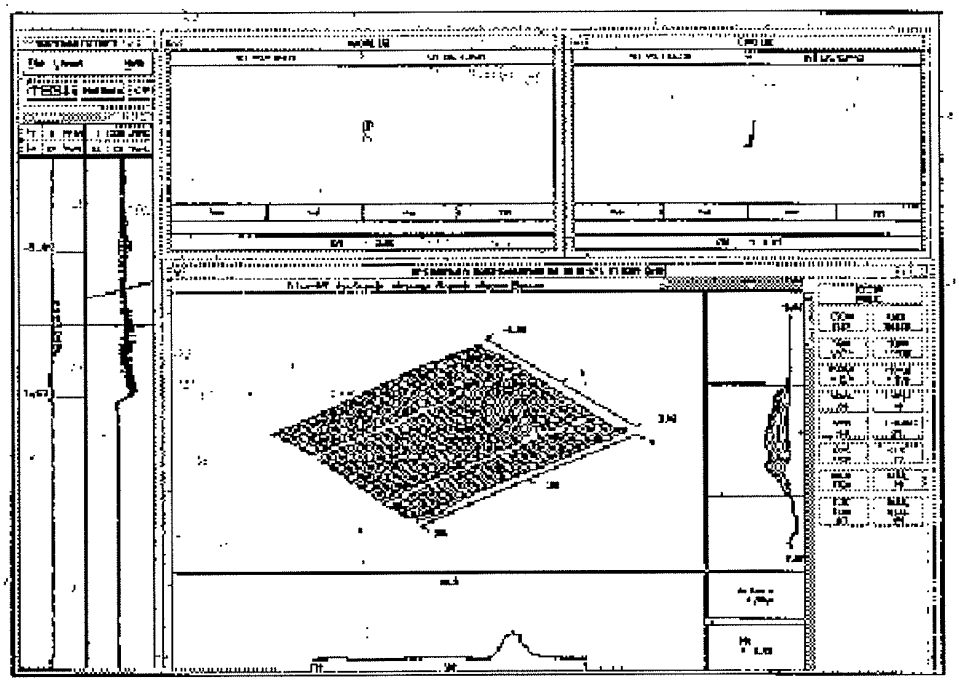

Figure A-16
Graphic documentation of the axial indication

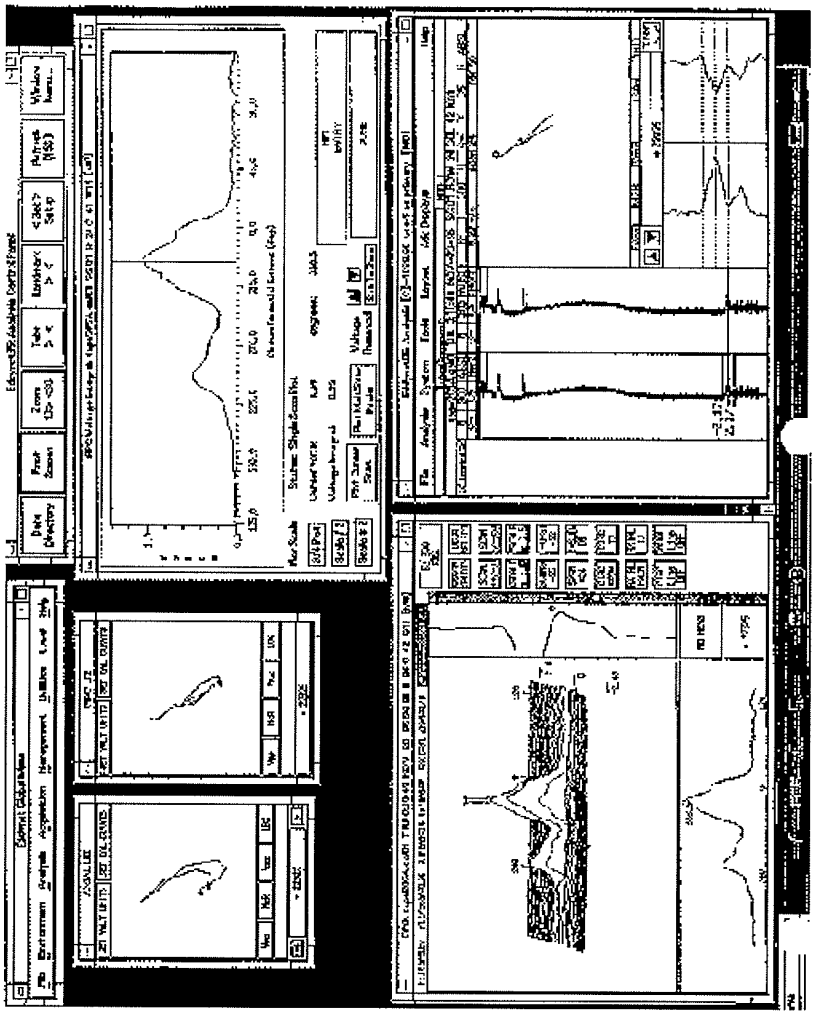

Figure A-17

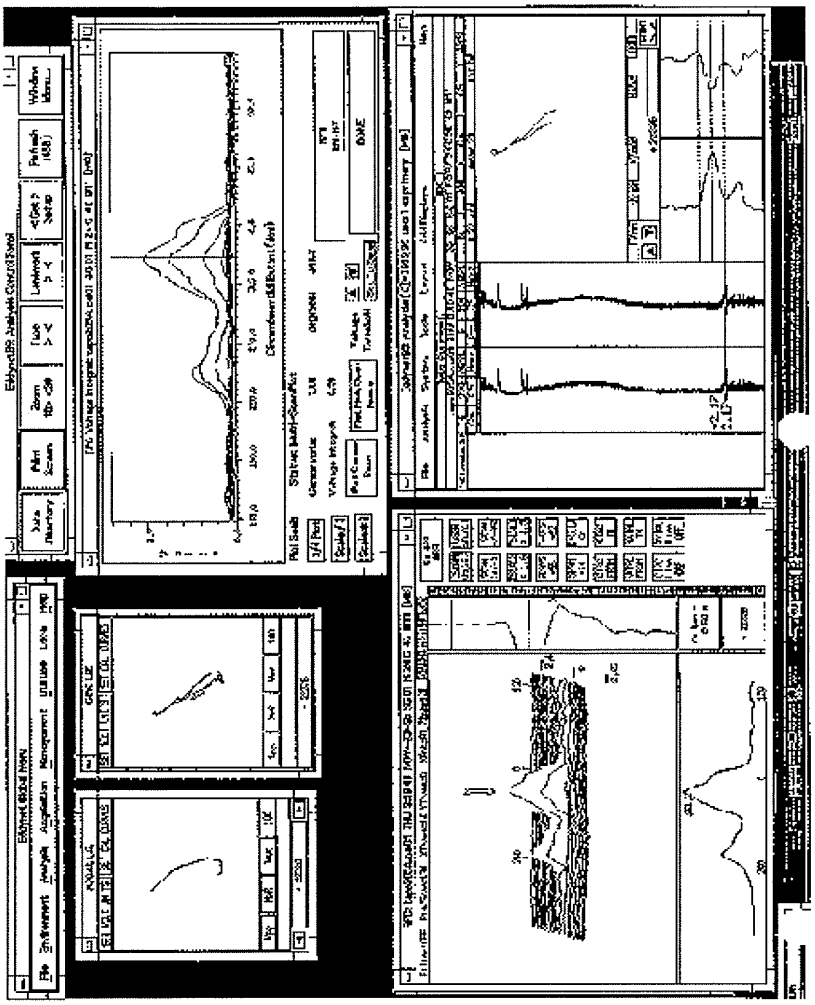

Figure A-18

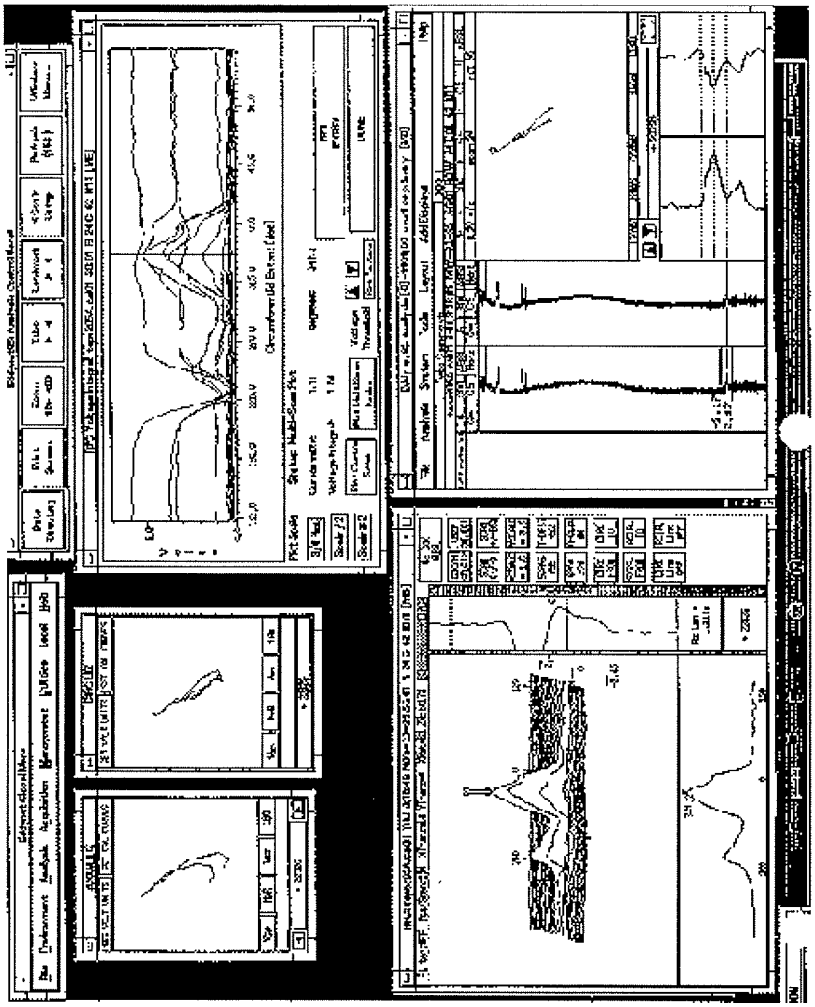

Figure A-19

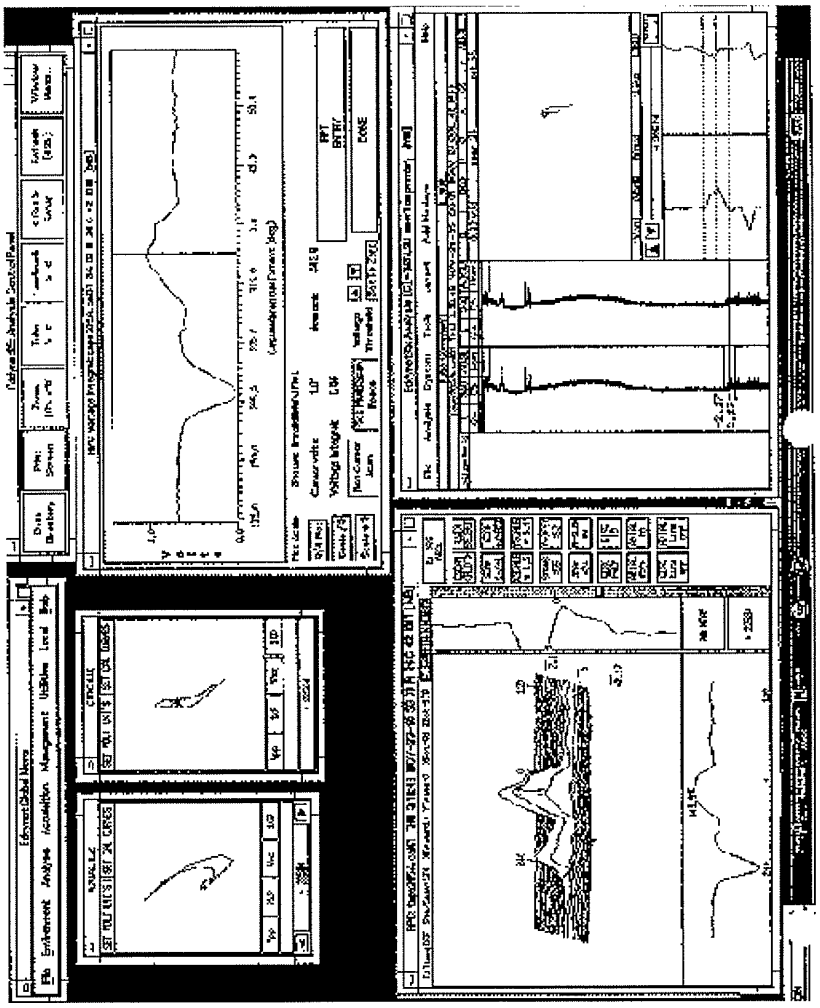

Figure A-20

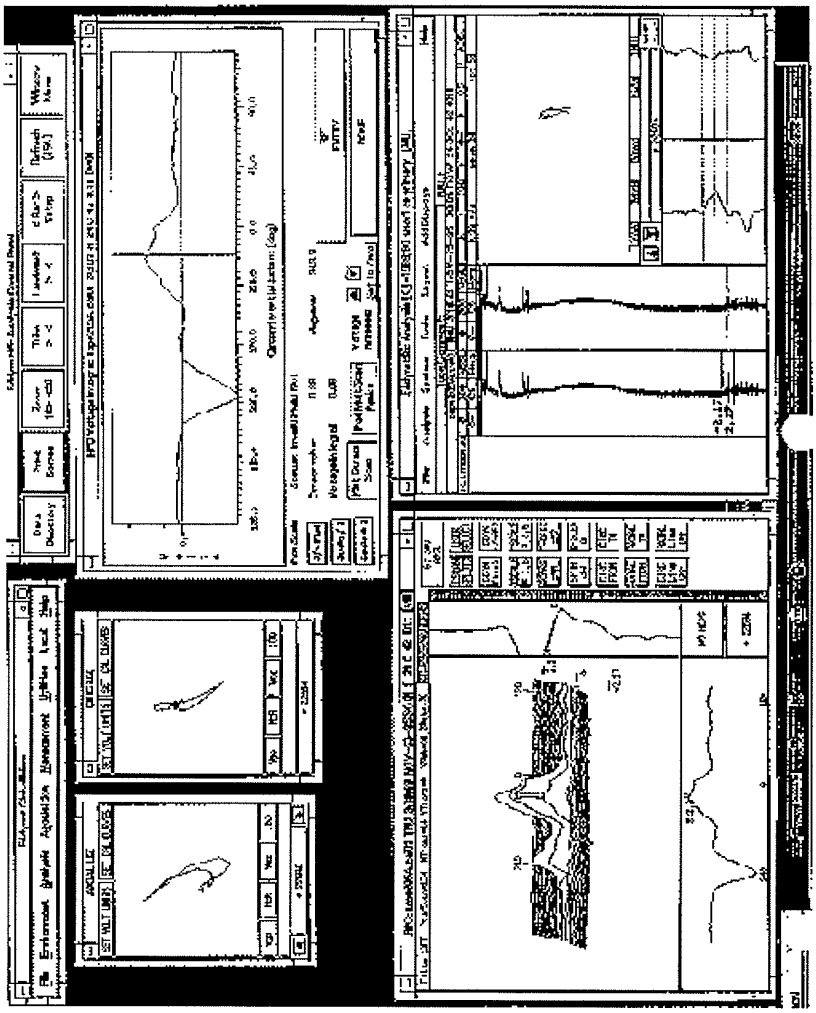

Figure A-21

B

TABULATION OF PULLED TUBE CRACK DEPTH PROFILES FROM DESTRUCTIVE EXAM

This Appendix includes the destructive examination data for the pulled tubes referenced in the body of the report. These data were compiled from original pulled tube examination reports as referenced in the data base table in Section 3. The data included here are tabular data of measured depth vs. angular position, and a plot of the tabular data to provide a visual image of the depth profile for each tube. Ligament data are included where these were reported; however, no adjustment to the depth profiles are made to account for the ligaments. Section 3 of the report provides the methods by which ligament adjustments were made to obtain a net depth profile.

Tabulation of Pulled Tube Crack Depth Profiles from Destructive Exam

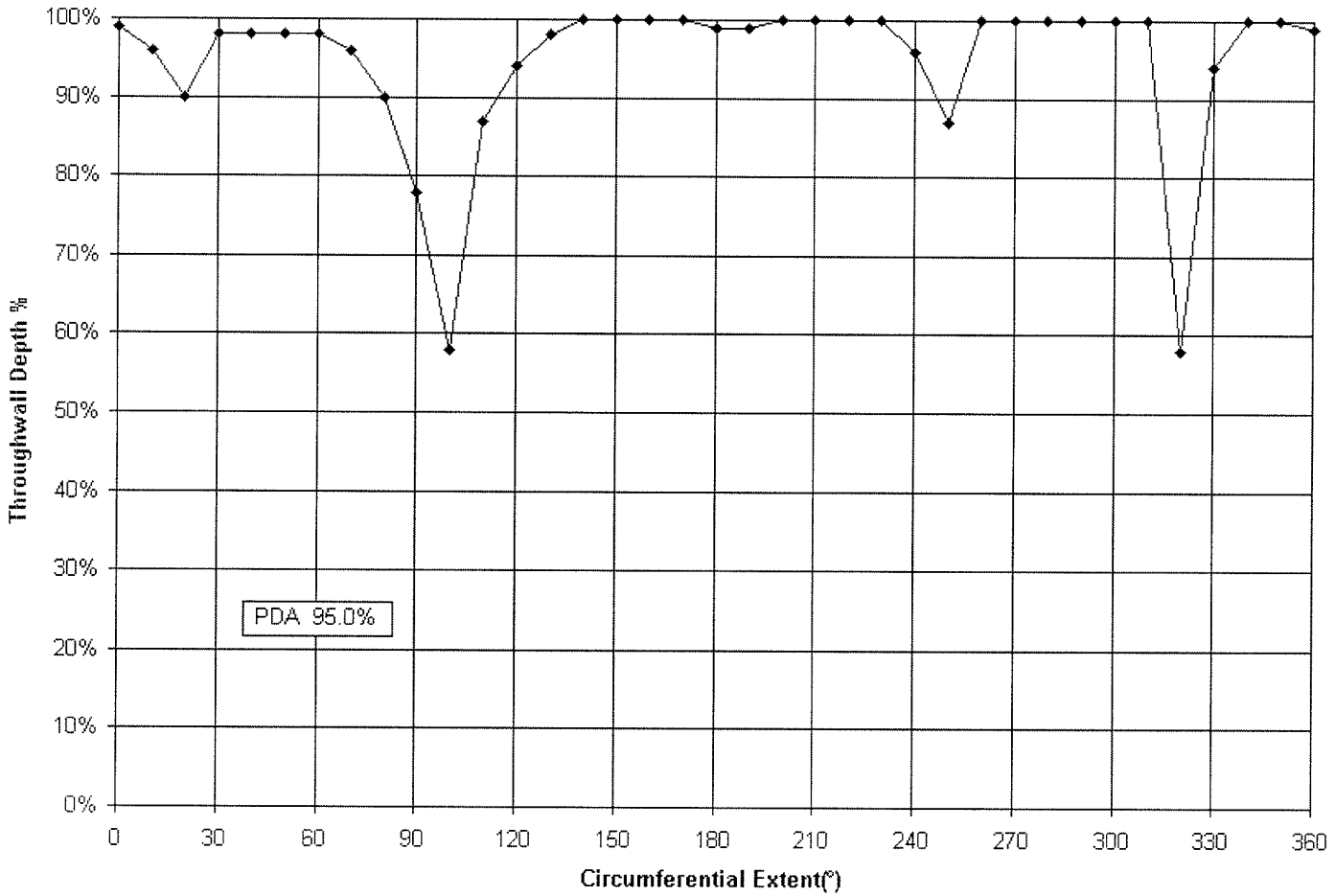

Figure B-1
Plant CA, R13L147; Destructive Examination Depth Profile

Plant :	**CA**	
Tube :	**R13L147**	
PDA :	**95.0%**	
Angle	Depth	Lig. Area
0	99.0%	
10	96.0%	
20	90.0%	
30	98.0%	
40	98.0%	
50	98.0%	
60	98.0%	
70	96.0%	
80	90.0%	
90	78.0%	
100	58.0%	
110	87.0%	
120	94.0%	
130	98.0%	
140	100.0%	
150	100.0%	
160	100.0%	
170	100.0%	
180	99.0%	
190	99.0%	
200	100.0%	
210	100.0%	
220	100.0%	
230	100.0%	
240	96.0%	
250	87.0%	
260	100.0%	
270	100.0%	
280	100.0%	
290	100.0%	
300	100.0%	
310	100.0%	
320	58.0%	
330	94.0%	
340	100.0%	
350	100.0%	
360	99.0%	

Tabulation of Pulled Tube Crack Depth Profiles from Destructive Exam

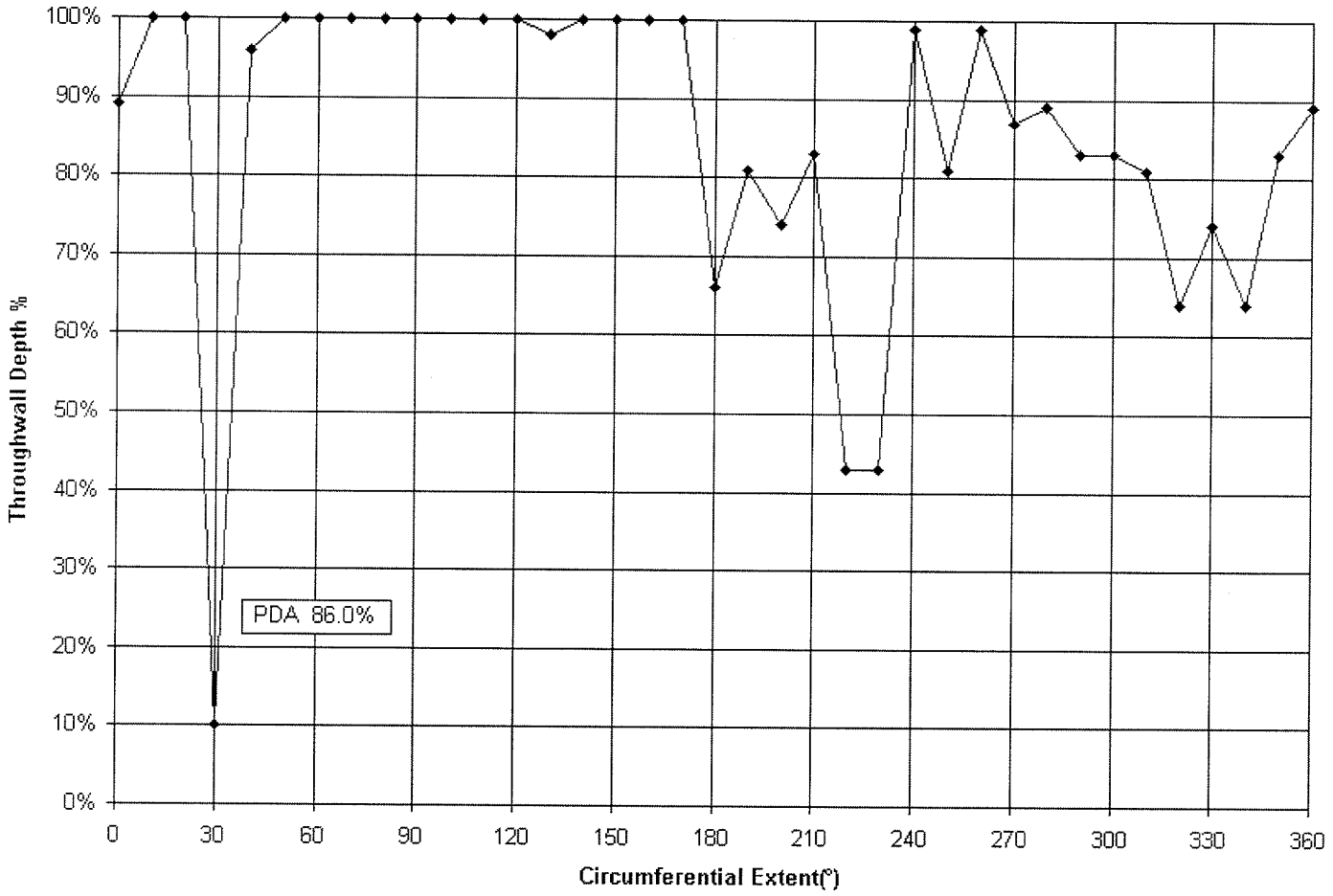

Figure B-2
Plant CA, R36L130; Destructive Examination Depth Profile

Plant :	**CA**	
Tube :	**R36L130**	
PDA :	**86.0%**	
Angle	Depth	Lig. Area
0	89.0%	
10	100.0%	
20	100.0%	
30	10.0%	
40	96.0%	
50	100.0%	
60	100.0%	
70	100.0%	
80	100.0%	
90	100.0%	
100	100.0%	
110	100.0%	
120	100.0%	
130	98.0%	
140	100.0%	
150	100.0%	
160	100.0%	
170	100.0%	
180	66.0%	
190	81.0%	
200	74.0%	
210	83.0%	
220	43.0%	
230	43.0%	
240	99.0%	
250	81.0%	
260	99.0%	
270	87.0%	
280	89.0%	
290	83.0%	
300	83.0%	
310	81.0%	
320	64.0%	
330	74.0%	
340	64.0%	
350	83.0%	
360	89.0%	

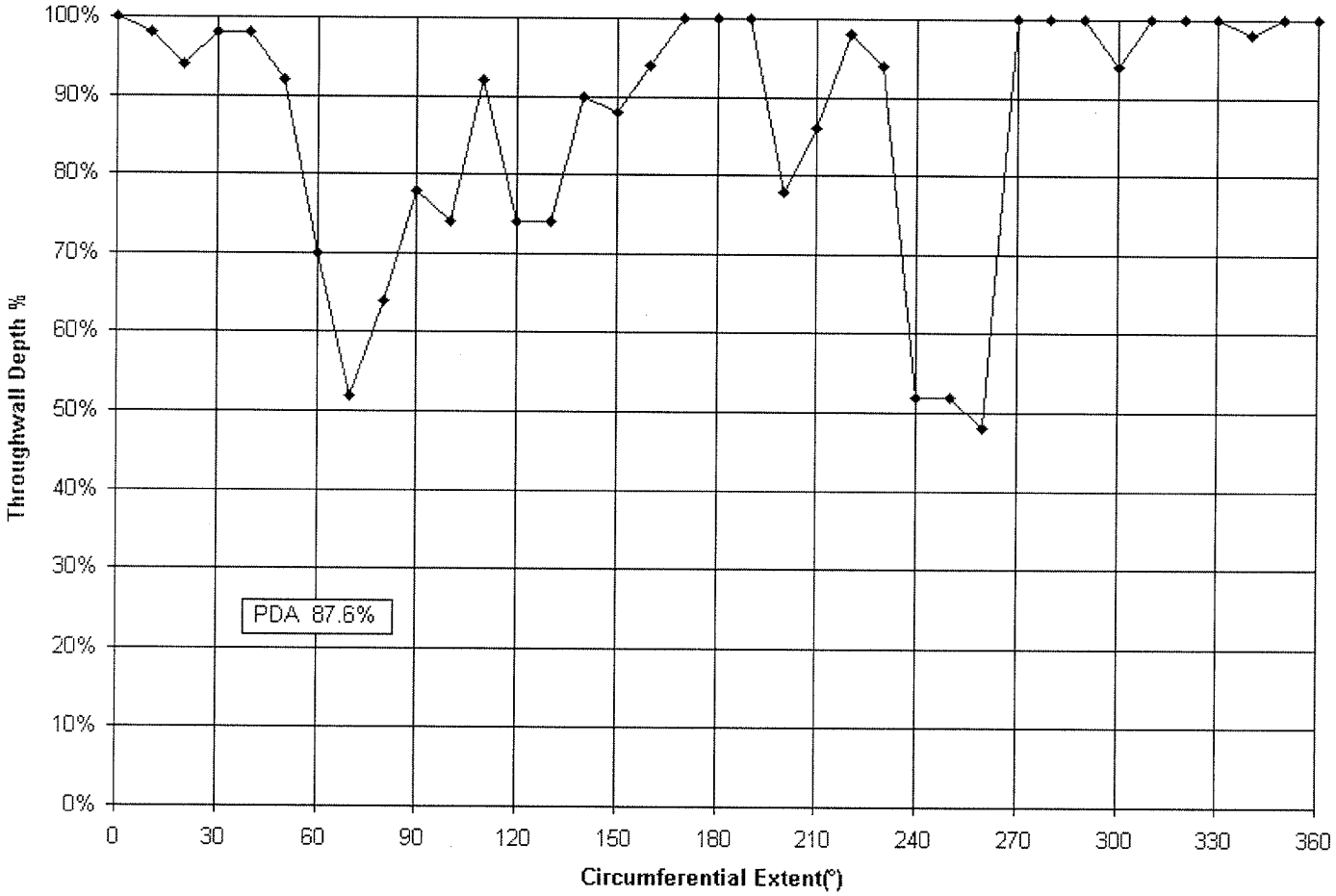

Figure B-3
Plant CA, R55L63; Destructive Examination Depth Profile

Plant :	**CA**	
Tube :	**R55L63**	
PDA :	**87.6%**	
Angle	Depth	Lig. Area
0	100.0%	
10	98.0%	
20	94.0%	
30	98.0%	
40	98.0%	
50	92.0%	
60	70.0%	
70	52.0%	
80	64.0%	
90	78.0%	
100	74.0%	
110	92.0%	
120	74.0%	
130	74.0%	
140	90.0%	
150	88.0%	
160	94.0%	
170	100.0%	
180	100.0%	
190	100.0%	
200	78.0%	
210	86.0%	
220	98.0%	
230	94.0%	
240	52.0%	
250	52.0%	
260	48.0%	
270	100.0%	
280	100.0%	
290	100.0%	
300	94.0%	
310	100.0%	
320	100.0%	
330	100.0%	
340	98.0%	
350	100.0%	
360	100.0%	

Tabulation of Pulled Tube Crack Depth Profiles from Destructive Exam

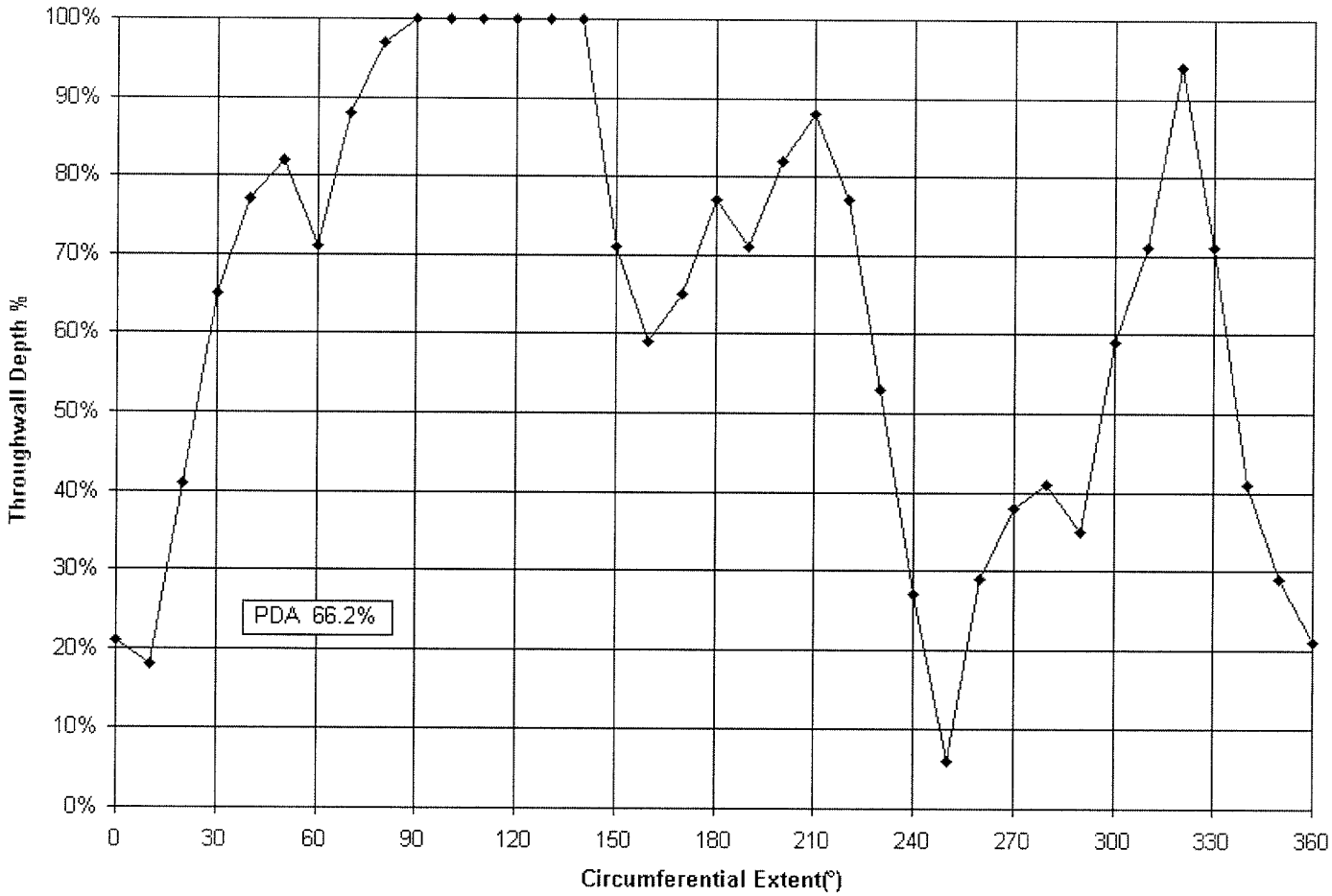

Figure B-4
Plant CA, R64L48; Destructive Examination Depth Profile

Plant :	**CA**	
Tube :	**R-64L48**	
PDA :	**66.2%**	
Angle	Depth	Lig. Area
0	21.0%	
10	18.0%	
20	41.0%	
30	65.0%	
40	77.0%	
50	82.0%	
60	71.0%	
70	88.0%	
80	97.0%	
90	100.0%	
100	100.0%	
110	100.0%	
120	100.0%	
130	100.0%	
140	100.0%	
150	71.0%	
160	59.0%	
170	65.0%	
180	77.0%	
190	71.0%	
200	82.0%	
210	88.0%	
220	77.0%	
230	53.0%	
240	27.0%	
250	6.0%	
260	29.0%	
270	38.0%	
280	41.0%	
290	35.0%	
300	59.0%	
310	71.0%	
320	94.0%	
330	71.0%	
340	41.0%	
350	29.0%	
360	21.0%	

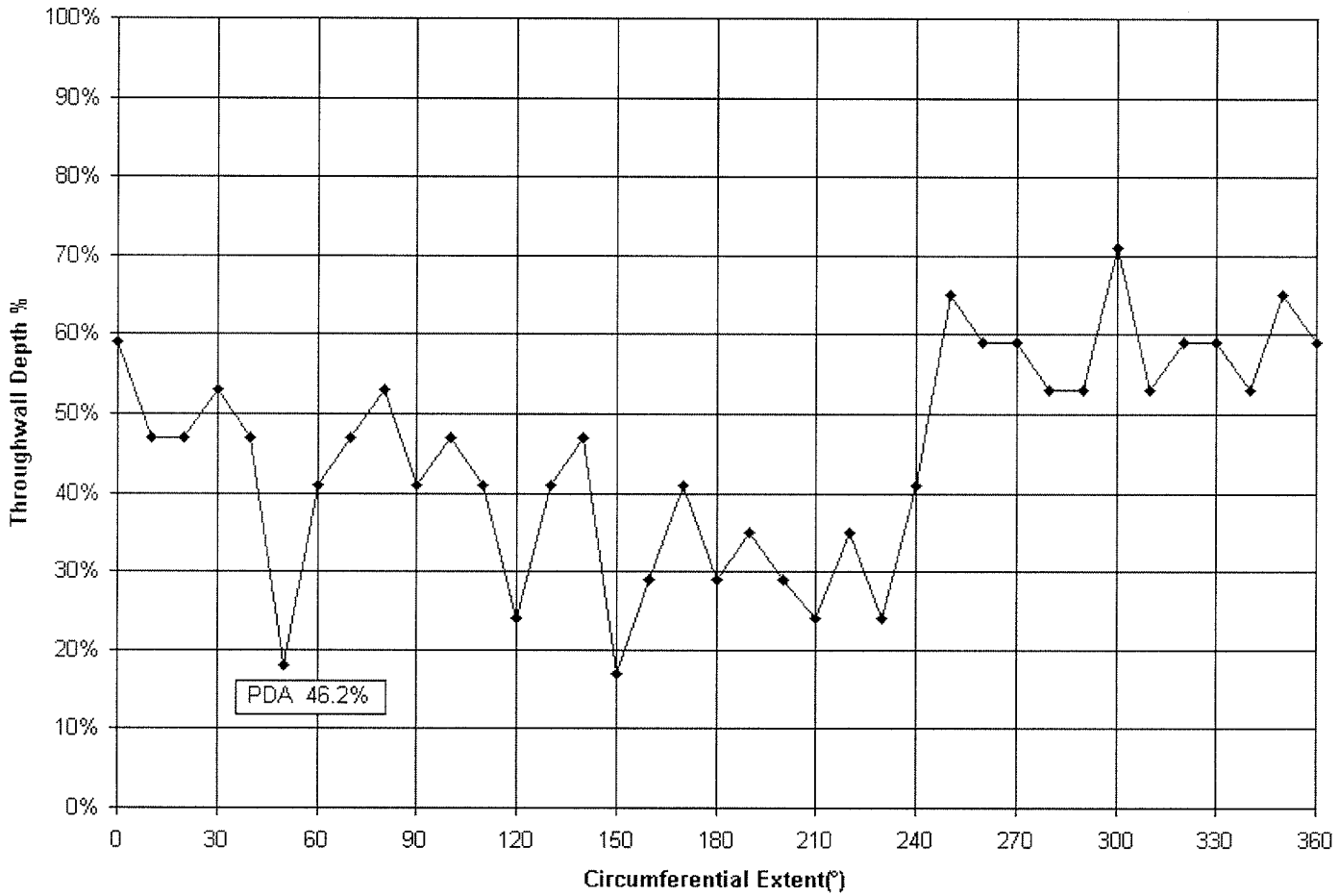

Figure B-5
Plant CA, R79L83; Destructive Examination Depth Profile

Plant :	**CA**	
Tube :	**R79L83**	
PDA :	**46.2%**	
Angle	Depth	Lig. Area
0	59.0%	
10	47.0%	
20	47.0%	
30	53.0%	
40	47.0%	
50	18.0%	
60	41.0%	
70	47.0%	
80	53.0%	
90	41.0%	
100	47.0%	
110	41.0%	
120	24.0%	
130	41.0%	
140	47.0%	
150	17.0%	
160	29.0%	
170	41.0%	
180	29.0%	
190	35.0%	
200	29.0%	
210	24.0%	
220	35.0%	
230	24.0%	
240	41.0%	
250	65.0%	
260	59.0%	
270	59.0%	
280	53.0%	
290	53.0%	
300	71.0%	
310	53.0%	
320	59.0%	
330	59.0%	
340	53.0%	
350	65.0%	
360	59.0%	

Tabulation of Pulled Tube Crack Depth Profiles from Destructive Exam

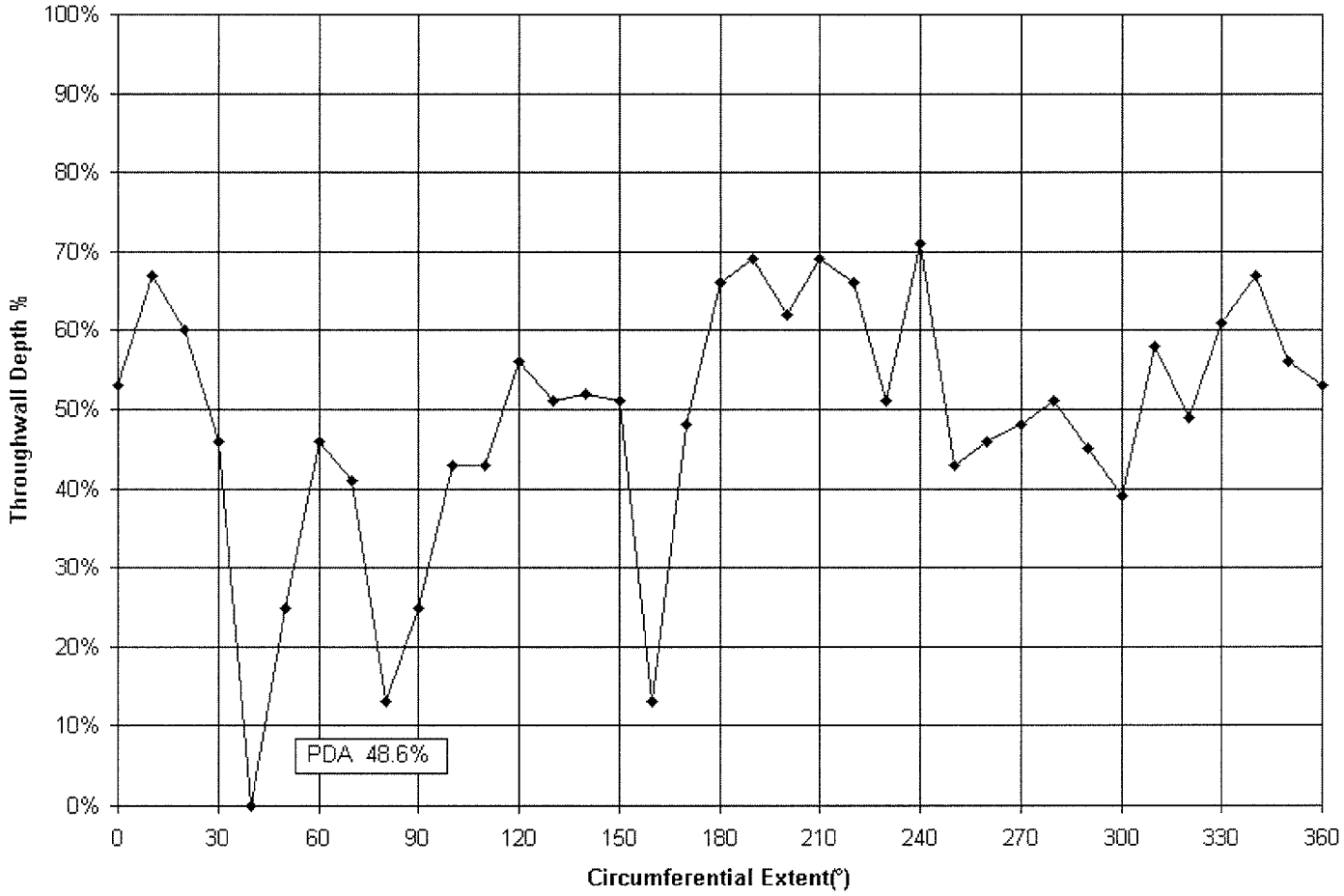

Figure B-6
Plant FM, R14L118; Destructive Examination Depth Profile

Plant :	**FM**	
Tube :	**R14L118**	
PDA :	**48.6%**	
Angle	Depth	Lig. Area
0	53.0%	
10	67.0%	
20	60.0%	
30	46.0%	
40	0.0%	
50	25.0%	
60	46.0%	
70	41.0%	
80	13.0%	
90	25.0%	
100	43.0%	
110	43.0%	
120	56.0%	
130	51.0%	
140	52.0%	
150	51.0%	
160	13.0%	
170	48.0%	
180	66.0%	
190	69.0%	
200	62.0%	
210	69.0%	
220	66.0%	
230	51.0%	
240	71.0%	
250	43.0%	
260	46.0%	
270	48.0%	
280	51.0%	
290	45.0%	
300	39.0%	
310	58.0%	
320	49.0%	
330	61.0%	
340	67.0%	
350	56.0%	
360	53.0%	

Tabulation of Pulled Tube Crack Depth Profiles from Destructive Exam

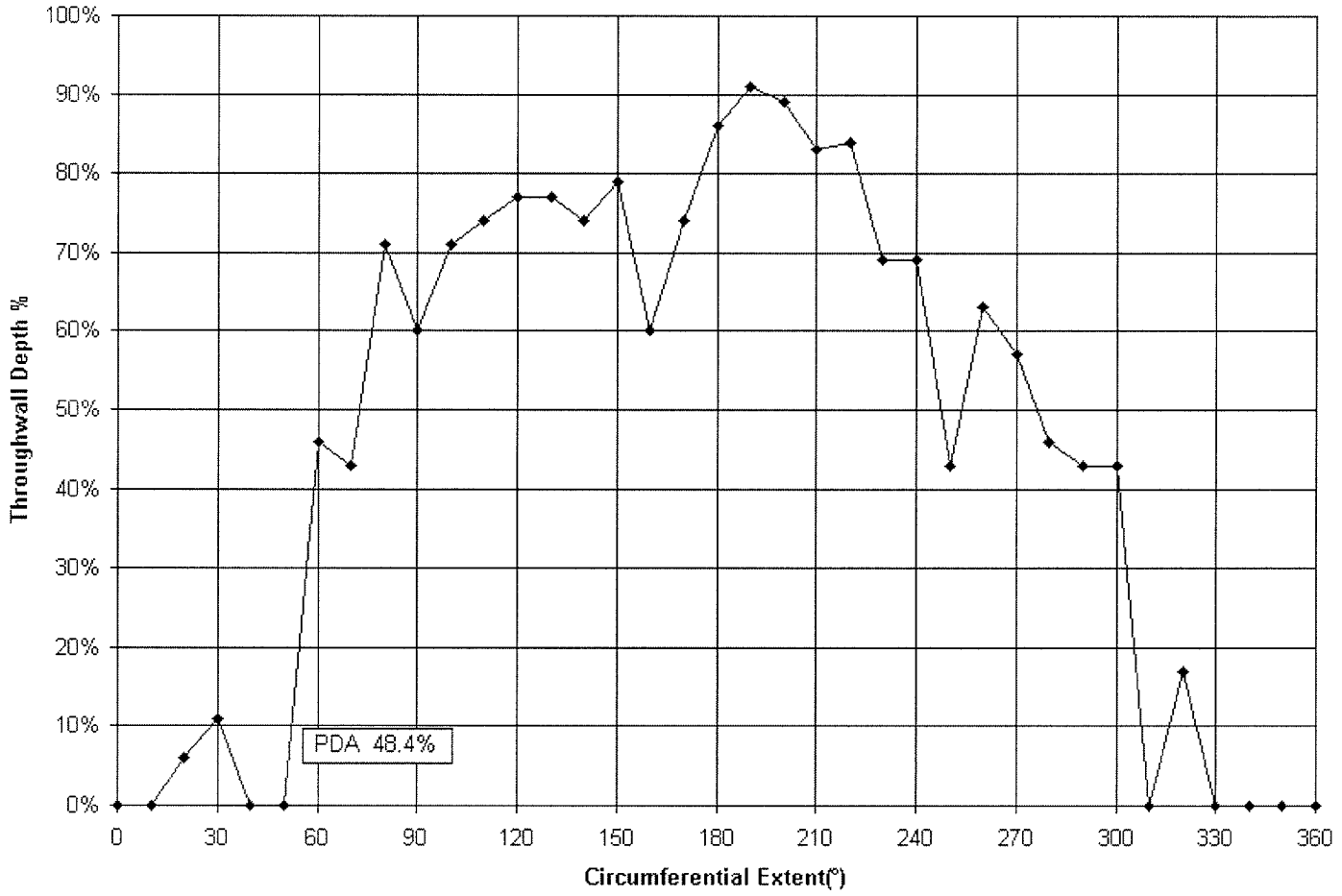

Figure B-7
Plant FM, R22L52; Destructive Examination Depth Profile

Plant :	**FM**	
Tube :	**R22L52**	
PDA :	**48.4%**	
Angle	Depth	Lig. Area
0	0.0%	
10	0.0%	
20	6.0%	
30	11.0%	
40	0.0%	
50	0.0%	
60	46.0%	
70	43.0%	
80	71.0%	
90	60.0%	
100	71.0%	
110	74.0%	
120	77.0%	
130	77.0%	
140	74.0%	
150	79.0%	
160	60.0%	
170	74.0%	
180	86.0%	
190	91.0%	
200	89.0%	
210	83.0%	
220	84.0%	
230	69.0%	
240	69.0%	
250	43.0%	
260	63.0%	
270	57.0%	
280	46.0%	
290	43.0%	
300	43.0%	
310	0.0%	
320	17.0%	
330	0.0%	
340	0.0%	
350	0.0%	
360	0.0%	

Tabulation of Pulled Tube Crack Depth Profiles from Destructive Exam

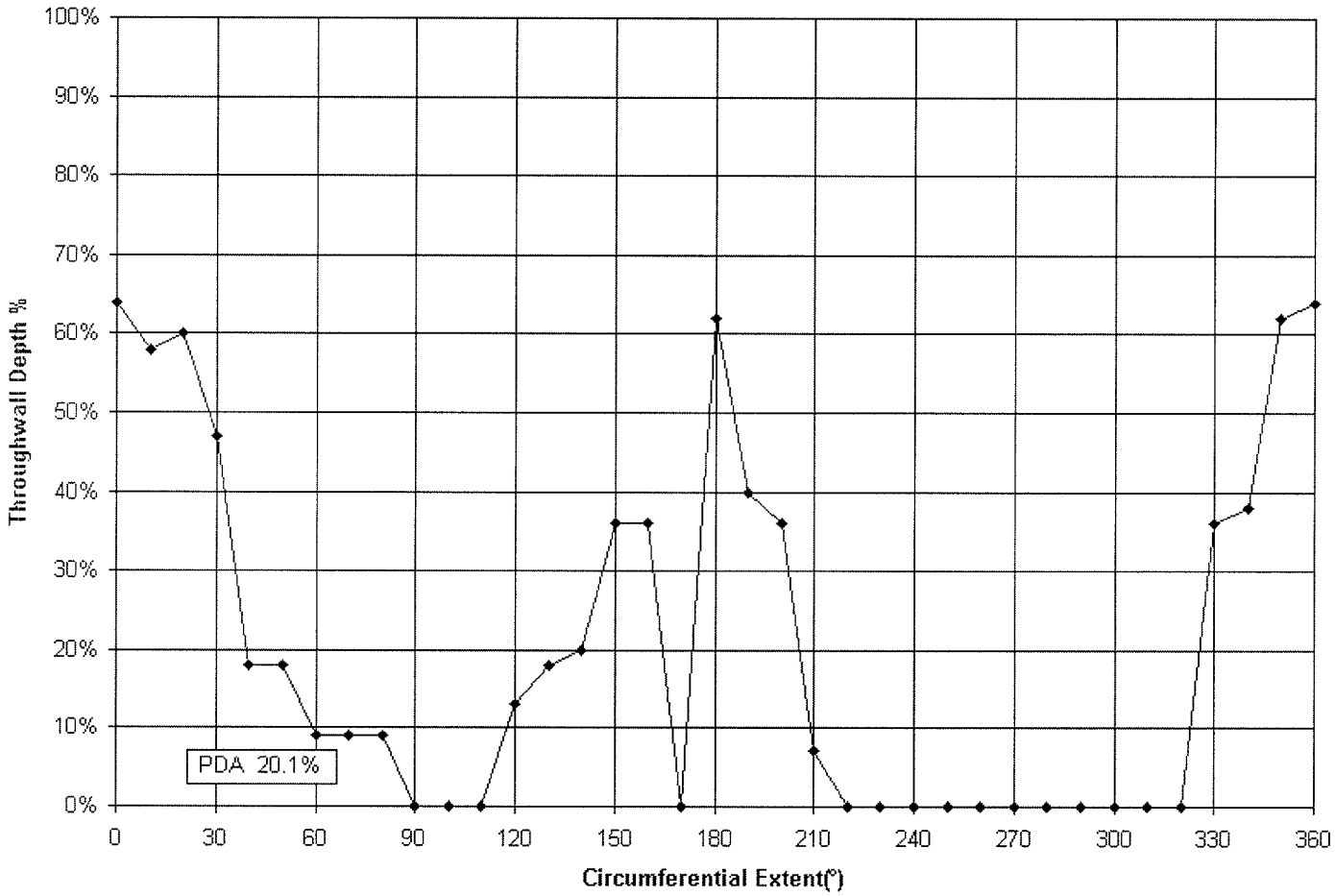

Figure B-8
Plant FM, R23L145; Destructive Examination Depth Profile

Plant :	**FM**	
Tube :	**R23L145**	
PDA :	**20.1%**	
Angle	Depth	Lig. Area
0	64.0%	
10	58.0%	
20	60.0%	
30	47.0%	
40	18.0%	
50	18.0%	
60	9.0%	
70	9.0%	
80	9.0%	
90	0.0%	
100	0.0%	
110	0.0%	
120	13.0%	
130	18.0%	
140	20.0%	
150	36.0%	
160	36.0%	
170	0.0%	
180	62.0%	
190	40.0%	
200	36.0%	
210	7.0%	
220	0.0%	
230	0.0%	
240	0.0%	
250	0.0%	
260	0.0%	
270	0.0%	
280	0.0%	
290	0.0%	
300	0.0%	
310	0.0%	
320	0.0%	
330	36.0%	
340	38.0%	
350	62.0%	
360	64.0%	

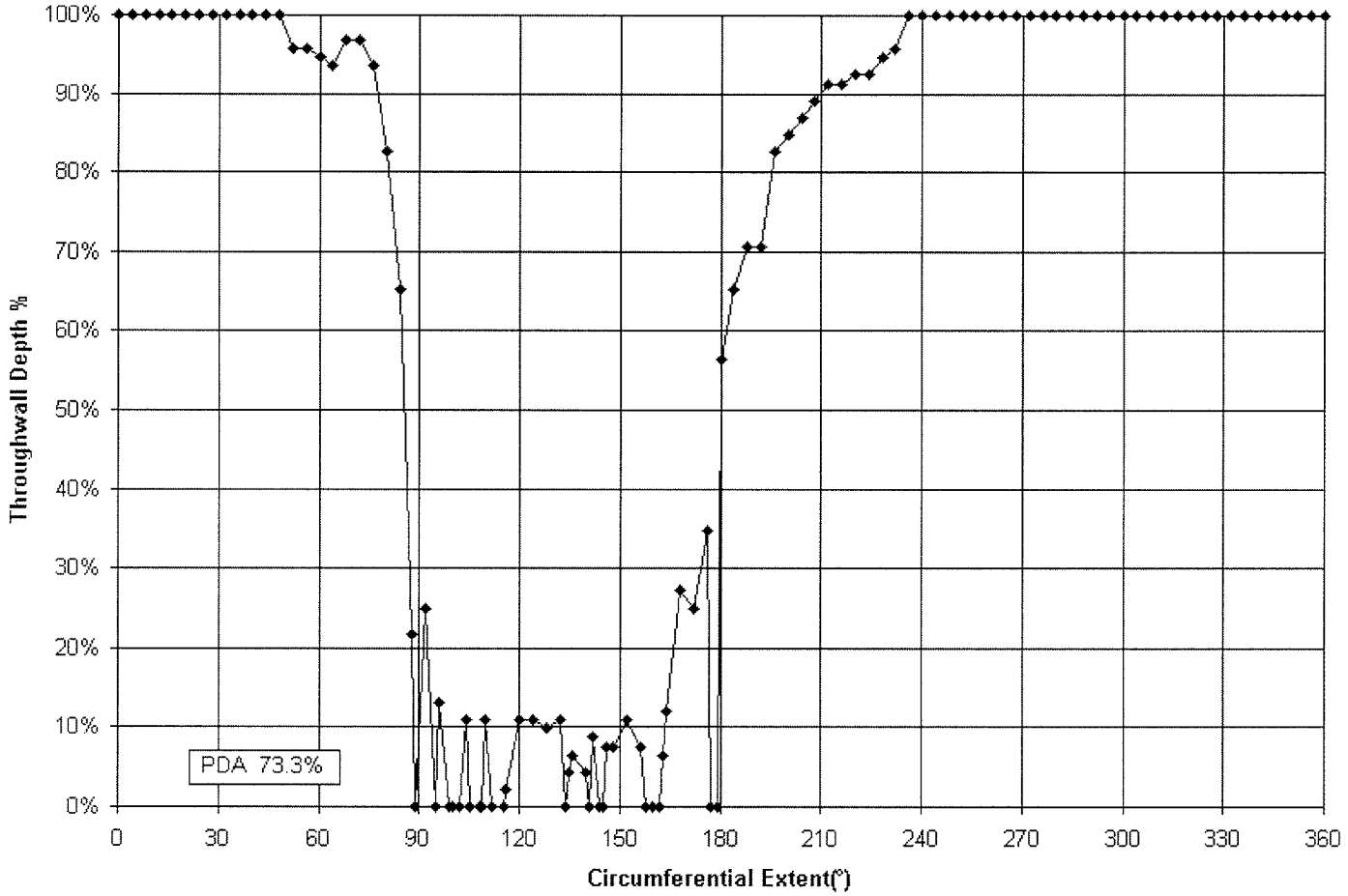

Figure B-9
Plant FM, R19L25; Destructive Examination Depth Profile

Plant :			**FM**					
Tube :			**R19L25**					
PDA :			**73.3%**					
Angle	Depth	Lig. Area	Angle	Depth	Lig. Area	Angle	Depth	Lig. Area
0	100.0%		116	2.2%		220	92.4%	
4	100.0%		120	10.9%		224	92.4%	
8	100.0%		124	10.9%		228	94.6%	
12	100.0%		128	9.8%		232	95.7%	
16	100.0%		132	10.9%		236	100.0%	
20	100.0%		134	0.0%		240	100.0%	
24	100.0%		135	4.3%		244	100.0%	
28	100.0%		136	6.5%		248	100.0%	
32	100.0%		140	4.3%		252	100.0%	
36	100.0%		141	0.0%		256	100.0%	
40	100.0%		142	8.7%		260	100.0%	
44	100.0%		144	0.0%		264	100.0%	
48	100.0%		145	0.0%		268	100.0%	
52	95.7%		146	7.6%		272	100.0%	
56	95.7%		148	7.6%		276	100.0%	
60	94.6%		152	10.9%		280	100.0%	
64	93.5%		156	7.6%		284	100.0%	
68	96.7%		158	0.0%		288	100.0%	
72	96.7%		160	0.0%		292	100.0%	
76	93.5%		162	0.0%		296	100.0%	
80	82.6%		163	6.5%		300	100.0%	
84	65.2%		164	12.0%		304	100.0%	
88	21.7%		168	27.2%		308	100.0%	
89	0.0%		172	25.0%		312	100.0%	
92	25.0%		176	34.8%		316	100.0%	
95	0.0%		177	0.0%		320	100.0%	
96	13.0%		179	0.0%		324	100.0%	
99	0.0%		180	56.5%		328	100.0%	
100	0.0%		184	65.2%		332	100.0%	
102	0.0%		188	70.7%		336	100.0%	
104	10.9%		192	70.7%		340	100.0%	
105	0.0%		196	82.6%		344	100.0%	
108	0.0%		200	84.8%		348	100.0%	
109	0.0%		204	87.0%		352	100.0%	
110	10.9%		208	89.1%		356	100.0%	
112	0.0%		212	91.3%		360	100.0%	
116	0.0%		216	91.3%				

Tabulation of Pulled Tube Crack Depth Profiles from Destructive Exam

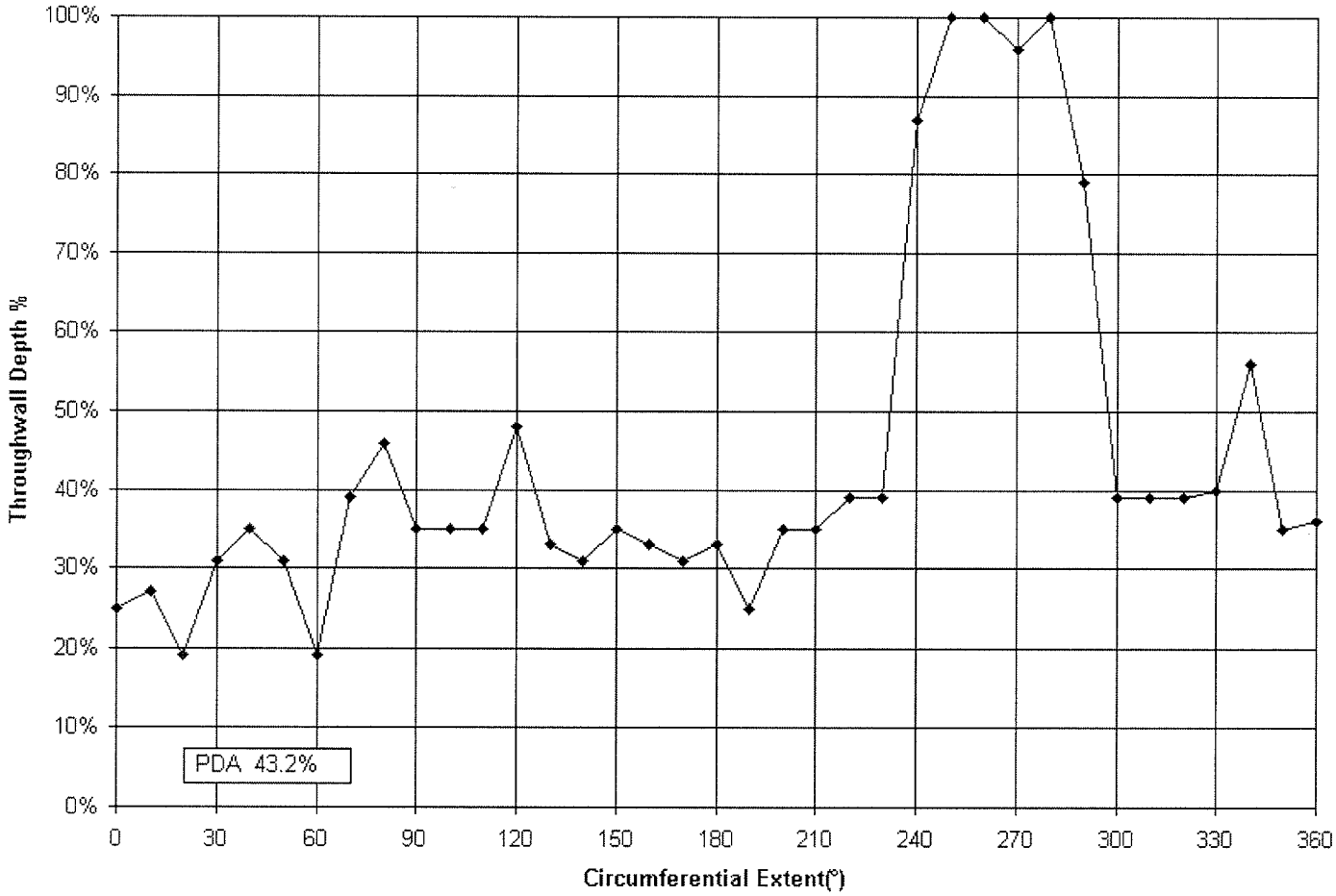

Figure B-10
Plant CB, R75L34; Destructive Examination Depth Profile

Plant :	**CB**	
Tube :	**R75L34**	
PDA :	**43.2%**	
Angle	Depth	Lig. Area
0	25.0%	
10	27.0%	
20	19.0%	
30	31.0%	
40	35.0%	
50	31.0%	
60	19.0%	
70	39.0%	
80	46.0%	
90	35.0%	
100	35.0%	
110	35.0%	
120	48.0%	
130	33.0%	
140	31.0%	
150	35.0%	
160	33.0%	
170	31.0%	
180	33.0%	
190	25.0%	
200	35.0%	
210	35.0%	
220	39.0%	
230	39.0%	
240	87.0%	
250	100.0%	
260	100.0%	
270	96.0%	
280	100.0%	
290	79.0%	
300	39.0%	
310	39.0%	
320	39.0%	
330	40.0%	
340	56.0%	
350	35.0%	
360	36.0%	

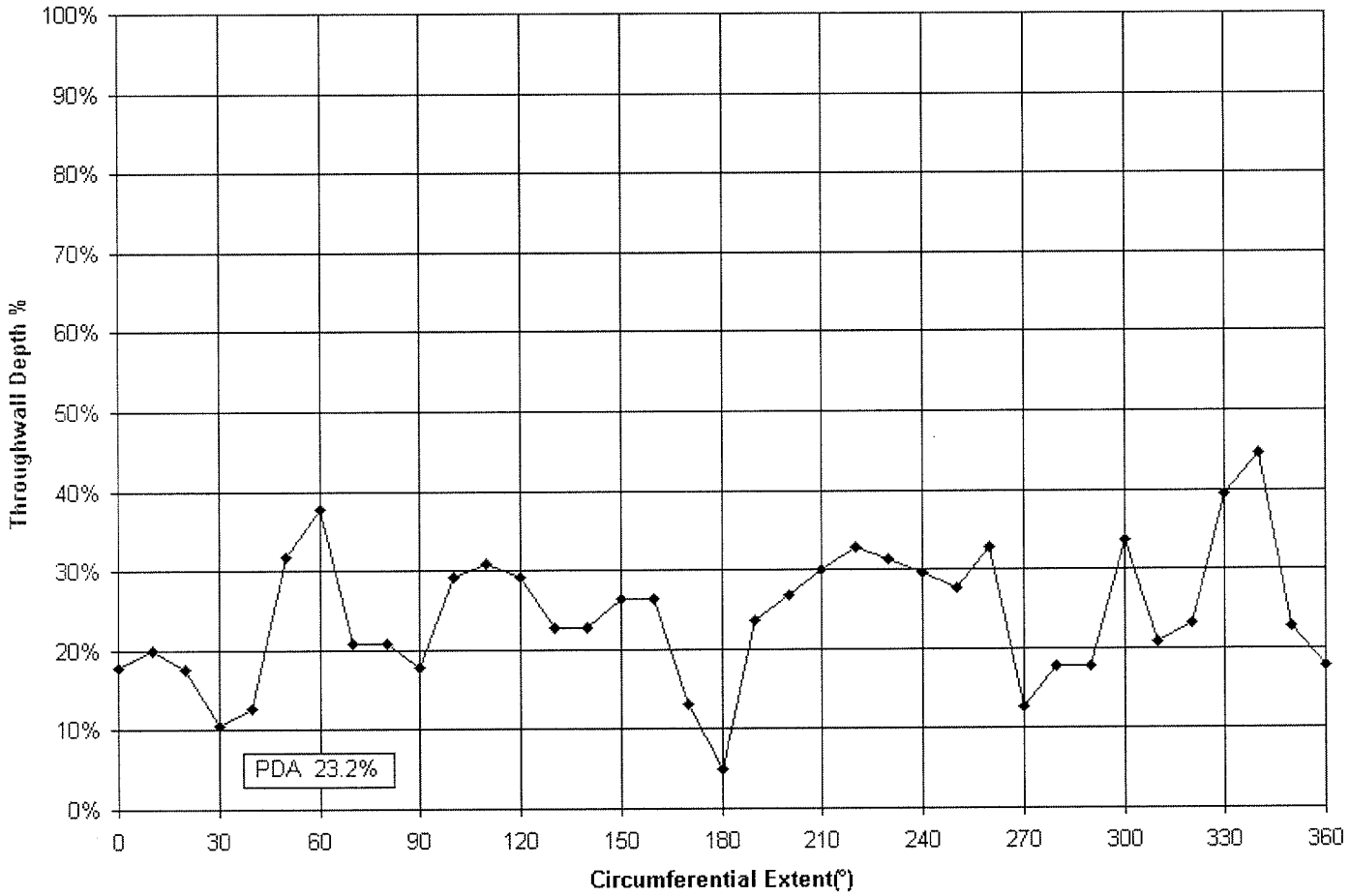

Figure B-11
Plant CB, R79L90; Destructive Examination Depth Profile

Plant :	**CB**	
Tube :	**R79L90**	
PDA :	**23.2%**	
Angle	Depth	Lig. Area
0	17.7%	
10	20.0%	
20	17.7%	
30	10.5%	
40	12.7%	
50	31.8%	
60	37.7%	
70	20.9%	
80	20.9%	
90	17.7%	
100	29.1%	
110	30.9%	
120	29.1%	
130	22.7%	
140	22.7%	
150	26.4%	
160	26.4%	
170	13.2%	
180	5.0%	
190	23.6%	
200	26.8%	
210	30.0%	
220	32.7%	
230	31.4%	
240	29.7%	
250	27.7%	
260	32.7%	
270	12.7%	
280	17.7%	
290	17.7%	
300	33.6%	
310	20.9%	
320	23.2%	
330	39.5%	
340	44.6%	
350	22.7%	
360	17.7%	

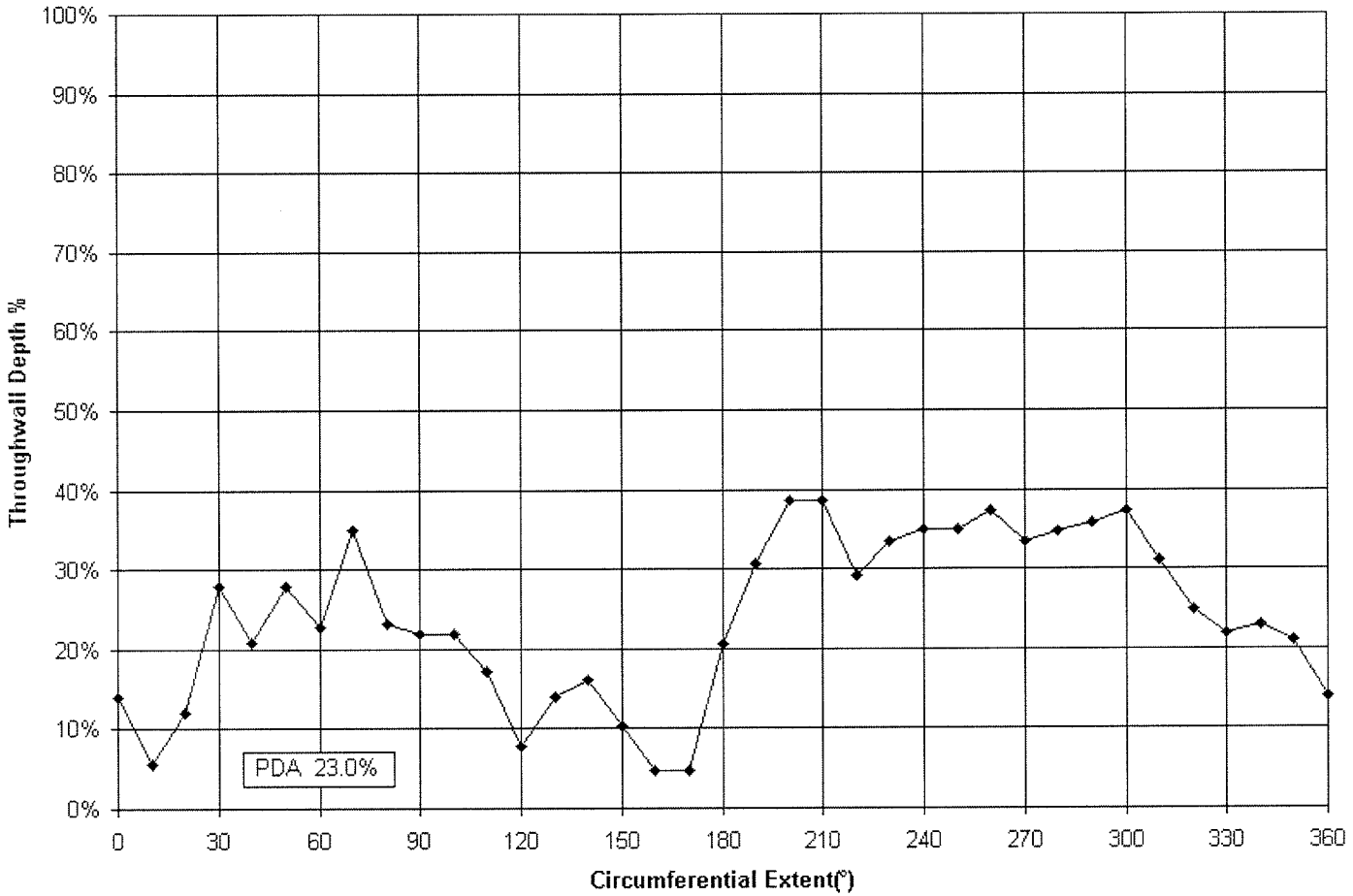

Figure B-12
Plant CB, R87L78; Destructive Examination Depth Profile

Plant :	**CB**	
Tube :	**R87L78**	
PDA :	**23.0%**	
Angle	Depth	Lig. Area
0	14.0%	
10	5.6%	
20	12.0%	
30	27.9%	
40	20.9%	
50	27.9%	
60	22.7%	
70	34.9%	
80	23.2%	
90	21.9%	
100	21.9%	
110	17.2%	
120	7.7%	
130	14.0%	
140	16.0%	
150	10.2%	
160	4.7%	
170	4.7%	
180	20.7%	
190	30.7%	
200	38.6%	
210	38.6%	
220	29.1%	
230	33.5%	
240	35.0%	
250	35.0%	
260	37.3%	
270	33.5%	
280	34.7%	
290	35.9%	
300	37.3%	
310	31.2%	
320	25.0%	
330	21.9%	
340	23.0%	
350	20.9%	
360	14.0%	

Tabulation of Pulled Tube Crack Depth Profiles from Destructive Exam

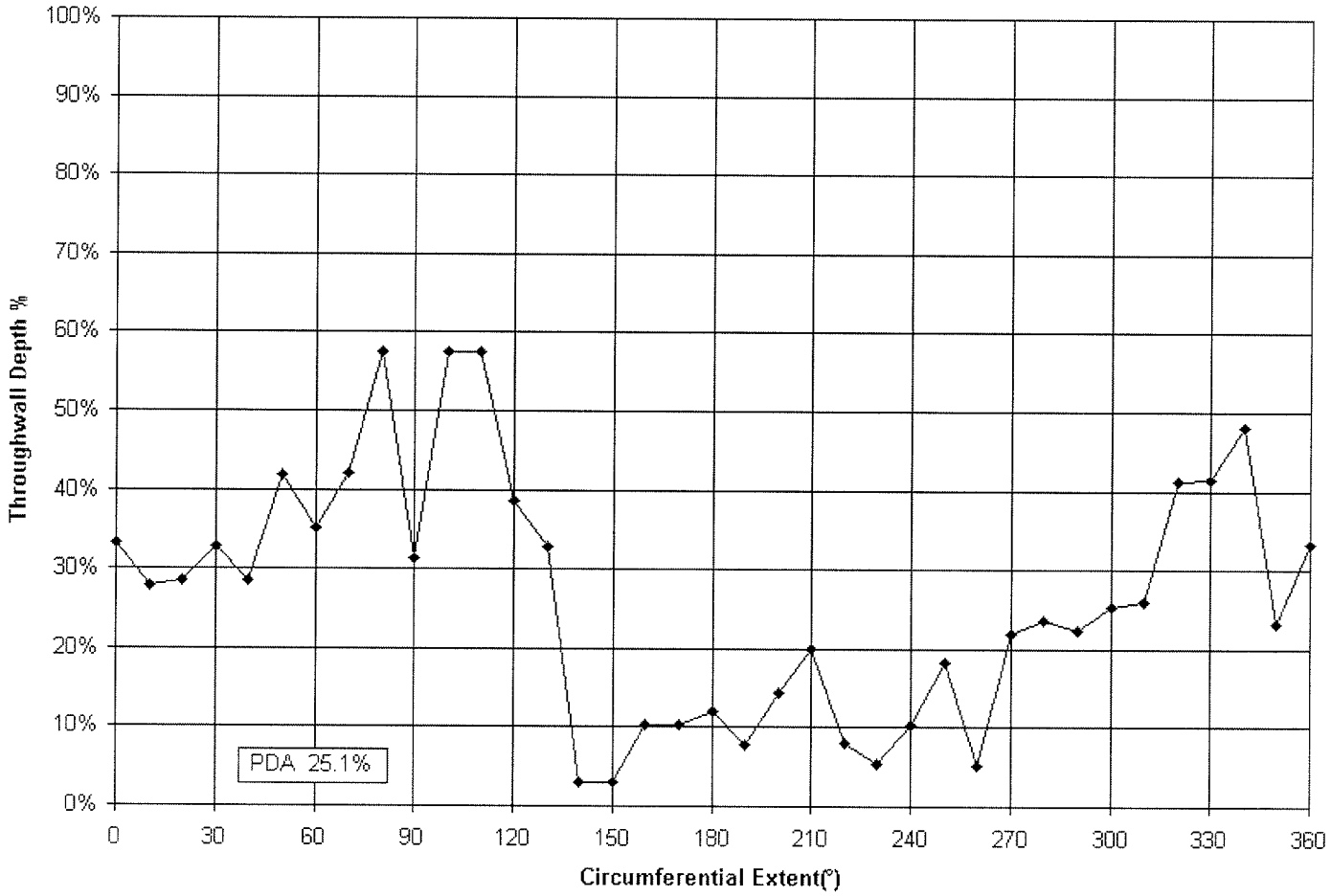

Figure B-13
Plant CB, R90L57; Destructive Examination Depth Profile

Plant :	**CA**	
Tube :	**R90L57**	
PDA :	**25.1%**	
Angle	Depth	Lig. Area
0	33.2%	
10	28.0%	
20	28.6%	
30	32.7%	
40	28.6%	
50	41.9%	
60	35.2%	
70	42.1%	
80	57.4%	
90	31.4%	
100	57.4%	
110	57.4%	
120	38.7%	
130	32.7%	
140	3.1%	
150	3.1%	
160	10.2%	
170	10.2%	
180	12.0%	
190	7.8%	
200	14.4%	
210	20.0%	
220	8.0%	
230	5.5%	
240	10.2%	
250	18.2%	
260	5.1%	
270	21.8%	
280	23.6%	
290	22.3%	
300	25.2%	
310	25.9%	
320	41.2%	
330	41.4%	
340	48.1%	
350	23.2%	
360	33.2%	

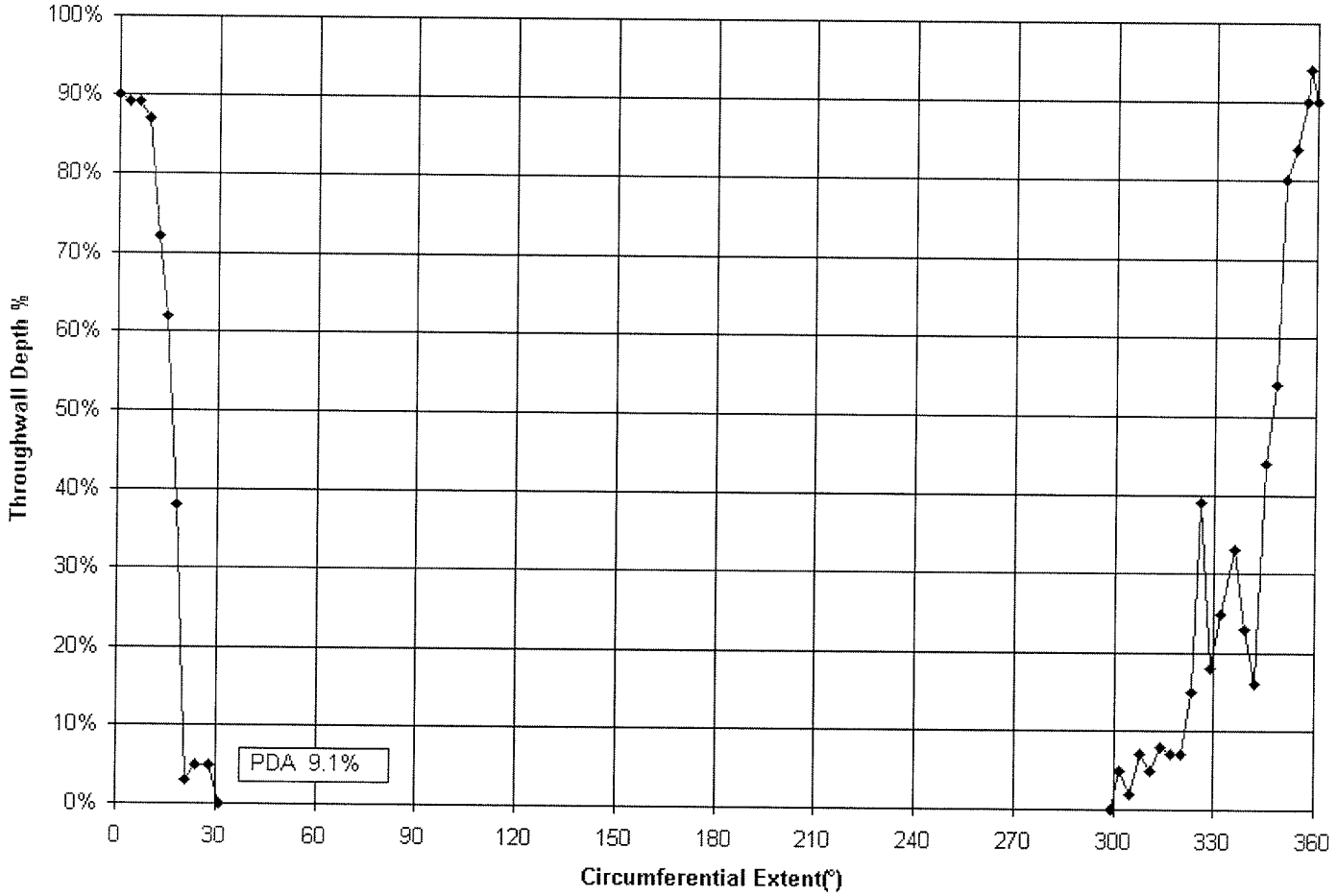

Figure B-14
Plant CC, R51L113; Destructive Examination Depth Profile

Plant :	**CC**	
Tube :	**R51L113**	
PDA :	**9.1%**	
Angle	Depth	Lig. Area
0	90.0%	
3	89.0%	
6	89.0%	
9	87.0%	
12	72.0%	
15	62.0%	
18	38.0%	
21	3.0%	
24	5.0%	
28	5.0%	
31	0.0%	
299	0.0%	
302	5.0%	
305	2.0%	
308	7.0%	
311	5.0%	
314	8.0%	
317	7.0%	
320	7.0%	
323	15.0%	
326	39.0%	
329	18.0%	
332	25.0%	
336	33.0%	
339	23.0%	
342	16.0%	
345	44.0%	
348	54.0%	
351	80.0%	
354	84.0%	
357	90.0%	
358	94.0%	
360	90.0%	

Tabulation of Pulled Tube Crack Depth Profiles from Destructive Exam

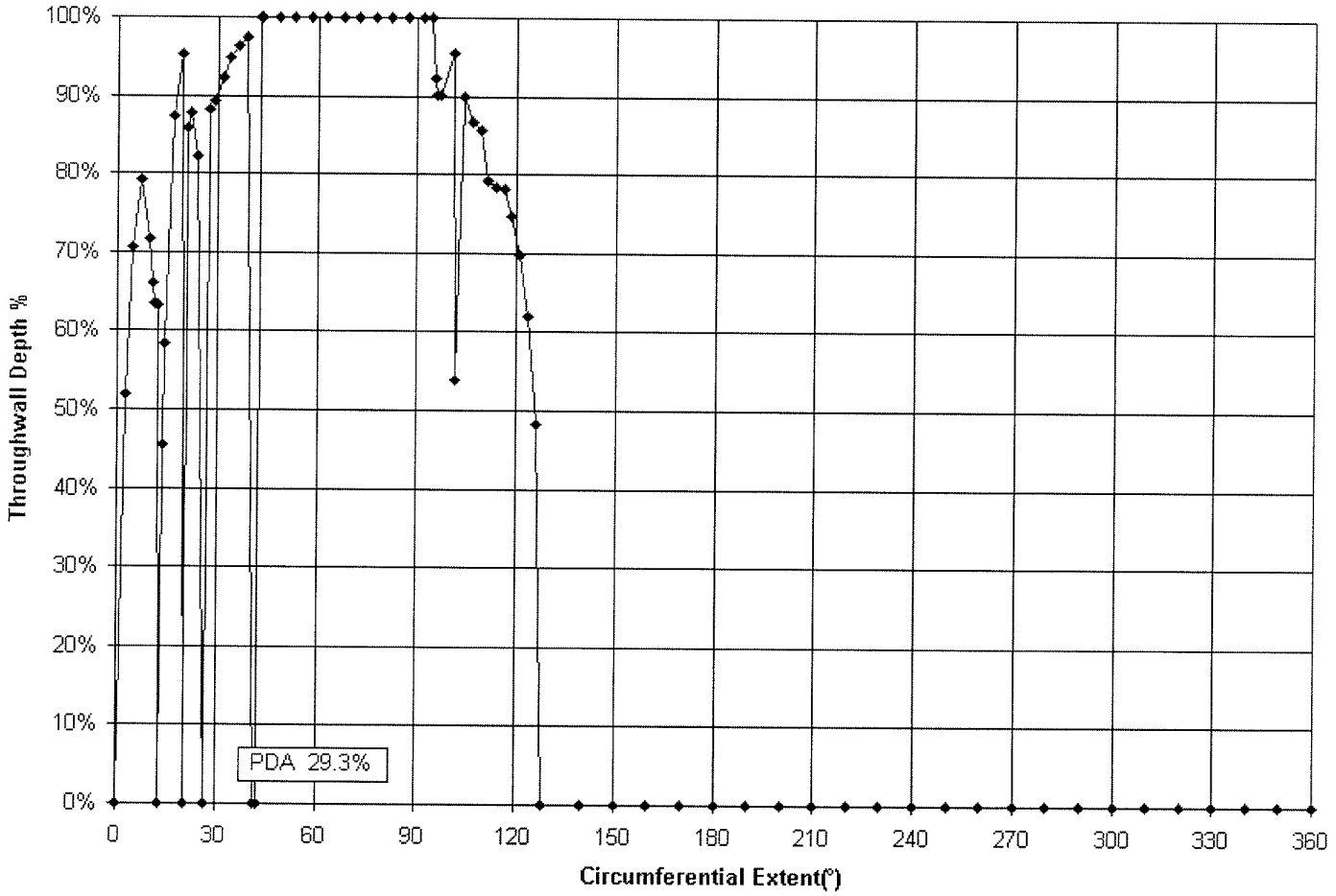

Figure B-15
Plant G, R18C36; Destructive Examination Depth Profile

Plant :				**G**				
Tube :				**R18C36**				
PDA :				**29.3%**				
Angle	Depth	Lig. Area	Angle	Depth	Lig. Area	Angle	Depth	Lig. Area
0	0.0%		92	100.0%		330	0.0%	
2	51.9%		94	100.0%		340	0.0%	
5	70.6%		95	92.2%		350	0.0%	
7	79.3%		96	90.1%		360	0.0%	
10	71.7%		97	90.2%				
10	66.1%		101	95.6%				
11	63.5%		102	53.9%				
12	63.3%		104	89.9%				
13	0.0%		107	86.7%				
14	45.5%		109	85.7%				
15	58.5%		111	79.1%				
17	87.3%		114	78.3%				
19	95.2%		116	78.0%				
20	0.0%		119	74.7%				
21	85.9%		121	69.7%				
22	87.7%		124	62.1%				
24	82.1%		126	48.2%				
27	0.0%		128	0.0%				
27	88.2%		140	0.0%				
29	89.3%		150	0.0%				
31	92.3%		160	0.0%				
34	94.9%		170	0.0%				
36	96.3%		180	0.0%				
39	97.5%		190	0.0%				
41	0.0%		200	0.0%				
42	0.0%		210	0.0%				
43	100.0%		220	0.0%				
44	100.0%		230	0.0%				
48	100.0%		240	0.0%				
53	100.0%		250	0.0%				
58	100.0%		260	0.0%				
63	100.0%		270	0.0%				
68	100.0%		280	0.0%				
73	100.0%		290	0.0%				
78	100.0%		300	0.0%				
82	100.0%		310	0.0%				
87	100.0%		320	0.0%				

Tabulation of Pulled Tube Crack Depth Profiles from Destructive Exam

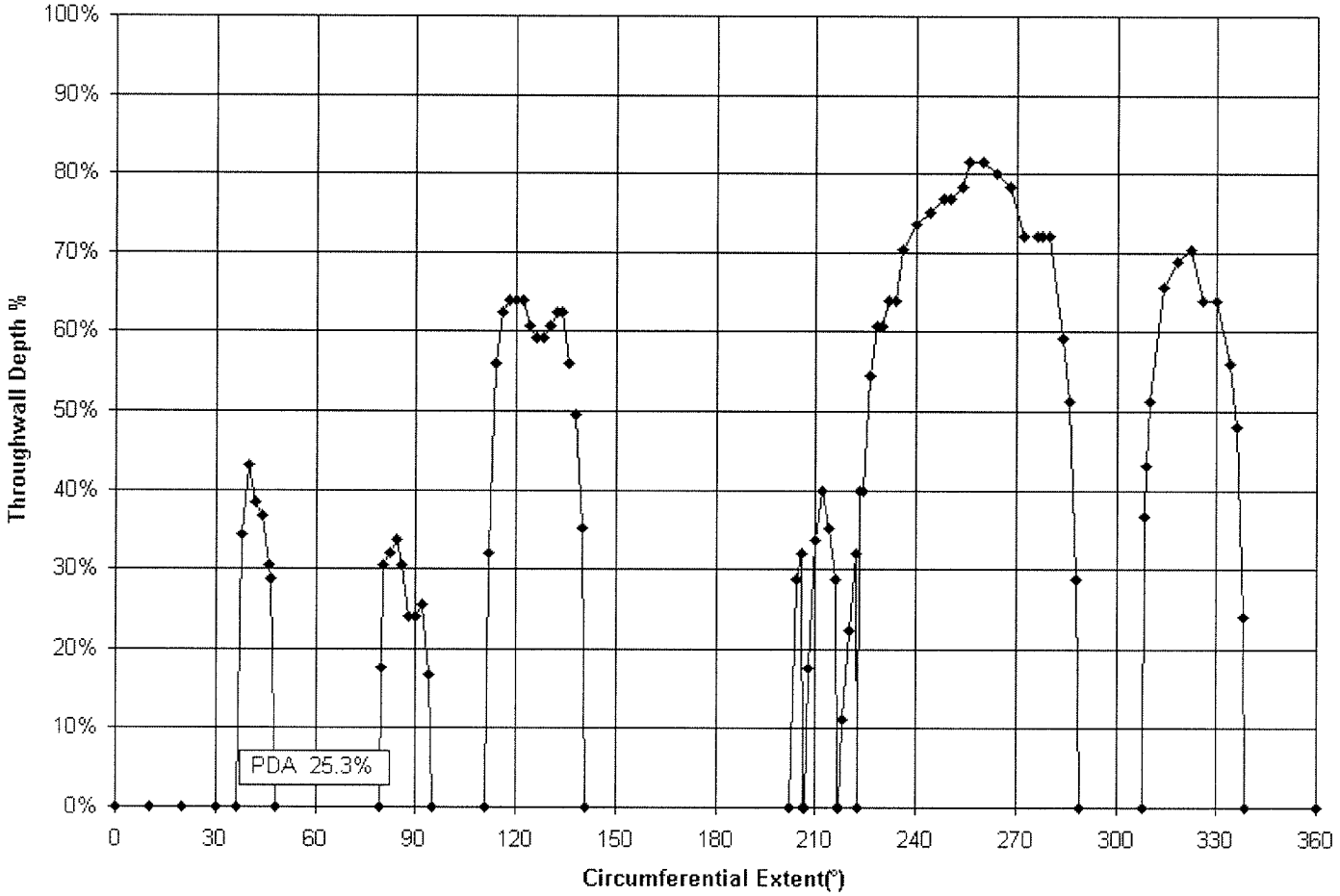

Figure B-16
Plant W, R15C23; Destructive Examination Depth Profile

Plant :			**W**					
Tube :			**R15C23**					
PDA :			**25.3%**					
Angle	Depth	Lig. Area	Angle	Depth	Lig. Area	Angle	Depth	Lig. Area
0	0.0%		138	49.6%		276	72.0%	
10	0.0%		140	35.2%		278	72.0%	
20	0.0%		141	0.0%		280	72.0%	
30	0.0%		202	0.0%		284	59.2%	
36	0.0%		204	28.8%		286	51.2%	
38	34.4%		206	32.0%		288	28.8%	
40	43.2%		207	0.0%		289	0.0%	
42	38.4%		207	0.0%		308	0.0%	
44	36.8%		208	17.6%		309	36.8%	
46	30.4%		210	33.6%		309	43.2%	
47	28.8%		212	40.0%		310	51.2%	
48	0.0%		214	35.2%		314	65.6%	
79	0.0%		216	28.8%		318	68.8%	
80	17.6%		217	0.0%		322	70.4%	
80	30.4%		217	0.0%		326	64.0%	
82	32.0%		218	11.2%		330	64.0%	
84	33.6%		220	22.4%		334	56.0%	
86	30.4%		222	32.0%		336	48.0%	
88	24.0%		223	0.0%		338	24.0%	
90	24.0%		223	40.0%		338	0.0%	
92	25.6%		224	40.0%		360	0.0%	
94	16.8%		226	54.4%				
95	0.0%		228	60.8%				
111	0.0%		230	60.8%				
112	32.0%		232	64.0%				
114	56.0%		234	64.0%				
116	62.4%		236	70.4%				
118	64.0%		240	73.6%				
120	64.0%		244	75.2%				
122	64.0%		248	76.8%				
124	60.8%		250	76.8%				
126	59.2%		254	78.4%				
128	59.2%		256	81.6%				
130	60.8%		260	81.6%				
132	62.4%		264	80.0%				
134	62.4%		268	78.4%				
136	56.0%		272	72.0%				

Tabulation of Pulled Tube Crack Depth Profiles from Destructive Exam

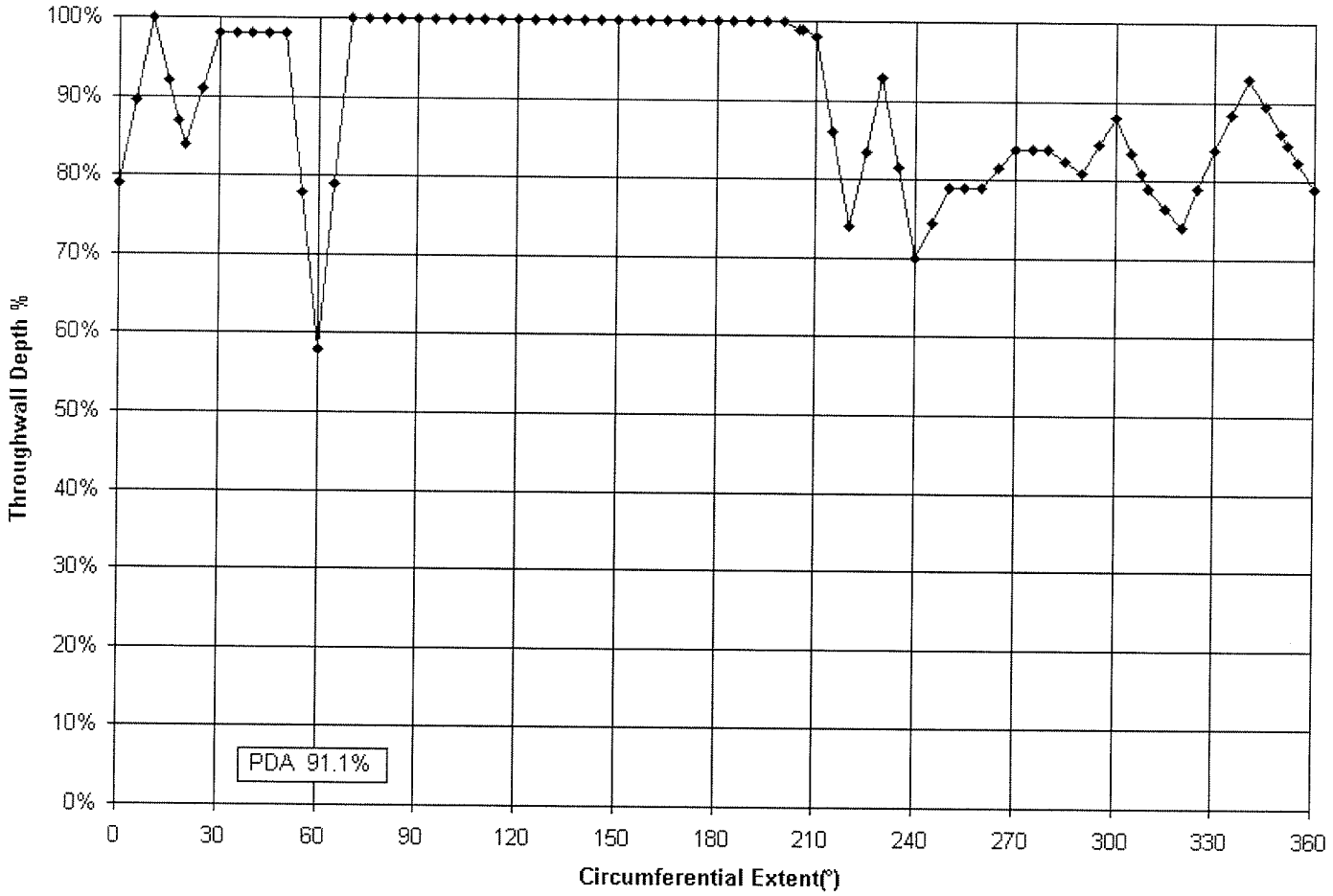

Figure B-17
Plant AA, R21C76; Destructive Examination Depth Profile

Plant :				**AA**				
Tube :				**R21C76**				
PDA :				**91.1%**				
Angle	Depth	Lig. Area	Angle	Depth	Lig. Area	Angle	Depth	Lig. Area
0	79.0%	0.000467	180	100.0%		352	84.6%	0.00056
5	89.5%		185	100.0%		355	82.5%	
10	100.0%		190	100.0%		360	79.0%	
15	92.0%		195	100.0%	0.00028			
18	87.0%	0.000333	200	100.0%				
20	84.0%	0.0004	205	99.0%				
25	91.0%		206	99.0%	0.000507			
30	98.0%		210	98.0%				
35	98.0%	7.00E-05	215	86.0%				
40	98.0%		220	74.0%	0.00038			
45	98.0%	7.00E-05	225	83.5%				
50	98.0%		230	93.0%				
55	78.0%		235	81.5%				
60	58.0%	0.00035	240	70.0%	0.000633			
65	79.0%		245	74.5%				
70	100.0%		250	79.0%				
75	100.0%		255	79.0%				
80	100.0%		260	79.0%				
85	100.0%		265	81.5%				
90	100.0%		270	84.0%	0.00038			
95	100.0%		275	84.0%				
100	100.0%		280	84.0%				
105	100.0%		285	82.5%				
110	100.0%		290	81.0%				
115	100.0%		295	84.5%				
120	100.0%		300	88.0%				
125	100.0%		305	83.5%				
130	100.0%	5.33E-05	308	80.8%	0.00024			
135	100.0%		310	79.0%				
140	100.0%		315	76.5%				
145	100.0%		320	74.0%				
150	100.0%		325	79.0%				
155	100.0%		330	84.0%	0.00028			
160	100.0%		335	88.5%				
165	100.0%		340	93.0%	0.00028			
170	100.0%		345	89.5%				
175	100.0%		350	86.0%				

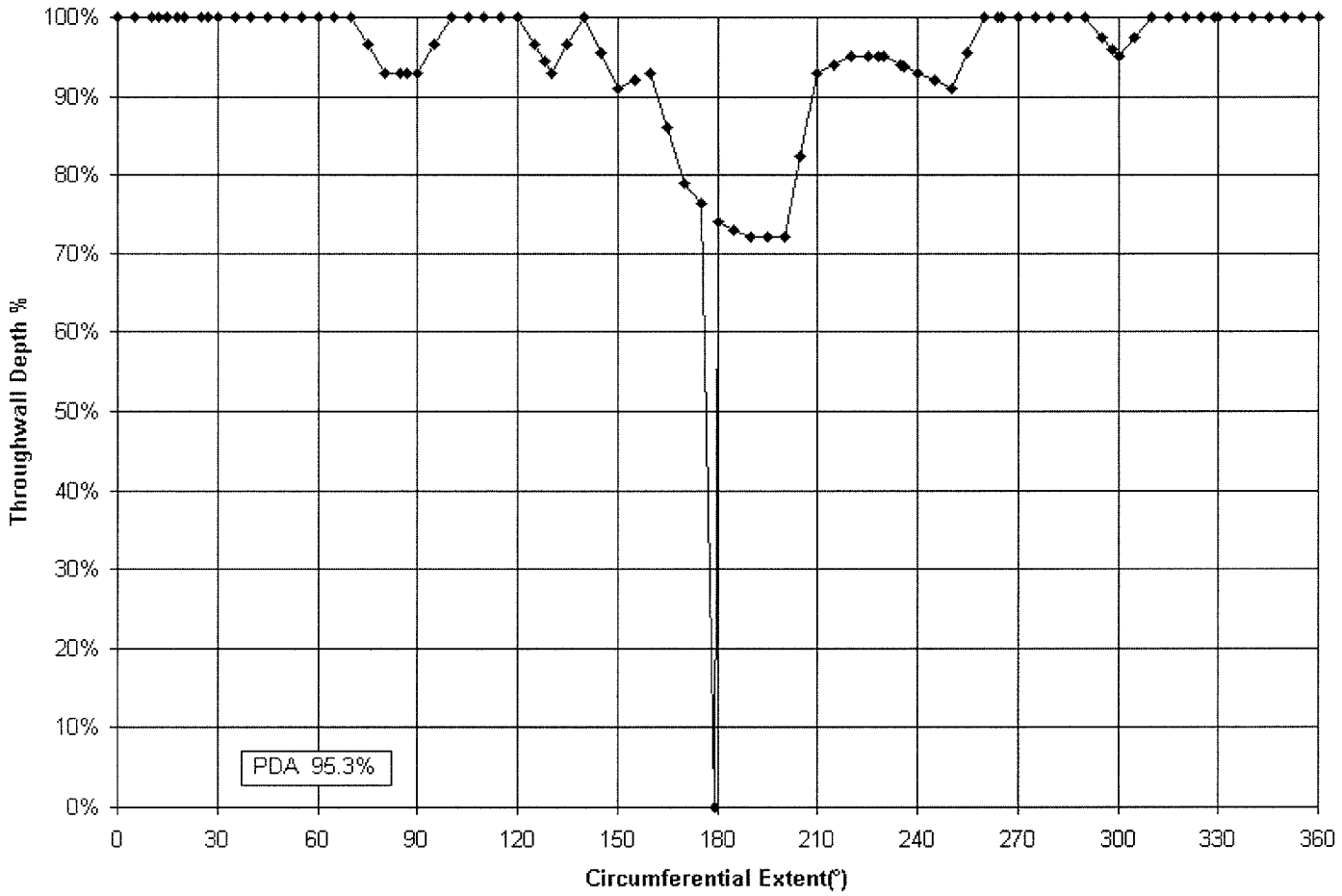

Figure B-18
Plant AA, R22C73; Destructive Examination Depth Profile

Plant :			**AA**					
Tube :			**R22C73**					
PDA :			**95.3%**					
Angle	Depth	Lig. Area	Angle	Depth	Lig. Area	Angle	Depth	Lig. Area
0	100.0%		160	93.0%		315	100.0%	
5	100.0%		165	86.0%		320	100.0%	9.33E-05
10	100.0%		170	79.0%	3.17E-05	325	100.0%	
12	100.0%	0.00026	175	76.5%		329	100.0%	0.000233
15	100.0%		179	0.0%	0.00043	330	100.0%	0.000128
18	100.0%	0.00022	180	74.0%	0.000717	335	100.0%	
20	100.0%		185	73.0%		340	100.0%	
25	100.0%		190	72.0%	0.00042	345	100.0%	0.000925
27	100.0%	0.000143	195	72.0%		350	100.0%	
30	100.0%		200	72.0%	0.000215	355	100.0%	
35	100.0%		205	82.5%		360	100.0%	
40	100.0%		210	93.0%				
45	100.0%		215	94.0%	0.00003			
50	100.0%	0.00011	220	95.0%				
55	100.0%		225	95.0%	4.67E-05			
60	100.0%		228	95.0%	3.33E-05			
65	100.0%		230	95.0%				
70	100.0%		235	94.0%	1.67 E-05			
75	96.5%		236	93.8%	0.000133			
80	93.0%		240	93.0%	0.000025			
85	93.0%		245	92.0%	0.00005			
87	93.0%	0.000287	250	91.0%				
90	93.0%		255	95.5%				
95	96.5%		260	100.0%				
100	100.0%	7.17E-05	264	100.0%	0.00005			
105	100.0%		265	100.0%				
110	100.0%		270	100.0%	1.67E-05			
115	100.0%	0.006667	275	100.0%				
120	100.0%		280	100.0%				
125	96.5%		285	100.0%				
128	94.5%	0.00043	290	100.0%				
130	93.0%		295	97.5%				
135	96.5%		298	96.0%	0.00086			
140	100.0%		300	95.0%				
145	95.5%		305	97.5%				
150	91.0%		310	100.0%				
155	92.0%	0.000105	312	100.0%	7.17E-05			

Tabulation of Pulled Tube Crack Depth Profiles from Destructive Exam

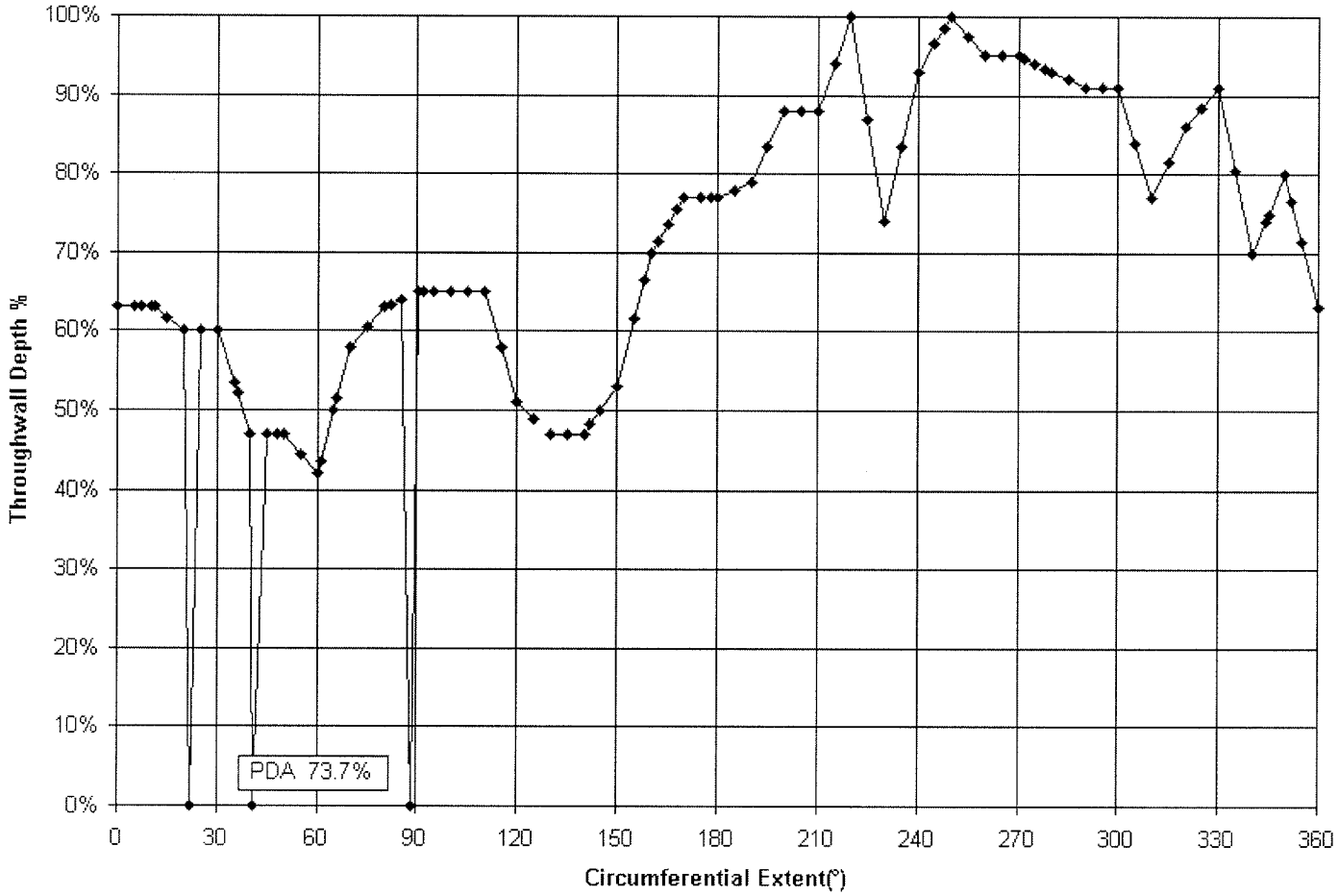

Figure B-19
Plant AA, R22C76; Destructive Examination Depth Profile

Plant :			**AA**					
Tube :			**R22C76**					
PDA :			**73.7%**					
Angle	Depth	Lig. Area	Angle	Depth	Lig. Area	Angle	Depth	Lig. Area
0	63.0%		130	47.0%		278	93.4%	3.33E-05
5	63.0%		135	47.0%		280	93.0%	
7	63.0%	0.000045	140	47.0%		285	92.0%	
10	63.0%		142	48.2%	2.83E-05	290	91.0%	
11	63.0%	7.33E-05	145	50.0%		295	91.0%	
15	61.5%		150	53.0%		300	91.0%	
20	60.0%		155	61.5%		305	84.0%	
22	0.0%	8.33E-06	158	66.6%	2.00E-05	310	77.0%	
25	60.0%		160	70.0%		315	81.5%	
30	60.0%	8.33E-05	162	71.4%	4.67E-05	320	86.0%	
35	53.5%		165	73.5%		325	88.5%	
36	52.2%		168	75.6%	0.000383	330	91.0%	
40	47.0%		170	77.0%		335	80.5%	
41	0.0%	0.00005	175	77.0%		340	70.0%	
45	47.0%		178	77.0%	9.33E-05	344	74.0%	3.33E-05
48	47.0%	0.000175	180	77.0%		345	75.0%	
50	47.0%		185	78.0%		350	80.0%	
55	44.5%	0.00003	190	79.0%		352	76.6%	2.33E-05
60	42.0%		195	83.5%		355	71.5%	
61	43.6%	4.67E-05	200	88.0%	0.00004	360	63.0%	
65	50.0%		205	88.0%				
66	51.6%	8.33E-05	210	88.0%				
70	58.0%	0.000133	215	94.0%	4.67E-05			
75	60.5%		220	100.0%				
80	63.0%		225	87.0%				
82	63.4%	6.67E-05	230	74.0%				
85	64.0%		235	83.5%				
88	0.0%	0.00035	240	93.0%	1.67E-05			
90	65.0%		245	96.5%				
92	65.0%	1.96E-06	248	98.6%	0.000187			
95	65.0%	1.44E-06	250	100.0%				
100	65.0%		255	97.5%				
105	65.0%		260	95.0%	9.33E-05			
110	65.0%		265	95.0%				
115	58.0%		270	95.0%				
120	51.0%		272	94.6%	0.000167			
125	49.0%		275	94.0%				

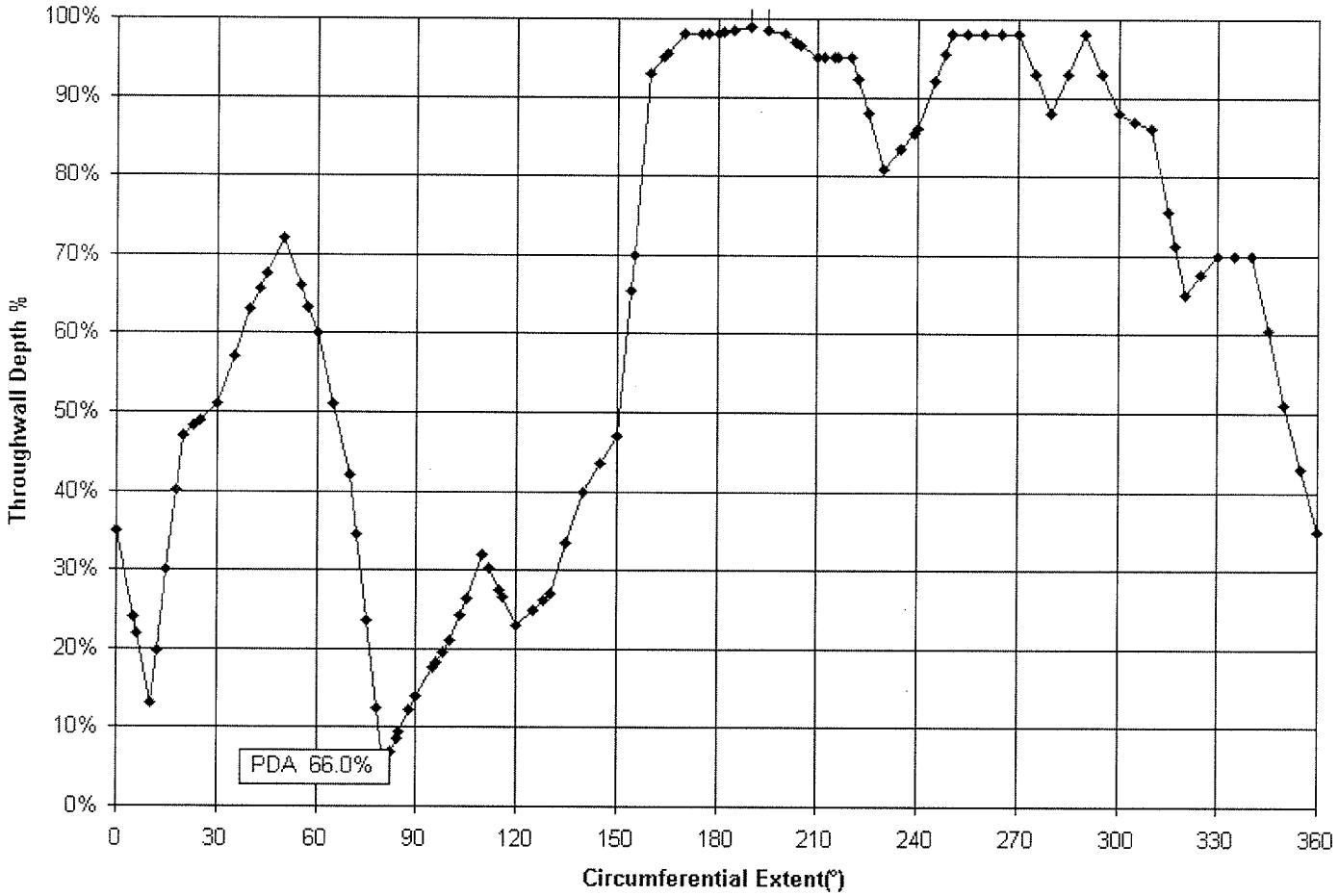

Figure B-20
Plant AA, R25C65; Destructive Examination Depth Profile

Plant :			**AA**					
Tube :			**R25C65**					
PDA :			**66.0%**					
Angle	Depth	Lig. Area	Angle	Depth	Lig. Area	Angle	Depth	Lig. Area
0	35.0%		112	30.2%		239	85.5%	0.00006
5	24.0%		115	27.5%		240	86.0%	
6	21.8%	1.67E-05	116	26.6%		245	92.0%	
10	13.0%		120	23.0%		248	95.6%	0.00015
12	19.8%	0.00001	125	25.0%		250	98.0%	
15	30.0%		128	26.2%		255	98.0%	0.00026
18	40.2%	0.00001	130	27.0%		260	98.0%	
20	47.0%		135	33.5%	0.000012	265	98.0%	
23	48.2%	1.17E-06	140	40.0%		270	98.0%	
25	49.0%		145	43.5%		275	93.0%	
30	51.0%		150	47.0%	3.73E-05	280	88.0%	6.67E-05
35	57.0%		154	65.4%	0.000205	285	93.0%	
40	63.0%		155	70.0%		290	98.0%	
43	65.7%	0.000187	160	93.0%	0.00006	295	93.0%	
45	67.5%		164	95.0%	0.0002	300	88.0%	
50	72.0%		165	95.5%		305	87.0%	
55	66.0%		170	98.0%		310	86.0%	
57	63.3%	2.93E-05	175	98.0%		315	75.5%	2.33E-05
60	60.0%		177	98.0%	0.000283	317	71.3%	3.33E-05
65	51.0%		180	98.0%		320	65.0%	
70	42.0%		182	98.2%	0.000167	325	67.5%	
72	34.6%	0.000016	185	98.5%	0.00018	330	70.0%	
75	23.5%		190	99.0%		335	70.0%	0.0001
78	12.4%	0.00001	193	9870.0%	0.000147	340	70.0%	
80	5.0%	6.67E-06	195	98.5%	9.33E-05	345	60.5%	
82	6.8%	1.33E-06	200	98.0%		350	51.0%	
84	8.6%	4.67E-05	203	97.1%	0.00025	355	43.0%	
85	9.5%		205	96.5%		360	35.0%	
88	12.2%	8.33E-05	210	95.0%				
90	14.0%		212	95.0%	0.000267			
95	17.5%		215	95.0%				
96	18.2%	0.00002	216	95.0%				
98	19.6%	0.00008	220	95.0%				
100	21.0%		222	92.2%				
103	24.3%	8.33E-06	225	88.0%				
105	26.5%		230	81.0%				
110	32.0%		235	83.5%				

Tabulation of Pulled Tube Crack Depth Profiles from Destructive Exam

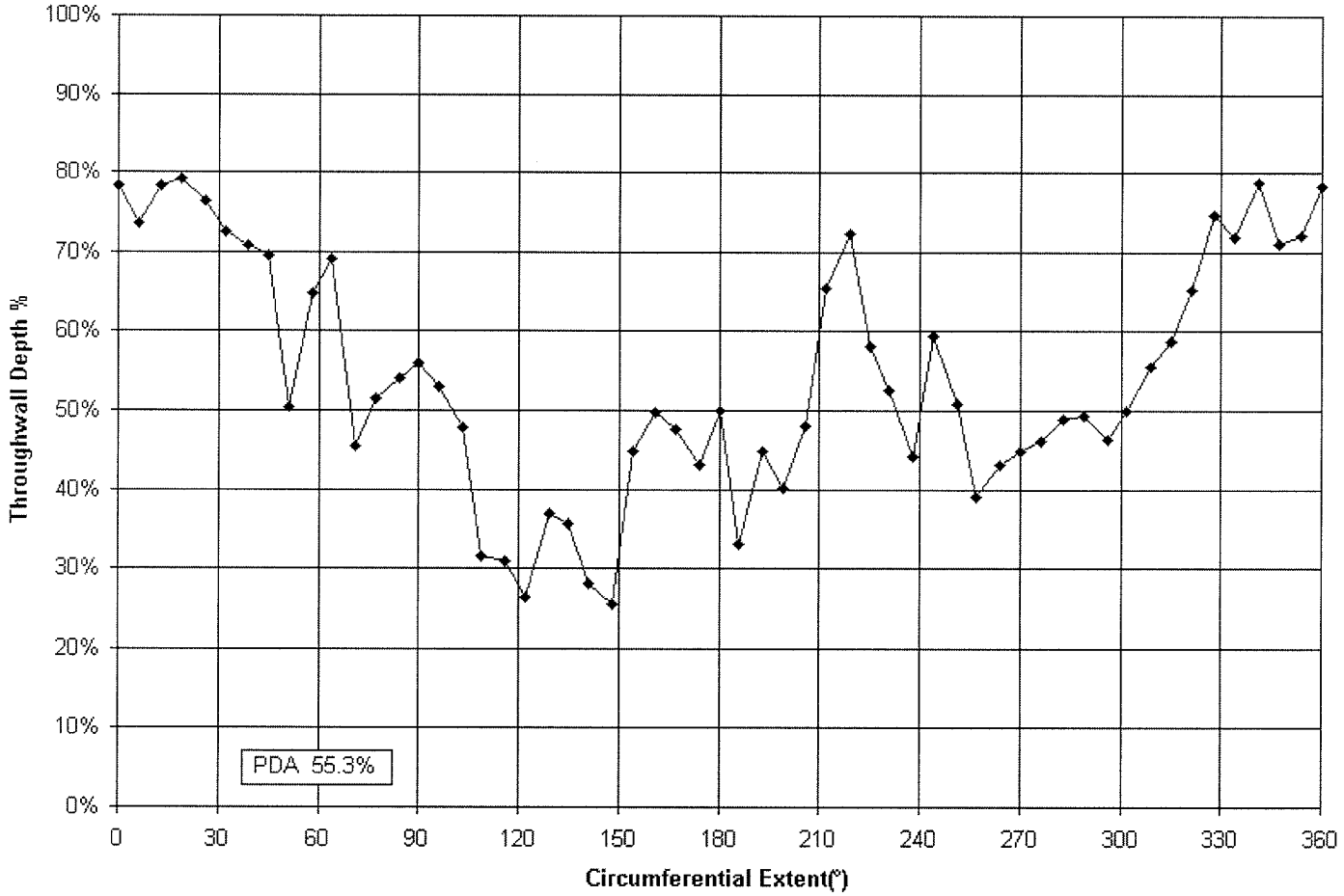

Figure B-21
Plant AB, R14C37; Destructive Examination Depth Profile

Plant :			**AB**		
Tube :			**R14C37**		
PDA :			**55.3%**		
Angle	Depth	Lig. Area	Angle	Depth	Lig. Area
0	78.4%		238	44.2%	4.64E-05
6	73.5%	0.000123	244	59.4%	6.21E-05
13	78.3%	0.000123	251	50.9%	7.8E-05
19	79.2%	0.000105	257	39.1%	3.34E-05
26	76.3%	0	264	43.1%	3.71E-05
32	72.5%	0.000245	270	44.9%	2.87E-05
39	70.9%	0.000305	276	46.1%	1.75E-05
45	69.5%	0.000274	283	48.9%	0.000117
51	50.4%	0.000275	289	49.3%	0.000118
58	64.8%	0.00042	296	46.3%	0.000137
64	69.1%	0.00038	302	50.1%	0.000161
71	45.6%	0.000266	309	55.5%	0.000167
77	51.4%	0.000423	315	58.7%	0.000143
84	54.0%	0.00052	321	65.2%	0
90	56.0%	0.00054	328	74.6%	0
96	52.9%	0.000245	334	71.8%	0
103	47.9%	0.000236	341	78.8%	0
109	31.5%	0.000318	347	71.1%	5.89E-05
116	30.9%	0.000373	354	72.0%	8.91E-05
122	26.5%	0.000317	360	78.4%	7.64E-05
129	37.0%	1.49E-05			
135	35.6%	2.71E-05			
141	28.2%	8.44E-05			
148	25.6%	0.000182			
154	44.9%	0.000162			
161	49.8%	0.000314			
167	47.7%	0.000248			
174	43.1%	0.000264			
180	50.0%	7.8E-05			
186	33.1%	5.25E-05			
193	44.8%	9.66E-05			
199	40.2%	9.39E-05			
206	48.0%	8.36E-05			
212	65.5%	5.41E-05			
219	72.3%	2.04E-05			
225	58.1%	1.43E-05			
231	52.5%	0			

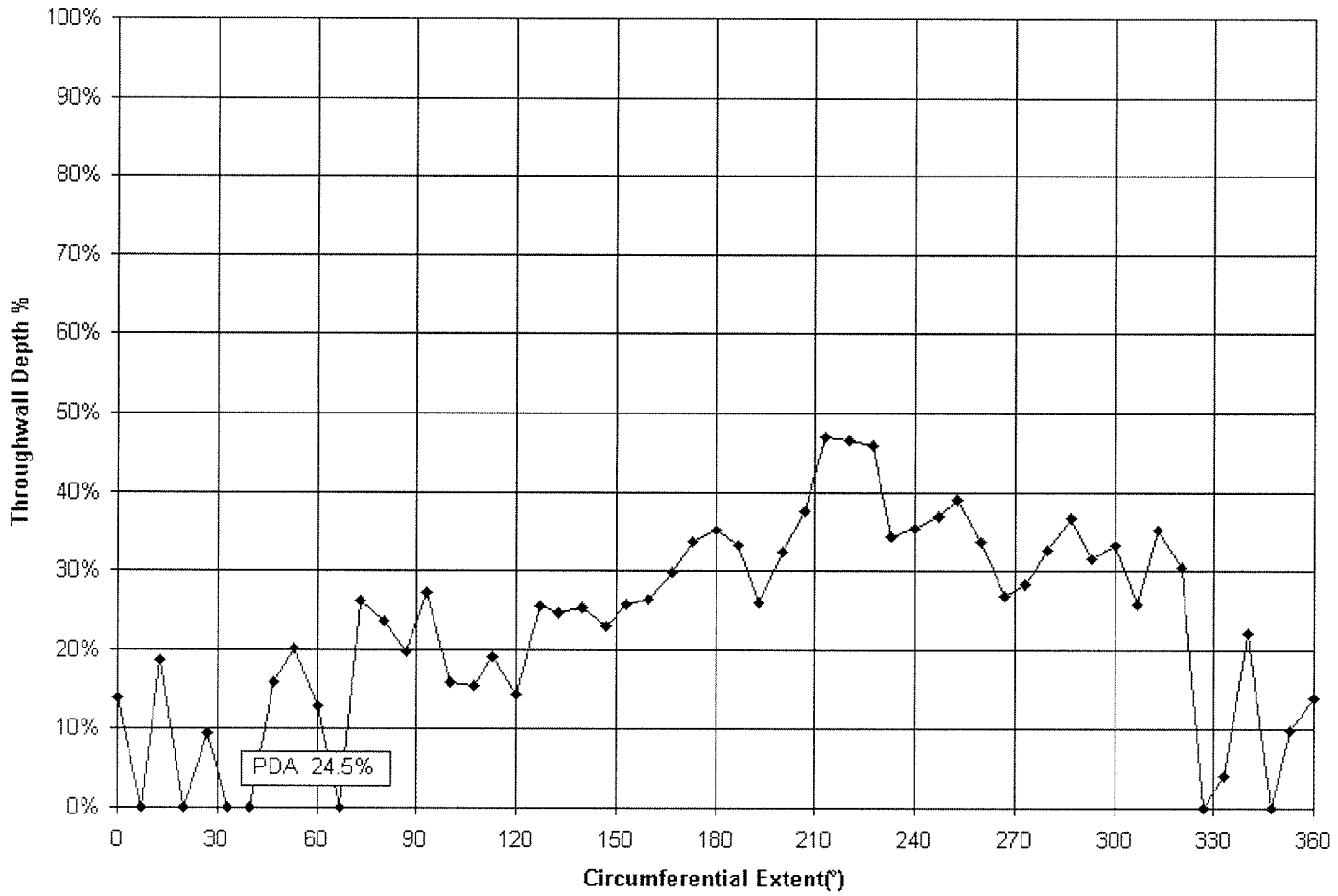

Figure B-22
Plant AB, R14C93; Destructive Examination Depth Profile

Plant :			**AB**		
Tube :			**R14C93**		
PDA :			**24.5%**		
Angle	Depth	Lig. Area	Angle	Depth	Lig. Area
0	14.0%	0	247	37.0%	0.000102
7	0.0%	0	253	39.1%	9.39E-05
13	18.7%	0	260	33.7%	4.27E-05
20	0.0%	0	267	26.8%	5.2E-05
27	9.4%	0	273	28.4%	0.000111
33	0.0%	0	280	32.7%	0.000104
40	0.0%	0	287	36.8%	0.000117
47	15.9%	0	293	31.5%	2.87E-05
53	20.1%	0	300	33.2%	3.71E-05
60	12.8%	0	307	25.8%	2.04E-05
67	0.0%	0	313	35.3%	1.59E-05
73	26.1%	4.46E-05	320	30.4%	1.49E-05
80	23.5%	0.000132	327	0.0%	0
87	19.8%	0.000156	333	4.1%	0
93	27.2%	9.87E-05	340	22.2%	0
100	15.9%	5.57E-05	347	0.0%	0
107	15.5%	5.01E-05	353	9.8%	0
113	19.0%	4.78E-05	360	14.0%	0
120	14.3%	4.64E-05			
127	25.5%	2.79E-05			
133	24.6%	9.55E-06			
140	25.3%	1.11E-05			
147	23.0%	6.31E-05			
153	25.8%	6.37E-05			
160	26.4%	0.000132			
167	29.8%	0.00018			
173	33.7%	0.000146			
180	35.3%	0.000102			
187	33.3%	0			
193	26.0%	6.69E-05			
200	32.5%	8.91E-05			
207	37.5%	0.00011			
213	47.0%	2.71E-05			
220	46.6%	7.8E-05			
227	45.9%	5.57E-05			
233	34.4%	4.78E-05			
240	35.5%	9.1E-05			

Tabulation of Pulled Tube Crack Depth Profiles from Destructive Exam

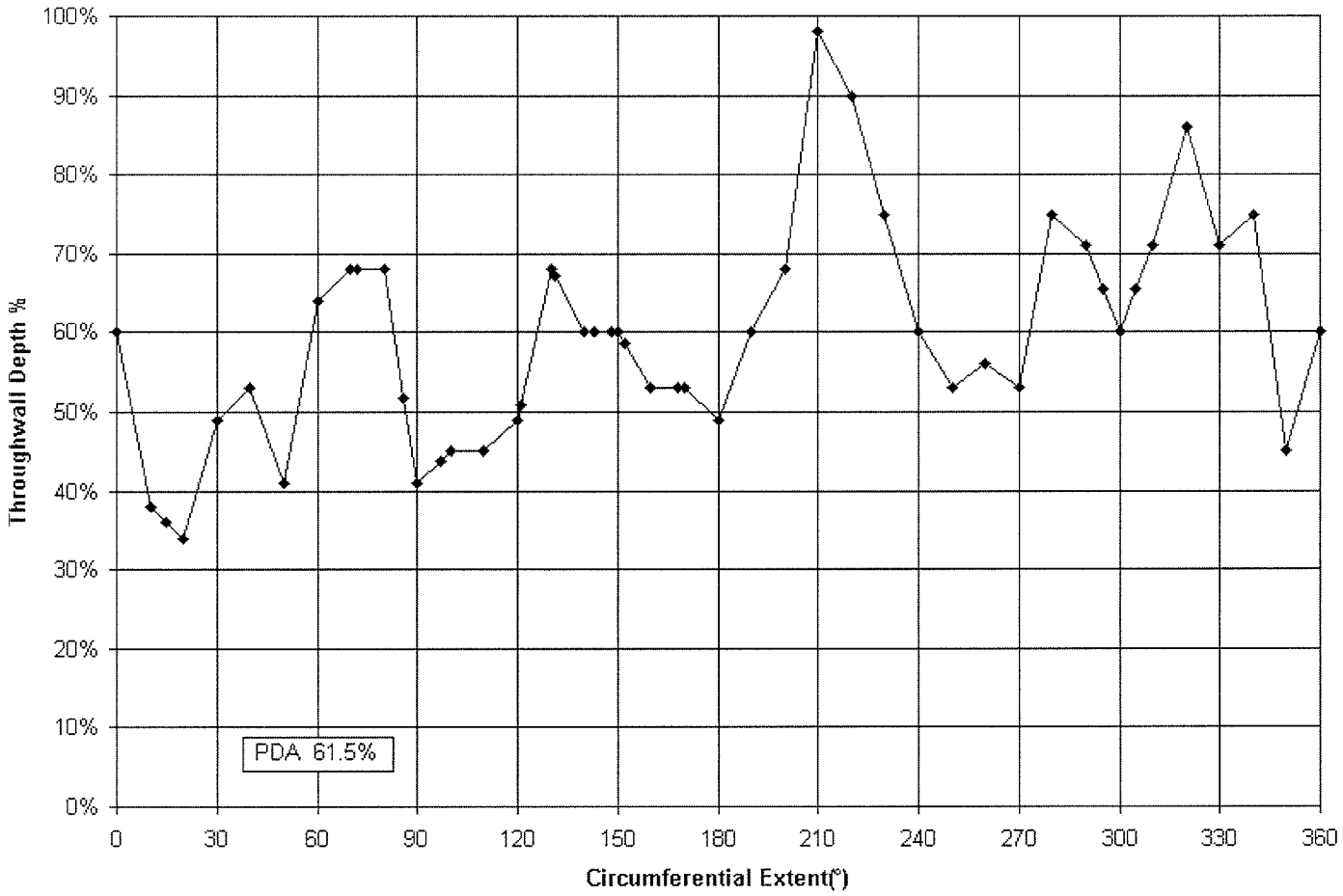

Figure B-23
Plant AB, R20C85; Destructive Examination Depth Profile

Plant :			**AB**		
Tube :			**R20C85**		
PDA :			**61.5%**		
Angle	Depth	Lig. Area	Angle	Depth	Lig. Area
0	60.0%	0.000361	270	53.0%	
10	38.0%		280	75.0%	0.000166
15	36.0%	0.000111	290	71.0%	
20	34.0%		295	65.5%	0.000217
30	49.0%	0.000311	300	60.0%	0.000217
40	53.0%		305	65.5%	0.00031
50	41.0%	0.000306	310	71.0%	
60	64.0%		320	86.0%	
70	68.0%		330	71.0%	
72	68.0%	0.000136	340	75.0%	
80	68.0%		350	45.0%	
86	51.8%	3.35E-05	360	60.0%	
90	41.0%				
97	43.8%	0.000133			
100	45.0%				
110	45.0%				
120	49.0%				
121	50.9%	0.000466			
130	68.0%				
131	67.2%	0.000266			
140	60.0%				
143	60.0%	0.000446			
148	60.0%	0.000122			
150	60.0%				
152	58.6%	3.35E-05			
160	53.0%	5.85E-05			
168	53.0%	0.000223			
170	53.0%				
180	49.0%				
190	60.0%				
200	68.0%				
210	98.0%				
220	90.0%				
230	75.0%				
240	60.0%				
250	53.0%				
260	56.0%				

Tabulation of Pulled Tube Crack Depth Profiles from Destructive Exam

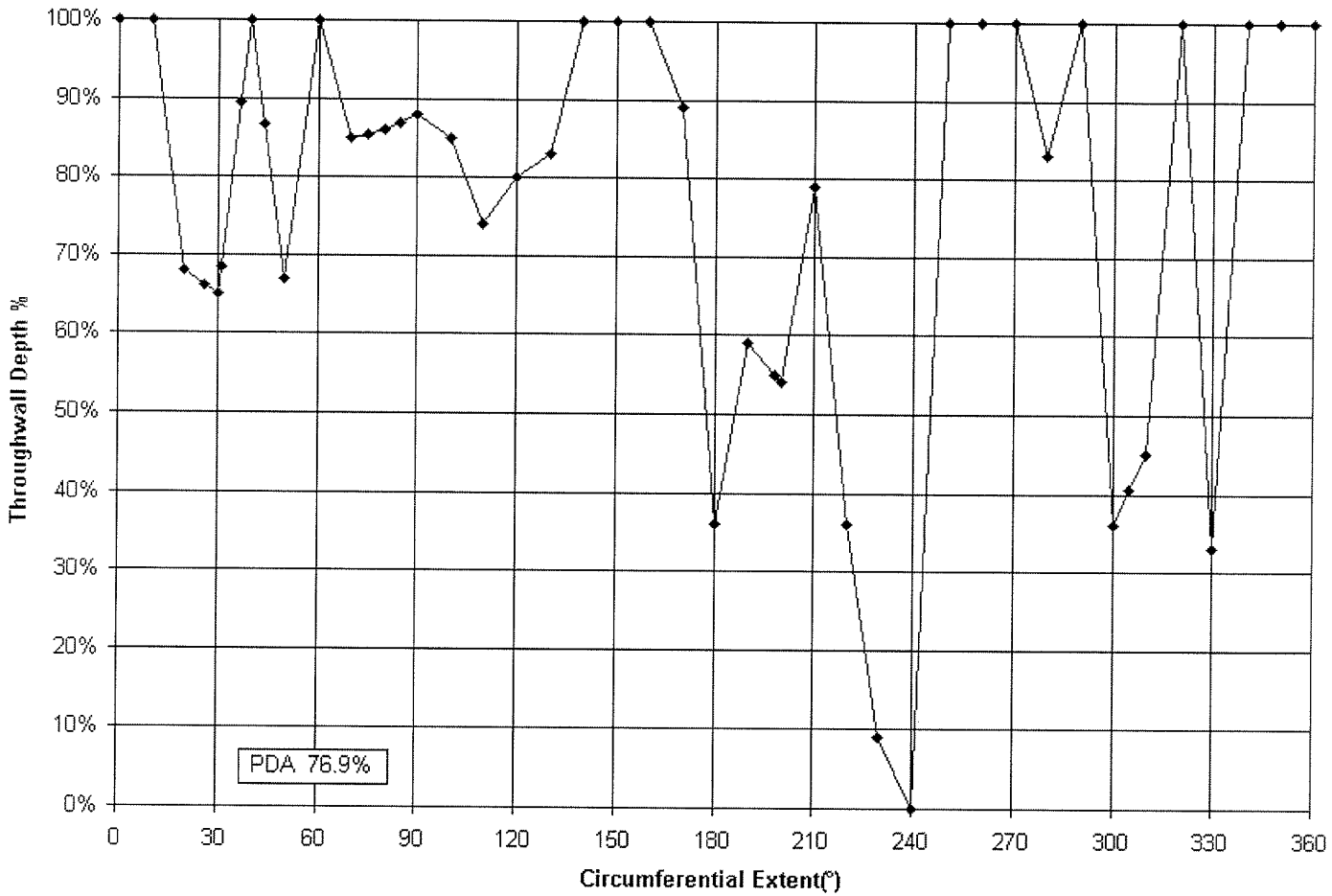

Figure B-24
Plant AB, R23C43; Destructive Examination Depth Profile

Plant :			**AB**		
Tube :			**R23C43**		
PDA :			**76.9%**		
Angle	Depth	Lig. Area	Angle	Depth	Lig. Area
0	100.0%	0.000685	300	36.0%	
10	100.0%		305	40.5%	0.000353
20	68.0%		310	45.0%	
26	66.2%	0.000481	320	100.0%	
30	65.0%		330	33.0%	
31	68.5%	0.000476	340	100.0%	
37	89.5%	0.001089	350	100.0%	
40	100.0%		360	100.0%	
44	86.8%	0.0005			
50	67.0%	0.00074			
60	100.0%				
70	85.0%				
75	85.5%	0.00108			
80	86.0%				
85	87.0%	0.00007			
90	88.0%				
100	85.0%				
110	74.0%	0.00198			
120	80.0%				
130	83.0%				
140	100.0%				
150	100.0%				
160	100.0%				
170	89.0%				
180	36.0%				
190	59.0%				
198	55.0%	0.000875			
200	54.0%				
210	79.0%				
220	36.0%				
230	9.0%				
240	0.0%				
250	100.0%				
260	100.0%	0.00033			
270	100.0%				
280	83.0%				
290	100.0%				

Tabulation of Pulled Tube Crack Depth Profiles from Destructive Exam

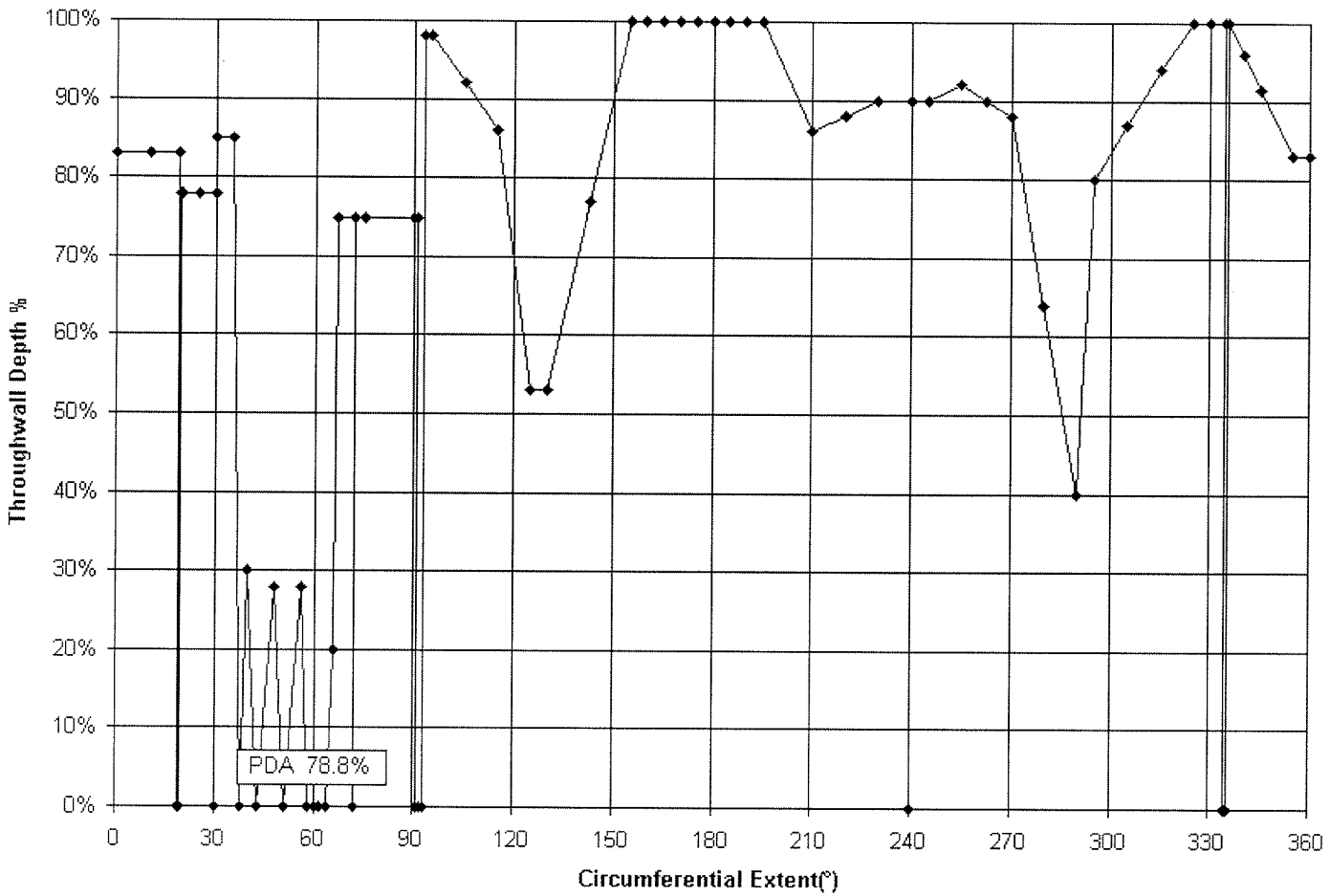

Figure B-25
Plant AB, R23C44; Destructive Examination Depth Profile

Plant :			**AB**					
Tube :			**R23C44**					
PDA :			**78.8%**					
Angle	Depth	Lig. Area	Angle	Depth	Lig. Area	Angle	Depth	Lig. Area
0.0	83.0%		93.0	0.0%		334.6	1	
10.0	83.0%	0.000129	93.0	98.0%		334.6	0	
18.8	83.0%		95.0	98.0%		335.0	0	
18.8	0.0%		105.0	92.0%		335.4	0	
19.0	0.0%		115.0	86.0%		335.4	1	
19.2	0.0%		125.0	53.0%		340.0	0.96	
19.2	78.0%		130.0	53.0%		345.0	0.915	
20.0	78.0%		143.0	77.0%		355.0	0.83	
25.0	78.0%	0.000043	155.0	100.0%		360.0	0.83	
29.9	78.0%		160.0	100.0%				
29.9	0.0%		165.0	100.0%				
30.0	0.0%		170.0	100.0%				
30.1	0.0%		175.0	100.0%				
30.1	85.0%		180.0	100.0%				
35.0	85.0%		185.0	100.0%				
38.0	0.0%		190.0	100.0%				
40.0	30.0%		195.0	100.0%				
43.0	0.0%		210.0	86.0%				
48.0	28.0%		220.0	88.0%				
51.0	0.0%		230.0	90.0%				
56.0	28.0%		239.8	90.0%				
58.0	0.0%		239.8	0.0%				
60.0	0.0%	0.00129	240.0	0.0%				
62.0	0.0%	0.00129	240.2	0.0%				
64.0	0.0%		240.2	90.0%				
66.0	20.0%		245.0	90.0%				
67.0	75.0%		255.0	92.0%				
71.8	75.0%		262.5	90.0%				
71.8	0.0%		270.0	88.0%				
72.0	0.0%		280.0	64.0%				
72.2	0.0%		290.0	40.0%				
72.2	75.0%		295.0	80.0%				
75.0	75.0%		305.0	87.0%				
90.0	75.0%	0.000516	315.0	94.0%				
91.0	75.0%		325.0	100.0%				
91.0	0.0%		330.0	100.0%				
92.0	0.0%		334.6	100.0%				

Tabulation of Pulled Tube Crack Depth Profiles from Destructive Exam

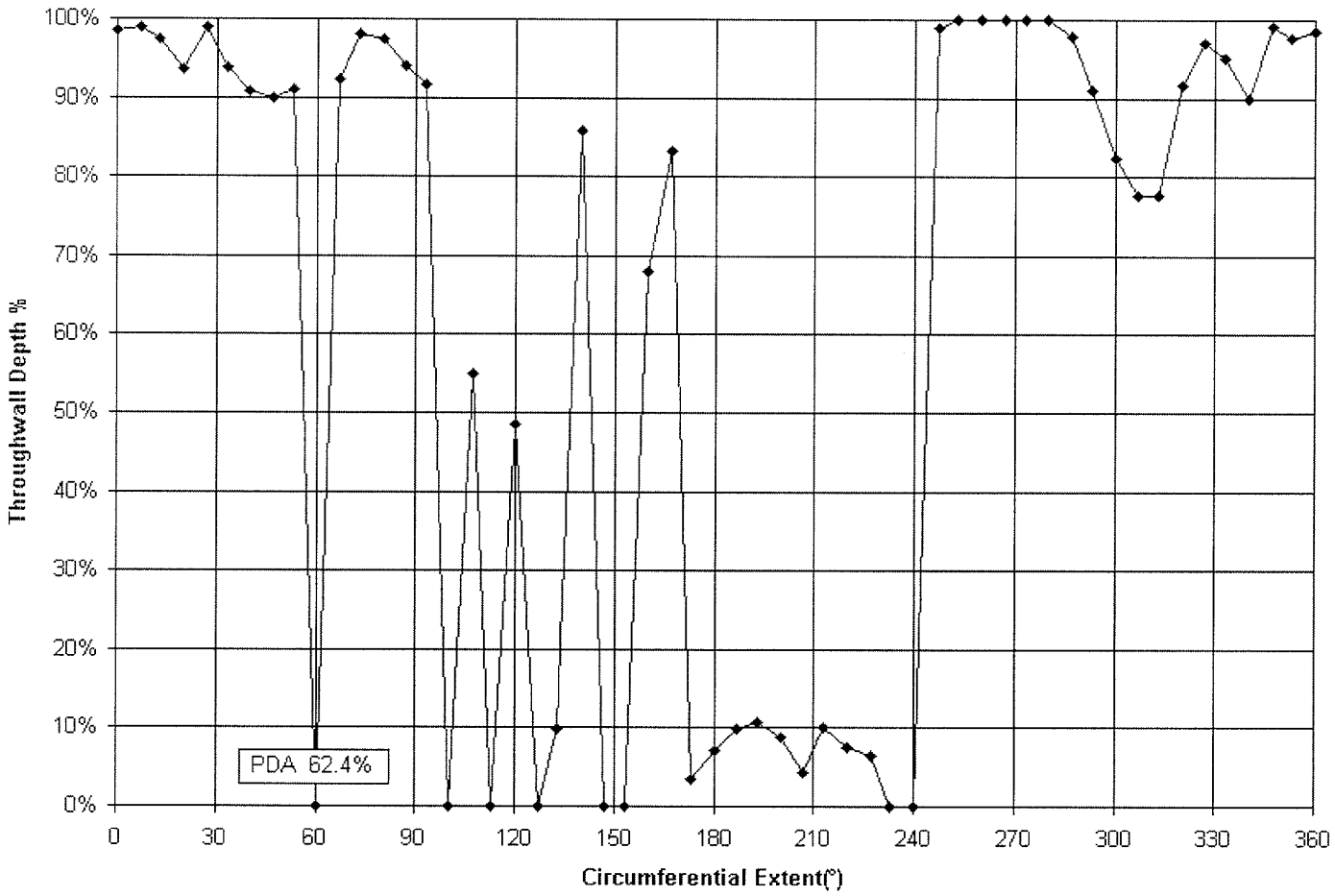

Figure B-26
Plant AB, R24C42; Destructive Examination Depth Profile

Plant :			**AB**		
Tube :			**R24C42**		
PDA :			**62.4%**		
Angle	Depth	Lig. Area	Angle	Depth	Lig. Area
0	0.986		247	0.989	1.49E-05
7	0.989	0	253	0.999	1.27E-05
13	0.974	2.23E-05	260	1	0
20	0.935	2.6E-05	267	1	0
27	0.99	2.6E-05	273	1	0
33	0.937	3.18E-05	280	1	0
40	0.908	0.000108	287	0.979	0
47	0.9	0.000108	293	0.91	0
53	0.909	6.21E-05	300	0.823	0
60	0	0.000217	307	0.776	0.000305
67	0.923	0.000215	313	0.777	0.000438
73	0.981	0.000186	320	0.917	0.000511
80	0.974	0	327	0.971	0.000208
87	0.94	0.000258	333	0.95	0
93	0.916	0.00022	340	0.899	0
100	0	0.000258	347	0.992	0
107	0.55	0	353	0.976	0
113	0	0	360	0.986	0
120	0.484	0			
127	0	0			
133	0.099	0			
140	0.858	0			
147	0	0			
153	0	0			
160	0.681	0			
167	0.833	0			
173	0.035	0			
180	0.071	0			
187	0.098	0			
193	0.108	0			
200	0.089	0			
207	0.043	0			
213	0.1	0			
220	0.076	0			
227	0.064	0			
233	0	0			
240	0	1.49E-05			

Tabulation of Pulled Tube Crack Depth Profiles from Destructive Exam

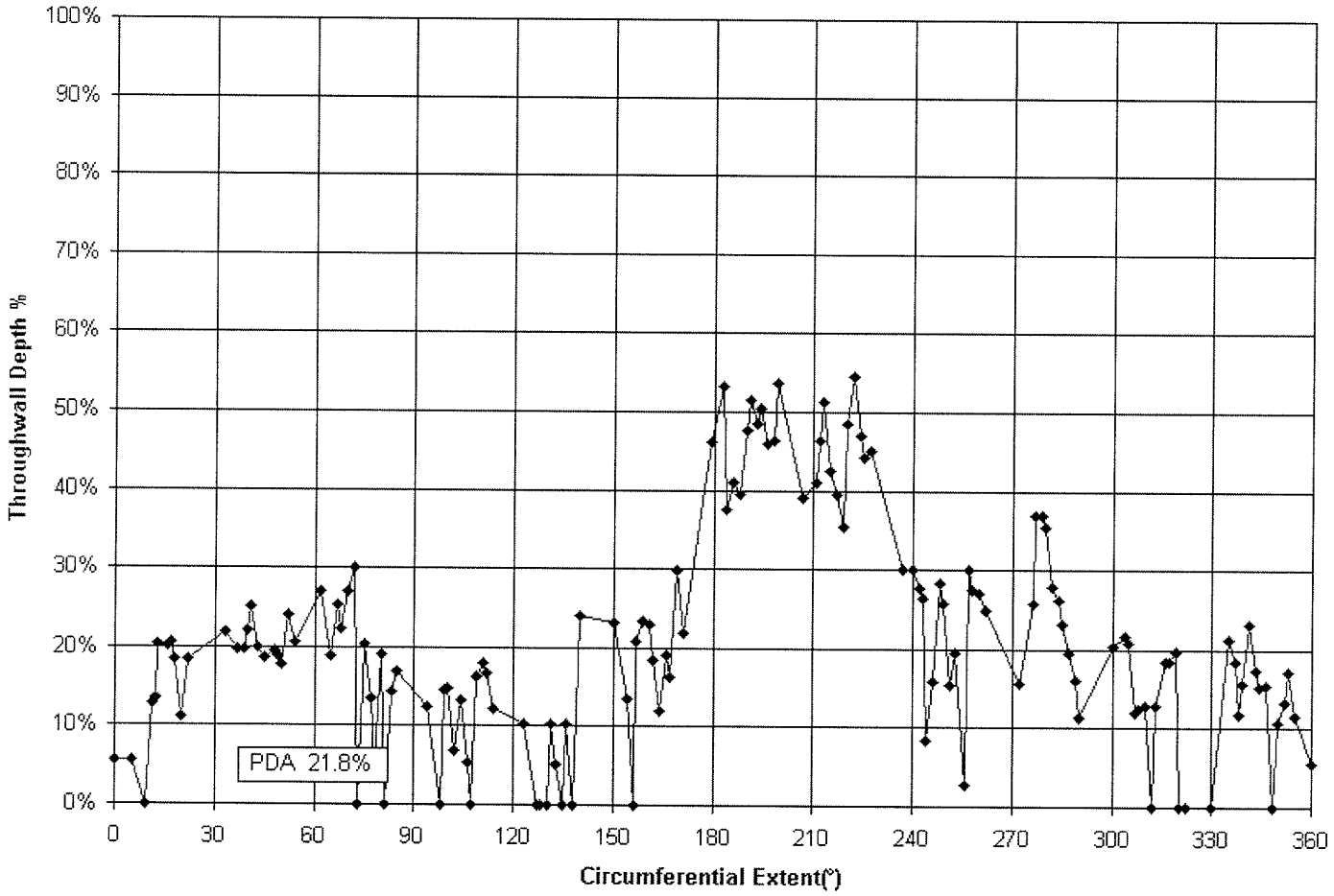

Figure B-27
Plant AB, R24C91; Destructive Examination Depth Profile

Plant :					**AB**				
Tube :					**R24C91**				
PDA :					**21.8%**				
Angle	Depth	Angle	Depth	Angle	Depth	Angle	Depth	Angle	Depth
0	5.6%	94	12.4%	186	41.0%	276	25.7%	360	5.6%
5	5.6%	98	0.0%	188	39.5%	277	37.0%		
9	0.0%	99	14.5%	190	47.6%	279	37.0%		
11	12.9%	100	14.7%	191	51.4%	280	35.4%		
12	13.5%	102	6.9%	193	48.6%	282	28.0%		
13	20.4%	104	13.4%	194	50.5%	284	26.2%		
16	20.1%	106	5.3%	196	45.9%	285	23.1%		
17	20.5%	107	0.0%	198	46.4%	287	19.6%		
18	18.5%	109	16.4%	199	53.6%	289	16.0%		
20	11.2%	111	18.0%	207	39.1%	290	11.3%		
22	18.4%	112	16.7%	211	41.0%	300	20.4%		
33	21.8%	114	12.2%	212	46.4%	304	21.6%		
37	19.8%	123	10.4%	213	51.2%	305	20.9%		
39	19.8%	127	0.0%	215	42.5%	307	12.0%		
40	22.2%	128	0.0%	217	39.4%	308	12.5%		
41	25.1%	130	0.0%	219	35.4%	310	12.8%		
43	19.9%	131	10.2%	220	48.5%	312	0.0%		
45	18.6%	133	5.1%	222	54.6%	313	12.8%		
48	19.5%	135	0.0%	224	47.1%	316	18.5%		
49	18.9%	136	10.3%	225	44.2%	317	18.4%		
50	17.8%	138	0.0%	227	45.0%	319	19.8%		
52	24.1%	140	24.1%	237	30.0%	320	0.0%		
54	20.5%	150	23.1%	240	30.0%	322	0.0%		
62	27.0%	154	13.5%	242	27.6%	330	0.0%		
65	18.9%	156	0.0%	243	26.3%	335	21.2%		
67	25.3%	157	20.8%	244	8.3%	337	18.5%		
68	22.4%	159	23.3%	246	15.8%	338	11.9%		
70	27.0%	161	23.0%	248	28.4%	339	15.7%		
72	30.0%	162	18.5%	249	25.7%	341	23.1%		
73	0.0%	164	12.1%	251	15.4%	343	17.3%		
75	20.3%	166	19.0%	253	19.6%	344	15.3%		
77	13.5%	167	16.3%	256	2.8%	346	15.5%		
78	5.1%	169	29.8%	257	30.0%	348	0.0%		
80	19.1%	171	21.9%	258	27.5%	350	10.8%		
81	0.0%	179	46.2%	260	27.0%	352	13.4%		
83	14.4%	183	53.3%	262	25.0%	353	17.1%		
85	16.9%	184	37.6%	272	15.7%	355	11.6%		

Tabulation of Pulled Tube Crack Depth Profiles from Destructive Exam

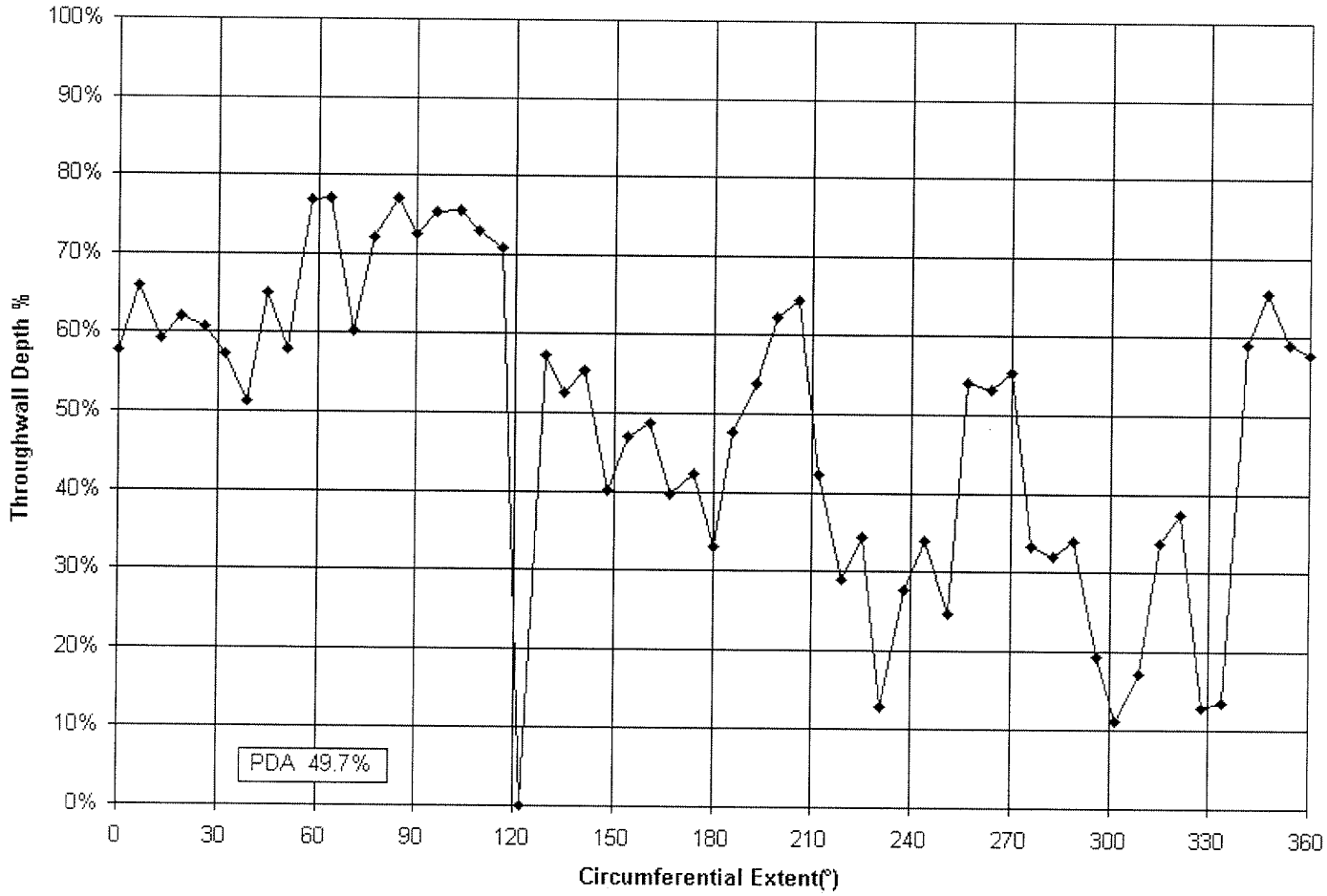

Figure B-28
Plant AB, R27C48; Destructive Examination Depth Profile

Plant :			**AB**		
Tube :			**R27C48**		
PDA :			**49.7%**		
Angle	Depth	Lig. Area	Angle	Depth	Lig. Area
0	57.7%		238	27.6%	9.47E-05
6	65.9%	0.000352	244	33.9%	2.23E-05
13	59.2%	0.000555	251	24.7%	7.99E-05
19	62.1%	0.000425	257	54.1%	5.89E-05
26	60.8%	0.000423	264	53.3%	0.00018
32	57.4%	0.000231	270	55.3%	0.000105
39	51.3%	0.000124	276	33.3%	0.000118
45	65.1%	0.000213	283	32.0%	6.69E-05
51	57.9%	0.000166	289	34.0%	6.05E-05
58	76.8%	0.000488	296	19.4%	5.57E-05
64	77.1%	0.00031	302	11.1%	1.75E-05
71	60.3%	0.000457	309	17.1%	1.86E-05
77	72.0%	0.000244	315	33.6%	2.23E-05
84	77.1%	0.000405	321	37.3%	1.75E-05
90	72.6%	0.000264	328	12.8%	9.29E-06
96	75.3%	0.000234	334	13.6%	0.000121
103	75.6%	0.000152	341	59.1%	0.00026
109	73.0%	0.000159	347	65.5%	0.000232
116	70.9%	3.34E-05	354	59.0%	0.00026
122	0.0%	0.000118	360	57.7%	0.00031
129	57.3%	0.00013			
135	52.6%	0.000126			
141	55.3%	4.78E-05			
148	40.2%	0.000137			
154	47.0%	0.000123			
161	48.7%	0.000241			
167	39.6%	0.000161			
174	42.2%	0.000184			
180	33.0%	7.48E-05			
186	47.6%	9.87E-05			
193	53.9%	0.000249			
199	62.3%	0.000244			
206	64.3%	0.000236			
212	42.3%	0.000124			
219	28.9%	0.000121			
225	34.4%	0.000132			
231	12.9%	9.39E-05			

Tabulation of Pulled Tube Crack Depth Profiles from Destructive Exam

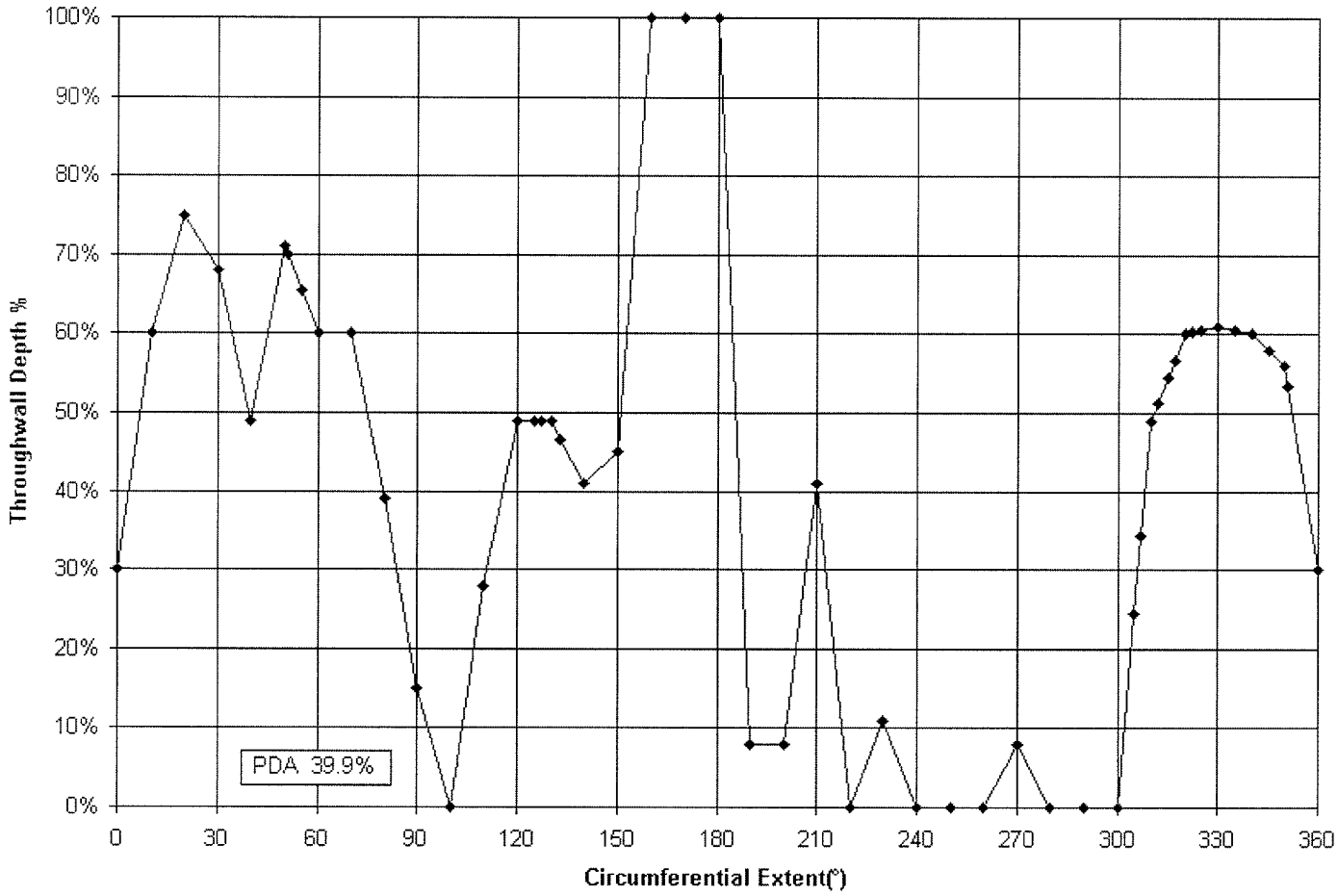

Figure B-29
Plant AB, R28C68; Destructive Examination Depth Profile

Plant :			**AB**		
Tube :			**R28C68**		
PDA :			**39.9%**		
Angle	Depth	Lig. Area	Angle	Depth	Lig. Area
0	30.0%		307	34.3%	0.00018
10	60.0%		310	0.49	
20	75.0%		312	0.512	8.75E-05
30	68.0%		315	0.545	0.00023
40	49.0%		317	0.567	5.95E-05
50	71.0%	0.00007	320	0.6	
51	69.9%	0.000105	322	0.602	0.000182
55	65.5%	0.000187	325	0.605	0.000176
60	60.0%	9.75E-05	330	0.61	
70	60.0%		335	0.605	0.00015
80	39.0%		340	0.6	
90	15.0%		345	0.58	0.000119
100	0.0%		350	0.56	
110	28.0%		351	0.534	0.000119
120	49.0%		360	0.3	
125	49.0%	5.25E-05			
127	49.0%	5.25E-05			
130	49.0%				
133	46.6%	5.25E-05			
140	41.0%				
150	45.0%				
160	100.0%				
170	100.0%				
180	100.0%	0.000138			
190	8.0%				
200	8.0%				
210	41.0%				
220	0.0%				
230	11.0%				
240	0.0%				
250	0.0%				
260	0.0%				
270	8.0%				
280	0.0%				
290	0.0%				
300	0.0%				
305	24.5%	0.000196			

Tabulation of Pulled Tube Crack Depth Profiles from Destructive Exam

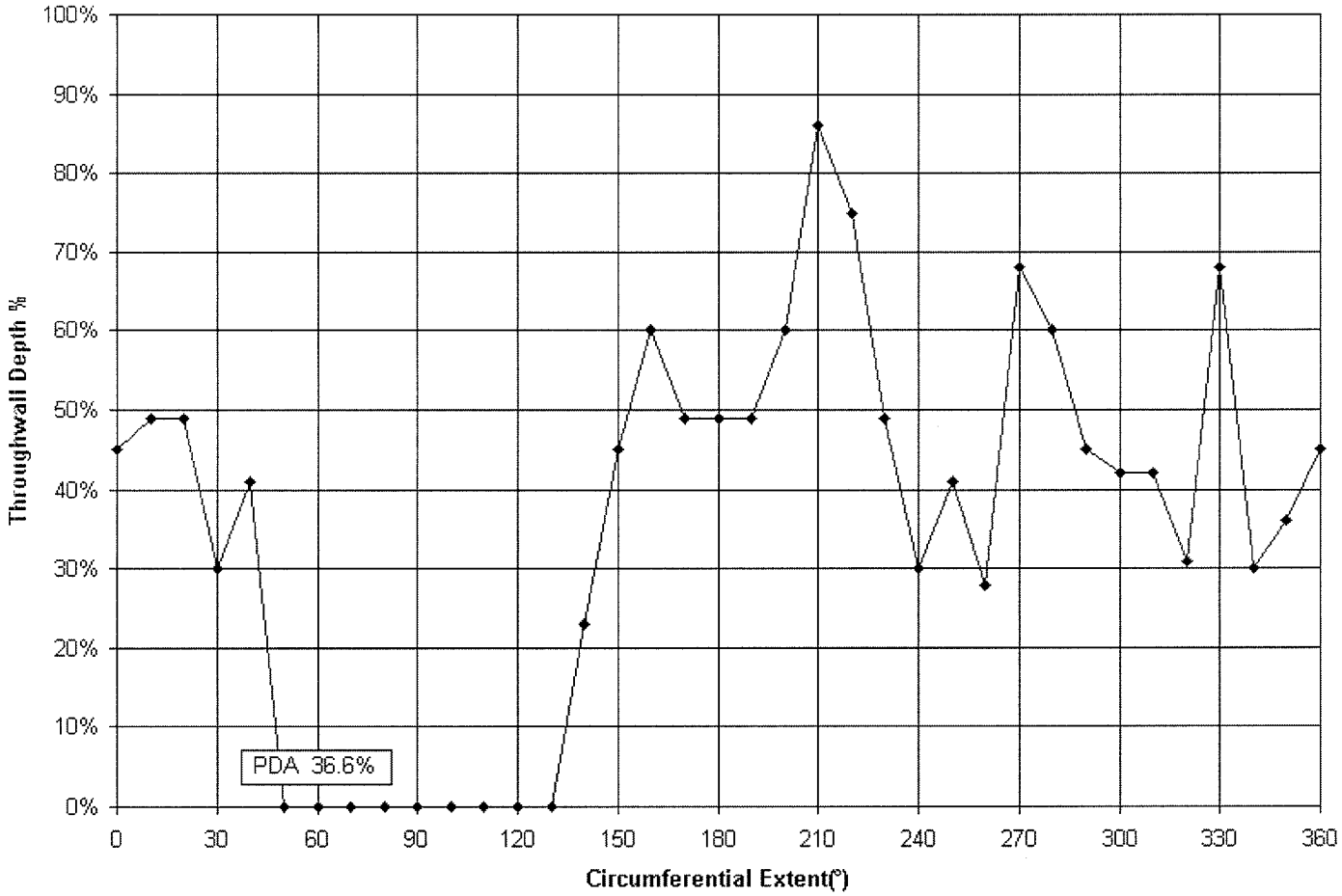

Figure B-30
Plant AB, R38C44; Destructive Examination Depth Profile

Plant :	**AB**	
Tube :	**R38C44**	
PDA :	**36.6%**	
Angle	Depth	Lig. Area
0	45.0%	
10	49.0%	
20	49.0%	
30	30.0%	
40	41.0%	
50	0.0%	
60	0.0%	
70	0.0%	
80	0.0%	
90	0.0%	
100	0.0%	
110	0.0%	
120	0.0%	
130	0.0%	
140	23.0%	
150	45.0%	
160	60.0%	
170	49.0%	
180	49.0%	
190	49.0%	
200	60.0%	
210	86.0%	
220	75.0%	
230	49.0%	
240	30.0%	
250	41.0%	
260	28.0%	
270	68.0%	
280	60.0%	
290	45.0%	
300	42.0%	
310	42.0%	
320	31.0%	
330	68.0%	
340	30.0%	
350	36.0%	
360	45.0%	

Tabulation of Pulled Tube Crack Depth Profiles from Destructive Exam

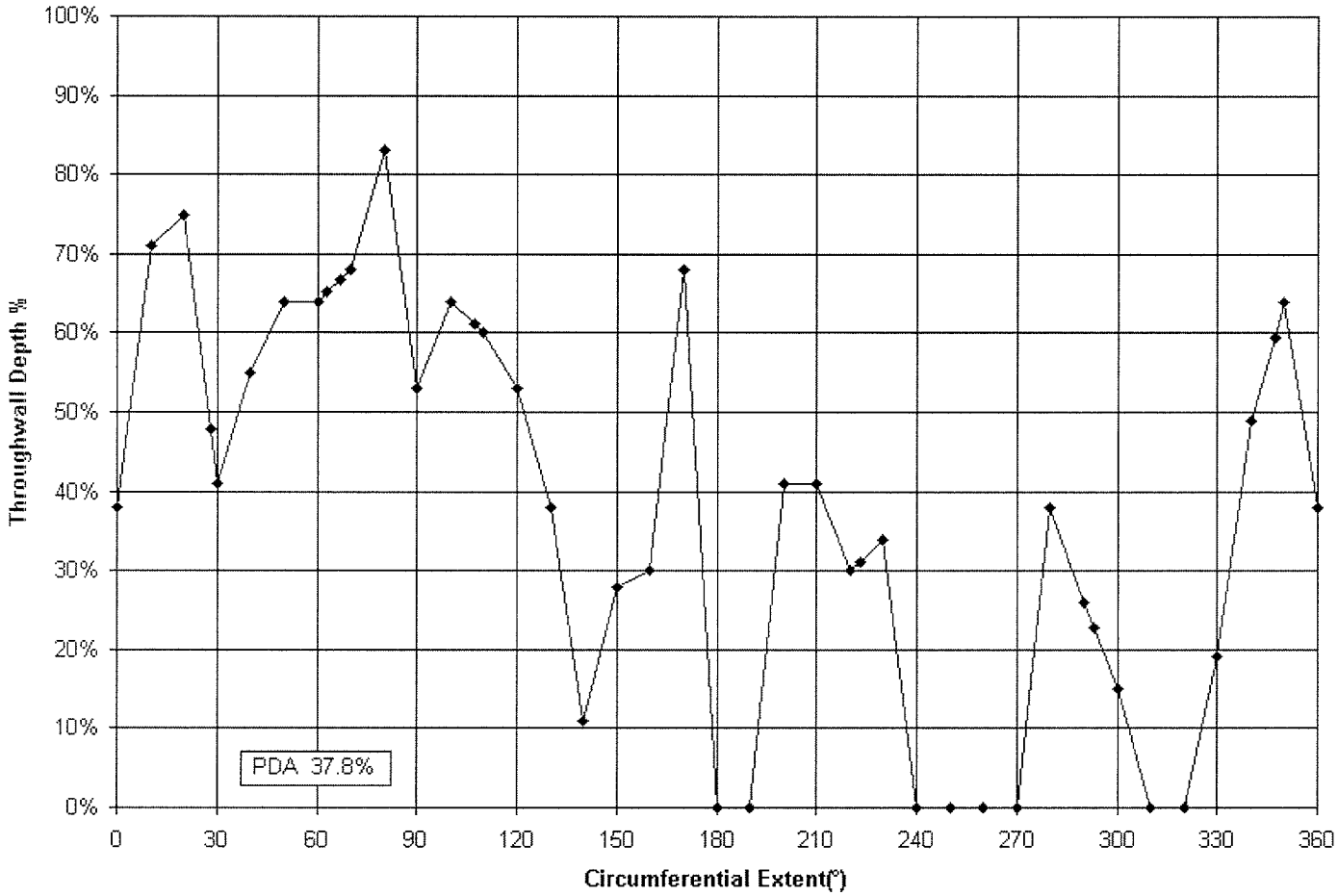

Figure B-31
Plant AB, R38C55; Destructive Examination Depth Profile

Plant :			**AB**		
Tube :			**R38C55**		
PDA :			**37.8%**		
Angle	Depth	Lig. Area	Angle	Depth	Lig. Area
0	38.0%	0.00013	310	0.0%	
10	71.0%		320	0.0%	
20	75.0%		330	19.0%	5.25E-05
28	47.8%	5.95E-05	340	49.0%	
30	41.0%		347	59.5%	5.95E-05
40	55.0%		350	64.0%	
50	64.0%		360	38.0%	
60	64.0%				
63	65.2%	0.000187			
67	66.8%	4.55E-05			
70	68.0%				
80	83.0%				
90	53.0%	0.000176			
100	64.0%				
107	61.2%	0.000161			
110	60.0%				
120	53.0%				
130	38.0%				
140	11.0%				
150	28.0%	0.000084			
160	30.0%				
170	68.0%				
180	0.0%				
190	0.0%				
200	41.0%				
210	41.0%				
220	30.0%				
223	31.2%	0.00022			
230	34.0%				
240	0.0%				
250	0.0%	0.00007			
260	0.0%				
270	0.0%				
280	38.0%				
290	26.0%				
293	22.7%	0.00026			
300	15.0%				

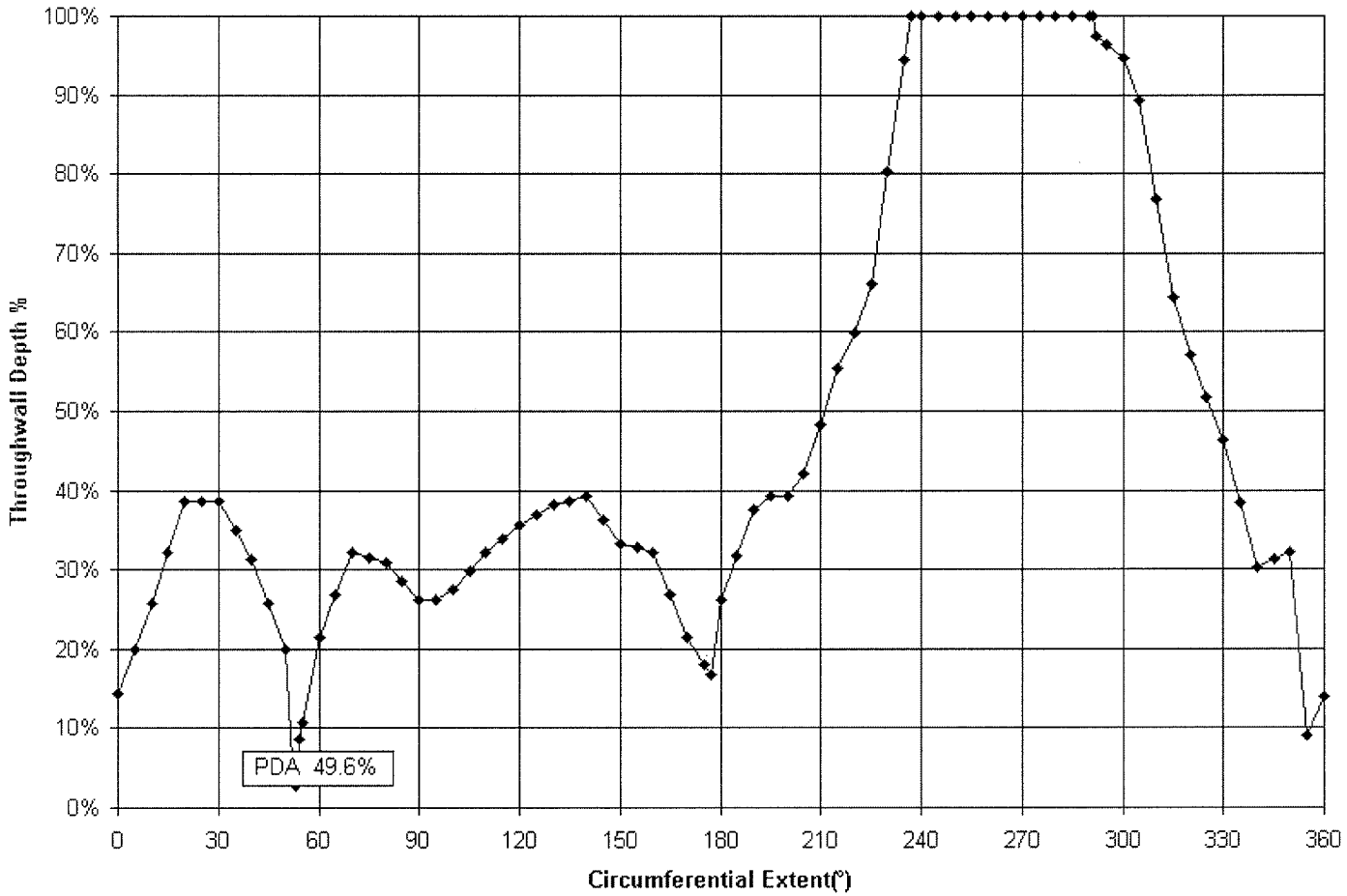

Figure B-32
Plant Q, R40C47; Destructive Examination Depth Profile

Plant :				**Q**				
Tube :				**R40C47**				
PDA :				**49.6%**				
Angle	Depth	Lig. Area	Angle	Depth	Lig. Area	Angle	Depth	Lig. Area
0	14.3%		170	21.4%		335	38.4%	
5	20.0%		175	18.0%		340	30.4%	
10	25.7%		177	16.7%		345	31.3%	
15	32.1%		180	26.2%		350	32.1%	
20	38.6%		185	31.8%		355	8.9%	
25	38.6%		190	37.5%		360	14.0%	
30	38.6%		195	39.3%				
35	35.0%		200	39.3%				
40	31.4%		205	42.0%				
45	25.7%		210	48.2%				
50	20.0%		215	55.4%				
52	5.7%		220	59.8%				
53	2.9%		225	66.1%				
54	8.6%		230	80.4%				
55	10.7%		235	94.4%				
60	21.4%		237	100.0%				
65	26.8%		240	100.0%				
70	32.1%		245	100.0%				
75	31.5%		250	100.0%				
80	31.0%		255	100.0%				
85	28.6%		260	100.0%				
90	26.2%		265	100.0%				
95	26.2%		270	100.0%				
100	27.4%		275	100.0%				
105	29.8%		280	100.0%				
110	32.1%		285	100.0%				
115	33.9%		290	100.0%				
120	35.7%		291	100.0%				
125	36.9%		292	97.3%				
130	38.1%		295	96.3%				
135	38.7%		300	94.6%				
140	39.3%		305	89.3%				
145	36.3%		310	76.8%				
150	33.3%		315	64.3%				
155	32.7%		320	57.1%				
160	32.1%		325	51.8%				
165	26.8%		330	46.4%				

Tabulation of Pulled Tube Crack Depth Profiles from Destructive Exam

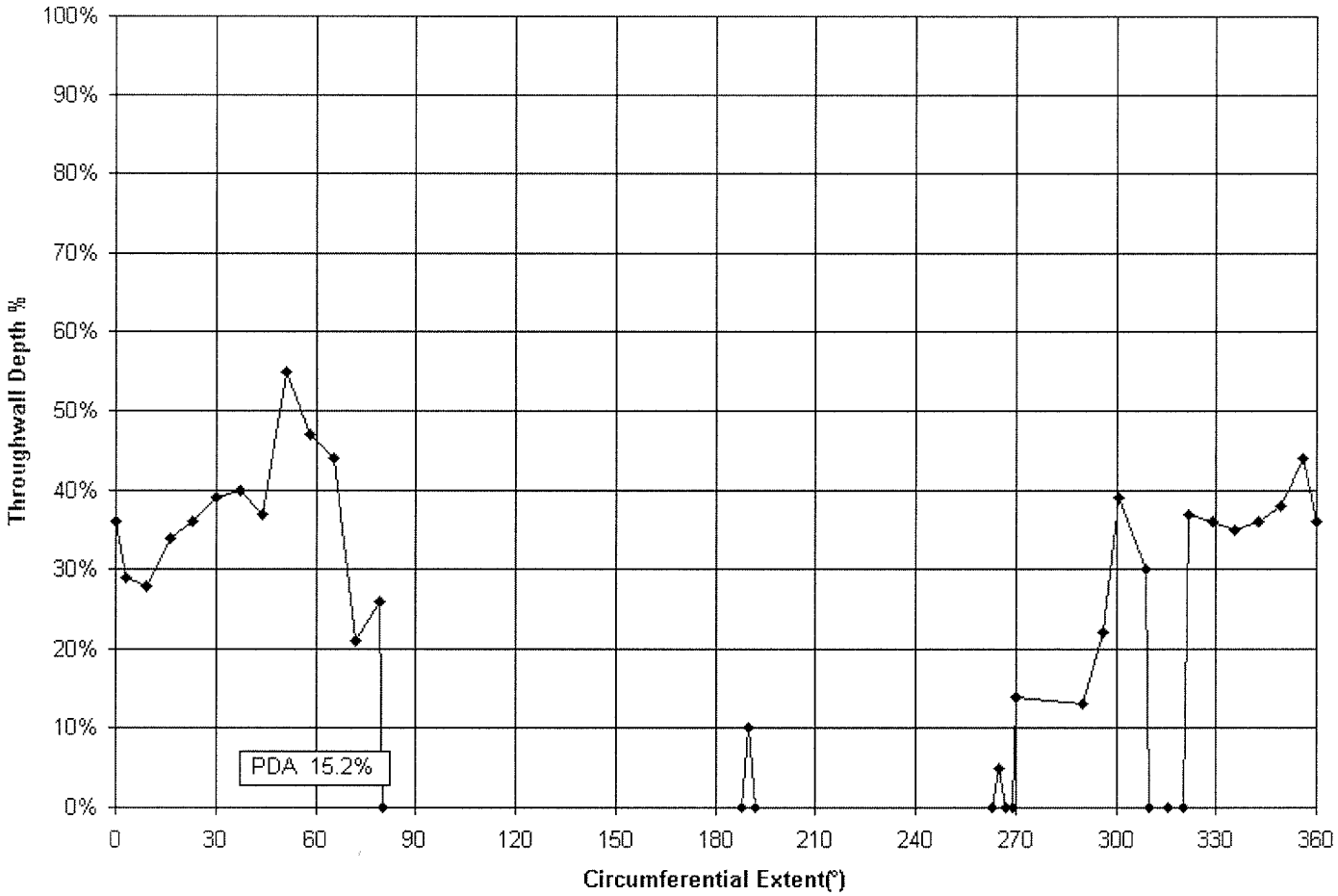

Figure B-33
Plant AC, R15C25; Destructive Examination Depth Profile

Plant :	**AC**	
Tube :	**R15C25**	
PDA :	**15.2%**	
Angle	Depth	Lig. Area
0	36.0%	
3	29.0%	
9	28.0%	
16	34.0%	
23	36.0%	
30	39.0%	
37	40.0%	
44	37.0%	
51	55.0%	
58	47.0%	
66	44.0%	
72	21.0%	
79	26.0%	
80	0.0%	
188	0.0%	
190	10.0%	
192	0.0%	
263	0.0%	
265	5.0%	
267	0.0%	
269	0.0%	
270	14.0%	
290	13.0%	
296	22.0%	
301	39.0%	
309	30.0%	
310	0.0%	
316	0.0%	
320	0.0%	
322	37.0%	
329	36.0%	
336	35.0%	
342	36.0%	
349	38.0%	
356	44.0%	
360	36.0%	

Tabulation of Pulled Tube Crack Depth Profiles from Destructive Exam

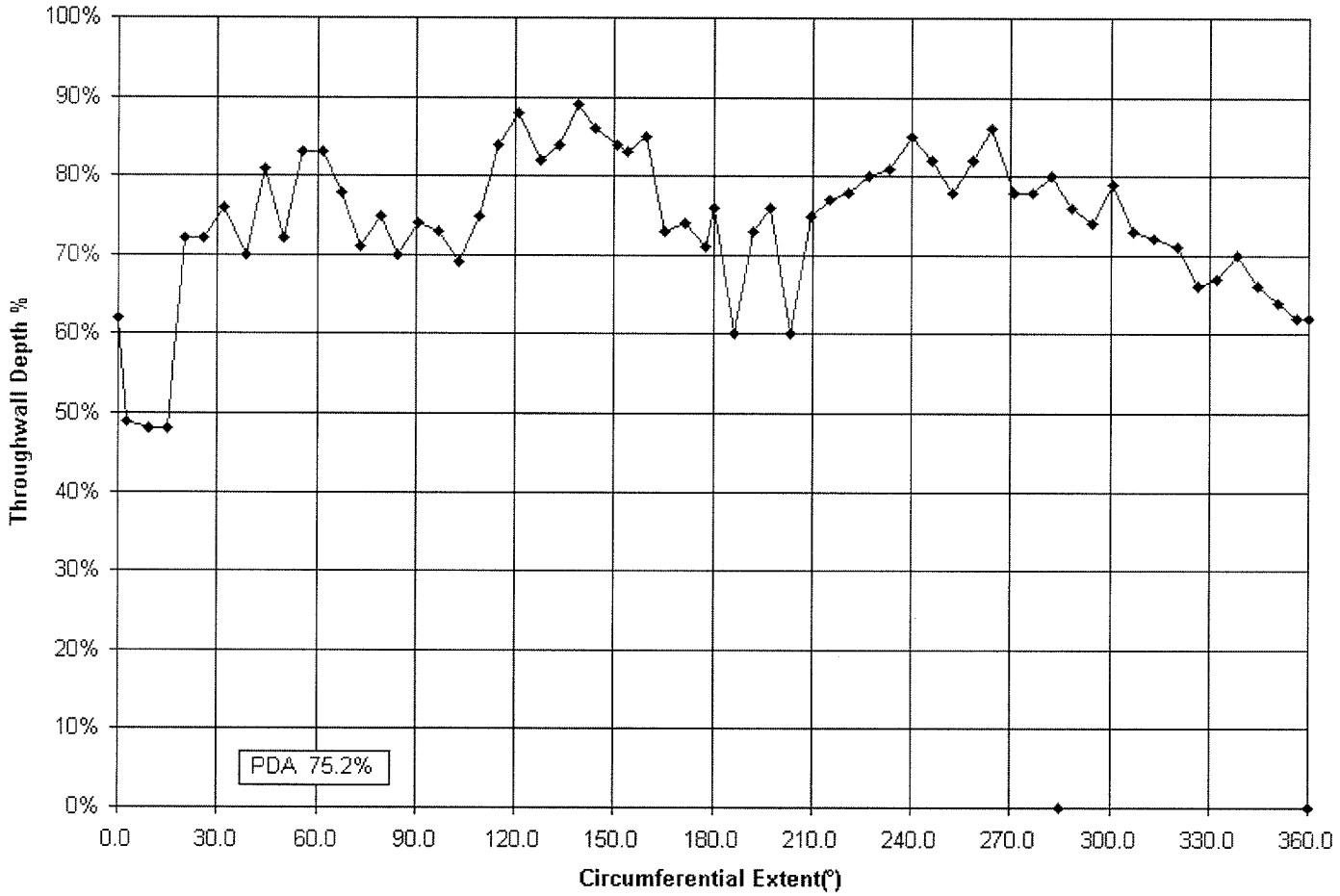

Figure B-34
Plant AC, R23C76; Destructive Examination Depth Profile

Plant :			**AC**		
Tube :			**R23C76**		
PDA :			**75.2%**		
Angle	Depth	Lig. Area	Angle	Depth	Lig. Area
0.0	62.0%		209.6	75.0%	
2.7	49.0%		215.5	77.0%	
9.1	48.0%		221.2	78.0%	
14.8	48.0%		227.2	80.0%	
19.9	72.0%		233.5	81.0%	
26.0	72.0%		239.9	85.0%	
32.1	76.0%		246.1	82.0%	
38.4	70.0%		252.3	78.0%	
44.2	81.0%		258.3	82.0%	
50.0	72.0%		264.4	86.0%	
55.8	83.0%		270.7	78.0%	
61.7	83.0%		276.8	78.0%	
67.5	78.0%		282.2	80.0%	
73.1	71.0%		288.6	76.0%	
79.3	75.0%		294.6	74.0%	
84.5	70.0%		301.0	79.0%	
90.8	74.0%		307.1	73.0%	
96.9	73.0%		313.2	72.0%	
102.8	69.0%		320.2	71.0%	
109.1	75.0%		326.3	66.0%	
114.9	84.0%		332.1	67.0%	
120.8	88.0%		338.6	70.0%	
127.5	82.0%		344.4	66.0%	
133.4	84.0%		350.5	64.0%	
138.8	89.0%		356.5	62.0%	
144.4	86.0%		360.0	62.0%	
151.0	84.0%				
153.9	83.0%				
159.5	85.0%				
165.3	73.0%				
171.5	74.0%				
177.8	71.0%				
180.4	76.0%				
186.5	60.0%				
192.1	73.0%				
197.4	76.0%				
203.5	60.0%				

Tabulation of Pulled Tube Crack Depth Profiles from Destructive Exam

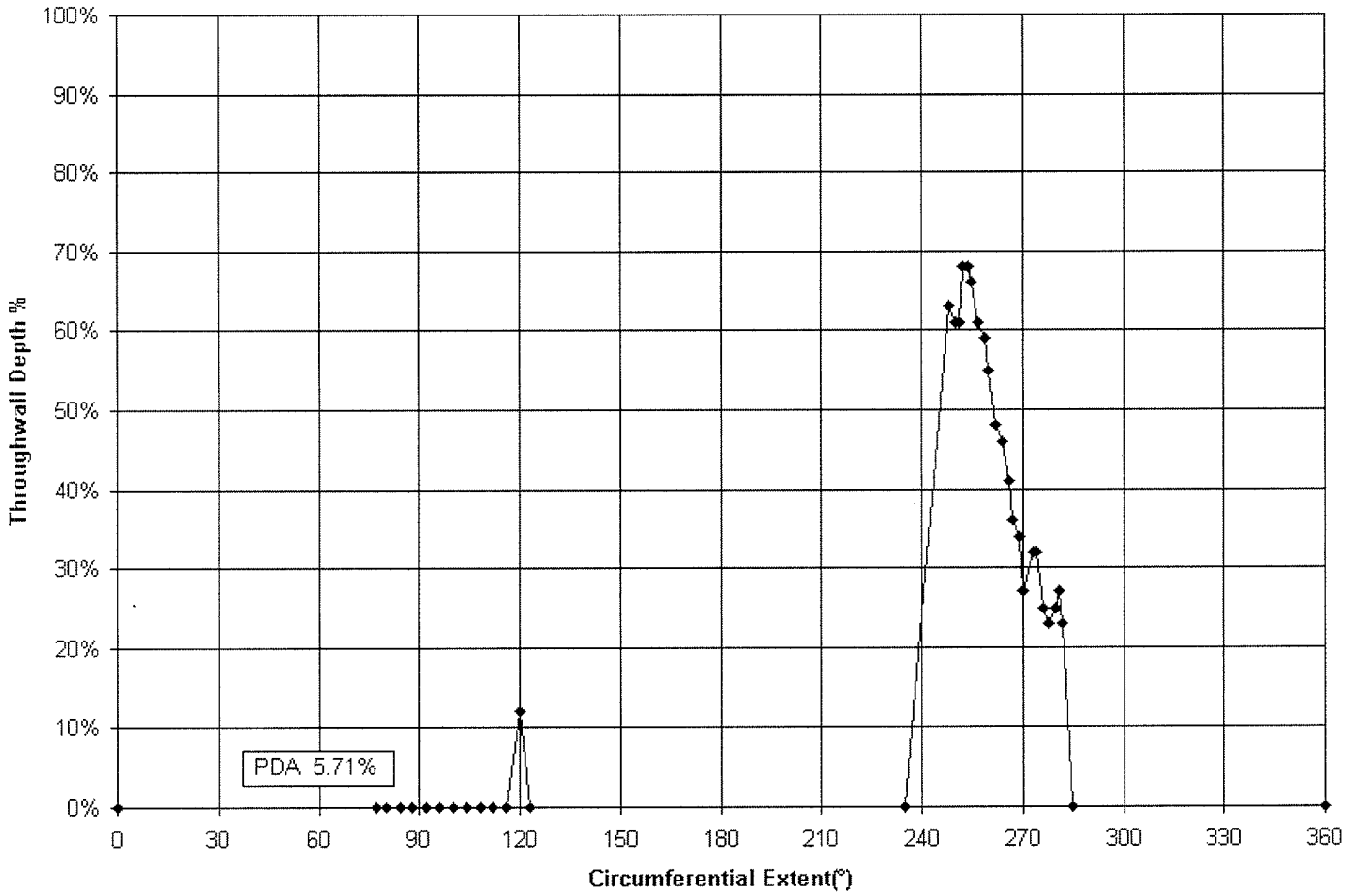

Figure B-35
Plant AC, R25C58; Destructive Examination Depth Profile

Plant :			**AC**		
Tube :			**R25C58**		
PDA :			**5.7%**		
Angle	Depth	Lig. Area	Angle	Depth	Lig. Area
0	0.0%		285	0.0%	
77	0.0%		360	0.0%	
80	0.0%				
84	0.0%				
88	0.0%				
92	0.0%				
96	0.0%				
100	0.0%				
104	0.0%				
108	0.0%				
112	0.0%				
116	0.0%				
120	12.0%				
123	0.0%				
235	0.0%				
248	63.0%				
250	61.0%				
251	61.0%				
252	68.0%				
254	68.0%				
255	66.0%				
257	61.0%				
259	59.0%				
260	55.0%				
262	48.0%				
264	46.0%				
266	41.0%				
267	36.0%				
269	34.0%				
270	27.0%				
273	32.0%				
274	32.0%				
276	25.0%				
278	23.0%				
280	25.0%				
281	27.0%				
282	23.0%				

Tabulation of Pulled Tube Crack Depth Profiles from Destructive Exam

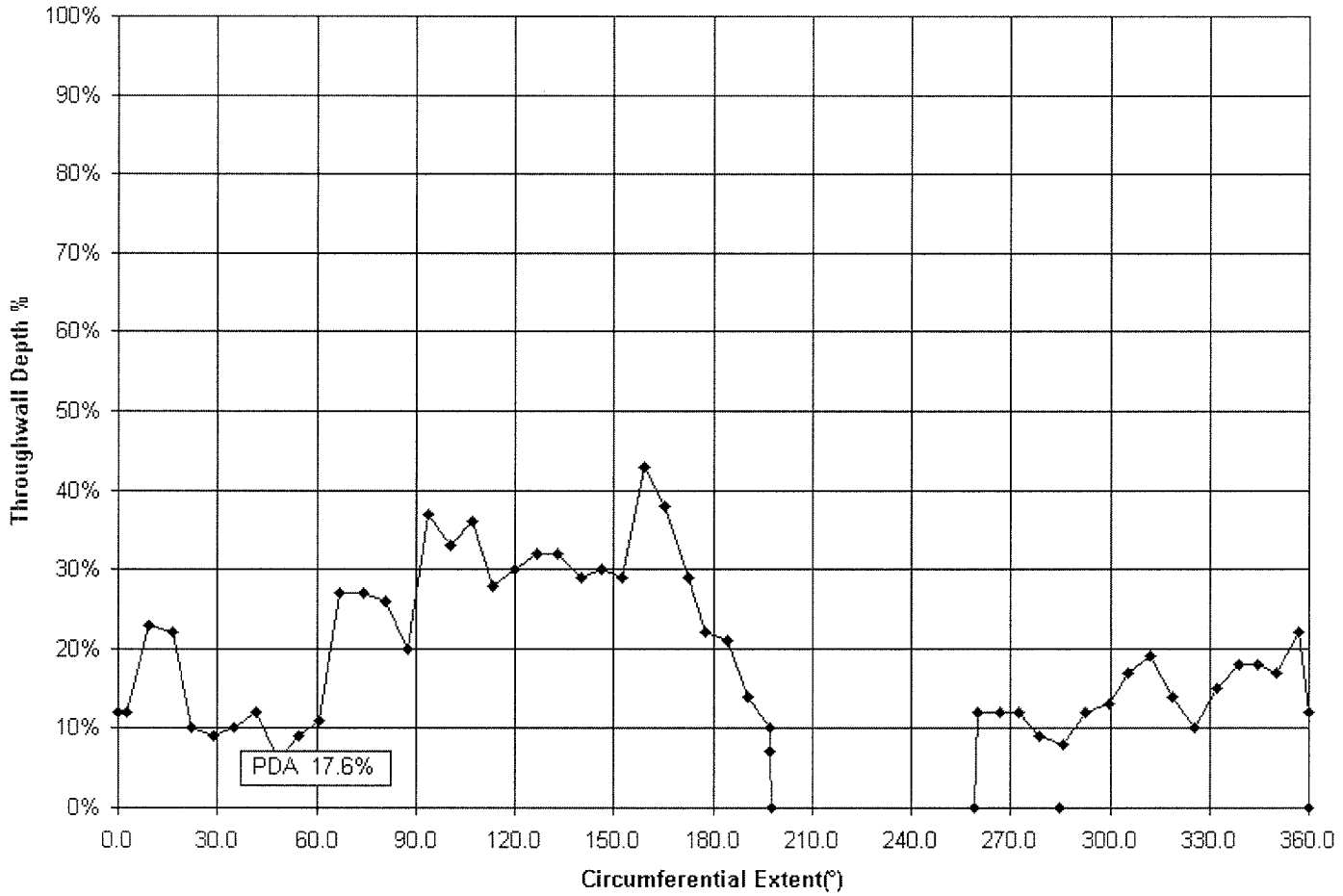

Figure B-36
Plant AC, R26C63; Destructive Examination Depth Profile

Plant :			**AC**		
Tube :			**R26C63**		
PDA :			**17.6%**		
Angle	Depth	Lig. Area	Angle	Depth	Lig. Area
0.0	12.0%		272.2	0.12	
2.5	12.0%		278.4	0.09	
9.4	23.0%		285.8	0.08	
16.6	22.0%		292.6	0.12	
22.1	10.0%		299.6	0.13	
28.7	9.0%		305.6	0.17	
35.1	10.0%		312.2	0.19	
41.5	12.0%		318.8	0.14	
48.3	6.0%		325.7	0.1	
54.6	9.0%		332.4	0.15	
60.6	11.0%		338.8	0.18	
67.0	27.0%		344.3	0.18	
74.2	27.0%		350.3	0.17	
80.9	26.0%		356.7	0.22	
87.4	20.0%		360	0.12	
93.7	37.0%				
100.3	33.0%				
107.0	36.0%				
113.4	28.0%				
119.9	30.0%				
126.5	32.0%				
133.1	32.0%				
139.9	29.0%				
146.2	30.0%				
152.6	29.0%				
158.9	43.0%				
165.2	38.0%				
172.3	29.0%				
177.9	22.0%				
184.5	21.0%				
190.8	14.0%				
197.1	10.0%				
197.5	7.0%				
198.0	0.0%				
259.0	0.0%				
259.9	12.0%				
266.6	12.0%				

Tabulation of Pulled Tube Crack Depth Profiles from Destructive Exam

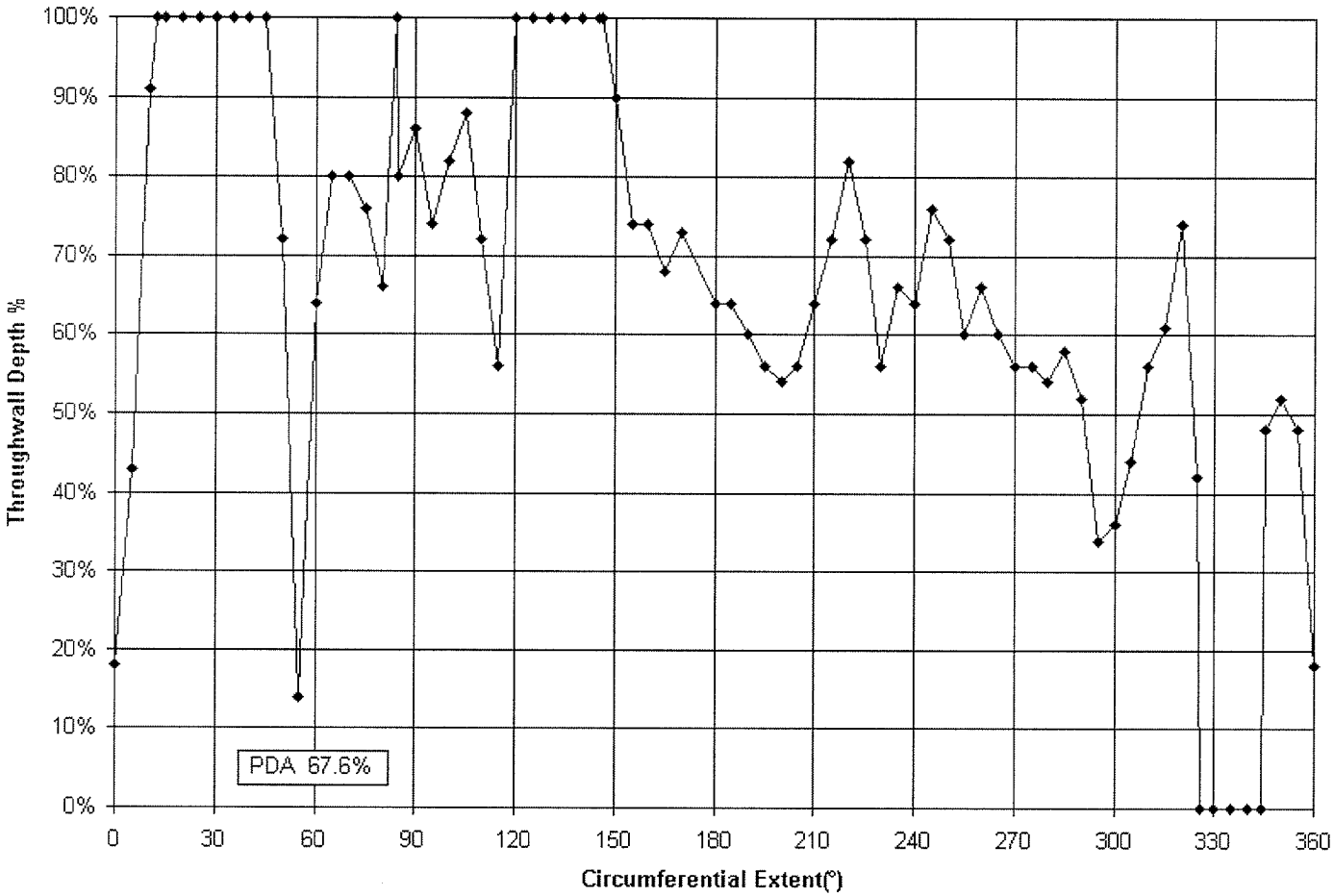

Figure B-37
Plant A, R18C42; Destructive Examination Depth Profile

Plant :			**A**					
Tube :			**R18C42**					
PDA :			**67.6%**					
Angle	Depth	Lig. Area	Angle	Depth	Lig. Area	Angle	Depth	Lig. Area
0	18.0%		170	73.0%		350	0.52	
5	43.0%		180	64.0%		355	0.48	
10	91.0%		185	64.0%		360	0.18	
12	100.0%		190	60.0%				
15	100.0%		195	56.0%				
20	100.0%		200	54.0%				
25	100.0%		205	56.0%				
30	100.0%		210	64.0%				
35	100.0%		215	72.0%				
40	100.0%		220	82.0%				
45	100.0%		225	72.0%				
50	72.0%		230	56.0%				
55	14.0%		235	66.0%				
60	64.0%		240	64.0%				
65	80.0%		245	76.0%				
70	80.0%		250	72.0%				
75	76.0%		255	60.0%				
80	66.0%		260	66.0%				
84	100.0%		265	60.0%				
85	80.0%		270	56.0%				
90	86.0%		275	56.0%				
95	74.0%		280	54.0%				
100	82.0%		285	58.0%				
105	88.0%		290	52.0%				
110	72.0%		295	34.0%				
115	56.0%		300	36.0%				
120	100.0%		305	44.0%				
125	100.0%		310	56.0%				
130	100.0%		315	61.0%				
135	100.0%		320	74.0%				
140	100.0%		325	42.0%				
145	100.0%		326	0.0%				
146	100.0%		330	0.0%				
150	90.0%		335	0.0%				
155	74.0%		340	0.0%				
160	74.0%		344	0.0%				
165	68.0%		345	48.0%				

C

TABULATION OF LABORATORY SPECIMEN CRACK DEPTH PROFILES FROM DESTRUCTIVE EXAM

This appendix includes the destructive examination data for the laboratory specimens referenced in the body of the report. These data generated during the laboratory effort for hardrolled tube cracking performed by Westinghouse supporting the circumferential crack program, and from data provided by ANO for circumferentially cracked laboratory specimens in explosively expanded tubes developed by ABB-CE in support of ANO programs. The hardrolled specimens, identified by specimen numbers in the form xx-yy-zz, were utilized in leak and burst test programs and thus, support the leak and burst test methodology sections of this report. The explosively expanded specimens, identified by specimens numbers in the form R0Cxx, were utilized principally in the NDE Performance Test, Section 5.7, to support development of NDE uncertainties for explosively expanded tubes.

The data included here are tabular data of measured depth vs. angular position, and a plot of the tabular data to provide a visual image of the depth profile for each tube. Ligament data are included where these were reported; however, no adjustment to the depth profiles are made to account for the ligaments. Section 3 of the report provides the methods by which ligament adjustments were made to obtain a net depth profile.

Tabulation of Laboratory Specimen Crack Depth Profiles from Destructive Exam

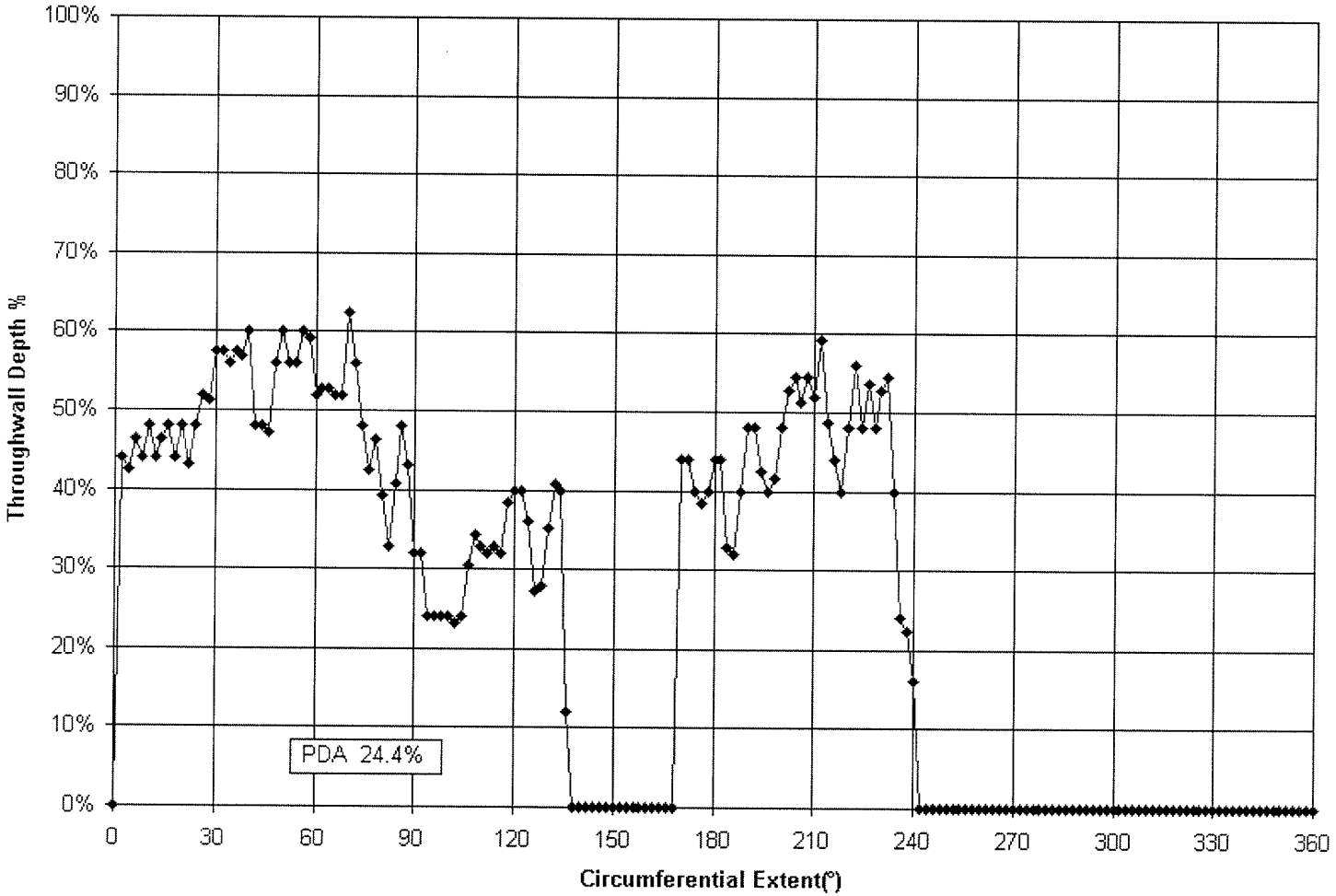

Figure C-1
LAB, 94-12-01A; Destructive Examination Depth Profile

Plant:	LAB								
Tube:	94-12-01A, ID, .875"								
PDA:	24.4%								
Angle	Depth	Angle	Depth	Angle	Depth	Angle	Depth	Angle	Depth
0	0.0%	74	48.0%	148	0.0%	220	48.0%	294	0
2	44.0%	76	42.4%	150	0.0%	222	56.0%	296	0
4	42.4%	78	46.4%	152	0.0%	224	48.0%	298	0
6	46.4%	80	39.2%	154	0.0%	226	53.6%	300	0
8	44.0%	82	32.8%	156	0.0%	228	48.0%	302	0
10	48.0%	84	40.8%	158	0.0%	230	52.8%	304	0
12	44.0%	86	48.0%	160	0.0%	232	54.4%	306	0
14	46.4%	88	43.2%	162	0.0%	234	40.0%	308	0
16	48.0%	90	32.0%	164	0.0%	236	24.0%	310	0
18	44.0%	92	32.0%	166	0.0%	238	22.4%	312	0
20	48.0%	94	24.0%	168	0.0%	240	16.0%	314	0
22	43.2%	96	24.0%	170	44.0%	242	0.0%	316	0
24	48.0%	98	24.0%	172	44.0%	244	0.0%	318	0
26	52.0%	100	24.0%	174	40.0%	246	0.0%	320	0
28	51.2%	102	23.2%	176	38.4%	248	0.0%	322	0
30	57.6%	104	24.0%	178	40.0%	250	0.0%	324	0
32	57.6%	106	30.4%	180	44.0%	252	0.0%	326	0
34	56.0%	108	34.4%	182	44.0%	254	0.0%	328	0
36	57.6%	110	32.8%	184	32.8%	256	0.0%	330	0
38	56.8%	112	32.0%	186	32.0%	258	0.0%	332	0
40	60.0%	114	32.8%	188	40.0%	260	0.0%	334	0
42	48.0%	116	32.0%	190	48.0%	262	0.0%	336	0
44	48.0%	118	38.4%	192	48.0%	264	0.0%	338	0
46	47.2%	120	40.0%	194	42.4%	266	0.0%	340	0
48	56.0%	122	40.0%	196	40.0%	268	0.0%	342	0
50	60.0%	124	36.0%	198	41.6%	270	0.0%	344	0
52	56.0%	126	27.2%	200	48.0%	272	0.0%	346	0
54	56.0%	128	28.0%	202	52.8%	274	0.0%	348	0
56	60.0%	130	35.2%	204	54.4%	276	0.0%	350	0
58	59.2%	132	40.8%	206	51.2%	278	0.0%	352	0
60	52.0%	134	40.0%	208	54.4%	280	0.0%	354	0
62	52.8%	136	12.0%	210	52.0%	282	0.0%	356	0
64	52.8%	138	0.0%	212	59.2%	284	0.0%	358	0
66	52.0%	140	0.0%	214	48.8%	286	0.0%	360	0
68	52.0%	142	0.0%	216	44.0%	288	0.0%		
70	62.4%	144	0.0%	218	40.0%	290	0.0%		
72	56.0%	146	0.0%			292	0.0%		

Tabulation of Laboratory Specimen Crack Depth Profiles from Destructive Exam

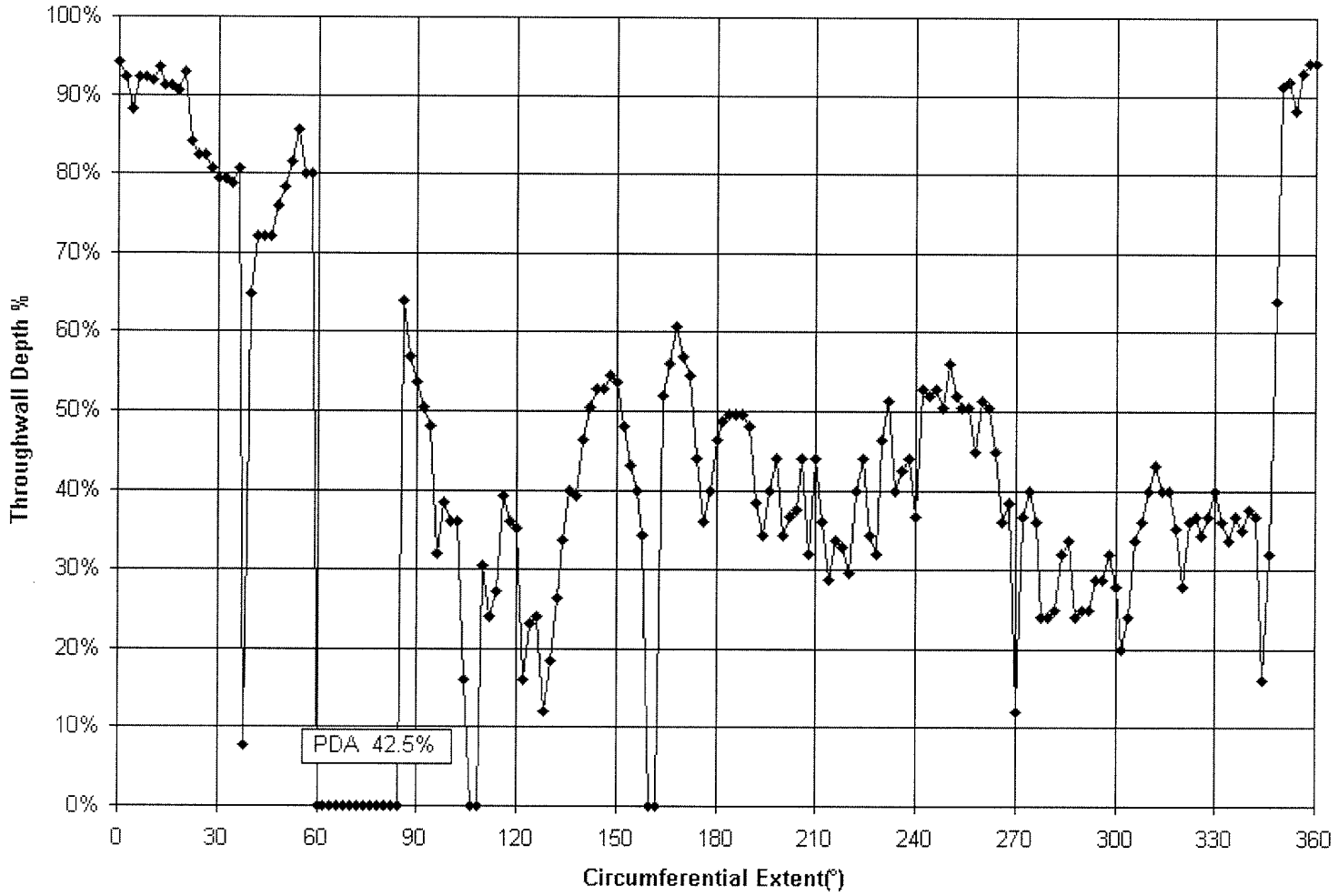

Figure C-2
LAB, 94-12-01B; Destructive Examination Depth Profile

Plant:	LAB												
Tube:	94-12-01B, ID, .875"												
PDA:	42.5%												
Angle	Depth	L/A	Angle	Depth	L/A	Angle	Depth	L/A	Angle	Depth	L/A	Angle	Depth
0	94.1%		74	0.0%		148	54.4%		222	40.0%		296	28.8%
2	92.4%		76	0.0%		150	53.6%		224	44.0%		298	32.0%
4	88.2%		78	0.0%		152	48.0%		226	34.4%		300	28.0%
6	92.4%		80	0.0%		154	43.2%		228	32.0%		302	20.0%
8	92.4%	0.00104255	82	0.0%		156	40.0%		230	46.4%		304	24.0%
10	91.8%		84	0.0%		158	34.4%		232	51.2%		306	33.6%
12	93.5%		86	64.0%		160	0.0%		234	40.0%		308	36.0%
14	91.2%		88	56.8%		162	0.0%		236	42.4%		310	40.0%
16	91.2%		90	53.6%		164	52.0%		238	44.0%		312	43.2%
18	90.6%		92	50.4%		166	56.0%		240	36.8%		314	40.0%
20	92.9%		94	48.0%		168	60.8%		242	52.8%		316	40.0%
22	84.1%		96	32.0%		170	56.8%		244	52.0%		318	35.2%
24	82.4%		98	38.4%		172	54.4%		246	52.8%		320	28.0%
26	82.4%		100	36.0%		174	44.0%		248	50.4%		322	36.0%
28	80.6%		102	36.0%		176	36.0%		250	56.0%		324	36.8%
30	79.4%		104	16.0%		178	40.0%		252	52.0%		326	34.4%
32	79.4%		106	0.0%		180	46.4%		254	50.4%		328	36.8%
34	78.8%		108	0.0%		182	48.8%		256	50.4%		330	40.0%
36	80.6%		110	30.4%		184	49.6%		258	44.8%		332	36.0%
38	7.8%		112	24.0%		186	49.6%		260	51.2%		334	33.6%
40	64.7%		114	27.2%		188	49.6%		262	50.4%		336	36.8%
42	72.0%		116	39.2%		190	48.0%		264	44.8%		338	35.0%
44	72.0%		118	36.0%		192	38.4%		266	36.0%		340	37.6%
46	72.0%		120	35.2%		194	34.4%		268	38.4%		342	36.8%
48	76.0%		122	16.0%		196	40.0%		270	12.0%		344	16.0%
50	78.4%		124	23.2%		198	44.0%		272	36.8%		346	32.0%
52	81.6%		126	24.0%		200	34.4%		274	40.0%		348	64.0%
54	85.6%		128	12.0%		202	36.8%		276	36.0%		350	91.2%
56	80.0%		130	18.4%		204	37.6%		278	24.0%		352	91.8%
58	80.0%		132	26.4%		206	44.0%		280	24.0%		354	88.2%
60	0.0%		134	33.6%		208	32.0%		282	24.8%		356	92.9%
62	0.0%		136	40.0%		210	44.0%		284	32.0%		358	94.1%
64	0.0%		138	39.2%		212	36.0%		286	33.6%		360	94.1%
66	0.0%		140	46.4%		214	28.8%		288	24.0%			
68	0.0%		142	50.4%		216	33.6%		290	24.8%			
70	0.0%		144	52.8%		218	32.8%		292	24.8%			
72	0.0%		146	52.8%		220	29.6%		294	28.8%			

Tabulation of Laboratory Specimen Crack Depth Profiles from Destructive Exam

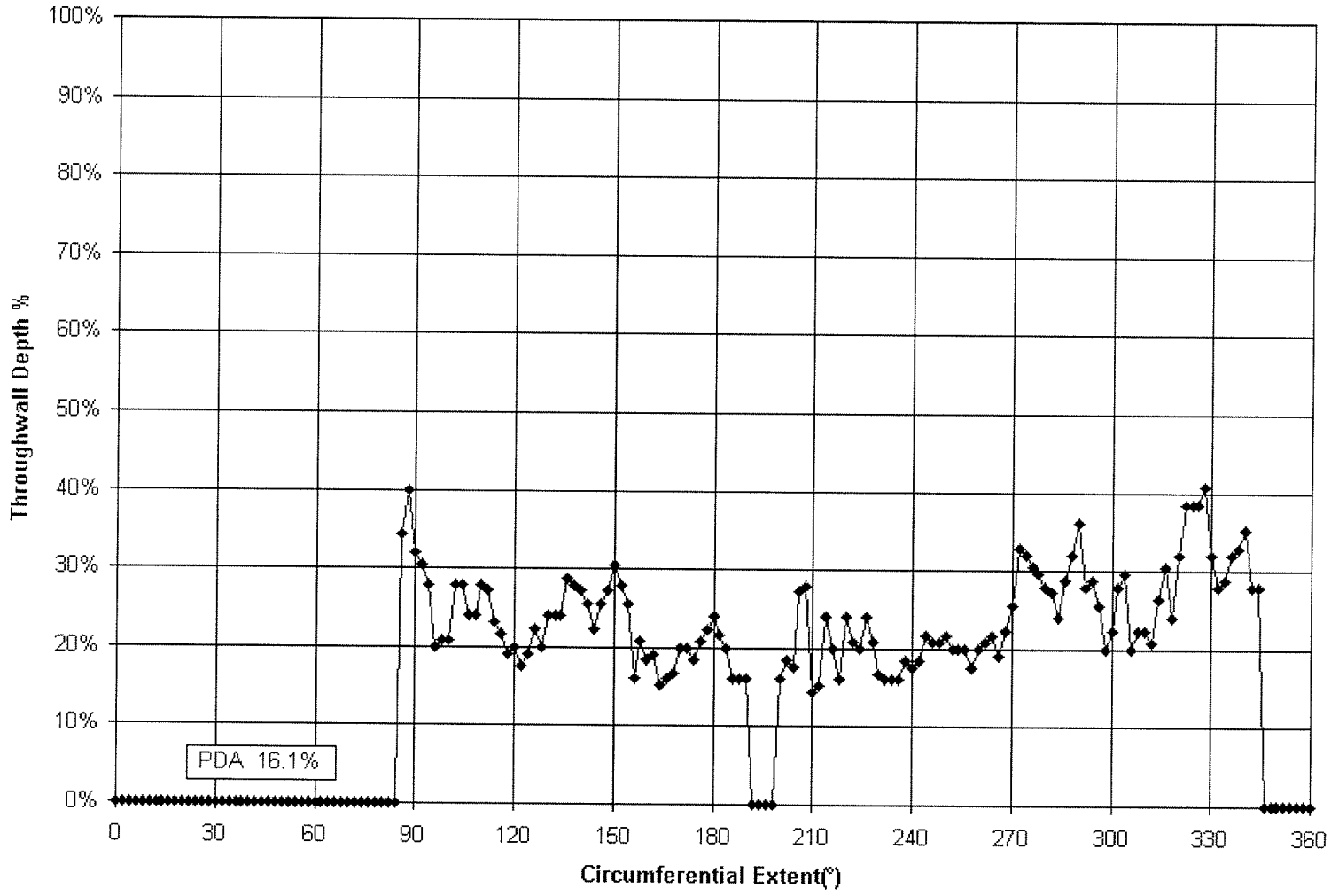

Figure C-3
LAB, 94-12-06A; Destructive Examination Depth Profiles

Plant:	LAB													
Tube:	94-12-06A, ID, .875"													
PDA:	16.1%													
Angle	Depth	L/A	Angle	Depth	L/A	Angle	Depth	L/A	Angle	Depth	L/A	Angle	Depth	L/A
0	0.0%		74	0.0%		148	27.2%		222	20.8%		296	25.6%	
2	0.0%		76	0.0%		150	30.4%	1.41E-03	224	20.0%		298	20.0%	
4	0.0%		78	0.0%		152	28.0%		226	24.0%		300	22.4%	
6	0.0%		80	0.0%		154	25.6%		228	20.8%		302	28.0%	
8	0.0%		82	0.0%		156	16.0%		230	16.8%		304	29.6%	
10	0.0%		84	0.0%		158	20.8%		232	16.0%		306	20.0%	
12	0.0%		86	34.4%		160	18.4%		234	16.0%		308	22.4%	
14	0.0%		88	40.0%		162	19.2%		236	16.0%		310	22.4%	
16	0.0%		90	32.0%		164	15.2%		238	18.4%		312	20.8%	
18	0.0%		92	30.4%		166	16.0%		240	17.6%		314	26.4%	
20	0.0%		94	28.0%		168	16.8%		242	18.4%		316	30.4%	
22	0.0%		96	20.0%		170	20.0%		244	21.6%		318	24.0%	0.0014
24	0.0%		98	20.8%		172	20.0%		246	20.8%		320	32.0%	
26	0.0%		100	20.8%		174	18.4%		248	20.8%		322	38.4%	
28	0.0%		102	28.0%		176	20.8%		250	21.6%		324	38.4%	
30	0.0%		104	28.0%		178	22.4%		252	20.0%		326	38.4%	
32	0.0%		106	24.0%		180	24.0%		254	20.0%		328	40.8%	
34	0.0%		108	24.0%		182	21.6%		256	20.0%		330	32.0%	
36	0.0%		110	28.0%		184	20.0%		258	17.6%		332	28.0%	
38	0.0%		112	27.2%		186	16.0%		260	20.0%		334	28.8%	
40	0.0%		114	23.2%		188	16.0%		262	20.8%		336	32.0%	
42	0.0%		116	21.6%		190	16.0%		264	21.6%		338	32.8%	
44	0.0%		118	19.2%		192	0.0%		266	19.2%		340	35.2%	
46	0.0%		120	20.0%		194	0.0%		268	22.4%		342	28.0%	
48	0.0%		122	17.6%		196	0.0%		270	25.6%		344	28.0%	
50	0.0%		124	19.2%		198	0.0%		272	32.8%		346	0.0%	
52	0.0%		126	22.4%		200	16.0%		274	32.0%		348	0.0%	
54	0.0%		128	20.0%		202	18.4%		276	30.4%		350	0.0%	
56	0.0%		130	24.0%		204	17.6%		278	29.6%		352	0.0%	
58	0.0%		132	24.0%		206	27.2%		280	28.0%		354	0.0%	
60	0.0%		134	24.0%		208	28.0%		282	27.2%		356	0.0%	
62	0.0%		136	28.8%		210	14.4%		284	24.0%		358	0.0%	
64	0.0%		138	28.0%		212	15.2%		286	28.8%		360	0.0%	
66	0.0%		140	27.2%		214	24.0%		288	32.0%				
68	0.0%		142	25.6%		216	20.0%		290	36.0%				
70	0.0%		144	22.4%		218	16.0%		292	28.0%				
72	0.0%		146	25.6%		220	24.0%		294	28.8%				

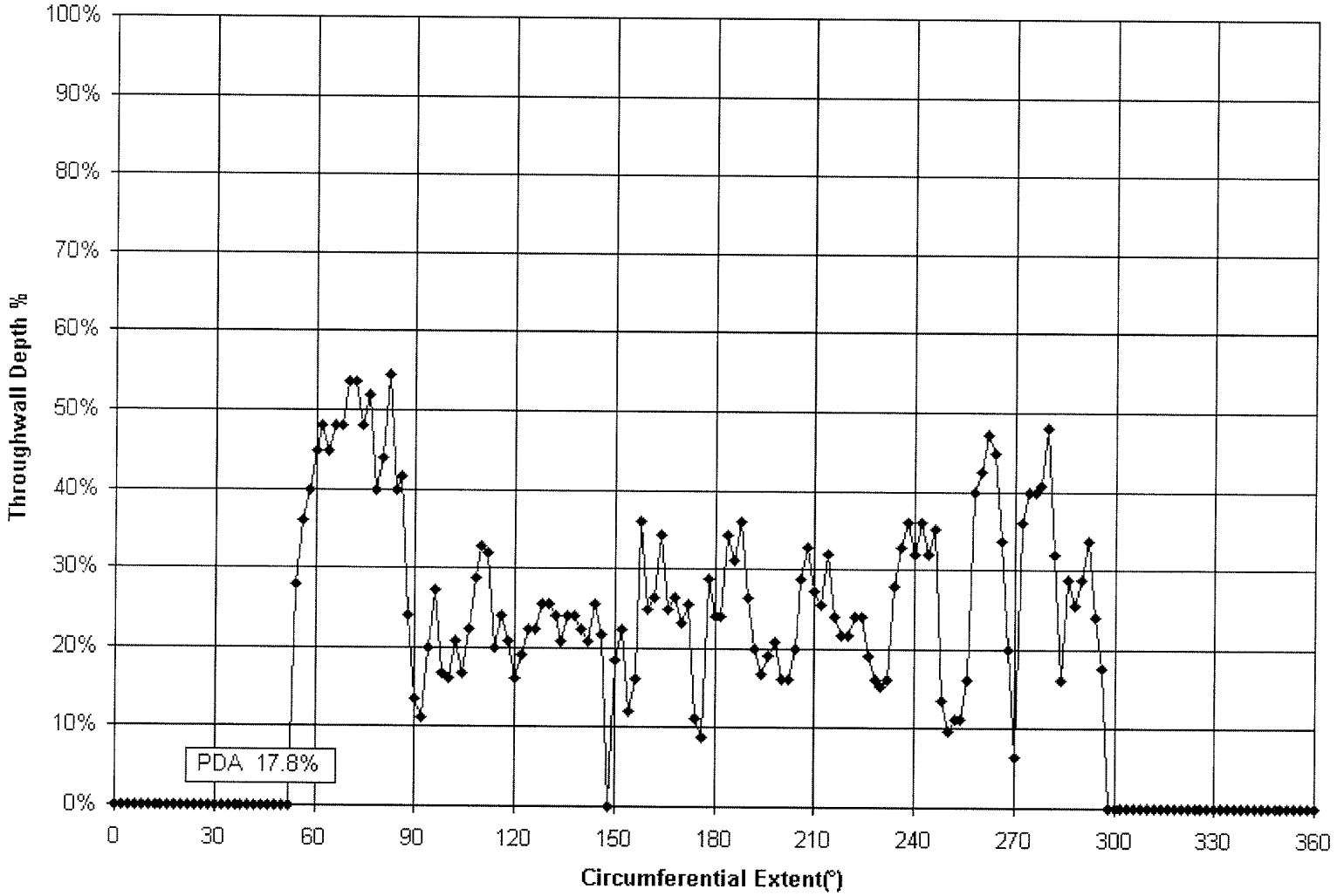

Figure C-4
LAB, 94-12-06B; Destructive Examination Depth Profile

Plant:	LAB													
Tube:	94-12-06B, ID, .875"													
PDA:	17.8%													
Angle	Depth	L/A	Angle	Depth	L/A	Angle	Depth	L/A	Angle	Depth	L/A	Angle	Depth	L/A
0	0.0%		74	48.0%		148	0.0%		222	24.0%		296	17.6%	
2	0.0%		76	52.0%		150	18.4%		224	24.0%		298	0.0%	
4	0.0%		78	40.0%		152	22.4%		226	19.2%		300	0.0%	
6	0.0%		80	44.0%		154	12.0%		228	16.0%		302	0.0%	
8	0.0%		82	54.4%		156	16.0%		230	15.2%		304	0.0%	
10	0.0%		84	40.0%	8.36E-04	158	36.0%		232	16.0%		306	0.0%	
12	0.0%		86	41.6%		160	24.8%		234	28.0%		308	0.0%	
14	0.0%		88	24.0%		162	26.4%		236	32.8%		310	0.0%	
16	0.0%		90	13.6%		164	34.4%		238	36.0%		312	0.0%	
18	0.0%		92	11.2%		166	24.8%		240	32.0%		314	0.0%	
20	0.0%		94	20.0%		168	26.4%		242	36.0%		316	0.0%	
22	0.0%		96	27.2%		170	23.2%		244	32.0%		318	0.0%	
24	0.0%		98	16.8%		172	25.6%		246	35.2%		320	0.0%	
26	0.0%		100	16.0%		174	11.2%		248	13.6%		322	0.0%	
28	0.0%		102	20.8%		176	8.8%		250	9.6%		324	0.0%	
30	0.0%		104	16.8%		178	28.8%		252	11.2%		326	0.0%	
32	0.0%		106	22.4%		180	24.0%		254	11.2%		328	0.0%	
34	0.0%		108	28.8%		182	24.0%		256	16.0%		330	0.0%	
36	0.0%		110	32.8%		184	34.4%		258	40.0%		332	0.0%	
38	0.0%		112	32.0%		186	31.2%		260	42.4%		334	0.0%	
40	0.0%		114	20.0%		188	36.0%		262	47.2%		336	0.0%	
42	0.0%		116	24.0%		190	26.4%		264	44.8%		338	0.0%	
44	0.0%		118	20.8%		192	20.0%		266	33.6%		340	0.0%	
46	0.0%		120	16.0%		194	16.8%		268	20.0%		342	0.0%	
48	0.0%		122	19.2%		196	19.2%		270	6.4%		344	0.0%	
50	0.0%		124	22.4%		198	20.8%		272	36.0%		346	0.0%	
52	0.0%		126	22.4%		200	16.0%		274	40.0%		348	0.0%	
54	28.0%		128	25.6%		202	16.0%		276	40.0%		350	0.0%	
56	36.0%		130	25.6%		204	20.0%		278	40.8%		352	0.0%	
58	40.0%		132	24.0%		206	28.8%		280	48.0%		354	0.0%	
60	44.8%		134	20.8%		208	32.8%		282	32.0%		356	0.0%	
62	48.0%		136	24.0%		210	27.2%		284	16.0%		358	0.0%	
64	44.8%		138	24.0%		212	25.6%		286	28.8%		360	0.0%	
66	48.0%		140	22.4%		214	32.0%		288	25.6%				
68	48.0%		142	20.8%		216	24.0%		290	28.8%				
70	53.6%		144	25.6%		218	21.6%		292	33.6%				
72	53.6%		146	21.6%		220	21.6%		294	24.0%				

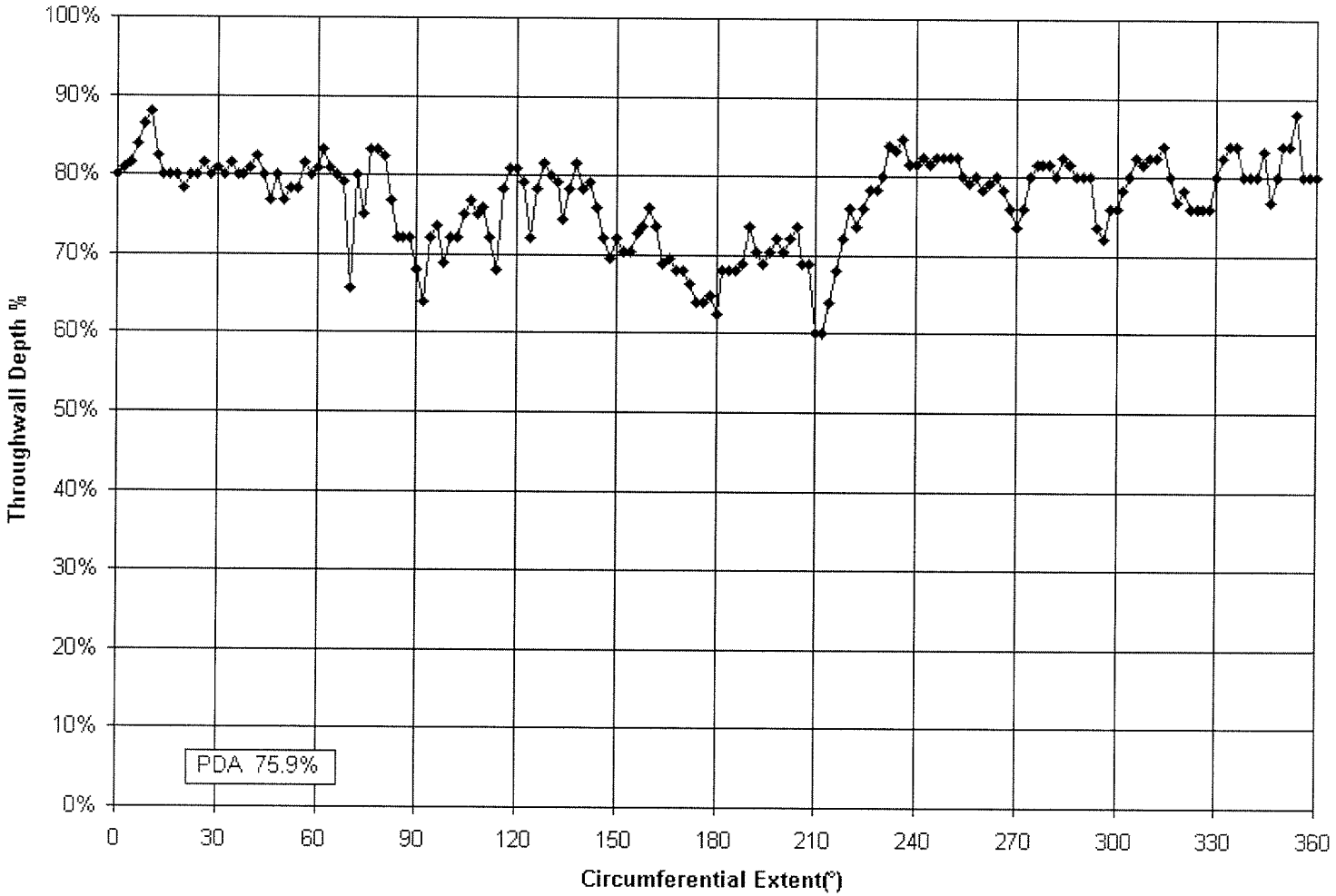

Figure C-5
LAB, 94-12-10A; Destructive Examination Depth Profile

Plant:	LAB													
Tube:	94-12-10A, ID, .875"													
PDA:	75.9%													
Angle	Depth	L/A	Angle	Depth	L/A	Angle	Depth	L/A	Angle	Depth	L/A	Angle	Depth	L/A
0	80.0%		74	75.2%		148	69.6%		222	73.6%		296	72.0%	
2	80.8%		76	83.2%		150	72.0%		224	76.0%		298	76.0%	
4	81.6%		78	83.2%		152	70.4%		226	78.4%		300	76.0%	
6	84.0%		80	82.4%		154	70.4%		228	78.4%		302	78.4%	
8	86.4%		82	76.8%		156	72.8%		230	80.0%		304	80.0%	
10	88.0%		84	72.0%		158	73.6%		232	84.0%		306	82.4%	
12	82.4%		86	72.0%		160	76.0%		234	83.2%		308	81.6%	
14	80.0%		88	72.0%		162	73.6%		236	84.8%		310	82.4%	
16	80.0%		90	68.0%	3.68E-04	164	68.8%		238	81.6%		312	82.4%	
18	80.0%		92	64.0%		166	69.6%		240	81.6%		314	84.0%	
20	78.4%		94	72.0%		168	68.0%	4.90E-04	242	82.4%		316	80.0%	
22	80.0%		96	73.6%		170	68.0%		244	81.6%		318	76.8%	
24	80.0%		98	68.8%		172	66.4%		246	82.4%		320	78.4%	
26	81.6%		100	72.0%		174	64.0%		248	82.4%		322	76.0%	
28	80.0%		102	72.0%		176	64.0%		250	82.4%		324	76.0%	
30	80.8%		104	75.2%		178	64.8%		252	82.4%		326	76.0%	
32	80.0%		106	76.8%		180	62.4%		254	80.0%		328	76.0%	
34	81.6%	3.68E-04	108	75.2%		182	68.0%		256	79.2%		330	80.0%	
36	80.0%		110	76.0%		184	68.0%		258	80.0%		332	82.4%	
38	80.0%		112	72.0%		186	68.0%		260	78.4%		334	84.0%	
40	80.8%		114	68.0%		188	68.8%		262	79.2%		336	84.0%	
42	82.4%		116	78.4%		190	73.6%		264	80.0%		338	80.0%	
44	80.0%	3.68E-04	118	80.8%		192	70.4%		266	78.4%		340	80.0%	
46	76.8%		120	80.8%		194	68.8%		268	76.0%		342	80.0%	
48	80.0%		122	79.2%		196	70.4%		270	73.6%		344	83.2%	
50	76.8%		124	72.0%		198	72.0%		272	76.0%		346	76.8%	
52	78.4%		126	78.4%		200	70.4%		274	80.0%		348	80.0%	
54	78.4%		128	81.6%		202	72.0%		276	81.6%		350	84.0%	3.06E-04
56	81.6%		130	80.0%		204	73.6%		278	81.6%		352	84.0%	
58	80.0%		132	79.2%		206	68.8%		280	81.6%		354	88.0%	
60	80.8%		134	74.4%		208	68.8%		282	80.0%		356	80.0%	2.45E-04
62	83.2%		136	78.4%		210	60.0%		284	82.4%		358	80.0%	
64	80.8%		138	81.6%		212	60.0%		286	81.6%		360	80.0%	
66	80.0%		140	78.4%		214	64.0%		288	80.0%				
68	79.2%		142	79.2%		216	68.0%		290	80.0%				
70	65.6%		144	76.0%		218	72.0%		292	80.0%				
72	80.0%		146	72.0%		220	76.0%		294	73.6%				

Tabulation of Laboratory Specimen Crack Depth Profiles from Destructive Exam

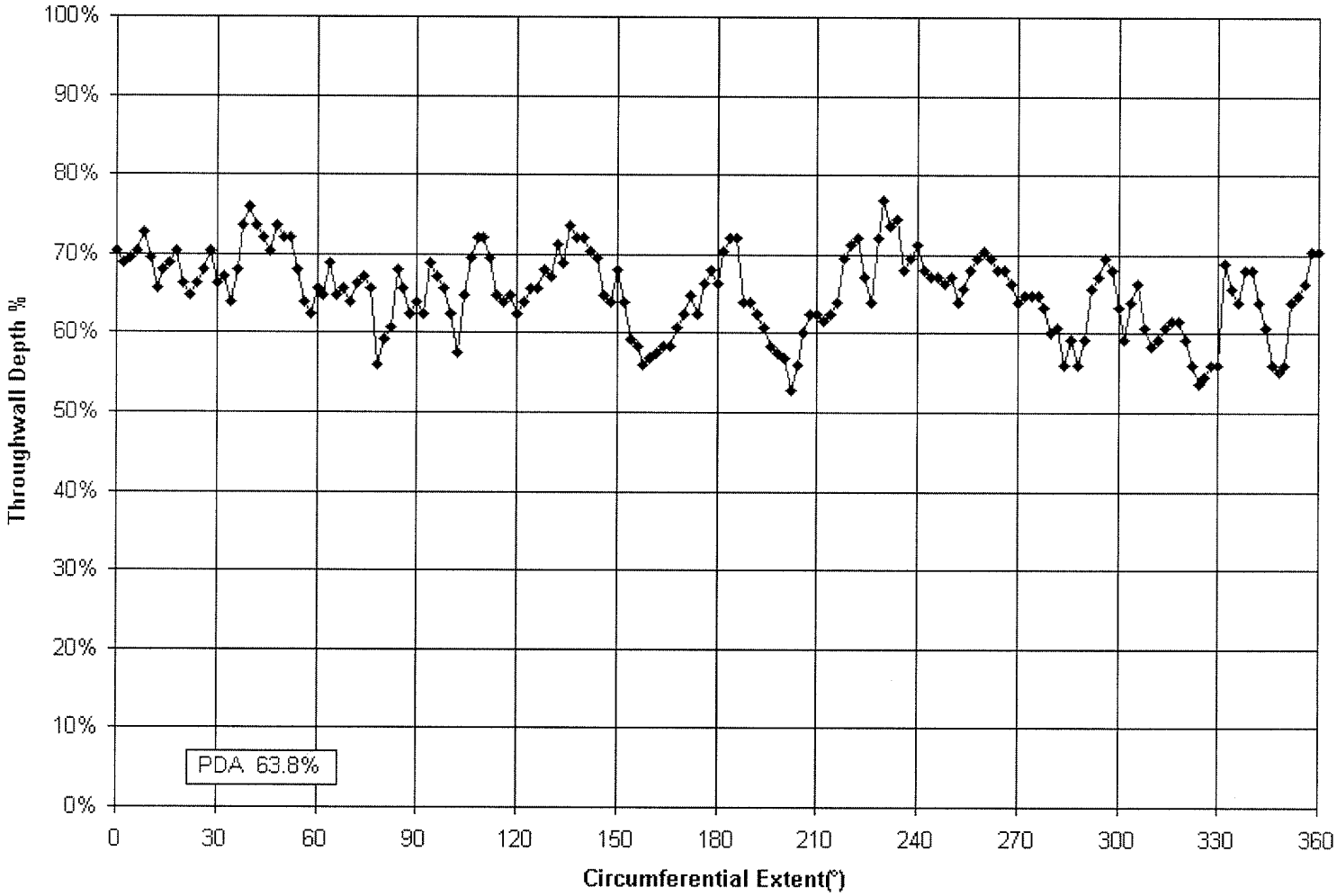

Figure C-6
LAB, 94-12-10B; Destructive Examination Depth Profile

Plant:	LAB													
Tube:	94-12-10B, ID, .875"													
PDA:	63.8%													
Angle	Depth	L/A	Angle	Depth	L/A	Angle	Depth	L/A	Angle	Depth	L/A	Angle	Depth	L/A
0	70.4%		74	67.2%		148	64.0%		222	72.0%		296	69.6%	
2	68.8%		76	65.6%		150	68.0%		224	67.2%		298	68.0%	
4	69.6%		78	56.0%		152	64.0%		226	64.0%		300	63.2%	
6	70.4%		80	59.2%		154	59.2%		228	72.0%		302	59.2%	
8	72.8%		82	60.8%		156	58.4%		230	76.8%		304	64.0%	
10	69.6%		84	68.0%		158	56.0%		232	73.6%		306	66.4%	
12	65.6%		86	65.6%		160	56.8%	3.26E-04	234	74.4%		308	60.8%	
14	68.0%		88	62.4%		162	57.6%		236	68.0%		310	58.4%	
16	68.8%		90	64.0%		164	58.4%		238	69.6%		312	59.2%	
18	70.4%		92	62.4%		166	58.4%		240	71.2%		314	60.8%	
20	66.4%		94	68.8%		168	60.8%	3.26E-04	242	68.0%		316	61.6%	
22	64.8%	3.26E-04	96	67.2%		170	62.4%		244	67.2%		318	61.6%	
24	66.4%		98	65.6%		172	64.8%		246	67.2%		320	59.2%	
26	68.0%		100	62.4%		174	62.4%		248	66.4%		322	56.0%	
28	70.4%		102	57.6%		176	66.4%		250	67.2%		324	53.6%	
30	66.4%		104	64.8%		178	68.0%		252	64.0%		326	54.4%	
32	67.2%		106	69.6%		180	66.4%		254	65.6%		328	56.0%	
34	64.0%		108	72.0%		182	70.4%		256	68.0%		330	56.0%	
36	68.0%		110	72.0%		184	72.0%		258	69.6%		332	68.8%	3.26E-04
38	73.6%		112	69.6%		186	72.0%		260	70.4%		334	65.6%	
40	76.0%		114	64.8%		188	64.0%		262	69.6%		336	64.0%	
42	73.6%		116	64.0%		190	64.0%		264	68.0%		338	68.0%	
44	72.0%		118	64.8%		192	62.4%		266	68.0%		340	68.0%	
46	70.4%		120	62.4%		194	60.8%		268	66.4%		342	64.0%	
48	73.6%		122	64.0%		196	58.4%		270	64.0%		344	60.8%	
50	72.0%		124	65.6%		198	57.6%		272	64.8%		346	56.0%	
52	72.0%		126	65.6%		200	56.8%	6.53E-04	274	64.8%		348	55.2%	
54	68.0%		128	68.0%		202	52.8%		276	64.8%		350	56.0%	
56	64.0%		130	67.2%		204	56.0%		278	63.2%	6.53E-04	352	64.0%	
58	62.4%		132	71.2%		206	60.0%		280	60.0%		354	64.8%	
60	65.6%		134	68.8%		208	62.4%		282	60.8%		356	66.4%	
62	64.8%		136	73.6%		210	62.4%		284	56.0%		358	70.4%	
64	68.8%		138	72.0%		212	61.6%		286	59.2%		360	70.4%	
66	64.8%		140	72.0%		214	62.4%		288	56.0%				
68	65.6%		142	70.4%		216	64.0%		290	59.2%				
70	64.0%		144	69.6%		218	69.6%		292	65.6%				
72	66.4%		146	64.8%		220	71.2%		294	67.2%	7.93E-04			

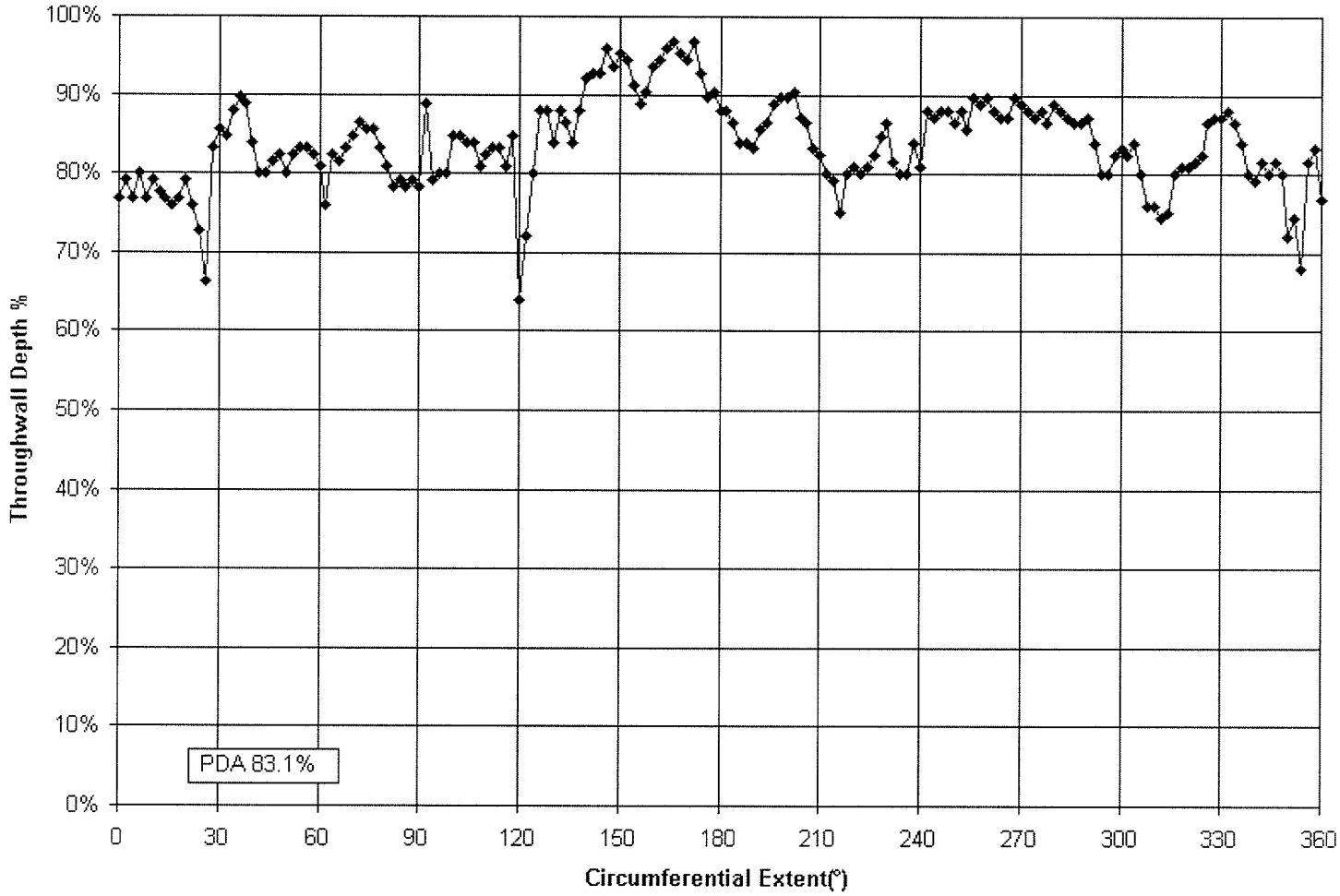

Figure C-7
LAB, 94-12-11A; Destructive Examination Depth Profile

Plant:	LAB													
Tube:	94-12-11A, ID, .875"													
PDA:	83.1%													
Angle	Depth	L/A	Angle	Depth	L/A	Angle	Depth	L/A	Angle	Depth	L/A	Angle	Depth	L/A
0	76.8%		74	85.6%		148	93.6%		222	80.0%		296	80.0%	
2	79.2%		76	85.6%		150	95.2%	3.23E-04	224	80.8%		298	82.4%	
4	76.8%		78	83.2%		152	94.4%		226	82.4%		300	83.2%	3.10E-04
6	80.0%		80	80.8%		154	91.2%		228	84.8%		302	82.4%	
8	76.8%		82	78.4%	9.35E-04	156	88.8%		230	86.4%		304	84.0%	
10	79.2%		84	79.2%		158	90.4%		232	81.6%		306	80.0%	
12	77.6%		86	78.4%		160	93.6%		234	80.0%		308	76.0%	
14	76.8%		88	79.2%		162	94.4%		236	80.0%		310	76.0%	
16	76.0%		90	78.4%		164	96.0%		238	84.0%		312	74.4%	
18	76.8%		92	88.8%		166	96.8%		240	80.8%		314	75.2%	
20	79.2%		94	79.2%		168	95.2%		242	88.0%		316	80.0%	
22	76.0%		96	80.0%		170	94.4%		244	87.2%		318	80.8%	
24	72.8%		98	80.0%		172	96.8%		246	88.0%	3.10E-04	320	80.8%	
26	66.4%		100	84.8%	2.49E-04	174	92.8%		248	88.0%		322	81.6%	
28	83.2%		102	84.8%		176	89.6%		250	86.4%		324	82.4%	
30	85.6%		104	84.0%		178	90.4%	4.30E-04	252	88.0%		326	86.4%	
32	84.8%		106	84.0%		180	88.0%		254	85.6%		328	87.2%	
34	88.0%		108	80.8%		182	88.0%		256	89.6%		330	87.2%	
36	89.6%		110	82.4%		184	86.4%		258	88.8%		332	88.0%	
38	88.8%		112	83.2%		186	84.0%	4.30E-04	260	89.6%		334	86.4%	
40	84.0%		114	83.2%		188	84.0%		262	88.0%		336	84.0%	
42	80.0%		116	80.8%		190	83.2%		264	87.2%		338	80.0%	
44	80.0%		118	84.8%		192	85.6%		266	87.2%		340	79.2%	
46	81.6%		120	64.0%		194	86.4%		268	89.6%		342	81.6%	
48	82.4%		122	72.0%		196	88.8%		270	88.8%		344	80.0%	
50	80.0%		124	80.0%		198	89.6%		272	88.0%		346	81.6%	
52	82.4%		126	88.0%		200	89.6%		274	87.2%	8.58E-04	348	80.0%	
54	83.2%		128	88.0%		202	90.4%		276	88.0%		350	72.0%	
56	83.2%		130	84.0%		204	87.2%		278	86.4%		352	74.4%	
58	82.4%		132	88.0%		206	86.4%		280	88.8%		354	68.0%	
60	80.8%		134	86.4%		208	83.2%		282	88.0%		356	81.6%	
62	76.0%		136	84.0%		210	82.4%		284	87.2%		358	83.2%	
64	82.4%		138	88.0%		212	80.0%		286	86.4%		360	76.8%	
66	81.6%		140	92.0%		214	79.2%		288	86.4%				
68	83.2%		142	92.8%		216	75.2%		290	87.2%				
70	84.8%		144	92.8%		218	80.0%		292	84.0%	3.10E-04			
72	86.4%		146	96.0%		220	80.8%		294	80.0%				

Tabulation of Laboratory Specimen Crack Depth Profiles from Destructive Exam

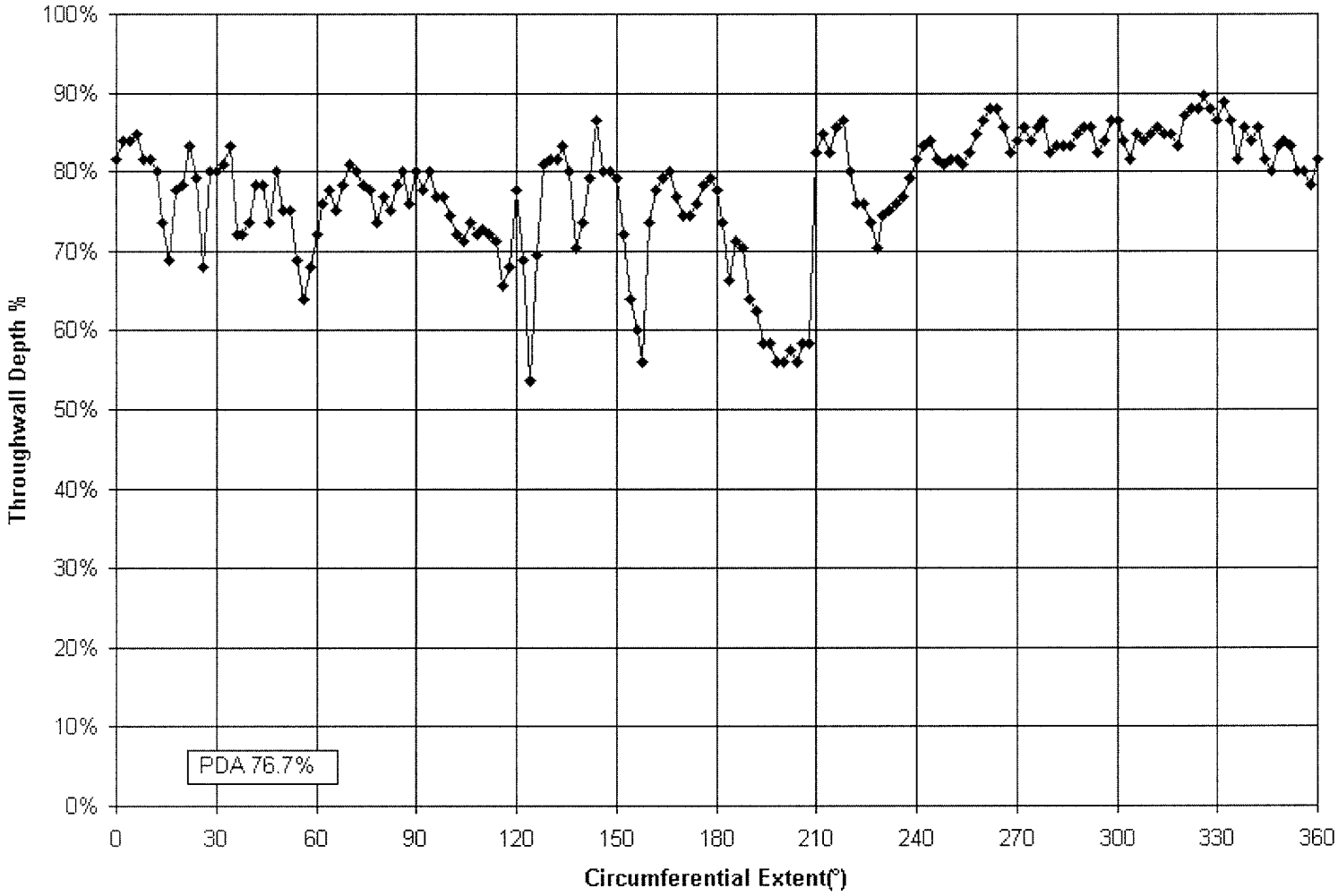

Figure C-8
LAB, 94-12-11B; Destructive Examination Depth Profile

Plant:	LAB												
Tube:	94-12-11B, ID, .875"												
PDA:	76.7%												
Angle	Depth	L/A	Angle	Depth	L/A	Angle	Depth	L/A	Angle	Depth	L/A	Angle	Depth
0	81.6%		74	78.4%		148	80.0%		222	76.0%		296	84.0%
2	84.0%		76	77.6%		150	79.2%		224	76.0%		298	86.4%
4	84.0%		78	73.6%		152	72.0%		226	73.6%		300	86.4%
6	84.8%		80	76.8%		154	64.0%		228	70.4%		302	84.0%
8	81.6%		82	75.2%		156	60.0%		230	74.4%		304	81.6%
10	81.6%		84	78.4%		158	56.0%		232	75.2%		306	84.8%
12	80.0%		86	80.0%		160	73.6%		234	76.0%		308	84.0%
14	73.6%		88	76.0%		162	77.6%		236	76.8%		310	84.8%
16	68.8%		90	80.0%		164	79.2%		238	79.2%		312	85.6%
18	77.6%		92	77.6%		166	80.0%		240	81.6%		314	84.8%
20	78.4%		94	80.0%		168	76.8%		242	83.2%		316	84.8%
22	83.2%		96	76.8%		170	74.4%		244	84.0%		318	83.2%
24	79.2%		98	76.8%		172	74.4%		246	81.6%		320	87.2%
26	68.0%		100	74.4%		174	76.0%		248	80.8%		322	88.0%
28	80.0%		102	72.0%		176	78.4%		250	81.6%		324	88.0%
30	80.0%		104	71.2%		178	79.2%		252	81.6%		326	89.6%
32	80.8%		106	73.6%		180	77.6%		254	80.8%		328	88.0%
34	83.2%		108	72.0%		182	73.6%		256	82.4%		330	86.4%
36	72.0%		110	72.8%		184	66.4%		258	84.8%		332	88.8%
38	72.0%		112	72.0%		186	71.2%		260	86.4%		334	86.4%
40	73.6%		114	71.2%	2.44E-04	188	70.4%		262	88.0%		336	81.6%
42	78.4%		116	65.6%		190	64.0%		264	88.0%		338	85.6%
44	78.4%		118	68.0%		192	62.4%		266	85.6%		340	84.0%
46	73.6%		120	77.6%		194	58.4%		268	82.4%		342	85.6%
48	80.0%		122	68.8%		196	58.4%		270	84.0%		344	81.6%
50	75.2%		124	53.6%		198	56.0%		272	85.6%		346	80.0%
52	75.2%		126	69.6%		200	56.0%		274	84.0%		348	83.2%
54	68.8%		128	80.8%		202	57.6%		276	85.6%		350	84.0%
56	64.0%		130	81.6%		204	56.0%		278	86.4%		352	83.2%
58	68.0%		132	81.6%		206	58.4%		280	82.4%		354	80.0%
60	72.0%		134	83.2%		208	58.4%		282	83.2%		356	80.0%
62	76.0%		136	80.0%		210	82.4%		284	83.2%		358	78.4%
64	77.6%		138	70.4%		212	84.8%		286	83.2%		360	81.6%
66	75.2%		140	73.6%		214	82.4%		288	84.8%			
68	78.4%		142	79.2%		216	85.6%		290	85.6%			
70	80.8%		144	86.4%		218	86.4%		292	85.6%			
72	80.0%		146	80.0%		220	80.0%		294	82.4%			

Tabulation of Laboratory Specimen Crack Depth Profiles from Destructive Exam

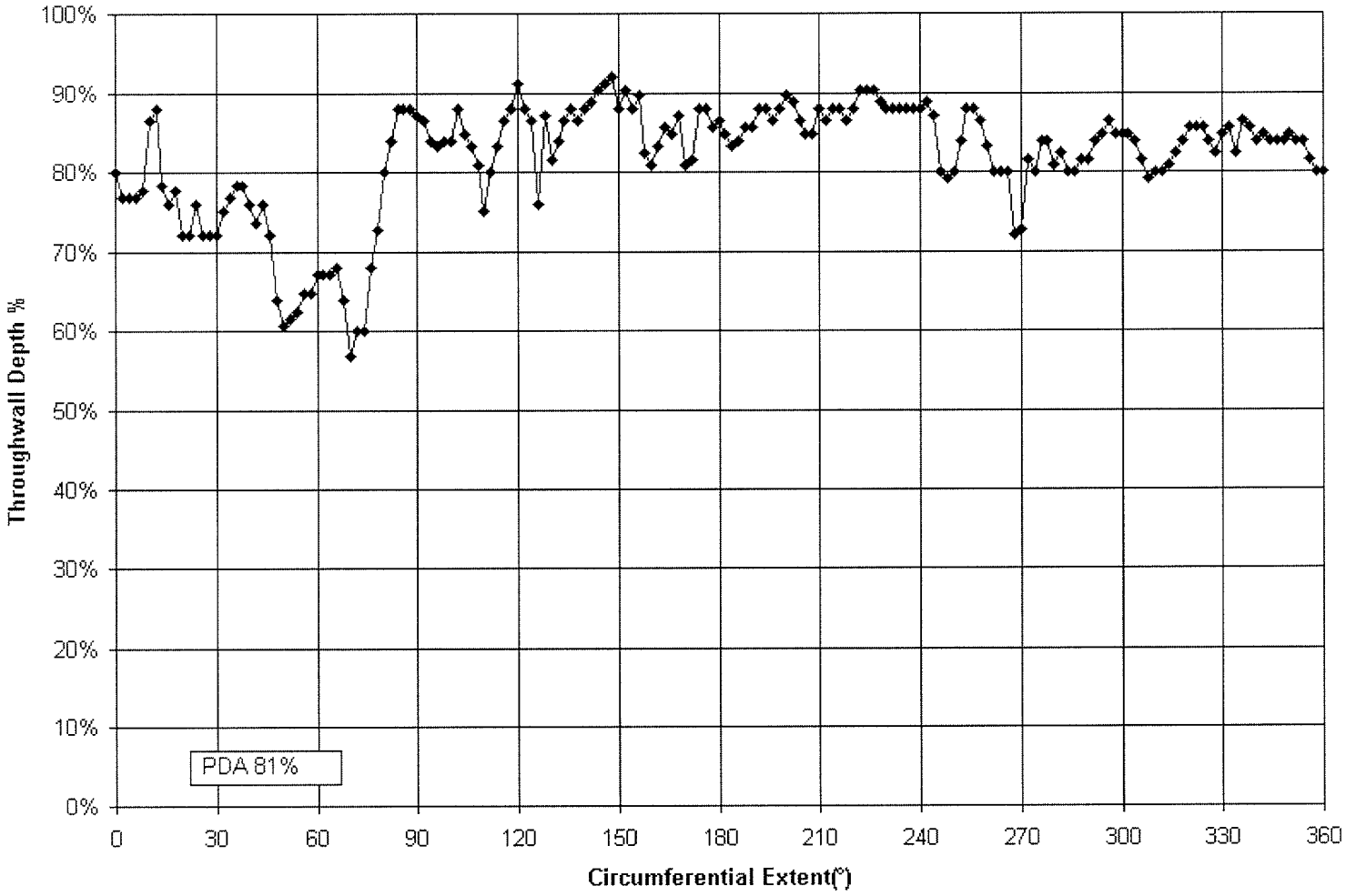

Figure C-9
LAB, 94-12-12A; Destructive Examination Depth Profile

Plant:	LAB													
Tube:	94-12-12A, ID, .875"													
PDA:	81.0%													
Angle	Depth	L/A	Angle	Depth	L/A	Angle	Depth	L/A	Angle	Depth	L/A	Angle	Depth	L/A
0	80.0%		74	60.0%		148	92.0%		222	90.4%		296	86.4%	
2	76.8%		76	68.0%		150	88.0%		224	90.4%		298	84.8%	
4	76.8%		78	72.8%		152	90.4%		226	90.4%		300	84.8%	
6	76.8%		80	80.0%		154	88.0%		228	88.8%		302	84.8%	
8	77.6%		82	84.0%		156	89.6%		230	88.0%		304	84.0%	
10	86.4%		84	88.0%		158	82.4%		232	88.0%		306	81.6%	
12	88.0%		86	88.0%		160	80.8%		234	88.0%		308	79.2%	
14	78.4%		88	88.0%		162	83.2%		236	88.0%		310	80.0%	
16	76.0%		90	87.2%		164	85.6%		238	88.0%		312	80.0%	
18	77.6%		92	86.4%		166	84.8%		240	88.0%		314	80.8%	
20	72.0%		94	84.0%		168	87.2%		242	88.8%		316	82.4%	
22	72.0%		96	83.2%		170	80.8%		244	87.2%		318	84.0%	
24	76.0%		98	84.0%		172	81.6%		246	80.0%		320	85.6%	
26	72.0%		100	84.0%		174	88.0%		248	79.2%		322	85.6%	
28	72.0%		102	88.0%		176	88.0%		250	80.0%		324	85.6%	
30	72.0%		104	84.8%		178	85.6%		252	84.0%		326	84.0%	
32	75.2%		106	83.2%		180	86.4%		254	88.0%		328	82.4%	
34	76.8%		108	80.8%		182	84.8%		256	88.0%		330	84.8%	
36	78.4%		110	75.2%		184	83.2%		258	86.4%		332	85.6%	
38	78.4%		112	80.0%		186	84.0%		260	83.2%		334	82.4%	
40	76.0%		114	83.2%		188	85.6%		262	80.0%		336	86.4%	
42	73.6%		116	86.4%		190	85.6%		264	80.0%		338	85.6%	
44	76.0%		118	88.0%		192	88.0%		266	80.0%		340	84.0%	
46	72.0%		120	91.2%		194	88.0%		268	72.0%		342	84.8%	
48	64.0%		122	88.0%		196	86.4%		270	72.8%		344	84.0%	
50	60.8%		124	86.4%		198	88.0%		272	81.6%		346	84.0%	
52	61.6%		126	76.0%		200	89.6%		274	80.0%		348	84.0%	
54	62.4%		128	87.2%		202	88.8%		276	84.0%		350	84.8%	
56	64.8%		130	81.6%		204	86.4%		278	84.0%		352	84.0%	
58	64.8%		132	84.0%		206	84.8%		280	80.8%		354	84.0%	
60	67.2%		134	86.4%		208	84.8%		282	82.4%		356	81.6%	
62	67.2%		136	88.0%		210	88.0%		284	80.0%		358	80.0%	
64	67.2%		138	86.4%		212	86.4%		286	80.0%		360	80.0%	
66	68.0%		140	88.0%		214	88.0%		288	81.6%				
68	64.0%		142	88.8%		216	88.0%		290	81.6%				
70	56.8%		144	90.4%		218	86.4%		292	84.0%				
72	60.0%		146	91.2%		220	88.0%		294	84.8%				

Tabulation of Laboratory Specimen Crack Depth Profiles from Destructive Exam

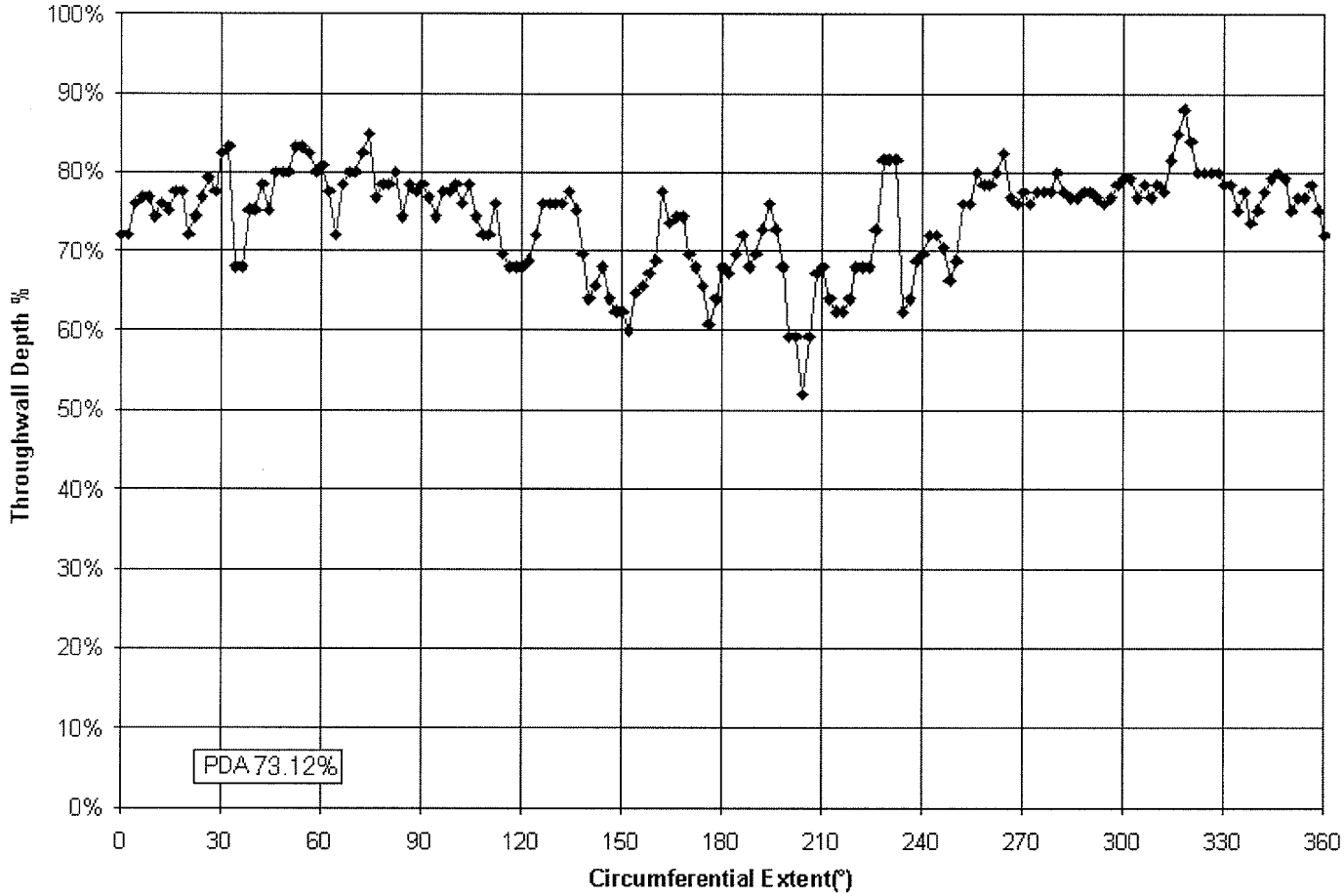

Figure C-10
LAB, 94-12-12B; Destructive Examination Depth Profile

Plant:	LAB													
Tube:	94-12-12B, ID, .875"													
PDA:	73.12%													
Angle	Depth	L/A	Angle	Depth	L/A	Angle	Depth	L/A	Angle	Depth	L/A	Angle	Depth	L/A
0	72.0%		74	84.8%		148	62.4%		222	68.0%		296	76.8%	
2	72.0%		76	76.8%		150	62.4%		224	68.0%		298	78.4%	
4	76.0%		78	78.4%		152	60.0%		226	72.8%		300	79.2%	
6	76.8%		80	78.4%		154	64.8%		228	81.6%		302	79.2%	
8	76.8%		82	80.0%		156	65.6%		230	81.6%		304	76.8%	
10	74.4%		84	74.4%		158	67.2%		232	81.6%		306	78.4%	
12	76.0%		86	78.4%		160	68.8%		234	62.4%		308	76.8%	
14	75.2%		88	77.6%		162	77.6%		236	64.0%		310	78.4%	
16	77.6%		90	78.4%		164	73.6%		238	68.8%		312	77.6%	
18	77.6%		92	76.8%		166	74.4%		240	69.6%		314	81.6%	
20	72.0%		94	74.4%		168	74.4%		242	72.0%		316	84.8%	
22	74.4%		96	77.6%		170	69.6%		244	72.0%		318	88.0%	
24	76.8%		98	77.6%		172	68.0%		246	70.4%		320	84.0%	
26	79.2%		100	78.4%		174	65.6%		248	66.4%		322	80.0%	
28	77.6%		102	76.0%		176	60.8%		250	68.8%		324	80.0%	
30	82.4%		104	78.4%		178	64.0%		252	76.0%		326	80.0%	
32	83.2%		106	74.4%		180	68.0%		254	76.0%		328	80.0%	
34	68.0%		108	72.0%		182	67.2%		256	80.0%		330	78.4%	
36	68.0%		110	72.0%		184	69.6%		258	78.4%		332	78.4%	
38	75.2%		112	76.0%		186	72.0%		260	78.4%		334	75.2%	
40	75.2%		114	69.6%		188	68.0%		262	80.0%		336	77.6%	
42	78.4%		116	68.0%		190	69.6%		264	82.4%		338	73.6%	
44	75.2%		118	68.0%		192	72.8%		266	76.8%		340	75.2%	
46	80.0%		120	68.0%		194	76.0%		268	76.0%		342	77.6%	
48	80.0%		122	68.8%		196	72.8%		270	77.6%		344	79.2%	
50	80.0%		124	72.0%		198	68.0%		272	76.0%		346	80.0%	
52	83.2%		126	76.0%		200	59.2%		274	77.6%		348	79.2%	
54	83.2%		128	76.0%		202	59.2%		276	77.6%		350	75.2%	
56	82.4%		130	76.0%		204	52.0%		278	77.6%		352	76.8%	
58	80.0%		132	76.0%		206	59.2%		280	80.0%		354	76.8%	
60	80.8%		134	77.6%		208	67.2%		282	77.6%		356	78.4%	
62	77.6%		136	75.2%		210	68.0%		284	76.8%		358	75.2%	
64	72.0%		138	69.6%		212	64.0%		286	76.8%		360	72.0%	
66	78.4%		140	64.0%		214	62.4%		288	77.6%				
68	80.0%		142	65.6%		216	62.4%		290	77.6%				
70	80.0%		144	68.0%		218	64.0%		292	76.8%				
72	82.4%		146	64.0%		220	68.0%		294	76.0%				

Tabulation of Laboratory Specimen Crack Depth Profiles from Destructive Exam

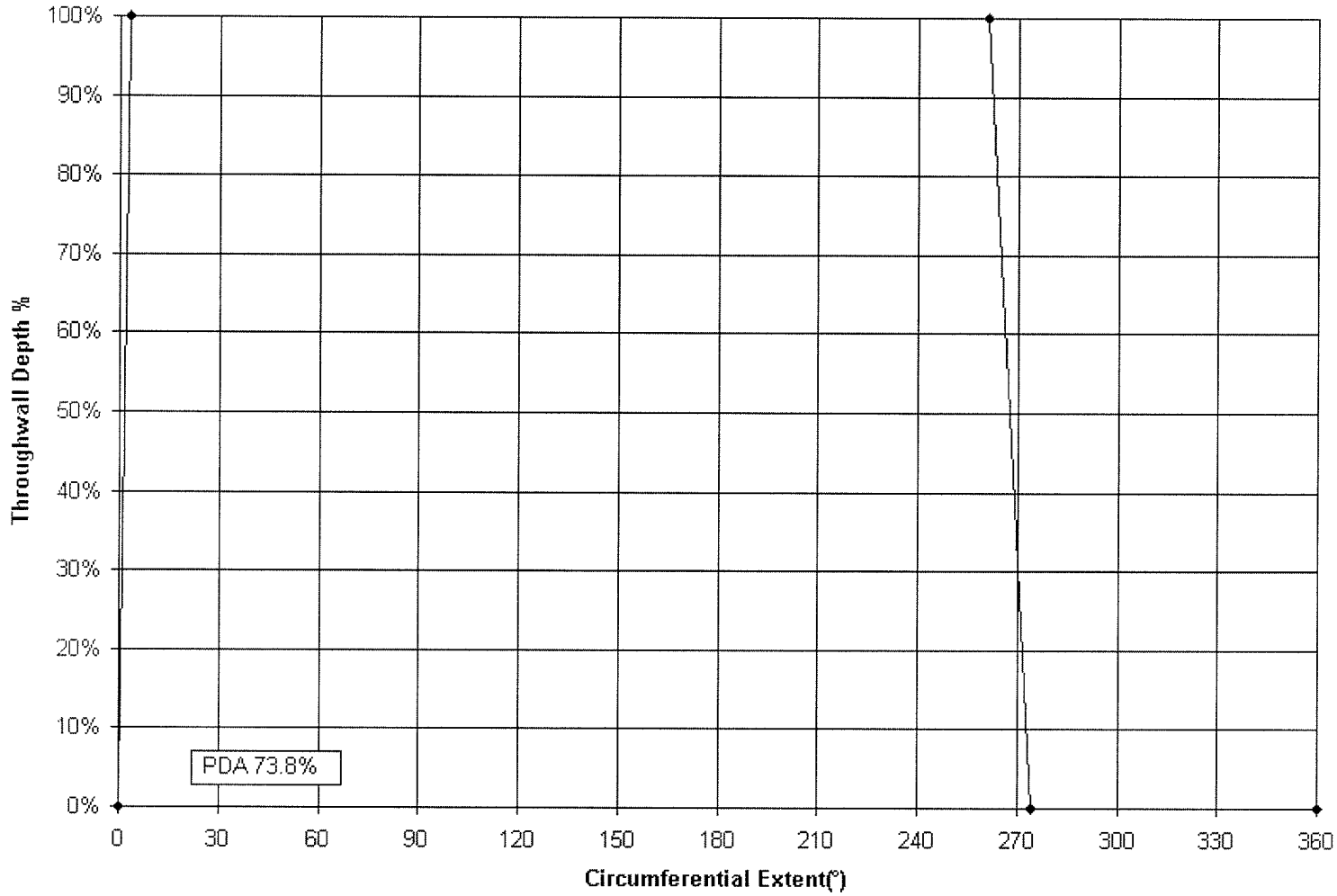

Figure C-11
LAB, 9-95-16T; Destructive Examination Depth Profile

Plant :	LAB	
Tube :	9-95-16T, ID, .875"	
PDA :	73.8%	
Angle	Depth	L/A
0	0.0%	
3	100.0%	
261	100.0%	
274	0.0%	
360	0.0%	

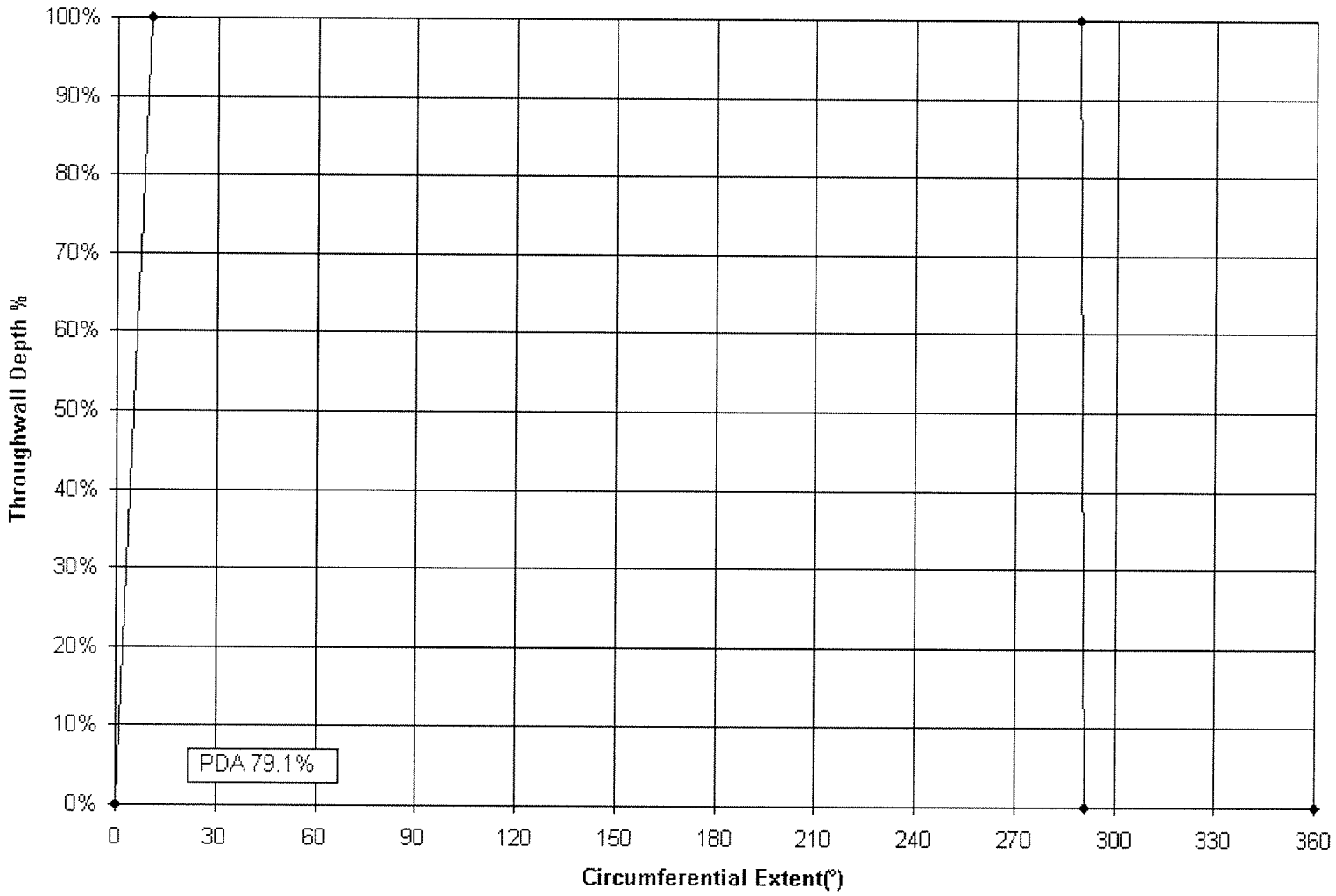

Figure C-12
LAB, 9-95-19T; Destructive Examination Depth Profile

Plant :	**LAB**	
Tube :	**9-95-19T, ID, .875"**	
PDA :	**79.1%**	
Angle	Depth	L/A
0	0.0%	
10	100.0%	
289	100.0%	
291	0.0%	
360	0.0%	

Tabulation of Laboratory Specimen Crack Depth Profiles from Destructive Exam

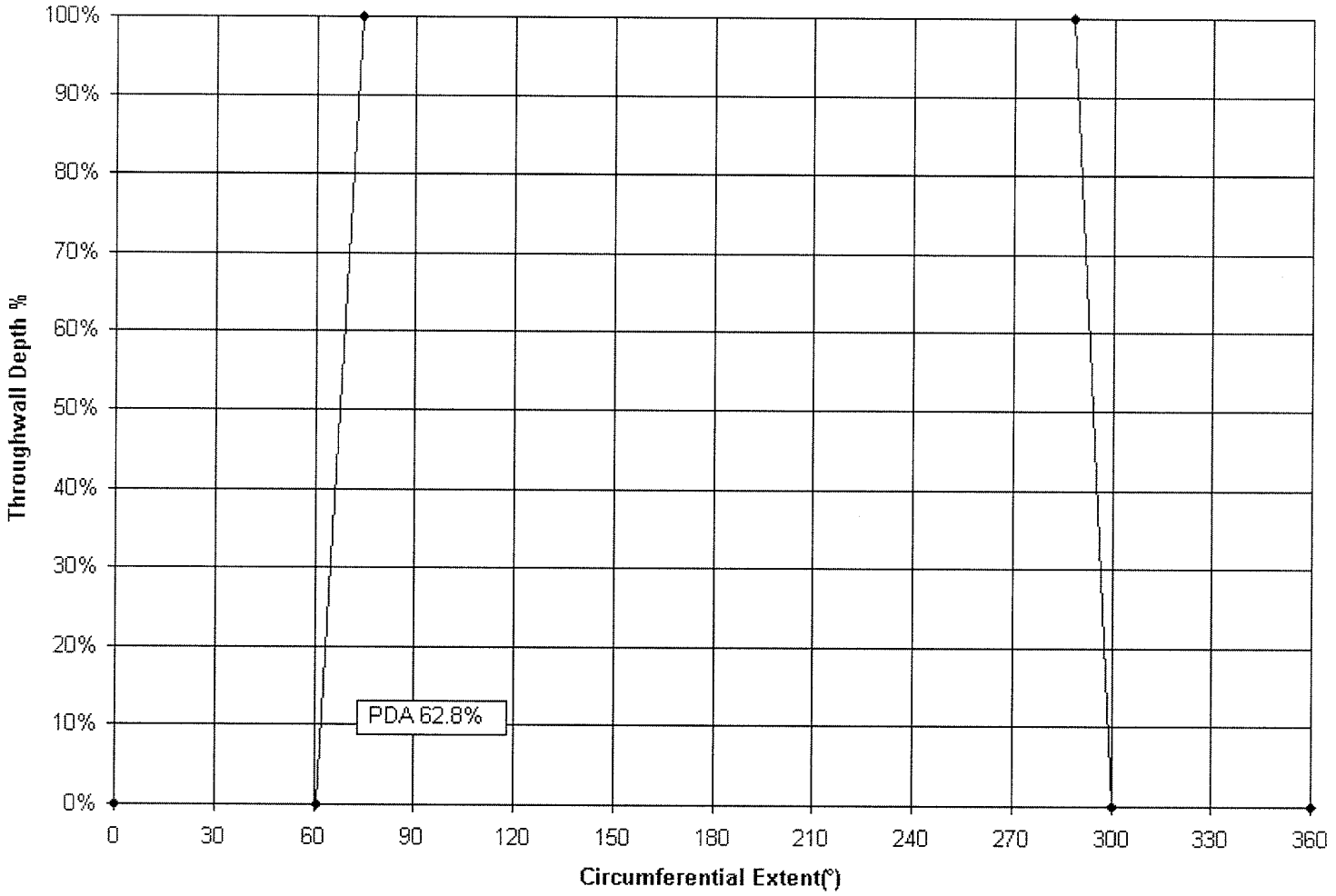

Figure C-13
LAB, 9-95-19B; Destructive Examination Depth Profile

Plant :	LAB	
Tube :	9-95-19B, ID, .875"	
PDA :	62.8%	
Angle	Depth	L/A
0	0.0%	
61	0.0%	
74	100.0%	
288	100.0%	
300	0.0%	
360	0.0%	

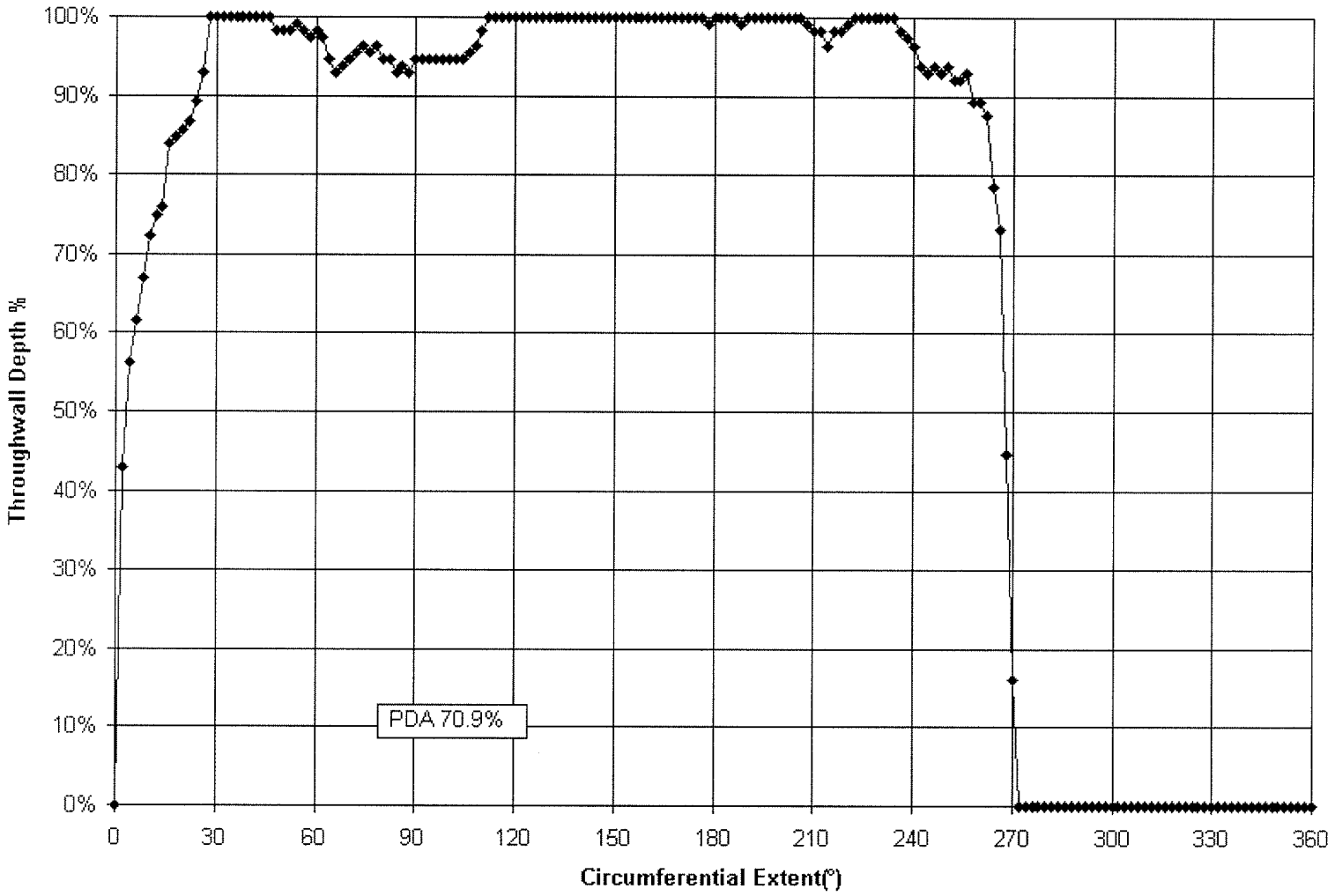

Figure C-14
LAB, 95-03-19; Destructive Examination Depth Profile

Plant:	LAB												
Tube:	95-03-19, OD, .875"												
PDA:	70.9%												
Angle	Depth	L/A	Angle	Depth	L/A	Angle	Depth	L/A	Angle	Depth	L/A	Angle	Depth
0	0.0%		74	96.4%		148	100.0%		222	100.0%		296	0.0%
2	42.9%		76	95.5%		150	100.0%		224	100.0%		298	0.0%
4	56.3%		78	96.4%		152	100.0%		226	100.0%		300	0.0%
6	61.6%		80	94.6%		154	100.0%		228	100.0%		302	0.0%
8	67.0%		82	94.6%		156	100.0%		230	100.0%		304	0.0%
10	72.3%		84	92.9%		158	100.0%		232	100.0%		306	0.0%
12	75.0%		86	93.8%		160	100.0%		234	100.0%		308	0.0%
14	75.9%		88	92.9%		162	100.0%		236	98.2%		310	0.0%
16	83.9%		90	94.6%		164	100.0%		238	97.3%		312	0.0%
18	84.8%		92	94.6%		166	100.0%		240	96.4%		314	0.0%
20	85.7%		94	94.6%		168	100.0%		242	93.8%		316	0.0%
22	86.6%		96	94.6%		170	100.0%		244	92.9%		318	0.0%
24	89.3%		98	94.6%		172	100.0%		246	93.8%		320	0.0%
26	92.9%		100	94.6%		174	100.0%		248	92.9%		322	0.0%
28	100.0%		102	94.6%		176	100.0%		250	93.8%		324	0.0%
30	100.0%		104	94.6%		178	99.1%		252	92.0%		326	0.0%
32	100.0%		106	95.5%		180	100.0%		254	92.0%		328	0.0%
34	100.0%		108	96.4%		182	100.0%		256	92.9%		330	0.0%
36	100.0%		110	98.2%		184	100.0%		258	89.3%		332	0.0%
38	100.0%		112	100.0%		186	100.0%		260	89.3%		334	0.0%
40	100.0%		114	100.0%		188	99.1%		262	87.5%		336	0.0%
42	100.0%		116	100.0%		190	100.0%		264	78.6%		338	0.0%
44	100.0%		118	100.0%		192	100.0%		266	73.2%	2.51E-04	340	0.0%
46	100.0%		120	100.0%		194	100.0%		268	44.6%		342	0.0%
48	98.2%		122	100.0%		196	100.0%		270	16.1%		344	0.0%
50	98.2%		124	100.0%		198	100.0%		272	0.0%		346	0.0%
52	98.2%		126	100.0%		200	100.0%		274	0.0%		348	0.0%
54	99.1%		128	100.0%		202	100.0%		276	0.0%		350	0.0%
56	98.2%		130	100.0%		204	100.0%		278	0.0%		352	0.0%
58	97.3%		132	100.0%		206	100.0%		280	0.0%		354	0.0%
60	98.2%		134	100.0%		208	99.1%		282	0.0%		356	0.0%
62	97.3%		136	100.0%		210	98.2%		284	0.0%		358	0.0%
64	94.6%		138	100.0%		212	98.2%		286	0.0%		360	0.0%
66	92.9%		140	100.0%		214	96.4%		288	0.0%			
68	93.8%		142	100.0%		216	98.2%		290	0.0%			
70	94.6%		144	100.0%		218	98.2%		292	0.0%			
72	95.5%		146	100.0%		220	99.1%		294	0.0%			

Tabulation of Laboratory Specimen Crack Depth Profiles from Destructive Exam

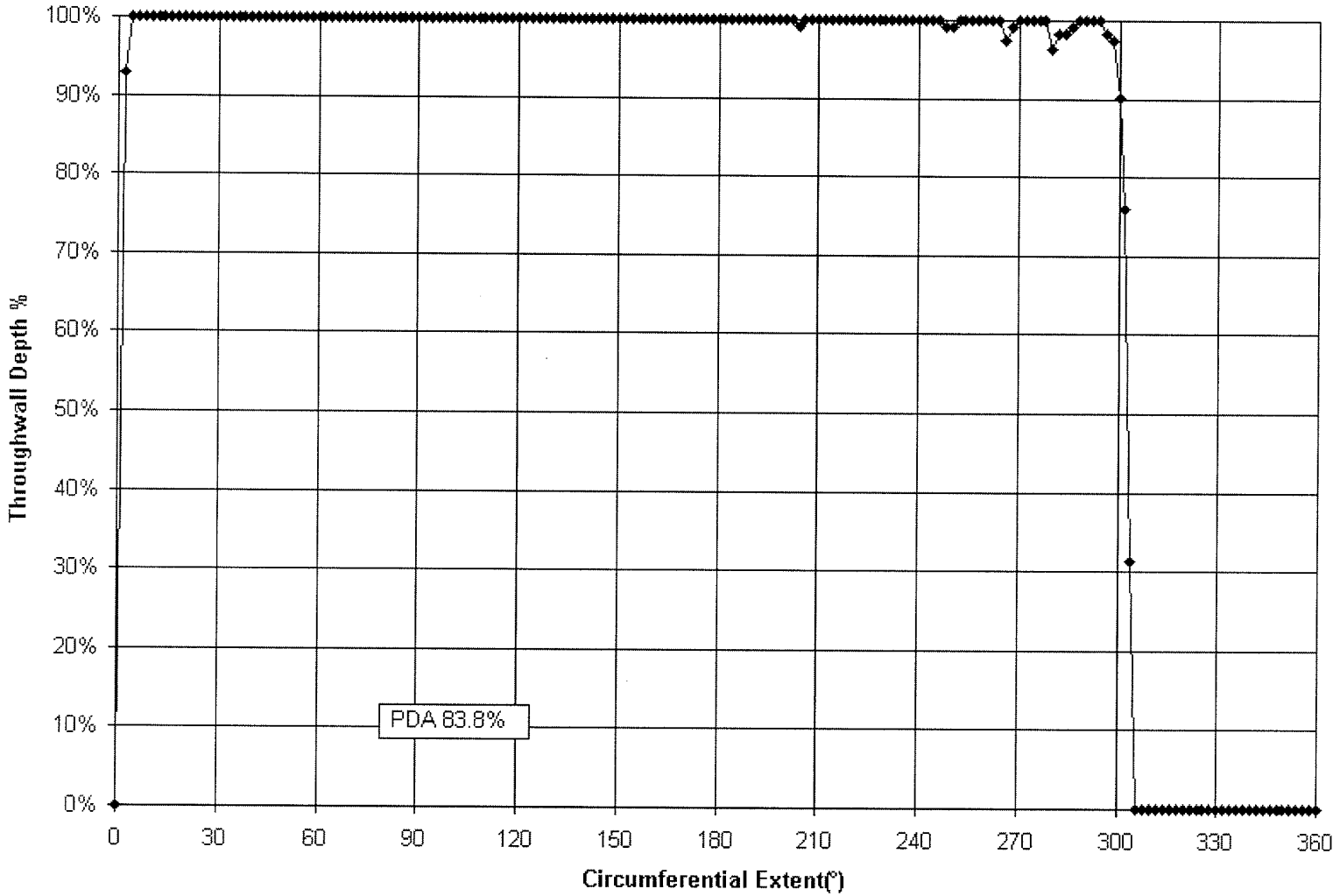

Figure C-15
LAB, 95-03-20; Destructive Examination Depth Profile

Plant:	LAB													
Tube:	95-03-20, OD, .875"													
PDA:	83.8%													
Angle	Depth	L/A	Angle	Depth	L/A	Angle	Depth	L/A	Angle	Depth	L/A	Angle	Depth	L/A
0	0.0%		74	100.0%		148	100.0%		222	100.0%		296	98.2%	
2	92.9%		76	100.0%		150	100.0%		224	100.0%		298	97.3%	
4	100.0%		78	100.0%		152	100.0%		226	100.0%		300	90.2%	
6	100.0%		80	100.0%		154	100.0%		228	100.0%		302	75.9%	
8	100.0%		82	100.0%		156	100.0%		230	100.0%		304	31.3%	
10	100.0%		84	100.0%		158	100.0%		232	100.0%		306	0.0%	
12	100.0%		86	100.0%		160	100.0%		234	100.0%		308	0.0%	
14	100.0%		88	100.0%		162	100.0%		236	100.0%		310	0.0%	
16	100.0%		90	100.0%		164	100.0%		238	100.0%		312	0.0%	
18	100.0%		92	100.0%		166	100.0%		240	100.0%		314	0.0%	
20	100.0%		94	100.0%		168	100.0%		242	100.0%		316	0.0%	
22	100.0%		96	100.0%		170	100.0%		244	100.0%		318	0.0%	
24	100.0%		98	100.0%		172	100.0%		246	100.0%		320	0.0%	
26	100.0%		100	100.0%		174	100.0%		248	99.1%		322	0.0%	
28	100.0%		102	100.0%		176	100.0%		250	99.1%		324	0.0%	
30	100.0%		104	100.0%		178	100.0%		252	100.0%		326	0.0%	
32	100.0%		106	100.0%		180	100.0%		254	100.0%		328	0.0%	
34	100.0%		108	100.0%		182	100.0%		256	100.0%		330	0.0%	
36	100.0%		110	100.0%		184	100.0%		258	100.0%		332	0.0%	
38	100.0%		112	100.0%		186	100.0%		260	100.0%		334	0.0%	
40	100.0%		114	100.0%		188	100.0%		262	100.0%		336	0.0%	
42	100.0%		116	100.0%		190	100.0%		264	100.0%		338	0.0%	
44	100.0%		118	100.0%		192	100.0%		266	97.3%		340	0.0%	
46	100.0%		120	100.0%		194	100.0%		268	99.1%		342	0.0%	
48	100.0%		122	100.0%		196	100.0%		270	100.0%		344	0.0%	
50	100.0%		124	100.0%		198	100.0%		272	100.0%		346	0.0%	
52	100.0%		126	100.0%		200	100.0%		274	100.0%		348	0.0%	
54	100.0%		128	100.0%		202	100.0%		276	100.0%		350	0.0%	
56	100.0%		130	100.0%		204	99.1%		278	100.0%		352	0.0%	
58	100.0%		132	100.0%		206	100.0%		280	96.4%		354	0.0%	
60	100.0%		134	100.0%		208	100.0%		282	98.2%		356	0.0%	
62	100.0%		136	100.0%		210	100.0%		284	98.2%		358	0.0%	
64	100.0%		138	100.0%		212	100.0%		286	99.1%		360	0.0%	
66	100.0%		140	100.0%		214	100.0%		288	100.0%				
68	100.0%		142	100.0%		216	100.0%		290	100.0%				
70	100.0%		144	100.0%		218	100.0%		292	100.0%				
72	100.0%		146	100.0%		220	100.0%		294	100.0%				

Tabulation of Laboratory Specimen Crack Depth Profiles from Destructive Exam

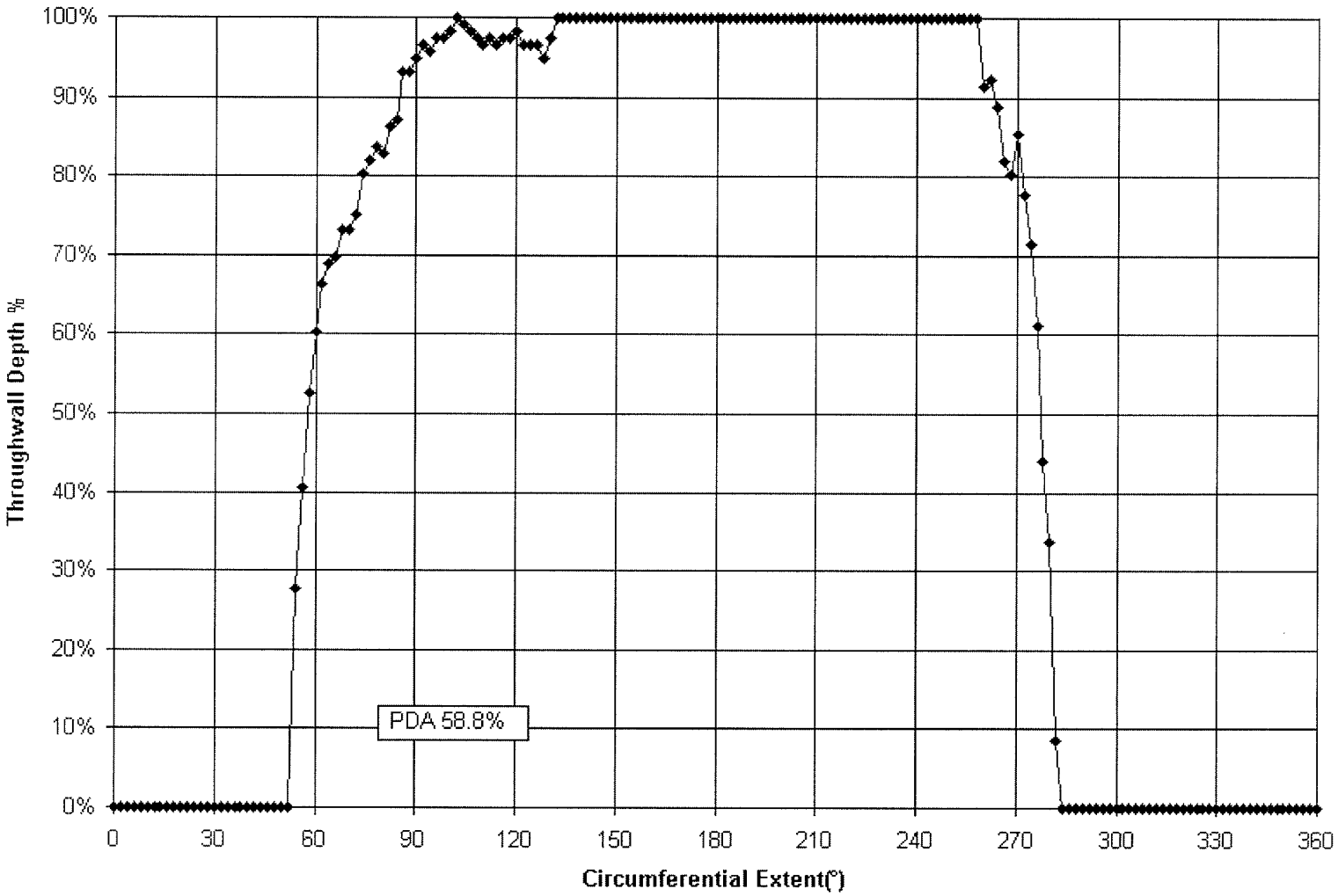

Figure C-16
LAB, 95-03-21; Destructive Examination Depth Profile

Plant:	LAB													
Tube:	95-03-21, OD, .875"													
PDA:	58.8%													
Angle	Depth	L/A	Angle	Depth	L/A	Angle	Depth	L/A	Angle	Depth	L/A	Angle	Depth	L/A
0	0.0%		74	80.2%		148	100.0%		222	100.0%		296	0.0%	
2	0.0%		76	81.9%		150	100.0%		224	100.0%		298	0.0%	
4	0.0%		78	83.6%		152	100.0%		226	100.0%		300	0.0%	
6	0.0%		80	82.8%		154	100.0%		228	100.0%		302	0.0%	
8	0.0%		82	86.2%		156	100.0%		230	100.0%		304	0.0%	
10	0.0%		84	87.1%		158	100.0%		232	100.0%		306	0.0%	
12	0.0%		86	93.1%		160	100.0%		234	100.0%		308	0.0%	
14	0.0%		88	93.1%		162	100.0%		236	100.0%		310	0.0%	
16	0.0%		90	94.8%		164	100.0%		238	100.0%		312	0.0%	
18	0.0%		92	96.6%		166	100.0%		240	100.0%		314	0.0%	
20	0.0%		94	95.7%		168	100.0%		242	100.0%		316	0.0%	
22	0.0%		96	97.4%		170	100.0%		244	100.0%		318	0.0%	
24	0.0%		98	97.4%		172	100.0%		246	100.0%		320	0.0%	
26	0.0%		100	98.3%		174	100.0%		248	100.0%		322	0.0%	
28	0.0%		102	100.0%		176	100.0%		250	100.0%		324	0.0%	
30	0.0%		104	99.1%		178	100.0%		252	100.0%		326	0.0%	
32	0.0%		106	98.3%		180	100.0%		254	100.0%		328	0.0%	
34	0.0%		108	97.4%		182	100.0%		256	100.0%		330	0.0%	
36	0.0%		110	96.6%		184	100.0%		258	100.0%		332	0.0%	
38	0.0%		112	97.4%		186	100.0%		260	91.4%		334	0.0%	
40	0.0%		114	96.6%		188	100.0%		262	92.2%		336	0.0%	
42	0.0%		116	97.4%		190	100.0%		264	88.8%		338	0.0%	
44	0.0%		118	97.4%		192	100.0%		266	81.9%		340	0.0%	
46	0.0%		120	98.3%		194	100.0%		268	80.2%		342	0.0%	
48	0.0%		122	96.6%		196	100.0%		270	85.3%		344	0.0%	
50	0.0%		124	96.6%		198	100.0%		272	77.6%		346	0.0%	
52	0.0%		126	96.6%		200	100.0%		274	71.6%		348	0.0%	
54	27.6%		128	94.8%		202	100.0%		276	61.2%		350	0.0%	
56	40.5%		130	97.4%		204	100.0%		278	44.0%		352	0.0%	
58	52.6%		132	100.0%		206	100.0%		280	33.6%		354	0.0%	
60	60.3%		134	100.0%		208	100.0%		282	8.6%		356	0.0%	
62	66.4%		136	100.0%		210	100.0%		284	0.0%		358	0.0%	
64	69.0%		138	100.0%		212	100.0%		286	0.0%		360	0.0%	
66	69.8%		140	100.0%		214	100.0%		288	0.0%				
68	73.3%		142	100.0%		216	100.0%		290	0.0%				
70	73.3%		144	100.0%		218	100.0%		292	0.0%				
72	75.0%		146	100.0%		220	100.0%		294	0.0%				

Tabulation of Laboratory Specimen Crack Depth Profiles from Destructive Exam

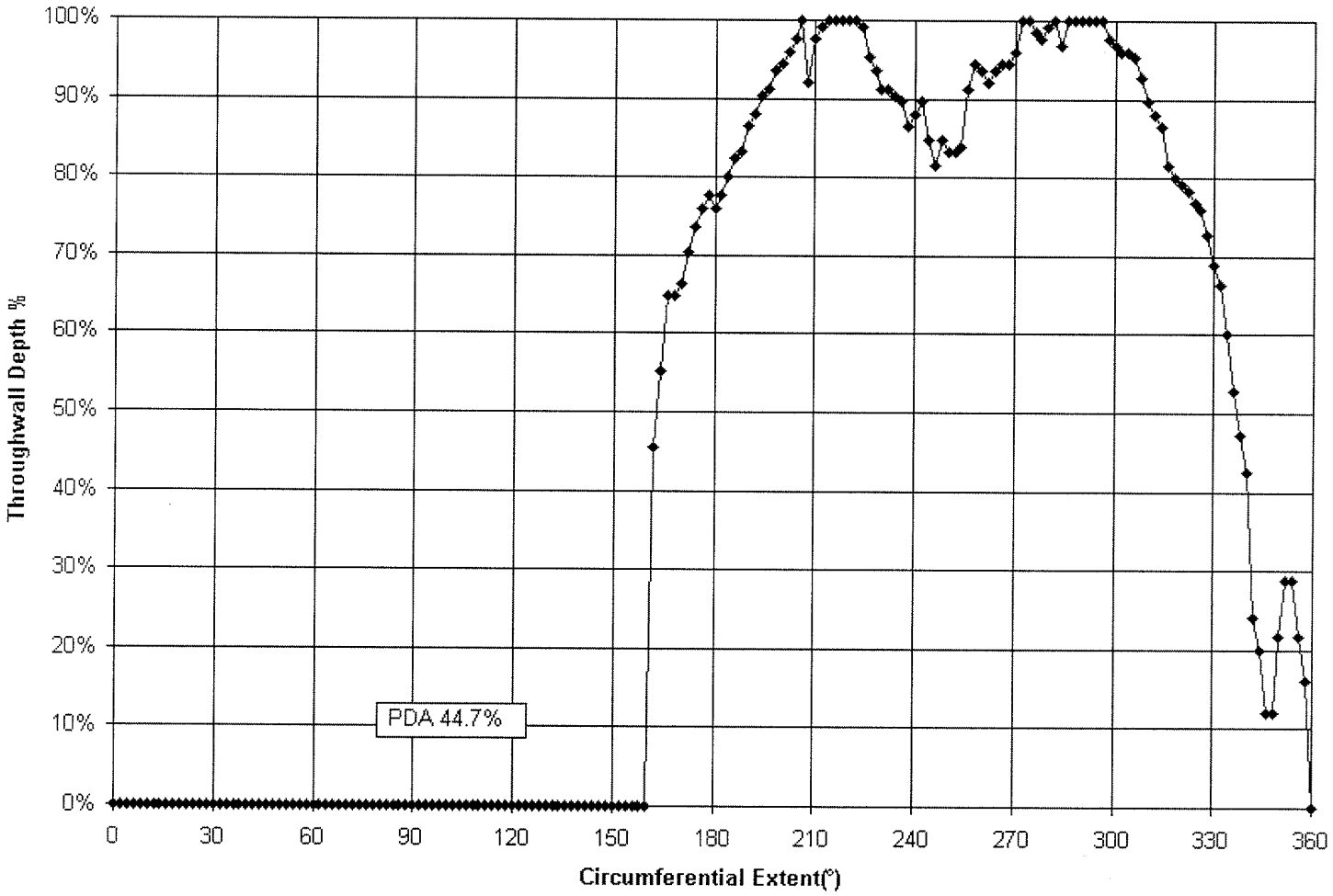

Figure C-17
LAB, 95-03-23; Destructive Examination Depth Profile

Plant:	LAB													
Tube:	95-03-23, OD, .875"													
PDA:	44.7%													
Angle	Depth	L/A	Angle	Depth	L/A	Angle	Depth	L/A	Angle	Depth	L/A	Angle	Depth	L/A
0	0.0%		74	0.0%		148	0.0%		222	100.0%		296	100.0%	
2	0.0%		76	0.0%		150	0.0%		224	99.2%		298	97.6%	
4	0.0%		78	0.0%		152	0.0%		226	95.2%		300	96.8%	
6	0.0%		80	0.0%		154	0.0%		228	93.6%		302	96.0%	
8	0.0%		82	0.0%		156	0.0%		230	91.2%		304	96.0%	
10	0.0%		84	0.0%		158	0.0%		232	91.2%		306	95.2%	
12	0.0%		86	0.0%		160	0.0%		234	90.4%		308	92.8%	
14	0.0%		88	0.0%		162	45.6%		236	89.6%		310	89.6%	
16	0.0%		90	0.0%		164	55.2%		238	86.4%		312	88.0%	
18	0.0%		92	0.0%		166	64.8%		240	88.0%		314	86.4%	
20	0.0%		94	0.0%		168	64.8%		242	89.6%		316	81.6%	
22	0.0%		96	0.0%		170	66.4%		244	84.8%		318	80.0%	
24	0.0%		98	0.0%		172	70.4%		246	81.6%		320	79.2%	
26	0.0%		100	0.0%		174	73.6%		248	84.8%		322	78.4%	
28	0.0%		102	0.0%		176	76.0%		250	83.2%		324	76.8%	
30	0.0%		104	0.0%		178	77.6%		252	83.2%		326	76.0%	
32	0.0%		106	0.0%		180	76.0%		254	84.0%		328	72.8%	
34	0.0%		108	0.0%		182	77.6%		256	91.2%		330	68.8%	
36	0.0%		110	0.0%		184	80.0%		258	94.4%		332	66.4%	
38	0.0%		112	0.0%		186	82.4%		260	93.6%		334	60.0%	
40	0.0%		114	0.0%		188	83.2%		262	92.0%		336	52.8%	
42	0.0%		116	0.0%		190	86.4%		264	93.6%		338	47.2%	
44	0.0%		118	0.0%		192	88.0%		266	94.4%		340	42.4%	
46	0.0%		120	0.0%		194	90.4%		268	94.4%		342	24.0%	
48	0.0%		122	0.0%		196	91.2%		270	96.0%		344	20.0%	
50	0.0%		124	0.0%		198	93.6%		272	100.0%		346	12.0%	
52	0.0%		126	0.0%		200	94.4%		274	100.0%		348	12.0%	
54	0.0%		128	0.0%		202	96.0%		276	98.4%		350	21.6%	
56	0.0%		130	0.0%		204	97.6%		278	97.6%		352	28.8%	
58	0.0%		132	0.0%		206	100.0%		280	99.2%		354	28.8%	
60	0.0%		134	0.0%		208	92.0%		282	100.0%		356	21.6%	
62	0.0%		136	0.0%		210	97.6%		284	96.8%		358	16.0%	
64	0.0%		138	0.0%		212	99.2%		286	100.0%		360	0.0%	
66	0.0%		140	0.0%		214	100.0%		288	100.0%				
68	0.0%		142	0.0%		216	100.0%		290	100.0%				
70	0.0%		144	0.0%		218	100.0%		292	100.0%				
72	0.0%		146	0.0%		220	100.0%		294	100.0%				

Tabulation of Laboratory Specimen Crack Depth Profiles from Destructive Exam

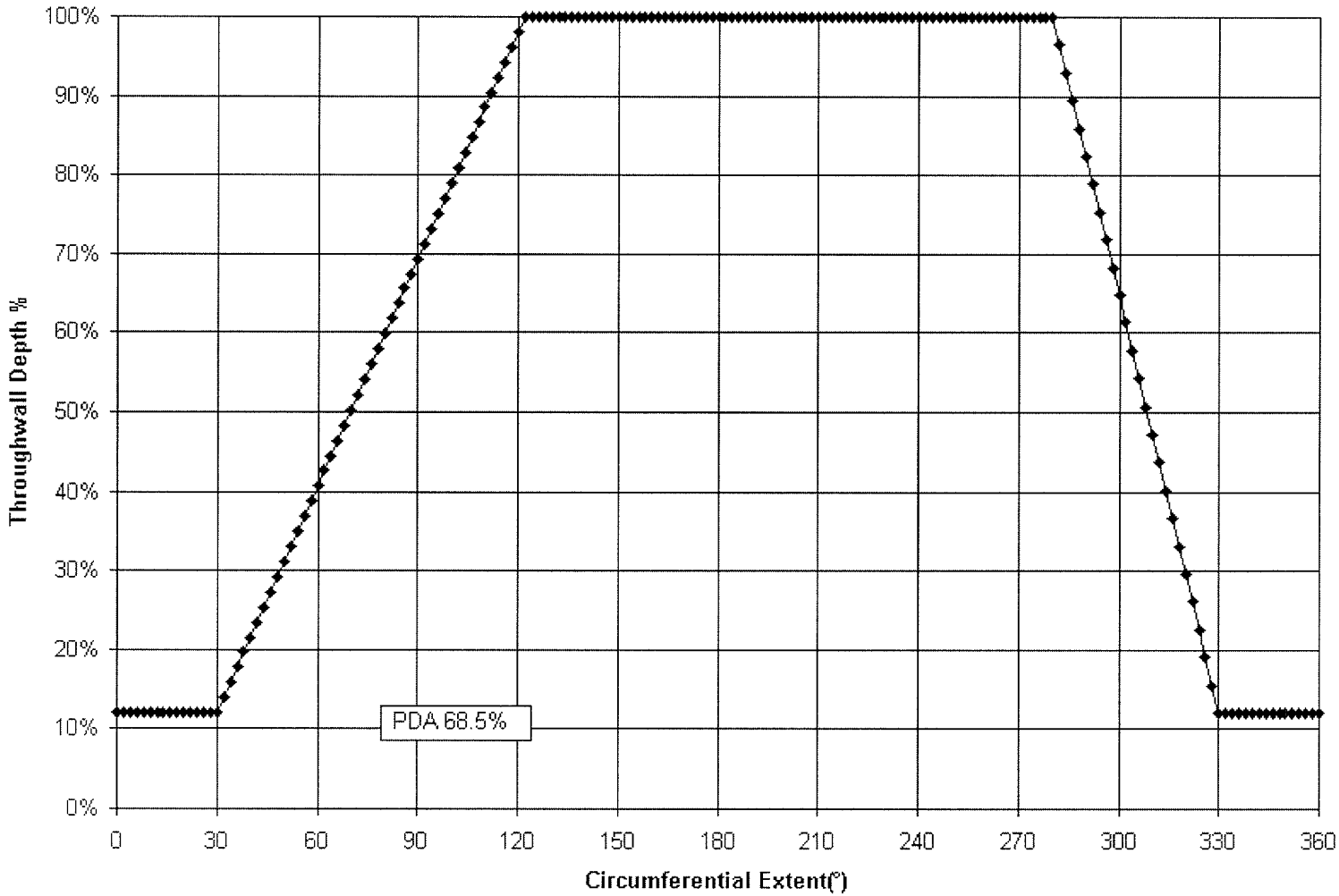

Figure C-18
LAB, 95-03-24; Destructive Examination Depth Profile

Plant:	LAB													
Tube:	95-03-24, OD, .875"													
PDA:	68.5%													
Angle	Depth	L/A	Angle	Depth	L/A	Angle	Depth	L/A	Angle	Depth	L/A	Angle	Depth	L/A
0	12.0%		74	54.1%		148	100.0%		222	100.0%		296	71.8%	
2	12.0%		76	56.0%		150	100.0%		224	100.0%		298	68.3%	
4	12.0%		78	57.9%		152	100.0%		226	100.0%		300	64.8%	
6	12.0%		80	59.8%		154	100.0%		228	100.0%		302	61.3%	
8	12.0%		82	61.7%		156	100.0%		230	100.0%		304	57.8%	
10	12.0%		84	63.7%		158	100.0%		232	100.0%		306	54.2%	
12	12.0%		86	65.6%		160	100.0%		234	100.0%		308	50.7%	
14	12.0%		88	67.5%		162	100.0%		236	100.0%		310	47.2%	
16	12.0%		90	69.4%		164	100.0%		238	100.0%		312	43.7%	
18	12.0%		92	71.3%		166	100.0%		240	100.0%		314	40.2%	
20	12.0%		94	73.2%		168	100.0%		242	100.0%		316	36.6%	
22	12.0%		96	75.1%		170	100.0%		244	100.0%		318	33.1%	
24	12.0%		98	77.0%		172	100.0%		246	100.0%		320	29.6%	
26	12.0%		100	79.0%		174	100.0%		248	100.0%		322	26.1%	
28	12.0%		102	80.9%		176	100.0%		250	100.0%		324	22.6%	
30	12.0%		104	82.8%		178	100.0%		252	100.0%		326	19.0%	
32	13.9%		106	84.7%		180	100.0%		254	100.0%		328	15.5%	
34	15.8%		108	86.6%		182	100.0%		256	100.0%		330	12.0%	
36	17.7%		110	88.5%		184	100.0%		258	100.0%		332	12.0%	
38	19.7%		112	90.4%		186	100.0%		260	100.0%		334	12.0%	
40	21.6%		114	92.3%		188	100.0%		262	100.0%		336	12.0%	
42	23.5%		116	94.3%		190	100.0%		264	100.0%		338	12.0%	
44	25.4%		118	96.2%		192	100.0%		266	100.0%		340	12.0%	
46	27.3%		120	98.1%		194	100.0%		268	100.0%		342	12.0%	
48	29.2%		122	100.0%		196	100.0%		270	100.0%		344	12.0%	
50	31.1%		124	100.0%		198	100.0%		272	100.0%		346	12.0%	
52	33.0%		126	100.0%		200	100.0%		274	100.0%		348	12.0%	
54	35.0%		128	100.0%		202	100.0%		276	100.0%		350	12.0%	
56	36.9%		130	100.0%		204	100.0%		278	100.0%		352	12.0%	
58	38.8%		132	100.0%		206	100.0%		280	100.0%		354	12.0%	
60	40.7%		134	100.0%		208	100.0%		282	96.5%		356	12.0%	
62	42.6%		136	100.0%		210	100.0%		284	93.0%		358	12.0%	
64	44.5%		138	100.0%		212	100.0%		286	89.4%		360	12.0%	
66	46.4%		140	100.0%		214	100.0%		288	85.9%				
68	48.3%		142	100.0%		216	100.0%		290	82.4%				
70	50.3%		144	100.0%		218	100.0%		292	78.9%				
72	52.2%		146	100.0%		220	100.0%		294	75.4%				

Tabulation of Laboratory Specimen Crack Depth Profiles from Destructive Exam

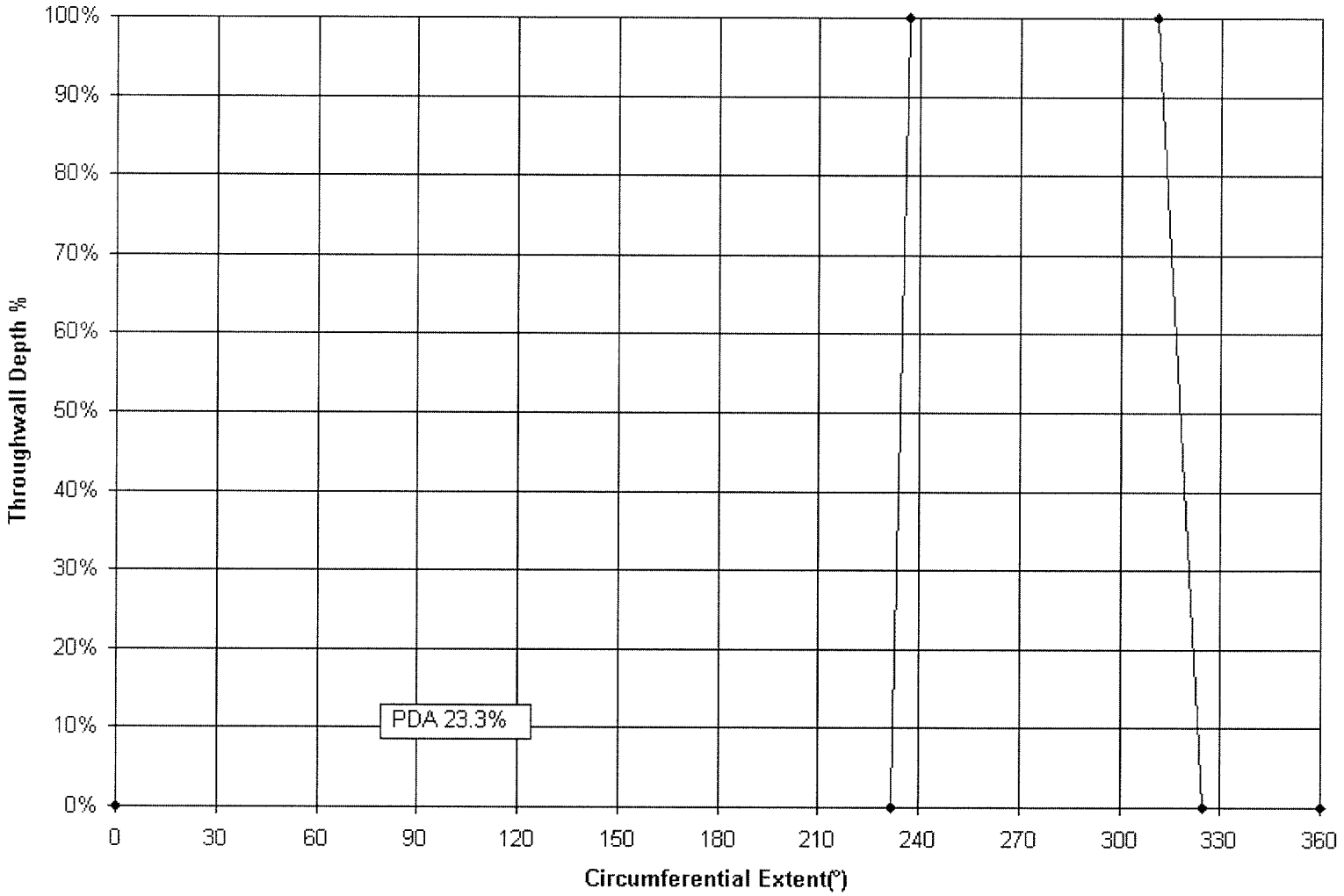

Figure C-19
LAB, 95-08-03B; Destructive Examination Depth Profile

Plant :	LAB	
Tube :	95-08-03B, OD, .875"	
PDA :	23.3%	
Angle	Depth	L/A
0	0.0%	
232	0.0%	
237	100.0%	
311	100.0%	
325	0.0%	
360	0.0%	

Tabulation of Laboratory Specimen Crack Depth Profiles from Destructive Exam

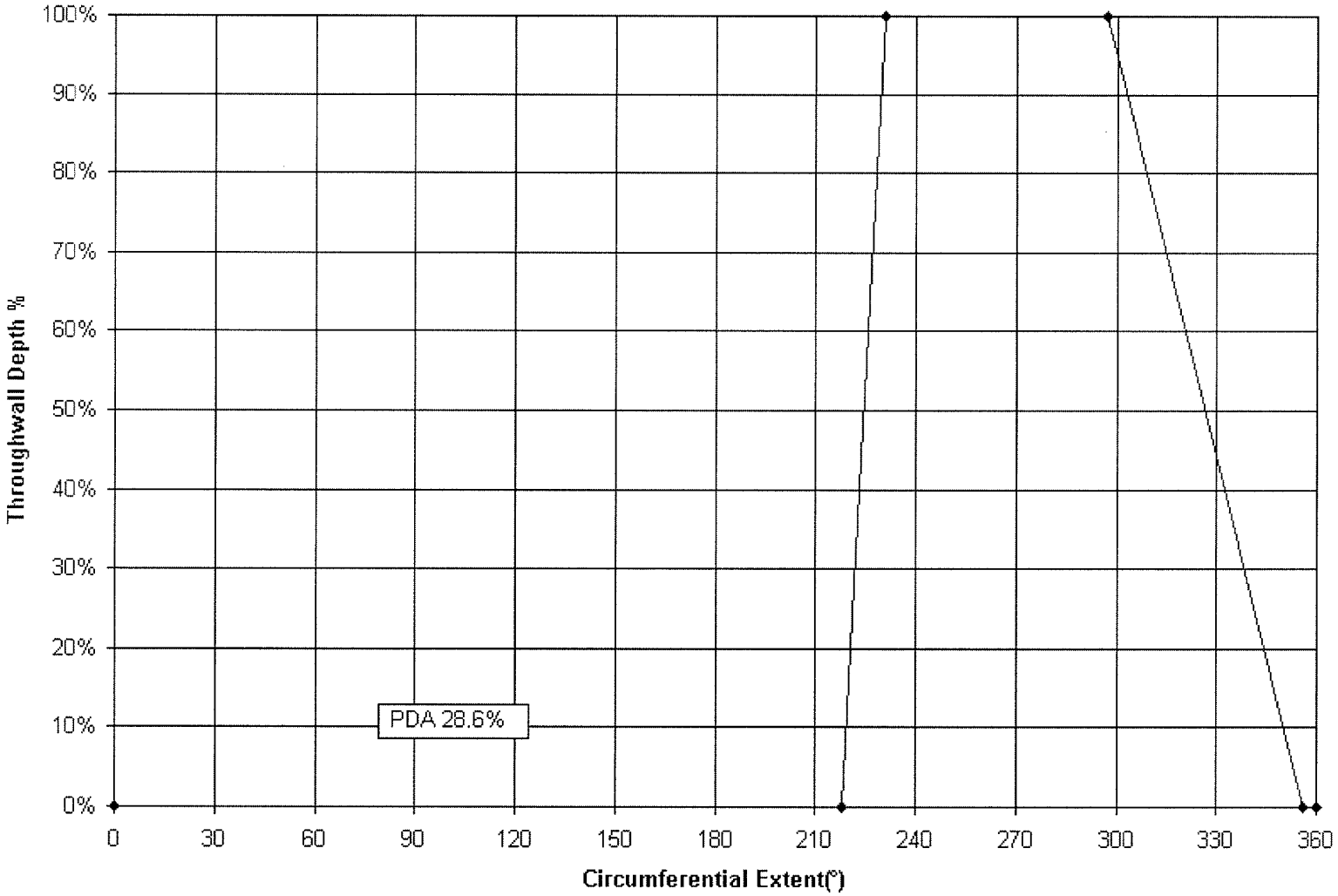

Figure C-20
LAB; 95-08-17B; Destructive Examination Depth Profile

Plant :	LAB	
Tube :	95-08-17B, OD, .875"	
PDA :	28.6%	
Angle	Depth	L/A
0	0.0%	
218	0.0%	
231	100.0%	
297	100.0%	
356	0.0%	
360	0.0%	

Tabulation of Laboratory Specimen Crack Depth Profiles from Destructive Exam

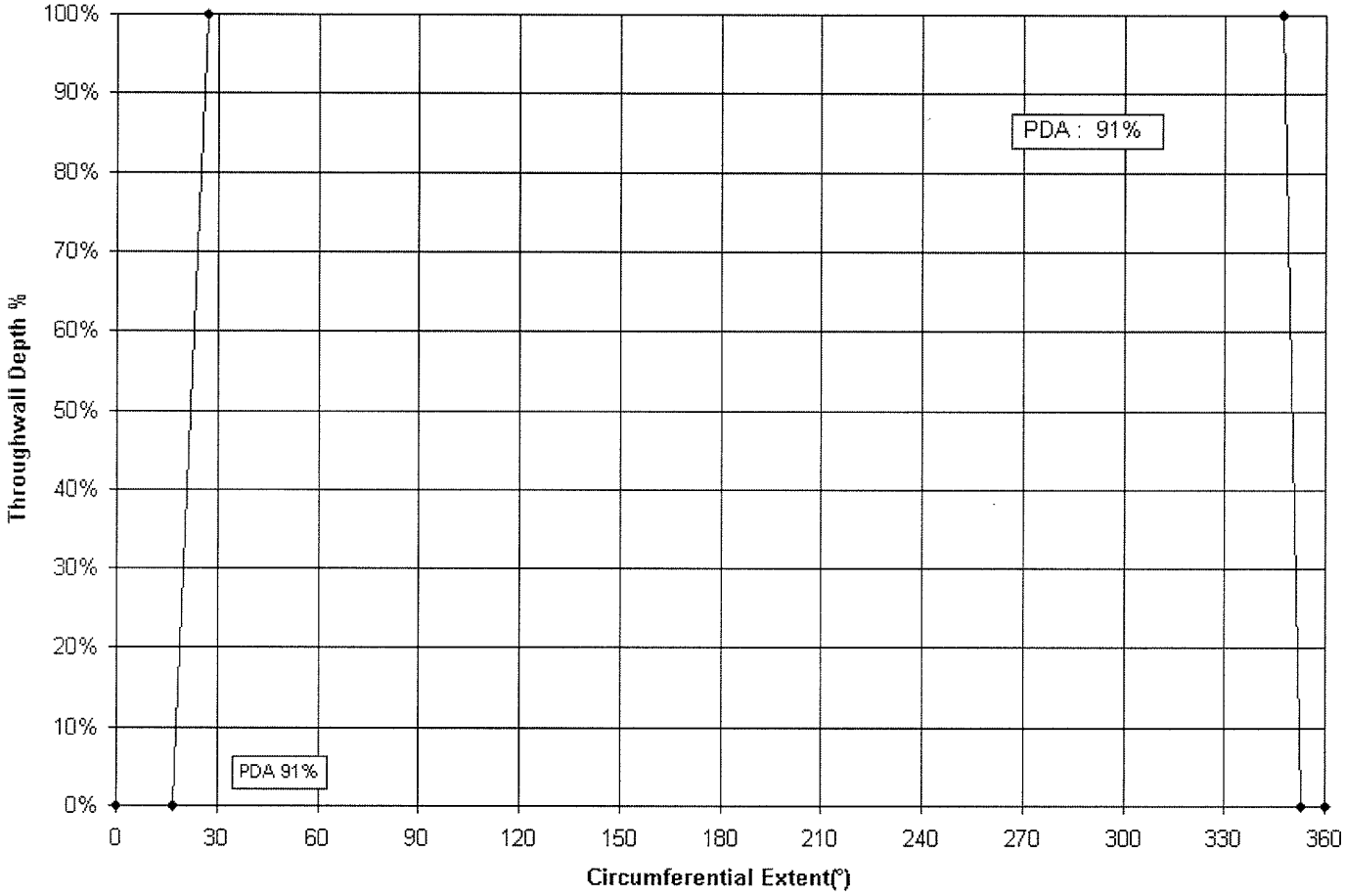

Figure C-21
LAB, 95-08-19T; Destructive Examination Depth Profile

Plant :	LAB	
Tube :	95-08-19T, OD, .875"	
PDA :	91.0%	
Angle	Depth	L/A
0	0.0%	
17	0.0%	
27	100.0%	
347	100.0%	
353	0.0%	
360	0.0%	

Tabulation of Laboratory Specimen Crack Depth Profiles from Destructive Exam

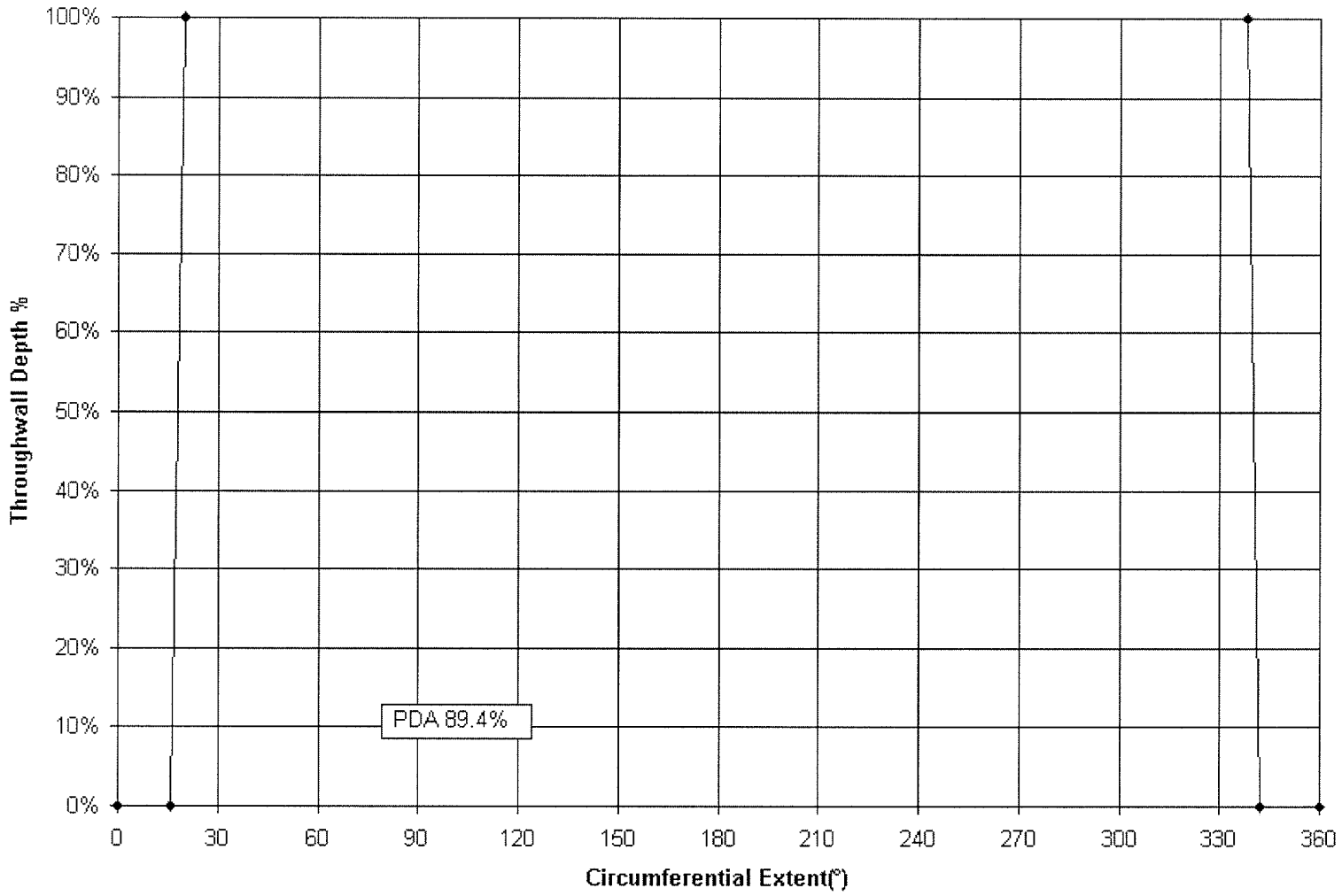

Figure C-22
LAB, 95-08-19B; Destructive Examination Depth Profile

Plant :	LAB	
Tube :	95-08-19B, OD, .875"	
PDA :	89.4%	
Angle	Depth	L/A
0	0.0%	
16	0.0%	
20	100.0%	
338	100.0%	
342	0.0%	
360	0.0%	

Tabulation of Laboratory Specimen Crack Depth Profiles from Destructive Exam

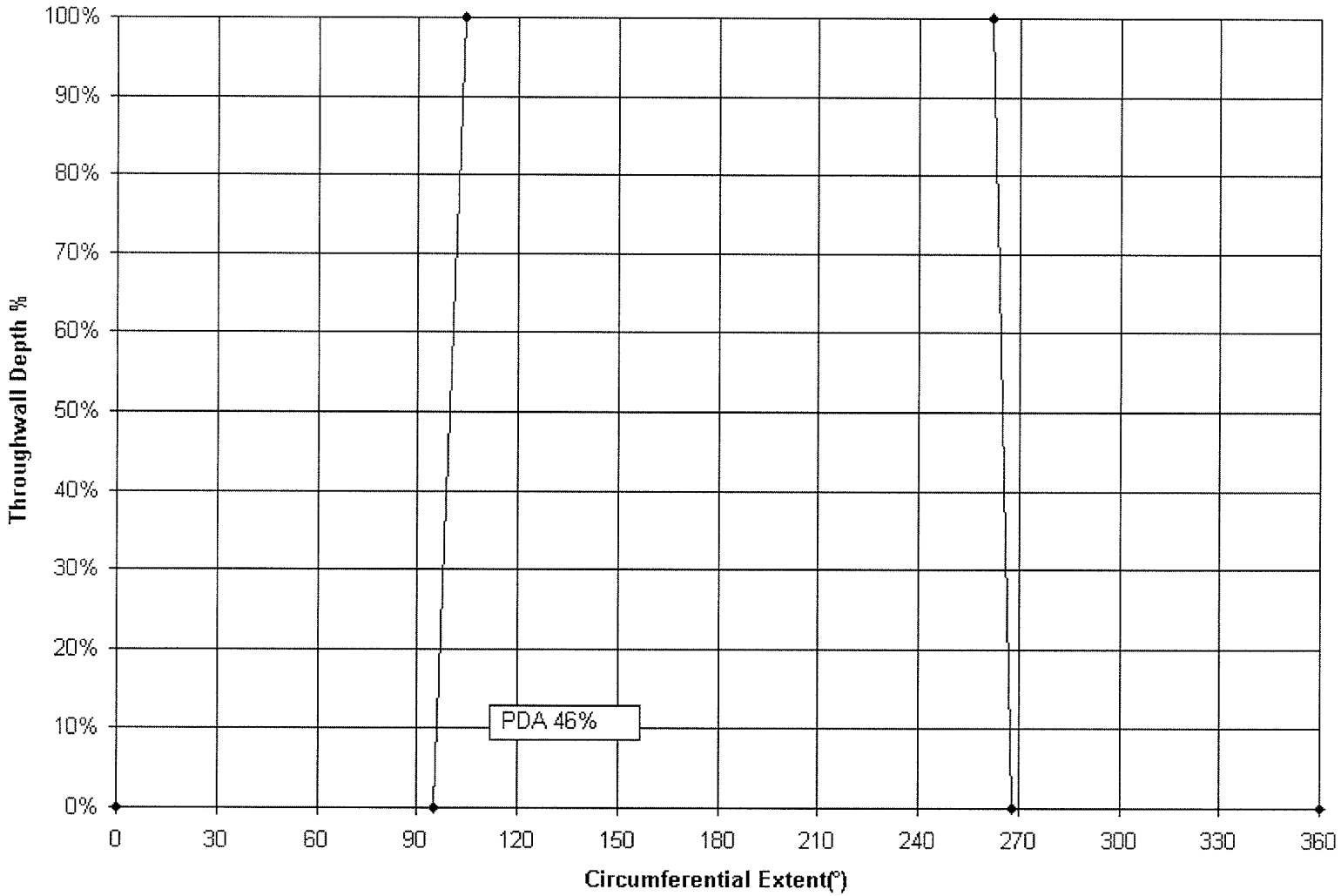

Figure C-23
LAB, 9-95-20T; Destructive Examination Depth Profile

Plant :	LAB	
Tube :	9-95-20T, OD, .875"	
PDA :	46.0%	
Angle	Depth	L/A
0	0.0%	
95	0.0%	
104	100.0%	
262	100.0%	
268	0.0%	
360	0.0%	

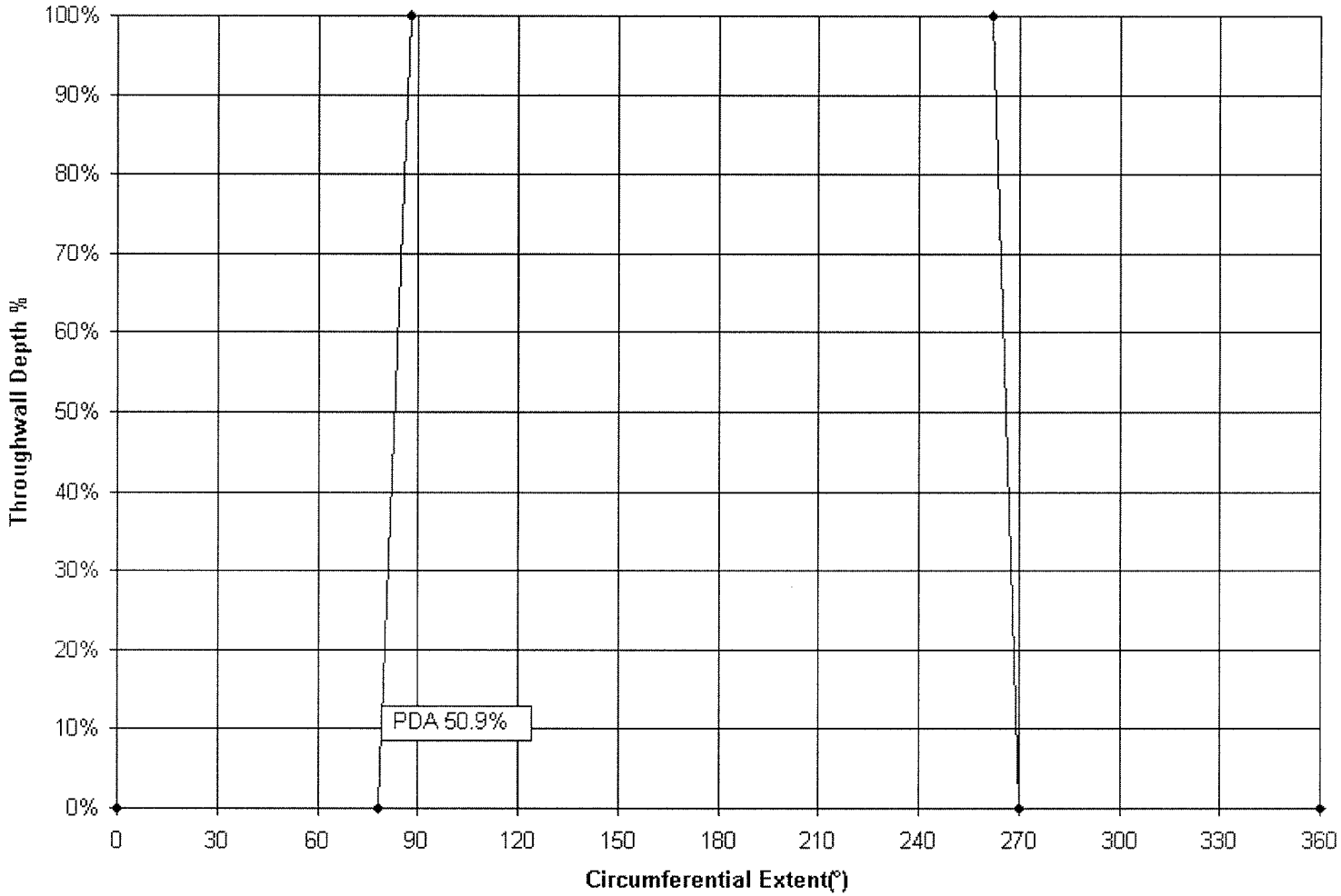

Figure C-24
LAB, 9-95-20B; Destructive Examination Depth Profile

Plant :	LAB	
Tube :	9-95-20B, OD, .875"	
PDA :	50.9%	
Angle	Depth	L/A
0	0.0%	
78	0.0%	
88	100.0%	
262	100.0%	
270	0.0%	
360	0.0%	

Tabulation of Laboratory Specimen Crack Depth Profiles from Destructive Exam

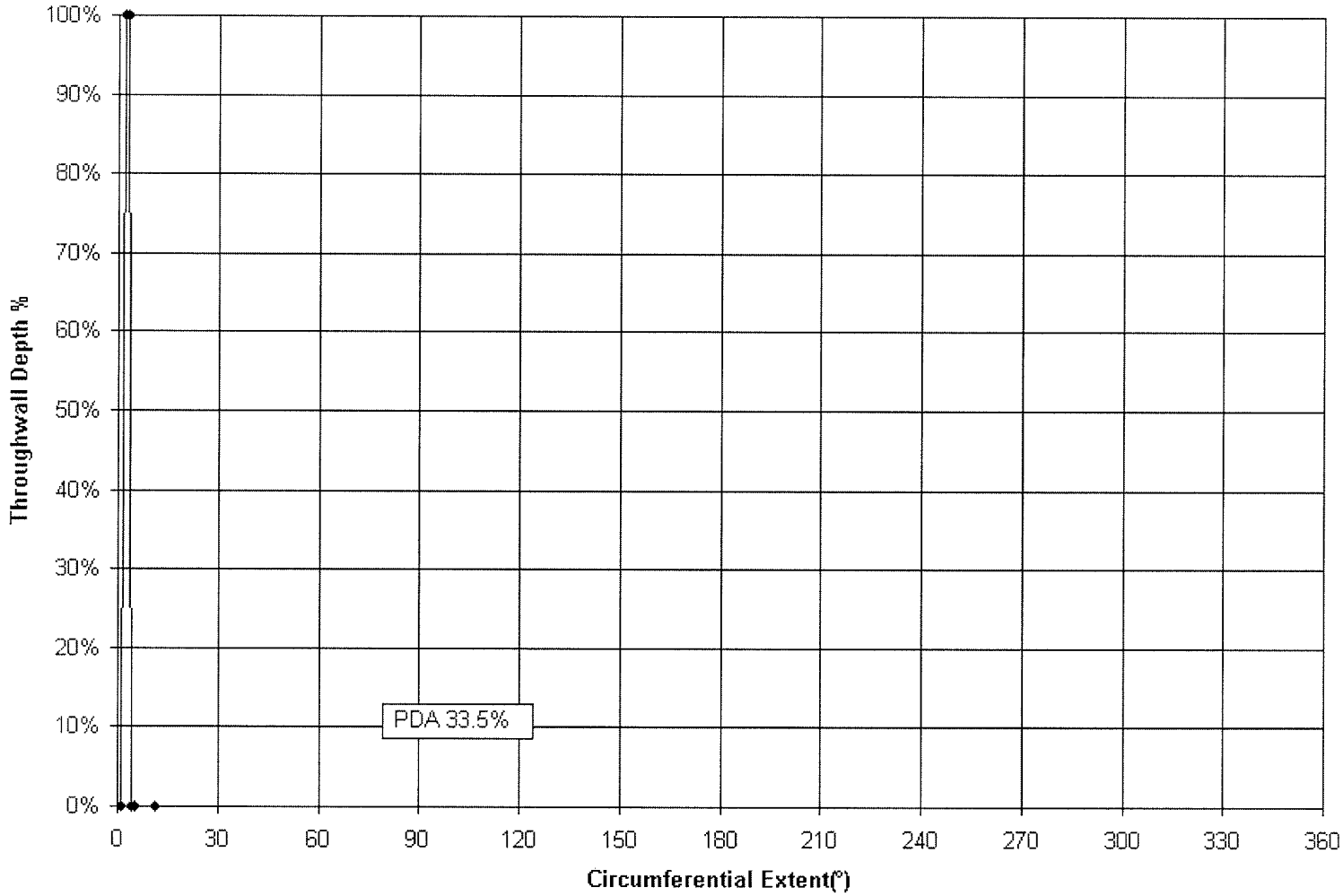

Figure C-25
LAB, 9-95-25B; Destructive Examination Depth Profile

Plant :	LAB	
Tube :	9-95-25B, OD, .875"	
PDA :	33.5%	
Angle	Depth	L/A
0	0.0%	
7	100.0%	
111	100.0%	
136	0.0%	
360	0.0%	

Tabulation of Laboratory Specimen Crack Depth Profiles from Destructive Exam

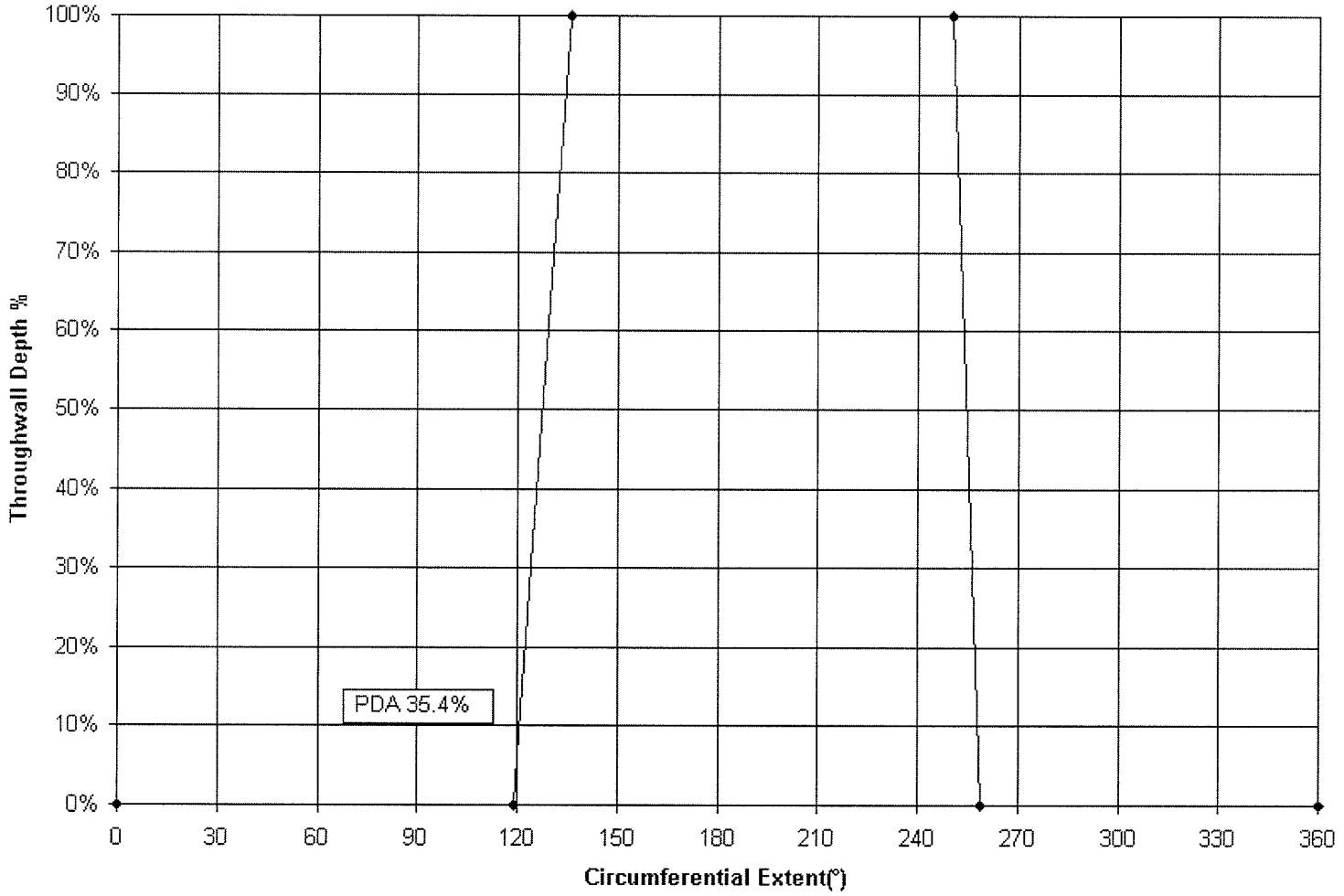

Figure C-26
LAB, 9-95-05T; Destructive Examination Depth Profile

Plant :	LAB	
Tube :	9-95-05T, ID, .75"	
PDA :	35.4%	
Angle	Depth	L/A
0	0.0%	
119	0.0%	
136	100.0%	
250	100.0%	
259	0.0%	
360	0.0%	

Tabulation of Laboratory Specimen Crack Depth Profiles from Destructive Exam

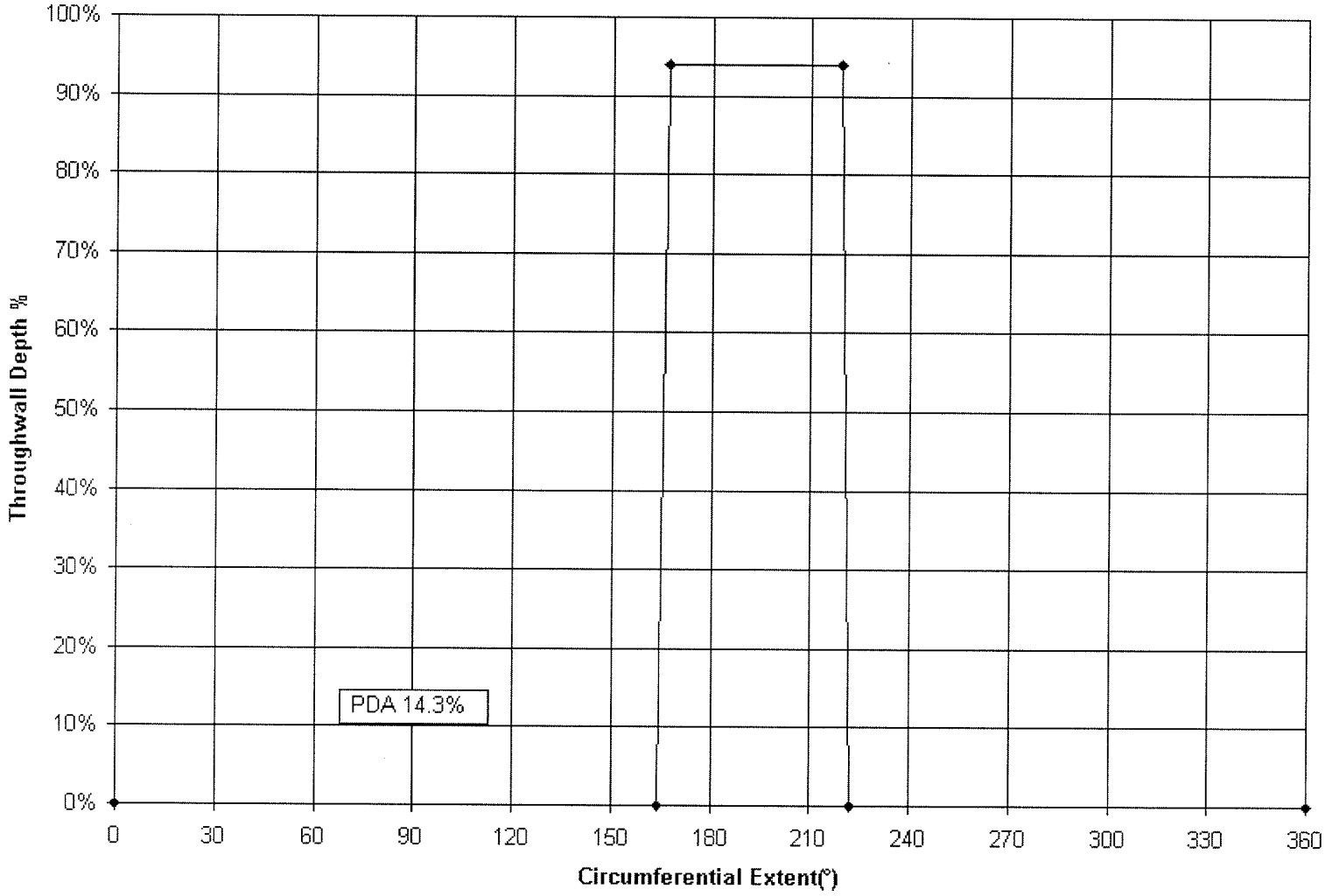

Figure C-27
LAB, 9-95-08T; Destructive Examination Depth Profile

Plant :	LAB	
Tube :	9-95-08T, ID, .75"	
PDA :	14.3%	
Angle	Depth	L/A
0	0.0%	
164	0.0%	
167	94.0%	
219	94.0%	
222	0.0%	
360	0.0%	

Tabulation of Laboratory Specimen Crack Depth Profiles from Destructive Exam

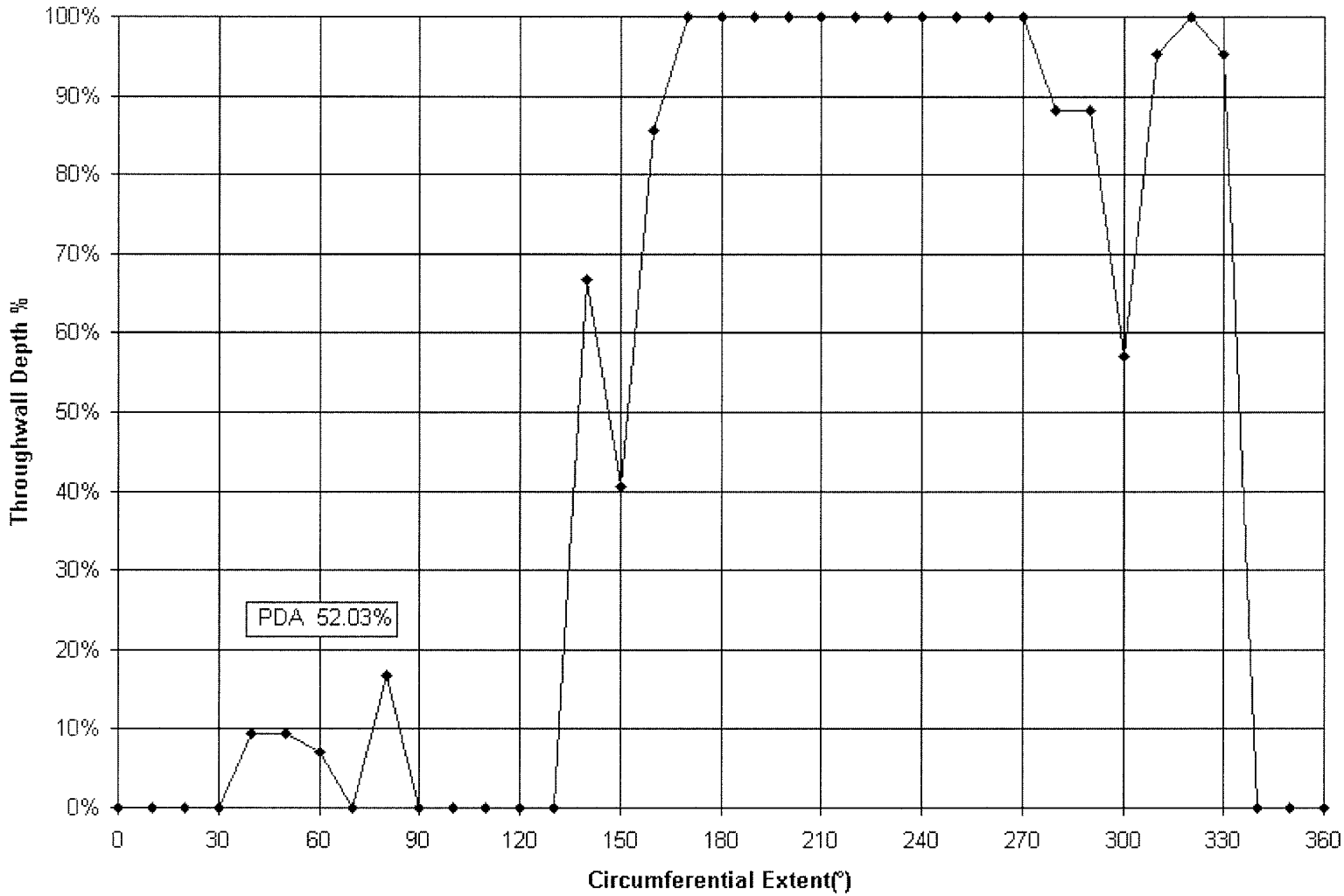

Figure C-28
LAB ANO, R0C1; Destructive Examination Depth Profile

Plant:	ANO LAB	
Tube :	R0C1, OD .75"	
PDA :	EX 52.03%	
Angle	Depth	Lig. Area
0	0.0%	
10	0.0%	
20	0.0%	
30	0.0%	
40	9.5%	
50	9.5%	
60	7.1%	
70	0.0%	
80	16.7%	
90	0.0%	
100	0.0%	
110	0.0%	
120	0.0%	
130	0.0%	
140	66.7%	
150	40.5%	
160	85.7%	
170	100.0%	
180	100.0%	
190	100.0%	
200	100.0%	
210	100.0%	
220	100.0%	
230	100.0%	
240	100.0%	
250	100.0%	
260	100.0%	
270	100.0%	
280	88.1%	
290	88.1%	
300	57.1%	
310	95.2%	
320	100.0%	
330	95.2%	
340	0.0%	
350	0.0%	
360	0.0%	

Tabulation of Laboratory Specimen Crack Depth Profiles from Destructive Exam

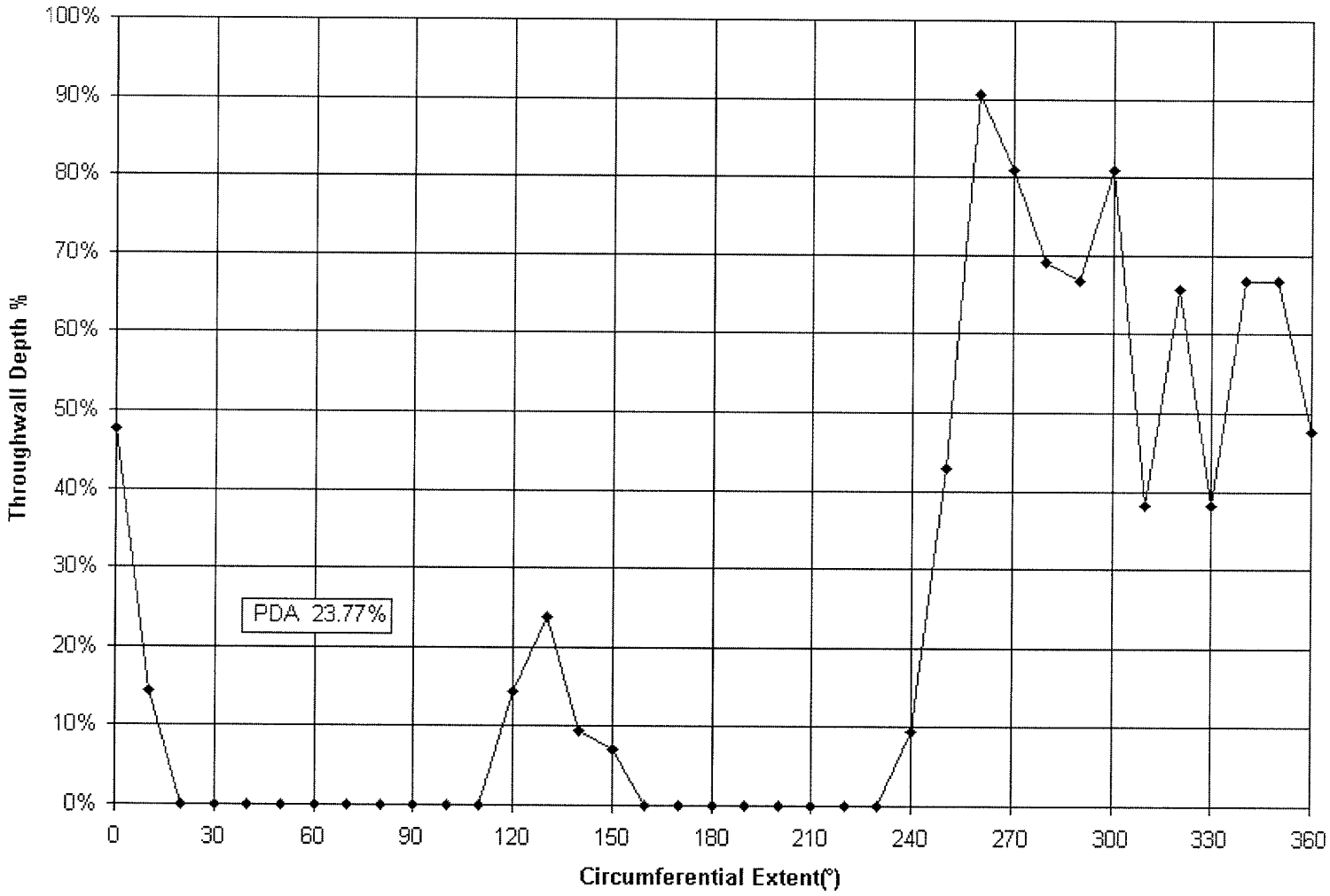

Figure C-29
LAB ANO, R0C2; Destructive Examination Depth Profile

Plant :	ANO LAB	
Tube :	R0C2, OD .75"	
PDA :	EX 23.77%	
Angle	Depth	Lig. Area
0	47.6%	
10	14.3%	
20	0.0%	
30	0.0%	
40	0.0%	
50	0.0%	
60	0.0%	
70	0.0%	
80	0.0%	
90	0.0%	
100	0.0%	
110	0.0%	
120	14.3%	
130	23.8%	
140	9.5%	
150	7.1%	
160	0.0%	
170	0.0%	
180	0.0%	
190	0.0%	
200	0.0%	
210	0.0%	
220	0.0%	
230	0.0%	
240	9.5%	
250	42.9%	
260	90.5%	
270	81.0%	
280	69.0%	
290	66.7%	
300	81.0%	
310	38.1%	
320	65.7%	
330	38.1%	
340	66.7%	
350	66.7%	
360	47.6%	

Tabulation of Laboratory Specimen Crack Depth Profiles from Destructive Exam

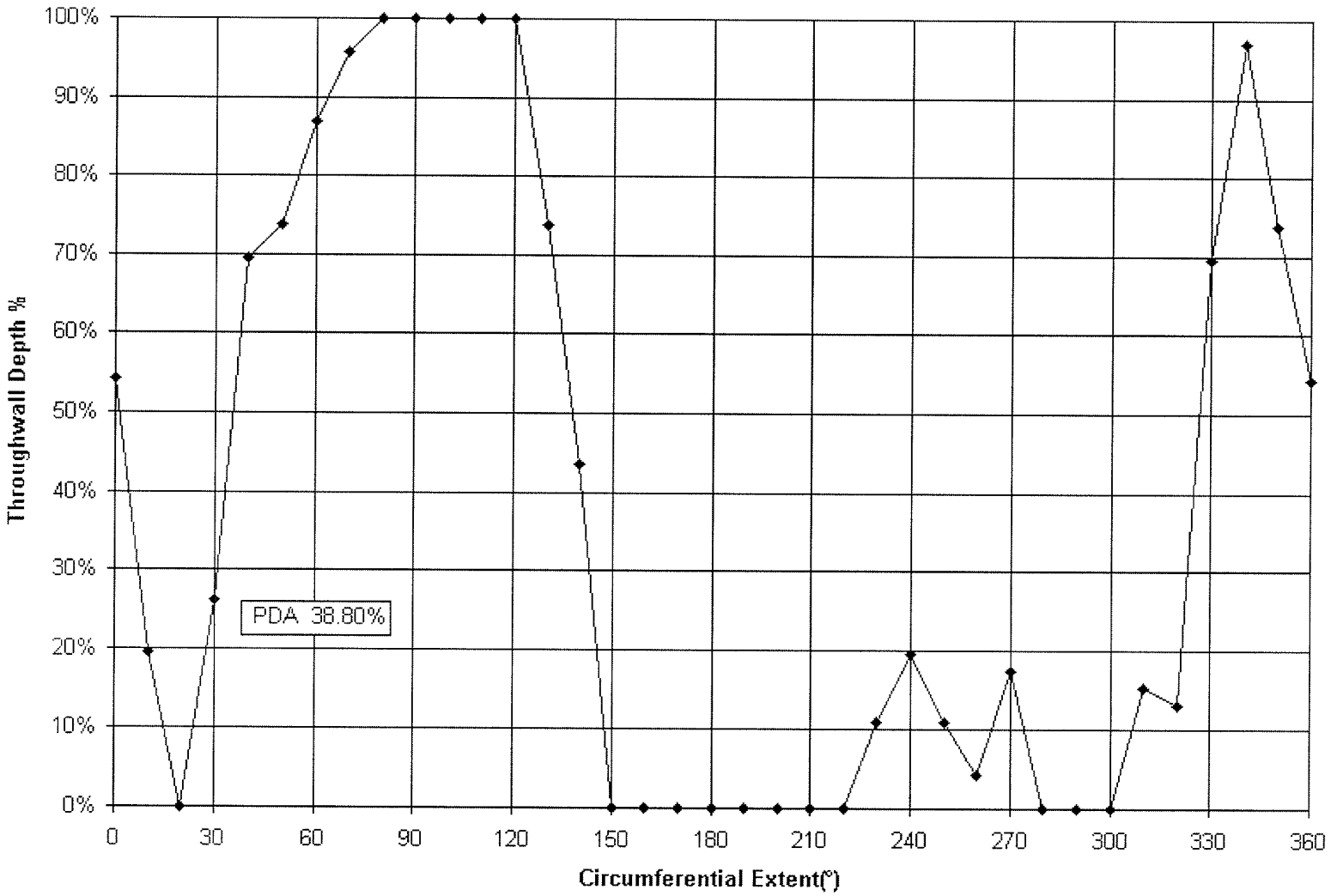

Figure C-30
LAB ANO, R0C3; Destructive Examination Depth Profile

Plant :	ANO LAB	
Tube :	R0C3, OD .75"	
PDA :	EX 38.8%	
Angle	Depth	Lig. Area
0	54.3%	
10	19.6%	
20	0.0%	
30	26.1%	
40	69.6%	
50	73.9%	
60	87.0%	
70	95.7%	
80	100.0%	
90	100.0%	
100	100.0%	
110	100.0%	
120	100.0%	
130	73.9%	
140	43.5%	
150	0.0%	
160	0.0%	
170	0.0%	
180	0.0%	
190	0.0%	
200	0.0%	
210	0.0%	
220	0.0%	
230	10.9%	
240	19.6%	
250	10.9%	
260	4.3%	
270	17.4%	
280	0.0%	
290	0.0%	
300	0.0%	
310	15.2%	
320	13.0%	
330	69.6%	
340	97.0%	
350	73.9%	
360	54.3%	

Tabulation of Laboratory Specimen Crack Depth Profiles from Destructive Exam

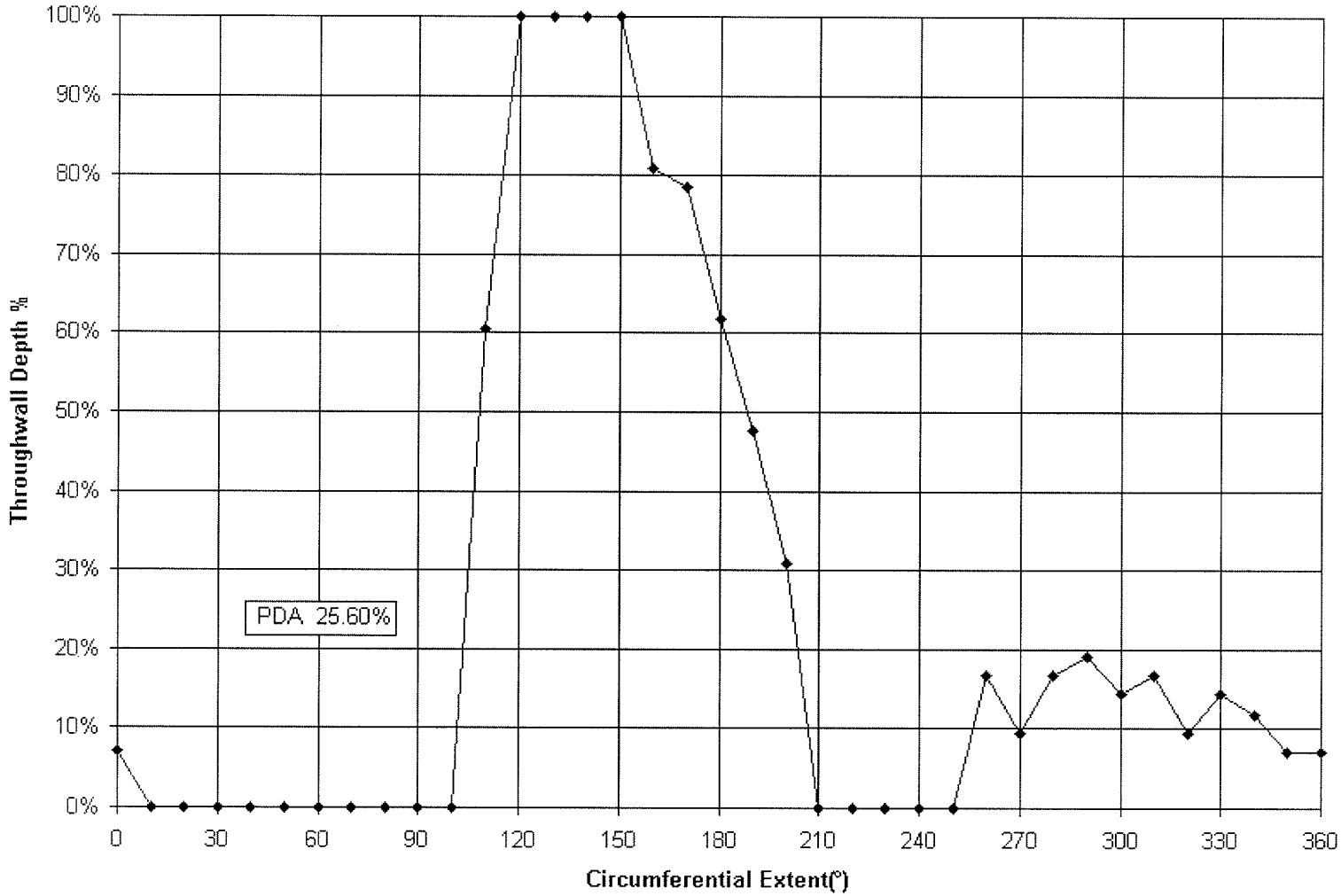

Figure C-31
LAB ANO, R0C4; Destructive Examination Depth Profile

Plant :	ANO LAB	
Tube :	R0C4, OD .75"	
PDA :	EX 25.6%	
Angle	Depth	Lig. Area
0	7.1%	
10	0.0%	
20	0.0%	
30	0.0%	
40	0.0%	
50	0.0%	
60	0.0%	
70	0.0%	
80	0.0%	
90	0.0%	
100	0.0%	
110	60.5%	
120	100.0%	
130	100.0%	
140	100.0%	
150	100.0%	
160	81.0%	
170	78.6%	
180	61.9%	
190	47.6%	
200	31.0%	
210	0.0%	
220	0.0%	
230	0.0%	
240	0.0%	
250	0.0%	
260	16.7%	
270	9.5%	
280	16.7%	
290	19.0%	
300	14.3%	
310	16.7%	
320	9.5%	
330	14.3%	
340	11.9%	
350	7.1%	
360	7.1%	

Tabulation of Laboratory Specimen Crack Depth Profiles from Destructive Exam

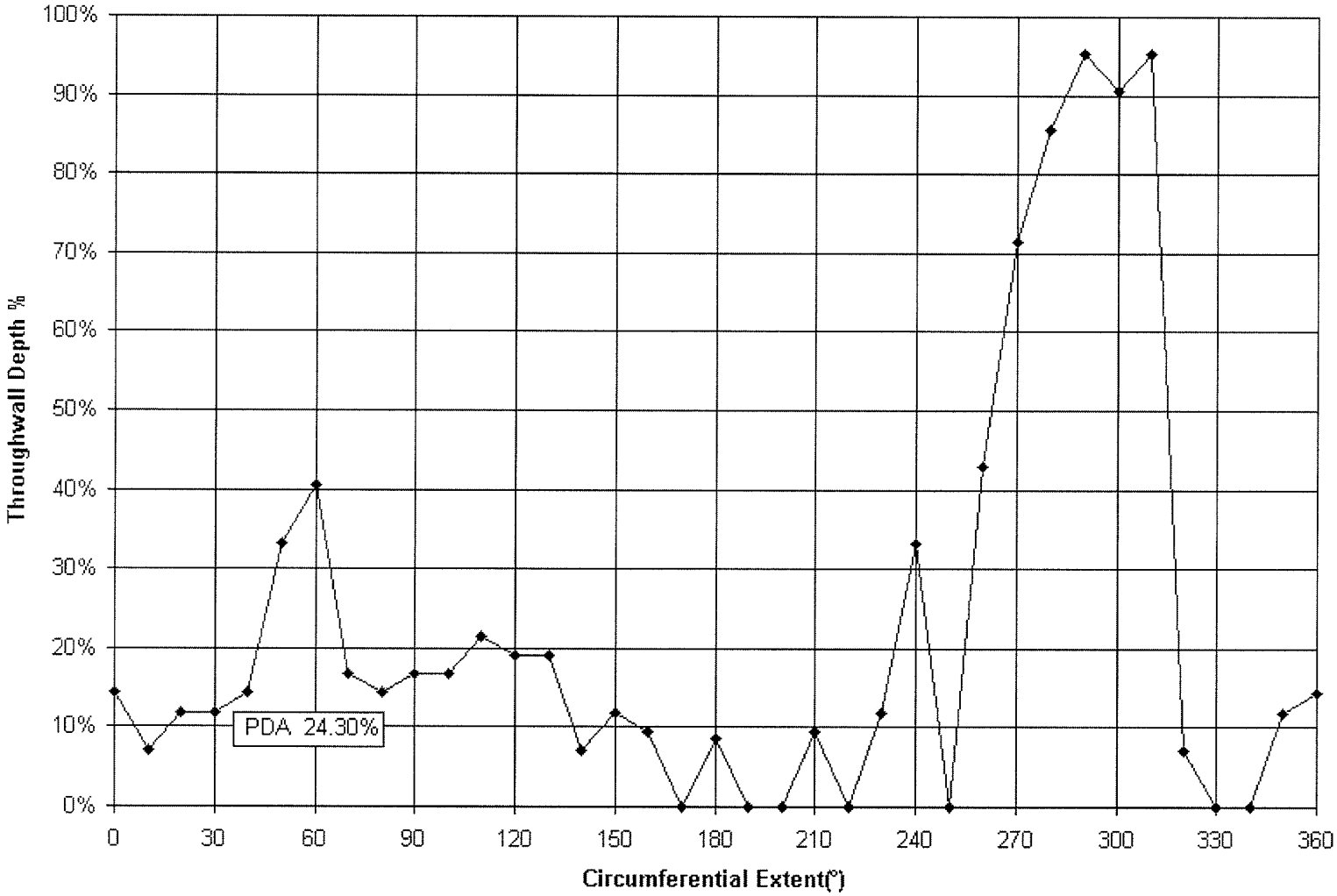

Figure C-32
LAB ANO, R0C5; Destructive Examination Depth Profile

Plant :	ANO LAB	
Tube :	R0C5, OD .75"	
PDA :	EX 24.3%	
Angle	Depth	Lig. Area
0	14.3%	
10	7.1%	
20	11.9%	
30	11.9%	
40	14.3%	
50	33.3%	
60	40.5%	
70	16.7%	
80	14.3%	
90	16.7%	
100	16.7%	
110	21.4%	
120	19.0%	
130	19.0%	
140	7.1%	
150	11.9%	
160	9.5%	
170	0.0%	
180	8.5%	
190	0.0%	
200	0.0%	
210	9.5%	
220	0.0%	
230	11.9%	
240	33.3%	
250	0.0%	
260	42.9%	
270	71.4%	
280	85.7%	
290	95.2%	
300	90.5%	
310	95.2%	
320	7.1%	
330	0.0%	
340	0.0%	
350	11.9%	
360	14.3%	

Tabulation of Laboratory Specimen Crack Depth Profiles from Destructive Exam

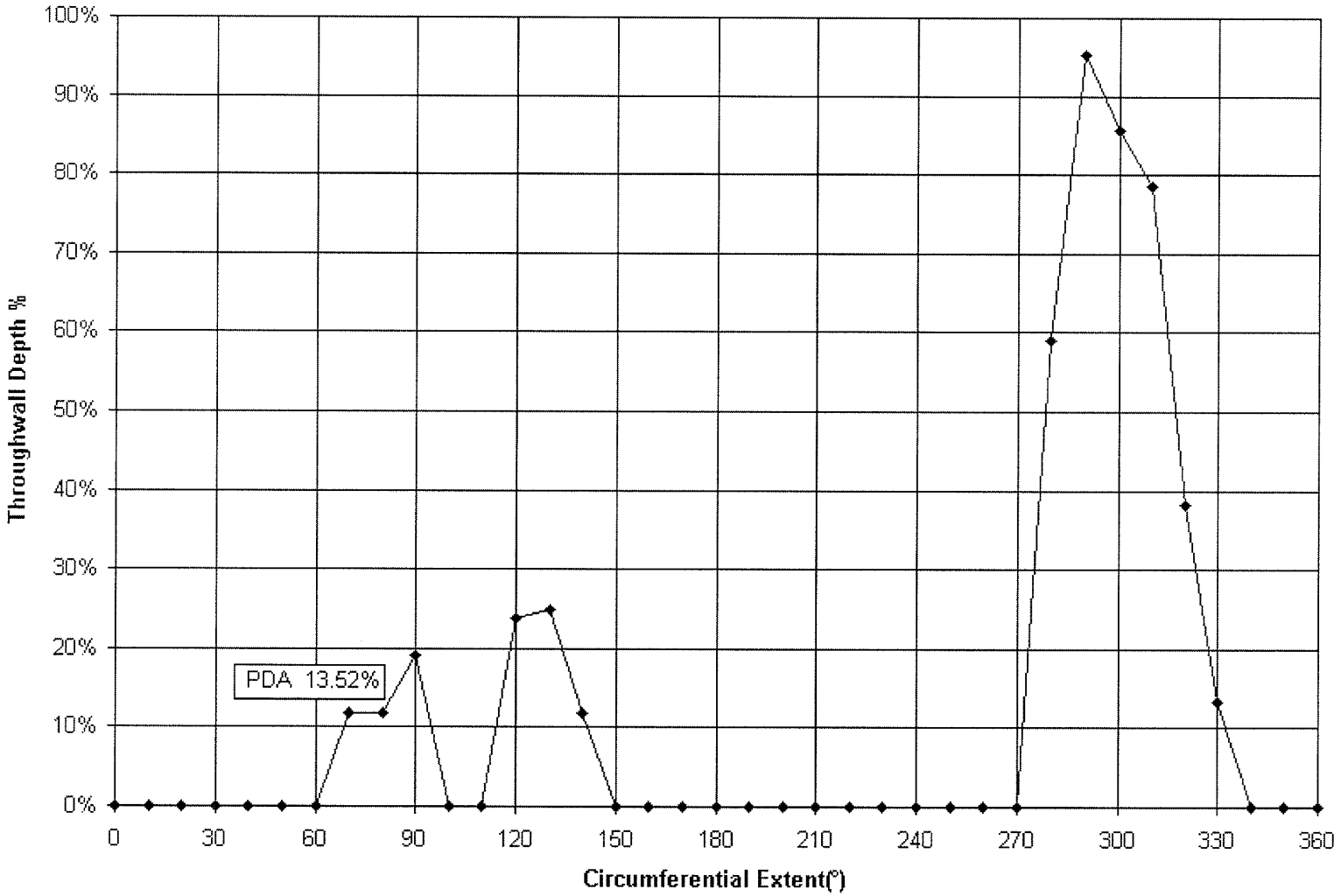

Figure C-33
LAB ANO, R0C6; Destructive Examination Depth Profile

Plant :	ANO LAB	
Tube :	R0C6, OD .75"	
PDA :	EX 13.52%	
Angle	Depth	Lig. Area
0	0	
10	0	
20	0	
30	0	
40	0	
50	0	
60	0	
70	0.119	
80	0.119	
90	0.19	
100	0	
110	0	
120	0.238	
130	0.248	
140	0.119	
150	0	
160	0	
170	0	
180	0	
190	0	
200	0	
210	0	
220	0	
230	0	
240	0	
250	0	
260	0	
270	0	
280	0.59	
290	0.952	
300	0.857	
310	0.786	
320	0.381	
330	0.133	
340	0	
350	0	
360	0	